Springer Transactions in Civil
and Environmental Engineering

Kishor Chandra Panda
Sudhirkumar V. Barai
Sriman Kumar Bhattacharyya

Shear Strengthening of T-beam with GFRP

A Systematic Approach

Springer

Springer Transactions in Civil and Environmental Engineering

More information about this series at http://www.springer.com/series/13593

Kishor Chandra Panda · Sudhirkumar V. Barai
Sriman Kumar Bhattacharyya

Shear Strengthening of T-beam with GFRP

A Systematic Approach

Springer

Kishor Chandra Panda
Department of Civil Engineering
Government College of Engineering,
Kalahandi
Bhawanipatna, Odisha
India

Sudhirkumar V. Barai
Department of Civil Engineering
Indian Institute of Technology Kharagpur
Kharagpur, West Bengal
India

Sriman Kumar Bhattacharyya
Department of Civil Engineering
Indian Institute of Technology Kharagpur
Kharagpur, West Bengal
India

ISSN 2363-7633 ISSN 2363-7641 (electronic)
Springer Transactions in Civil and Environmental Engineering
ISBN 978-981-10-7759-3 ISBN 978-981-10-7760-9 (eBook)
https://doi.org/10.1007/978-981-10-7760-9

Library of Congress Control Number: 2018938372

Printed on acid-free paper

This Springer imprint is published by the registered company Springer Nature Singapore Pte Ltd.
part of Springer Nature
The registered company address is: 152 Beach Road, #21-01/04 Gateway East, Singapore 189721, Singapore

The best way to predict the future is to design it.

—Buckminster Fuller

Dedicated to

The Structural Life Savers!

Foreword

Infrastructure deficit has been one of the biggest issues the world is facing for the last two decades. The deficit hypothesis postulates that a decline in the public capital formation (i.e. infrastructure) will lower private sector productivity and, therefore, lower a nation's real income while weakening its international competitiveness. Around the world, civil infrastructure—that represents 70% of the country's total infrastructure—is declining rapidly and will need nearly $6 trillion investment.

Why are we in such dire straits? A primary reason is that the average expected maintenance-free life for a structure built today is approximately 18.5 years. When we compare this short life expectancy of our modern structures to that of some historical and still functioning structures like the Great Stupas of Sanchi in India (200 BC), the Pont du Gard in France (15 BC) and the Pantheon in Rome (118 AD), a rather disturbing trend emerges: our modern construction materials and technologies produce structures with serviceable lives that are far shorter than those produced by two-millennia-old technologies! Major factors responsible for this dismal reality are the corrosion of steel in our reinforced concrete structures (curiously enough, steel was not present in any of the old structures cited above) and a faster rate of deterioration and ageing of structural systems used today. A second reason for our current infrastructure crisis has to do with decades of deferred maintenance work that has resulted in deterioration and decay of our structural systems occurring at an ever-increasing rate. All materials deteriorate with time, and the deterioration rate is further increased by factors such as severe weather, overload, fatigue, pollutions/chemicals, structural settlement and lack of timely maintenance. Clearly, we need not only to improve upon our building technologies, design philosophies and construction materials, but also to find ways of

rehabilitating the current inventory of structures using materials, processes and techniques that provide repair and strengthening solutions that are both long-lasting and cost-effective.

There are several solutions proposed for combating the problem of corrosion of steel in concrete. One of these is the use of high-performance concrete, concrete that on account of its dense and refined pore system has a greater resistance to the ingress of chloride ions and hence a greater ability to protect the reinforcing steel from corrosion. This being said, in the case of high-performance concrete, one is also faced with an increased material brittleness and a lower fracture toughness resulting in a lower resistance to cracking and an easier ingress of chlorides.

With regard to steel, there have been numerous advances as well. Both epoxy-coated steels and micro-alloyed steels have all come into the vanguard from time to time. These have also unfortunately not produced a "cure-all" solution for the problem of corrosion. Fully alloyed steels (e.g. stainless steel) have shown significant promise, but the prohibitive cost of such steels unfortunately fails to produce a "workable" solution.

A very effective solution that has come into the spotlight of late is that of the use of fibre-reinforced polymers (FRPs). Used extensively for over several decades by both the defence and the aerospace industries, FRPs are high-specific-strength and high-specific-stiffness materials that are also non-corrosive, lightweight and magnetically neutral. As in the case of aerospace applications, the high specific strengths and stiffness of FRPs make them very attractive for civil applications where large structural sizes, need for large volumes of materials and growing labour costs make their use logical and more efficient. Not surprisingly, FRPs are fast replacing steel as a material of choice in both new construction and rehabilitation projects.

Of the two failure modes—flexural and shear—the shear mode of failure tends to be highly brittle and catastrophic. This was evident in the Concorde overpass failure of 2006 in Montreal. It is now well accepted that FRPs are ideal materials for shear strengthening.

This book covers *Basic Introduction on Shear Strengthening* in Chap. 1. An extensive review of the literature is presented in Chap. 2. *Experimental Programmes on Shear Strengthening of RC T-beams Using GFRP Sheets* are described in Chap. 3. *Analysis of Results* from such experimental programmes is presented in Chap. 4. *Model on Shear Strengthening of RC T-beams with GFRP Sheets* is highlighted in Chap. 5. *Numerical Approaches Applied to Shear Strengthening Predictions* are presented in Chap. 6. All these chapters are well written and provide a coherent and clear view of the current state of the art.

I would like to compliment the authors of the book: Dr. Kishor Chandra Panda, Prof. Sudhirkumar V. Barai and Prof. Sriman Kumar Bhattacharyya, for this significant undertaking and for producing a volume that is useful not only for the

scholars in the field but also for the practising engineers. My gratitude is also to the publisher of the book, Springer Publication, for recognizing the importance of the topic. I wish them all the success.

Vancouver, BC, Canada

Nemkumar (Nemy) Banthia
Ph.D., PEng, FACI, FCAE, FICI, FCSCE, FRSC
Professor, Distinguished University Scholar &
Canada Research Chair in Infrastructure
Rehabilitation, CEO and Scientific Director: Canada
India Research Center of Excellence
(IC-IMPACTS.com), Editor-in-Chief: J of Cement
and Concrete Composites (Elsevier)

Department of Civil Engineering
The University of British Columbia

Preface

The fibre-based reinforcement in reinforced concrete structure has been started since 1930. However, actual development and research into the use of these materials for strengthening and retrofitting concrete structures started in the 1980s by the initiatives of the National Science Foundation (NSF) and the Federal Highway Administration (FHWA). First retrofitting of concrete structures using fibre-reinforced polymer (FRP) materials was reported in Germany in 1978. Same kinds of investigations to retrofit concrete structures were reported in Europe and Japan in the 1980s. The Japanese civil engineers realized that this was the answer to their severe earthquake threat, and they were the first to fully commercialize composites for repair and retrofit. To date, many thousands of structures have been strengthened in Japan, and it is now the material of choice for seismic strengthening of concrete structures. Externally bonded FRP systems have been applied to strengthen concrete, masonry, timber, steel and cast iron. These have been used in structural elements such as beams, slabs, columns, walls, joints/connections, chimneys, domes, tunnels, silos, pipes and trusses.

The development of the design guidelines for the field application of externally bonded FRP systems is ongoing in Europe, Japan, Canada and the USA. In the last 20 years, Japan Society of Civil Engineers (JSCE, 2001) and the Japan Concrete Institute (JCI, 1997 and 1998) made several publications related to FRP systems in concrete structures. Past research and field applications of FRP for rehabilitation and strengthening of concrete structural elements are described in ACI Committee 440 (2002). In Europe, Task Group 9.3 of the International Federation for Structural Concrete (FIB) published a bulletin on design guidelines for FRP reinforcement for concrete structures (FIB Bulletin 14, 2001). Canadian Standards Association (CSA) approved the code "Design and Construction of Building Components with Fibre-Reinforced Polymer" (CSA 2002).

Most of the research studies and field applications, however, were undertaken for flexural strengthening and for retrofitting of columns. Research studies on *shear strengthening of beams with fibre-reinforced polymer* are sparse and are mostly limited to relatively small beams. The research in this area exists since 1992 (Berset 1992). Shear failure of reinforced concrete (RC) beam is a type of failure mode that

has a catastrophic effect. If an RC beam, deficient in shear strength, is overloaded, shear failure may occur suddenly without advance warning of distress. Shear deficiency of the beam may occur due to many reasons such as insufficient shear reinforcement or reduction in steel area due to corrosion, increased service load and construction errors. In addition, there is an urgent need to upgrade the shear resistance of older RC structures to meet the current seismic design standards in high seismic regions. In this situation, externally bonded FRP reinforcement may be used effectively in strengthening the concrete beams weak in shear.

The present book is divided into six chapters. The general introduction to strengthening of structures with FRP, motivation for shear strengthening and shear strengthening configuration using FRP is outlined in Chap. 1. The existing literature relevant to the shear study and critical observation on it are presented in Chap. 2. The details of a novel technique for shear strengthening—an experimental approach—are described in Chap. 3. Major experimental findings of RC T-beams strengthened in shear with GFRP sheets for all phases of experimental works are presented in Chap. 4. A theoretical approach on the evaluation of shear strengthening of beams with GFRP sheets is presented in Chap. 5. Comparison of the effectiveness of GFRP using ACI guidelines with the present experimental results is also demonstrated. Numerical approach on the evaluation of shear strengthening of beams using commercial finite element software (ANSYS) is presented in Chap. 6.

In the present book, the authors have documented the procedure and results of experimental investigation of forty-five simply supported RC T-beams, out of which nine beams are used as control beams with and without transverse steel reinforcements and rest thirty-six beams were strengthened in shear with GFRP sheets and strips in different configurations, orientations and variation of layers for each type of stirrup spacing. All the beams were tested at the structural engineering laboratory of IIT Kharagpur using 300T UTM. The test results demonstrate the advantage of using an externally applied, epoxy-bonded GFRP sheet and strips of specified layers to increase the shear capacity of the beams. The shear resistance due to GFRP obtained from the experimental investigation was compared with the shear resistance predicted by the ACI 440.2R-02 guidelines. Numerical studies were also carried out using commercial finite element software (ANSYS). The analysis results agree reasonably well with the experimental results.

Finally, the authors would like to thank the readers for their keen interest on the subject area.

Bhawanipatna, India — Kishor Chandra Panda
Kharagpur, India — Sudhirkumar V. Barai
Kharagpur, India — Sriman Kumar Bhattacharyya
August 2017

Acknowledgement

A fascinating journey began with the objective in mind to contribute to the field of retrofitting, kept on moving with wide exposure of information, gathering of knowledge and application and finally giving shape in the form of this book. It has become possible due to the direct and indirect contributions of many well-wishers, who have provided the requisite support to stand determined, motivated to move forward, provided strength to overcome the obstacles in reaching the goal.

The authors have gained immense knowledge through the works of several researchers in the field of rehabilitation, retrofitting and strengthening of structures and are grateful to all of them. Authors also acknowledge the help and support received from IIT Kharagpur during the progress of the research work.

The authors wish to express sincere gratitude to the editorial team of Springer, especially Swati Meherishi and Aparajita Singh. The authors also wish to thank all those who helped directly and indirectly and made this book possible.

The authors express their sincere thanks and regards to Profs. S. Majumdar, N. Dhang, B. Maiti, D. Maiti, L. S. Ramachandra and all other faculty members of IIT Kharagpur for their valuable suggestions at different stages of the investigation for their kind support and cooperation.

This book could not have been completed without the full support and cooperation of the authors' family members. Authors are especially grateful to their family members for their patience and understanding while enduring the completion of the book.

Dr. Panda expresses his sincere regards and gratitude to his co-authors Prof. S. K. Bhattacharyya and Prof. Sudhirkumar Barai for their continuous motivation, guidance and support in the investigation. They have inspired and extended necessary academic help in carrying out the research work during his

Ph.D. Programme. He also thank all co-researchers, namely Sarat, Priya, Pabitra, Debasish, Shailendra, Rajendra, Praduymna, Chakradhar, Rashmi and all others for their friendly co-operation and help, and he also sincerely thank all the staff members of structural laboratory of IIT Kharagpur for their kind support and co-operation.

Kishor Chandra Panda
Sudhirkumar V. Barai
Sriman Kumar Bhattacharyya

Contents

About the Authors

Kishor Chandra Panda is currently working as Professor in the Department of Civil Engineering, Government College of Engineering, Kalahandi, Bhawanipatna (a constituent college of Biju Patnaik University of Technology, Odisha) and is a former Professor of Institute of Technical Education and Research, Siksha 'O' Anusandhan (Deemed to be University), Bhubaneswar, Odisha-751030, India. In 2010, he obtained his Ph.D. (Eng.) from the Indian Institute of Technology Kharagpur, India. He received his B.E. (Civil) from Utkal University, IGIT, Saranga, Talcher, in 1990 and M.Sc. Eng. (civil) with specialization in structural engineering in 1992, from Sambalpur University, REC, Rourkela, India (presently NIT Rourkela). His research interests are FRP-concrete composite systems, strengthening, rehabilitation and retrofitting of structures, durability of concrete structure in marine environment, self-compacting concrete using different types of waste material, sustainable material in construction field and bacterial concrete. He has published more than 100 papers in journals and conference proceedings and chapters. He has guided 16 M.Tech. students and 1 Ph.D. student. He is a member of some professional bodies like ICI, ISTE and IET.

Sudhirkumar V. Barai holds B.E. (civil) and M.E. (civil) with specialization in structural engineering from Maharaja Sayajirao (M.S.) University of Baroda and a Ph.D. (Eng.) from the Indian Institute of Science, Bangalore. He is a Professor of structural engineering at the Department of Civil Engineering, Indian Institute of Technology Kharagpur, Kharagpur, India. His research interests include computational intelligence applications, structural health monitoring and concrete technology. He has published more than 200 papers in leading national/international journals and conferences. He is a fellow of the Association of Consulting Civil Engineers, India, and Institution of Engineers, India. He is also the co-author (with Shailendra Kumar) of the book 'Concrete Fracture Models and Applications', which has recently been published by Springer.

Sriman Kumar Bhattacharyya is the Deputy Director of the Indian Institute of Technology Kharagpur (IIT Kharagpur), Kharagpur, India. Formerly, he was the Director of the Council of Scientific & Industrial Research (CSIR)-Central Building Research Institute at Roorkee. He is a Professor and Ex-head of Civil Engineering at IIT Kharagpur. His research interests include fluid–structure interactions, structural health monitoring, sustainability of materials and fibre-reinforced polymer (FRP)-concrete composite systems. He is a fellow of the Indian National Academy of Engineering, Institution of Engineers, India, and Institution of Structural Engineering. He has travelled to different countries in connection with his research.

Chapter 1
Introduction

1.1 General

Civil engineering structures such as bridges, monumental buildings, tall towers, dams, harbours, offshore structures, etc., deteriorate due to several reasons. The deterioration of the structures is primarily due to ageing, aggressive environment, industrial pollution, faulty design or construction and different natural disasters. Demolition and rebuilding of the deteriorating infrastructure are the major concerns faced by the nation today due to economic crisis and several other issues. Therefore, the development of simple rehabilitation and strengthening techniques which are safe, efficient and cost-effective presents a powerful challenge for the construction industry. The use of externally applied fibre-reinforced polymer (FRP) as a strengthening element for reinforced concrete structures has gained tremendous popularity and interest because of its high strength-to-weight ratio, high stiffness-to-weight ratio, corrosion resistance, durability, non-magnetic, non-conductive and superior resistance to chemical attack as well as the ease in installation.

Composites consist of a mixture or a combination of two or more distinctive different materials which are insoluble in each other and differ in chemical composition. These composites combine the strength of the fibres with the firmness of the polymer resins. This is also known as polymer matrix, which is reinforced with fibres or other reinforcing material to provide desirable reinforcing characteristics in one or more directions. The composite materials are anisotropic nature different than conventional construction materials such as concrete, steel and aluminium. The properties of the composite differ depending on the direction of fibres used. The applications of FRP composite have been widely used in aerospace, marine, automobile, electrical, transportation and civil engineering structures due to the numerous benefits of the material. The strength of the composite materials comes largely from the fibre, which are generally used as glass, carbon or aramid. Fibres are the principal load carrying members. The matrix does not carry any tensile load

K. C. Panda et al., *Shear Strengthening of T-beam with GFRP*, Springer Transactions in Civil and Environmental Engineering, https://doi.org/10.1007/978-981-10-7760-9_1

directly which surrounds the fibre and keeps them in a proper location and correct orientations. It acts as a filler material and holds the fibres together and acts as the medium by which the load is transferred through the fibre. The matrix also protects the fibre from environmental damage caused by elevated temperature and humidity.

Research studies on *shear strengthening with fibre reinforced polymer* are sparse and are mostly limited to relatively small beams. The research in this area exists since 1992. Shear failure of a reinforced concrete (RC) beam is a type of failure mode that has a catastrophic effect. If an RC beam, insufficient in shear strength, is overloaded, shear failure may occur suddenly without prior warning. Shear deficiency of the beam may occur due to several reasons such as deficient transverse steel in beam or decrease in reinforcement area due to corrosion, construction errors and increased service load. The shear resistance of older RC structures is also needed to be upgraded to meet the present seismic design standards in high seismic zones. In this situation, externally bonded FRP reinforcement may be used effectively in strengthening the concrete beams weak in shear.

1.2 Background

In early days, the traditional method of external reinforcing was provided by steel plate bonding and steel or concrete column jacketing. The flexural capacity of concrete members increases by using steel plates bonding to the tension zones of concrete members. This traditional method of external reinforcing has been used over the world to strengthen civil engineering structures such as bridges and buildings, etc. However, the major drawbacks of this technique were identified by the corrosion of steel plates, deterioration of the bond between concrete and steel interfaces and also the installation difficulties. To overcome the external reinforcing by steel plates, researchers investigated FRP strengthening as an alternative to this method.

1.3 Reasons for Strengthening with FRP

FRP may be used either to rehabilitate and restore the strength of a damaged, weakened structures or partially deteriorated structural member or to strengthen and retrofit a sound structural member to resist higher loads in case of a faulty design or construction error, in case of a change in use of loading, or for a seismic upgrade. FRP may be used to increase the flexural and shear capacity of structural members such as columns, beams, slabs and walls. The strengthening of culvert and bridges can be done using FRP without decrease of vertical clearance. FRP can be applied in a different range of environmental conditions to reduce environmentally induced deterioration. Some reasons for strengthening with FRP are as follows:

In an earthquake vulnerable zone, a structure needs to be light and flexible to absorb the movement and have lesser effect of earthquake, but adding weight to the structure can increase the mass and therefore the chances of failure, in this condition FRP is an ideal choice. Sometimes a structure needs to perform in a manner that it was not designed for and needs to be strengthening the structures with FRP to take the additional and changed loads. Some structures degrade due to aging and environmental factors, however with careful preparation may be restored to their original capacity. FRP can be used to repair and protect structural members from aggressive chemical or environmental attack because it is highly resistant to chemical degradation.

1.4 Motivation for Shear Strengthening

A clear understanding of the mechanism involved in the role of shear in RC T-beams externally strengthened with FRP sheet requires large test data to identify the effect of different parameters. Shear failure takes place in brittle manner without any warning of distress. Therefore, it is very important to understand the effect of shear loading on the strength, stiffness and ductility of RC T-beams strengthened in shear with glass fibre reinforced polymer (GFRP) sheet and strips in different configuration, distribution, orientation and various layers. The tests were carefully conducted to identify the modes of failure of T-beams with and without GFRP sheet and strips. The behaviour of RC T-beams strengthened in shear with GFRP sheets and the influence of transverse steel reinforcement (stirrups) on the shear resistance was throughly studied.

1.5 Shear Strengthening Configurations Using FRP

The shear capacity of concrete beams may be increased using FRP as external reinforcement, FRP sheets are typically bonded to the beam surface. The configuration of FRP includes the application of these on the available beam surfaces to the beam, and the fibre orientations.

Generally four varieties of FRP configurations such as full wrapping, U-jacket, side-bonding and U-jacket with anchorage are observed in the literature for rectangular beams as shown in Fig. 1.1.

Whereas for T-beams, three types of FRP configurations such as full wrapping, U-jacket and side-bonding are observed as shown in Fig. 1.2.

Mechanical anchorage could be added at the free ends of the FRP for U-jacket only (as shown in Fig. 1.3), but usually this is not practicable.

For the application of FRP, generally continuous FRP sheets or a series of FRP strips may be used as shown in Fig. 1.4.

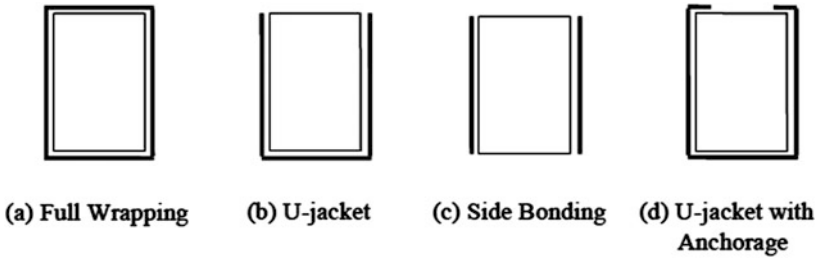

Fig. 1.1 FRP configurations of rectangular beams

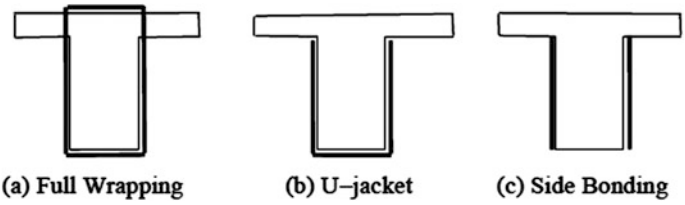

Fig. 1.2 FRP configurations of T-beams

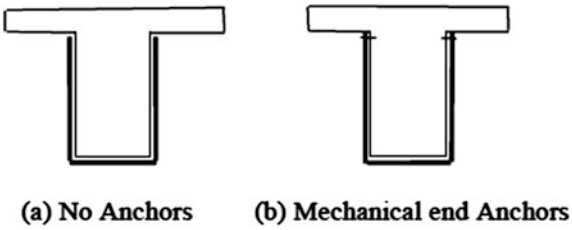

Fig. 1.3 Mechanical anchorage

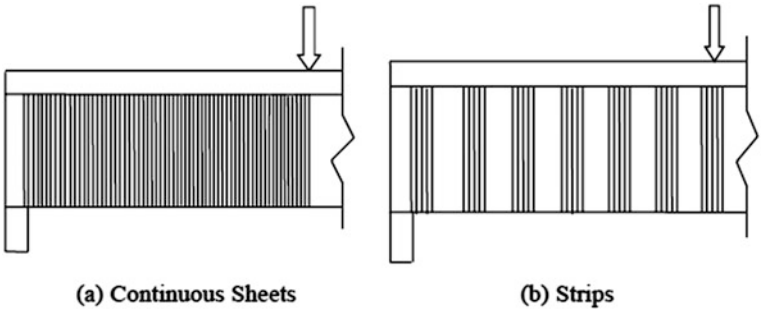

Fig. 1.4 FRP patterns

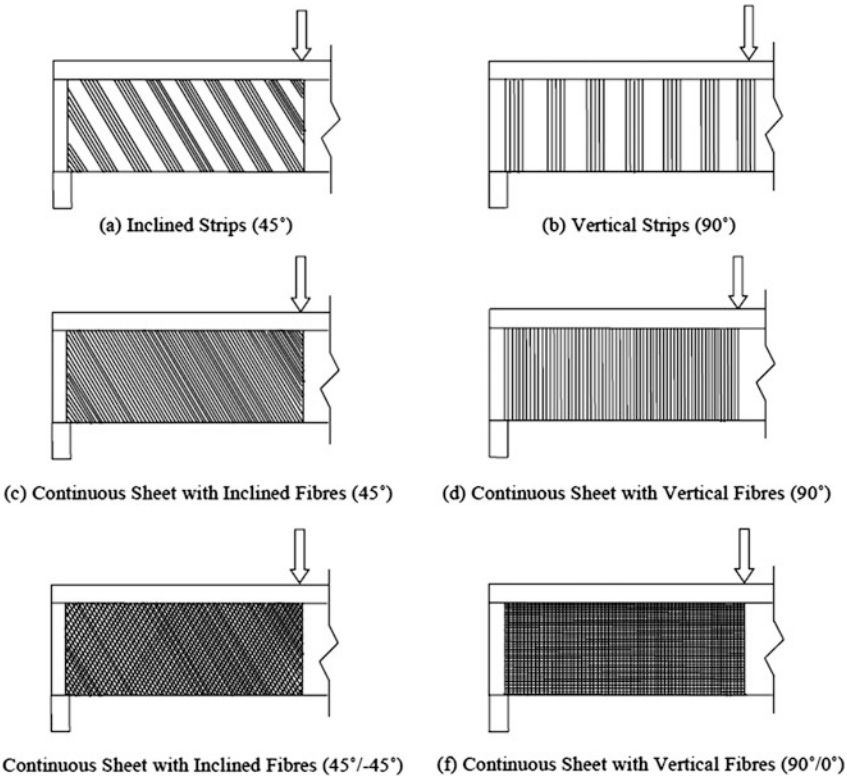

Fig. 1.5 FRP orientations

The fibres in the FRP sheet may be unidirectional; the FRP orientation may be vertical (90° to the longitudinal axis of the beam) or normal to the expected shear crack (45° to the longitudinal axis of the beam). The fibres may also be oriented in the multiple directions in (45°/−45°) and (90°/0°) as shown in Fig. 1.5. In Fig. 1.5a, b, the orientations of FRP strips are 45° and 90° to the longitudinal axis of the beam, respectively. In Fig. 1.5c, d, the orientations of the FRP sheet are 45° and 90° to the longitudinal axis of the beam, respectively. In Fig. 1.5e, f, the orientations of FRP sheet are (45°/−45°) and (90°/0°) to the longitudinal axis of the beam, respectively.

1.6 Summary

This chapter presents the general introduction to strengthening of structural elements, background information, the motivation for shear strengthening and shear strengthening configurations generally adopted using FRP.

Chapter 2
Shear Strengthening—A State-of-the-Art Review

2.1 Application of FRP—Present Status

Concrete structures, exposed to aggressive environment, are susceptible to chemical attacks such as carbonation and chloride contamination and destroy the alkaline barrier of cement matrix. This gives rise to spalling of concrete, degradation of steel and several other phenomena. Distressed concrete structures cannot be abandoned to develop a new construction. Instead, recourse is taken to rehabilitate or strengthen such deteriorated structures using different structural materials. Use of FRP composite in rehabilitating concrete and other structural elements has started way back in 1978 as reported in literature. However, fibre as reinforcement to concrete structures has started since around 1930. Extensive use of FRP in strengthening concrete structures in Europe and Japan has been reported in 1980 (Fardis and Khalili 1981).

First application of external bonded FRP system to reinforced concrete bridges was reported by Meier (1987) in Switzerland for flexural strengthening. In Japan, in 1980s, FRP system was first applied to increase the confinement of the column (Fardis and Khalili 1981). FRP systems have been increasing globally from a few projects 10 years ago to several thousand today (Bakis et al. 2002). After the 1995, Hyogoken Nanbu Earthquake, the application of FRP has been increased in Japan (Nanni 1995). Nowadays, FRP systems are widely used to strengthen masonry works, timber and steel structures, apart from concrete structures. FRP system is also used in various structural elements such as columns, beams, slabs, walls, beam–column joints, chimneys, domes, silos, tunnels, pipes and trusses, etc.

The development of the design guidelines of externally bonded FRP systems is still in progress in United States, Japan, Europe and Canada. In the last 20 years, several papers published by Japan Concrete Institute (JCI 1997, 1998) and Japan Society of Civil Engineers (JSCE 2001) related to FRP systems applied in concrete structures (Neale 2000; Dolan et al. 1999; Sheheta et al. 1999; Saadatmanesh and Ehsani 1998). The use of FRP composites as reinforcing material for concrete has

K. C. Panda et al., *Shear Strengthening of T-beam with GFRP*, Springer Transactions in Civil and Environmental Engineering, https://doi.org/10.1007/978-981-10-7760-9_2

been demonstrated by Uomoto et al. (2002). ACI committee 440 (2002) reported the field application for FRP strengthening and rehabilitation in ACI guidelines. International Federation for Structural Concrete (FIB) published a bulletin on design guidelines for FRP strengthening for concrete structures (FIB Bulletin 14 2001). Canadian Standards Association (CSA) developed the code 'Design and Construction of Building Components with Fibre Reinforced Polymer' (CSA 2002).

The state-of-the-art review in the area of shear strengthening of RC beams with externally bonded fibre-reinforced polymer is presented in this chapter.

The literature review is presented in the following five classified groups.

- Experimental studies on RC rectangular beams, strengthened in shear with FRP
- Experimental studies on RC T-beams, strengthened in shear with FRP
- Experimental studies of shear effect on RC beam–column joints, strengthened with FRP
- Theoretical studies on RC beams, strengthened in shear with FRP
- Numerical studies on RC beams, strengthened in shear with FRP.

2.2 Experimental Studies on RC Rectangular Beams, Strengthened in Shear with FRP

A brief review of the experimental studies carried out by researchers on shear strengthening is presented in Table 2.1.

Berset (1992) had performed the first research study on shear strengthening of RC beams using FRP materials at the Massachusetts Institute of Technology. The author had tested RC rectangular beams with and without shear strengthening reinforcement in the form of GFRP laminates bonded to the vertical sides in the shear-critical zones, and developed a simple analytical model for the contribution of the external reinforcement to shear capacity.

Uji (1992) had conducted experimental investigation on eight rectangular beams, externally bonded with continuous FRP sheets fully wrapped around (Fig. 1.1a) the beam (Fig. 1.1c) and concluded that FRP had substantially increased the shear capacity of the strengthened beams without stirrups. Also, it was shown that the strain of stirrups of two beams with both stirrups and wrapped FRP was smaller than that in beams without FRP and stirrups did not yield throughout the tests.

Al-Sulaimani et al. (1994) had conducted experimental studies on 16 small-scale rectangular beams using GFRP strips and sheets bonded on U-jacketing (Fig. 1.1b) and the side of the beam (Fig. 1.1c). From these tests, the author concluded that the strengthening effect of 80% reached for U-jacketing.

Sato et al. (1996) had conducted experimental studies on six rectangular beams using CFRP sheets bonded on the side of the beam (Fig. 1.1c) and U-jacketing (Fig. 1.1b). The authors had concluded from the results that the use of CFRP

Table 2.1 Brief review of RC rectangular beams, strengthened in shear with FRP

Author/year	Geometry	Type of beam	Type of FRP	FRP configurations	FRP distributions	FRP orientations
Uji (1992)	Beam span (L) < 2 m	$a/d > 2.5$, Regular beams	CFRP	Side shape, wrapped around	One, two layers continuous sheet	90°, 45°
Al-Sulaimani et al. (1994)	L = 1.25 m	$a/d > 2.5$	GFRP	Side shapes, U-shape	One layer continuous sheet, strips (GFRP)	90°
Sato et al. (1996)	L = 2–4 m	$a/d > 2.5$	CFRP	Side shape, U-shape	One, two layers continuous sheet, strips	90°
Taerwe et al. (1997)	L > 4 m	$a/d > 2.5$	CFRP	U-shape, wrapped around	Strips	90°
Umezu et al. (1997)	L = 2–4 m	$a/d > 2.5$	CFRP, AFRP	Wrapped around	One, two layers continuous sheet, strips	90°
Funakawa et al. (1997)	L > 4 m	$a/d > 2.5$	CFRP	Wrapped around	One, two layers continuous sheet	90°
Araki et al. (1997)	L < 2 m	$a/d < 2.5$ (Deep beams)	CFRP, AFRP	Wrapped around	One, two layers continuous sheet, strips	90°
Norries et al. (1997)	L = 2.44 m and L = 1.22 m	$a/d > 2.5$	CFRP	Tension face and side faces	One layer continuous sheet	90°, 45°
Triantafillou (1998)	L = 1.0 m	$a/d > 2.5$	CFRP	Side shape	Strips	90°, 45°
Chaallal et al. (1998)	L = 1.3 m	$a/d > 2.5$	CFRP	Side shape	One layer, two layer strips	90°, 45°
Khalifa et al. (1999)	Two span continuous L = 2.29 m	$a/d > 2.5$	CFRP	U-shape, wrapped around	One, two layers continuous sheet, strips	90°, 0°
Taljsten and Elfgren (2000)	L = 4.5 m	$a/d > 2.5$	CFRP	Side shape	One, two layers continuous sheet, strips	+45°, −45°
Li et al. (2001)	L = 1.35 m	$a/d < 2.5$	CFRP	Side shape	One layer continuous sheet, strips	90°

(continued)

Table 2.1 (continued)

Author/year	Geometry	Type of beam	Type of FRP	FRP configurations	FRP distributions	FRP orientations
Khalifa and Nanni (2002)	L = 3.05 m	$a/d > 2.5$	CFRP	U-shape	One layer continuous sheet	90°
LI et al. (2002)	L = 2.7 m	$a/d > 2.5$	CFRP	Side shape	Continuous fabrics	45°/135°
Pellegrinoand Modena (2002)	L = 2.7 m	$a/d > 2.5$	CFRP	Side shape	One, two, three layers continuous sheet	90°
Adhikary et al. (2004)	L = 3.5 m	$a/d > 2.5$	CFRP and AFRP	U-shape, wrapped around, U-shape with anchorage	One layer continuous sheet	90°
Zhang et al. (2004)	L = 36 in.	$a/d < 2.5$	CFRP	U-shape	One, two layers continuous sheet, and strips	90°, 45°
Zhang and Hsu (2005)	L = 1.22 m	$a/d > 2.5$	CFRP	Side shape	One layer continuous sheet, strips	90°, 45°, 0°
Cao et al. (2005)	L = 2 m	$a/d > 2.5$, $a/d < 2.5$	CFRP and GFRP	Wrapped around	Strips	90°
Islam et al. (2005)	L = 2.0 m	$a/d < 2.5$	CFRP	Side shape	Strips, grids and wraps	90° wrap, 45° strips, 45° grids
Carolin and Taljsten (2005)	L = 3.5–4.5 m	$a/d > 2.5$	CFRP	Side shape and wrapped around	Sheets with different fibre thickness	90°, 45°, 0°
Guadagnini et al. (2006)	L = 2.3–1.0 m	$a/d > 2.5$, $a/d < 2.5$	GFRP, CFRP	Wrapped around	Glass fibre bars	90°
Mosallam and Banerjee (2007)	L = 3.62 m	$a/d < 2.5$	GFRP, CFRP	U-shape	One, two layers continuous sheet, and strips	90°
Leung et al. (2007)	L = 3.8–0.95 m	$a/d > 2.5$	CFRP	Side shape, U-shape, wrapped around	Strips	90°

increases the shear strength significantly. They also deduced that the beam strengthened with U-jacket CFRP is more effective than those attached to the side faces.

Taerwe et al. (1997) had conducted experimental studies on five rectangular beams strengthened with U-jacket FRP sheets (Fig. 1.1b) with different FRP distributions such as continuous sheets or strips and finally observed the shear failure in four beams and bending failure in one beam. The authors had concluded that FRP increases the shear capacity in a way similar to that of internal stirrups.

Umezu et al. (1997) had conducted experimental studies on 26 rectangular beams with carbon fibre sheets and aramid fibre sheets wrapped around the beams (Fig. 1.1a). The authors observed the peak loading at the moment when diagonal cracking penetrated into the upper edge of beam, usually it did not occur at the moment when the FRP ruptured.

Funakawa et al. (1997) carried out experimental investigation on four rectangular beams, externally bonded with continuous FRP sheets fully wrapped around (Fig. 1.1a), and observed that the beams failed by FRP rupture. FRP sheets of various thicknesses are used in the test and it was concluded that the increase of shear capacity is due to the increase of FRP thickness and also FRP fibres did not reach their ultimate tensile strength at the time of beam failure.

Araki et al. (1997) had conducted experimental studies on 13 rectangular beams with different types of fibres, different amount of FRP and steel stirrups. FRP was wrapped around the beams (Fig. 1.1a). The authors had concluded that the failure mode was the diagonal tension failure. Rupture of FRP sheets was not observed when the maximum load was achieved in strengthened beam but the FRP sheets ruptured in most of the beams after the maximum load was attained.

Norries et al. (1997) had studied both experimentally and analytically the behaviour of damaged or understrength concrete having small-scale rectangular beams retrofitted with thin CFRP sheets, bonded to tension face and side faces (Fig. 1.1c). The authors had concluded from the test results that when the CFRP fibres were placed perpendicular to cracks in the beam, a large increase in strength and stiffness was observed and the modes of failure were brittle whereas when the fibre was placed obliquely to the cracks in the beam, a smaller increase in strength and stiffness was observed, however, the failure mode was ductile.

Chaallal et al. (1998) had studied both experimentally and analytically on small-scale rectangular RC beams strengthened in shear using externally bonded unidirectional CFRP strips, bonded to side faces (Fig. 1.1c). The authors had concluded from the results that the strengthening method increases the effectiveness while substantially reducing shear cracking. Also, observed RC beams strengthened by diagonal side strips out-performed those strengthened with vertical side strips in terms of strength, stiffness and crack propagation. Also, the author had proposed the following equation to calculate the shear contribution of bonded FRPs in the ACI format (ACI 318-95 1999):

$$V_f = \phi_f A_f f_f \frac{(\sin\beta + \cos\beta)d}{s_f}$$

where f_f is the tensile strength of FRP, $\phi_f = 0.8$ is the material reduction factor for the FRP, A_f is the cross-sectional area of a pair of FRP strips, β is the angle of the fibre orientation measured clockwise from the horizontal direction for the left side of the beam, d is the effective depth of the beam and s_f is the spacing of FRP strips measured along the longitudinal axis.

Triantafillou (1998) had undertaken the study with an aim to increase the test database on shear strengthening of concrete using FRP and developed an analytical model for the design of such members based on ultimate limit states. The experimental studies had conducted on rectangular beams of smaller size, strengthened in shear with CFRP with different configurations and at various area fractions. The analytical study resulted in a model for the contribution of FRP to shear capacity in analogy with steel stirrups, with an effective FRP strain that decreases with the increasing FRP axial rigidity.

$$V_f = \frac{0.9}{\gamma_f}\rho_f E_f \varepsilon_{fe} b_w d(1 + \cot\beta)\sin\beta$$

where E_f is the modulus of elasticity of FRP, $\rho_f = \frac{2t_f}{b_w}$ is the FRP area fraction, t_f is the thickness of the FRP, b_w is the width of the RC beam, γ_f is the partial safety factor for the tensile strength of FRP which was proposed to be about 1.15, 1.20 and 1.25 for CFRP, AFRP and GFRP, respectively (Triantafillou and Fardis 1997), and ε_{fe} is an effective FRP strain at failure which was obtained from the regression of experimental data of beam tests.

The relation between ε_{fe} and $\rho_f E_f$ is obtained here from the best-fit second-order equation up to $\rho_f E_f = 1$ GPa and by the equation of a straight line for $\rho_f E_f > 1$ GPa, given as follows:

$$0 \le \rho_f E_f \le 1:$$

$$\varepsilon_{fe} = 0.0119 - 0.0205(\rho_f E_f) + 0.0104(\rho_f E_f)^2$$

$$\rho_f E_f > 1:$$

$$\varepsilon_{fe} = -0.00065(\rho_f E_f) + 0.00245$$

It was shown from the model that for the values of $\rho_f E_f$ up to about 0.4 GPa the FRP contribution to shear strength increases almost linearly with $\rho_f E_f$ reaching a maximum, beyond which it drops slightly and then increases again slightly.

The disadvantage of this model was that no discrimination was made between the various strengthening schemes or failure modes. As a result, the predicted FRP

contribution was the same, for example, for wrapping and side-bonding, which was clearly incorrect.

Khalifa et al. (1999) had studied the response of two span continuous RC rectangular beams with shear deficiencies, strengthened with externally bonded CFRP sheets. The studied parameters include the amount of transverse steel shear reinforcement, amount of CFRP, strengthening schemes, and 90% ply combination. The authors had concluded that the externally bonded CFRP may be used to enhance the shear capacity of the beams in positive and negative moment regions and increase in shear strength varying from 22 to 135%.

Taljsten and Elfgren (2000) had conducted experimental studies on full-scale rectangular RC beams by providing the CFRP fabrics by different methods and tests. The purpose of the tests was twofold: First, the shear capacity of the beams was studied both before and after strengthening and second, three different methods of applying the fabrics (Hand lay-up systems, vacuum injection system and prepreg system) were studied. The authors had concluded that a very good strengthening effect almost 300% in shear with CFRP composite beams. It was even possible to reach a 100% with completely fractured beams.

Li et al. (2001) had studied the effect of shear strengthening of five RC rectangular beams of small sizes with different CFRP sheets on stress distribution, initial cracks, crack propagation and ultimate strength. The authors had concluded from the results that the stiffness increased while increasing the CFRP sheet area at the flank and showed that strengthening the entire lateral faces of the beam was not necessary. The strengthened beam with CFRP on the lateral faces delayed the appearance of the first cracks in concrete and significantly increased the ultimate strength in comparison with normal beams.

Khalifa and Nanni (2002) had studied the shear behaviour and modes of failure of simply supported RC rectangular beams designed with shear deficiencies and externally strengthened with CFRP sheets. The parameters investigated in this study included transverse steel, shear span-to-effective depth ratio (a/d), as well as amount and distribution of CFRP. The authors had concluded from the experimental result that the contribution of externally bonded CFRP significantly increases the shear strength from 40 to 138%.

Li et al. (2002) had conducted experimental investigation on 16 full-scale rectangular RC beams with or without the CFRP fabrics with point load at one-third of the length and studied the shear strengthening effect. The authors had concluded from the experimental results that the contribution of CFRP fabrics on ultimate force decreases as the longitudinal steel bar sections and stirrup spacing was reduced.

Pellegrino and Modena (2002) had presented the modelling of the shear behaviour of RC beams strengthened with CFRP sheets and also experimentally investigated 11 beams with and without the transverse steel reinforcement, and with different amount of CFRP shear strengthening bonded to both the sides of the beams (Fig. 1.1c). The authors had pointed out a general improvement of shear capacity for the strengthened beams.

Taljsten (2003) had presented the strengthening effect of RC beams with CFRP for shear. The author had concluded from the test results that concrete beams can be strengthened for shear and that fabric or laminates should be placed perpendicular to the shear crack and also from strain measurements, it was shown that the thinner the fibre used the better the utilization of the fabric.

Adhikary et al. (2004) had conducted experimental investigation on nine RC beams without the provision of shear reinforcement but wrapping with fibre material and studied the effect of extending the length of sheet on the top surface of the beam to delay or prevent sheet debonding and the test parameters considered were the types of fibres, the wrapping schemes, and the length of bonded anchorage (Fig. 1.1a, b, d). The authors had concluded from the experimental results that FRP with bonded anchorage is much more effective than U-wrap scheme. Also a new design methodology based on the effective strain in the FRP sheet at failure was proposed. This new methodology uses two separate equations: when FRP sheet debonding is dominant and when bonded anchorage is provided to the top surface of the beams.

Zhang et al. (2004) had carried out experimental investigation on 16 deep beams, externally bonded with CFRP laminate; the parameter studied the effect of shear span-to-effective depth ratio, various CFRP types and configurations on the shear behaviour, and modes of failure of deep beams with shear deficiencies after strengthening with CFRP laminates. The authors had concluded from the test results that the shear strength of the deep beam increased with CFRP laminates, when the (a/d) ratio decreased, but it depends on the CFRP configuration.

Zhang and Hsu (2005) had conducted experimental studies on 11 RC beams without the steel shear reinforcement and strengthened with carbon fibre strips and fabrics applied on both sides of the beams (Fig. 1.1c) at various orientations with respect to the axis of the beam. The authors had concluded from the results that the externally applied epoxy bonded CFRP system increases the shear capacity of RC beams also the performance of diagonal side strips is better than vertical side strips in arresting the shear crack propagation and ultimate shear strength.

Islam et al. (2005) had presented an experimental investigation on six identical structurally deficient deep beams, strengthened in shear using carbon fibre strips, grids and wraps, and tested to failure. The authors had observed from the test results that the enhancement of shear strength was about 40% as compared with control specimen.

Cao et al. (2005) had presented an experimental investigation on the debonding failure state in which totally 18 RC beams were tested in three series with or without the use of transverse reinforcement and externally shear strengthened with complete wraps (Fig. 1.1a). The variables considered are shear span (a) to effective depth (d) ratio (range 1.4–3.0) and amount of external FRP reinforcement, but the compressive strength of concrete was the same for all the series, and they had studied the strain distribution in the FRP strips intersected by the critical shear crack and the shear capacity at debonding. The authors had concluded from the results

that the FRP strain distribution was non-uniform. Shear resistance contributed by the FRP was predicted through the use of a strain distribution factor.

Carolin and Taljsten (2005) had conducted experimental investigation on RC rectangular beams of 3.5–4.5 m long and strengthened in shear using CFRP and had studied the parameters such as fatigue, anchorage and others. Different modes of failure have been identified, such as fibre rupture, anchorage and combinations thereof. They also studied the strain field in shear span of beams simultaneously subjected to shear and bending.

Guadagnini et al. (2006) had studied experimentally the shear behaviour of six RC rectangular beams by conducting 12 tests. Half of the beams were reinforced with steel reinforcement in flexure, while other half were reinforced with glass fibre bars. The authors investigated the variation in the shear behaviour of beams characterized by different types of shear failure, different shear span-to-depth ratios (a/d), ranging from 1.1 to 3.3. Shear reinforcement was not provided in the first phase, while glass and carbon shear reinforcement was provided in the second phases to enable shear failure.

Mosallam and Banerjee (2007) had experimentally studied nine RC rectangular beams of three different classes, as-built, repaired and retrofitted and externally reinforced with FRP composites. Three composite systems were used for retrofit and repair evaluation such as carbon/epoxy wet lay-up, carbon/epoxy procured strips and E-glass/epoxy wet lay-up. The authors had concluded from the results that the FRP strengthening provided substantial increase in ultimate strength of strengthened and repaired beams as compared to the pre-cracked and as-built beams.

Leung et al. (2007) had experimentally studied geometrically similar beams with 180, 360 and 720 mm depth and strengthened in shear with CFRP strips in both U-jacket (Fig. 1.1b) and fully wrapped around (Fig. 1.1a). The authors had concluded that the strengthening effectiveness may significantly decrease with the member size for beams strengthened with CFRP strips in the U-jacket. The strengthening effectiveness was independent of member size for beams with fully wrapped strips.

Sundarraja and Rajamohan (2009) had studied the effectiveness of a RC beam in terms of width and spacing of inclined GFRP strips, spacing of internal steel stirrups and the additional shear capacity due to GFRP strips. The studied parameters include shear strengthening effect, failure modes and load–deflection behaviour of RC beams bonded externally with inclined GFRP strips on the shear region of the beam.

Baggio et al. (2014) had studied the effectiveness of nine RC shear deficient slender beams using CFRP, GFRP and fibre-reinforced cementitious matrix (FRCM). The studied parameters include three different FRPs, presence and type of FRP anchors. The results of the study revealed that FRP sheet enhances the shear capacity, and u-wrapped FRP sheets with full depth strengthening perform better as compared to u-wrapped FRP sheets with partial strengthening. The authors further improved the shear capacity and ductility of failure using FRP anchors.

Li and Leung (2017) had studied the effectiveness of a six shear strengthened beams with CFRP strips and six normal beams with varying a/d ratio ranging from 1.0 to 3.5. The results of the study revealed that FRP shear contribution increases initially with increasing *a/d* ratio up to 2, thereafter slightly decreases when the *a/d* is beyond 2.

2.3 Experimental Studies on RC T-beams, Strengthened in Shear with FRP

Several works have been carried out by different researchers on experimental studies of RC T-beams strengthened in shear with FRP. The brief review of the experimental studies on shear strengthening is presented in Table 2.2.

Chajes et al. (1995) had studied the effectiveness of 12 under-reinforced RC T-beams of small sizes using the externally applied composite fabrics made of aramid, E-glass and graphite fibres bonded to the web of the T-beam (Fig. 1.2b). The authors had concluded from the results that the beam tested with external reinforcement showed an increase in ultimate shear capacity of 60–150% of control beam.

Sato et al. (1997) had presented experimental investigation on two RC T-beams, and concluded that FRP strengthened beam with mechanical anchorage was more effective than FRP strengthened beam without mechanical anchorage (Fig. 1.3a, b).

Khalifa and Nanni (2000) had studied experimentally the performance of six simply supported RC T-beams without shear reinforcement, but externally strengthening with CFRP sheets. The parameters had investigated in this study were wrapping schemes, anchorage. The authors had concluded from the experimental results that the CFRP sheet can increase the shear capacity of the externally strengthened beam significantly, i.e. from 35 to 145% and also found that U-wrap with end anchorage was the most effective configuration and the proposed design approach from ACI format as well as Eurocode format was conservative and acceptable.

Deniaud and Cheng (2001) had conducted experimental investigation on the behaviour of full-scale RC T-beams of size (length = 3.7 m, width of web = 140 mm, width of flange = 400 mm, depth of flange = 150 mm, and depth of web = 450 mm) strengthened externally to the web of the T-beams such as uniaxial glass fibre, uniaxial carbon fibre, and triaxial glass fibre and studied the interaction of concrete, steel stirrups and external fibre-reinforced polymer sheets. The authors had concluded that FRP sheet increases the maximum shear strengths from 77.4 to 117.3% over beams without FRP and also observed that the enhancement of shear strength was dependent on both the type of FRP and the amount of internal shear reinforcement.

Chaallal et al. (2002) had conducted experimental investigation on the performance of RC T-girders strengthened in shear using epoxy bonded bidirectional

Table 2.2 Brief review on RC T-beams, strengthened in shear with FRP

Author/year	Geometry	Type of beam	Types of FRP	FRP configurations	FRP distributions	FRP orientations
Chajes et al. (1995)	L < 2.0 m (48 in.)	*a/d* > 2.5	CFRP, AFRP, GFRP	U-shape	One layer continuous sheet	90°, 45°
Sato et al. (1997)	L < 2 m	*a/d* > 2.5	CFRP	U-shape	One layer	90°
Khalifa and Nanni (2000)	L = 3.05 m	*a/d* > 2.5	CFRP	U-shape	One layer, two layers continuous sheet, strips	90°, 0°
Deniaud and Cheng (2001)	L = 3.7 m	*a/d* > 2.5	CFRP, GFRP	U-shape	One layer continuous sheet, strips	90°, 45°
Chaallal et al. (2002)	L = 6.095 m	*a/d* < 2.5	CFRP	U-shape	One, two and three layers continuous sheet	90°
Micelli et al. (2002)	L = 2.743 m	*a/d* < 2.5	CFRP, AFRP	U-shape, U-shape with anchorage	One, two layers continuous sheet	90°
Deniaud and Cheng (2003)	L = 3.0 m	*a/d* > 2.5	CFRP, GFRP	U-shape	One layer continuous sheet	90°, 45°, 0°
Bousselham and Chaallal (2006a, b)	L = 3.0 m	*a/d* < 2.5, *a/d* > 2.5	CFRP	U-shape	One layer, two layers continuous sheet	90°
Bousselham and Chaallal (2008)	L = 3.0–4.52 m	*a/d* > 2.5	CFRP	U-shape	Half, one layer, two layers continuous sheet	90°
Panda et al. (2011a)	L = 2.5 m	*a/d* > 2.5	GFRP	Side shape	One, two and three layers continuous sheet	90°
Panda et al. (2012)	L = 2.5 m	*a/d* > 2.5	GFRP	U-shape	One, two and three layers continuous sheet	90°
Panda et al. (2011b, c, 2013a)	L = 2.5 m	*a/d* > 2.5	GFRP	U-shape and side shape	One layer strips in shear zone	90°, 45°
Panda et al. (2013b)	L = 2.5 m	*a/d* > 2.5	GFRP	U-shape, side shape, U-shape with anchorage	One layer in shear zone	90°

CFRP sheets and had studied the effectiveness using the CFRP with single, double and triple layer with shear span-to-effective depth ratio (a/d = 2) and with different stirrups spacings. The authors had concluded that for unwrapped specimen, the values for shear predicted by ACI model are conservative for beams developing arch action and the ultimate shear capacity was underestimated by 40–80% and for wrapped specimens, the maximum shear force generally increased with the number of CFRP layers, but this increase was not only a function of number of layers but also it depends on the internal shear steel reinforcement.

Micelli et al. (2002) had conducted experimental studies on 12 RC T-Joists without transverse shear reinforcement but externally strengthened with CFRP and AFRP sheets in an epoxy matrix using wet lay-up technique. The authors had concluded that an increase in the amount of FRP did not result in a proportional increase in the shear capacity, as expected by design equations, but all the beams showed a considerable increase in stiffness. The experimental results were compared with the results obtained analytically and it was found that theoretical calculations resulted in non-conservative values.

Deniaud and Cheng (2003) had carried out experimental investigation on four controlled RC T-beams by eight tests of size (length = 3.0 m, width of web = 140 mm, width of flange = 400 mm, depth of flange = 400 mm, depth of web = 250 mm) and strengthened externally with three types of FRP, uniaxial glass fibre, uniaxial carbon fibre and triaxial glass fibre to the web of the T-beams, and had studied the parameters, i.e. interaction of concrete, steel stirrups and external fibre-reinforced polymer sheets. The authors had concluded from the experimental results that FRP reinforcement was increased the maximum shear strength between 15.4 and 42.2% over the beams with no FRP and the magnitude of the shear capacity dependant not only on the types of FRP but also on the amount of internal shear reinforcement.

Bousselham and Chaallal (2006a) had conducted experimental investigation on six RC T-beams strengthened externally with CFRP composites and studied the parameters such as CFRP ratio, the transverse steel reinforcement ratio and the type of beams. The authors had concluded from the test results that the enhancement of shear capacity was significant in slender beams whereas it was very modest in deep beams. They also observed that the addition of internal transverse steel in slender beams resulted in significant decrease of the gain in shear capacity, whereas in deep beams, the addition of transverse steel had no effect on the shear capacity.

Bousselham and Chaallal (2006b) had conducted 22 tests on 4520 mm long T-beams retrofitted in shear with CFRP. The parameters investigated were the internal shear steel reinforcement ratio, CFRP ratio and the shear span-to-depth ratio (a/d). The authors had concluded that the contribution of CFRP to the shear resistance is not in proportion to the CFRP thickness provided.

Bousselham and Chaallal (2008) had conducted 22 tests on 4520 mm long T-beams retrofitted in shear with CFRP. The parameters investigated were the internal shear steel reinforcement ratio, CFRP ratio and the shear span-to-depth ratio (a/d). The authors had concluded that the contribution of CFRP to the shear resistance is not in proportion to the CFRP thickness provided.

Panda et al. (2010) had studied experimentally the performance of nine simply supported RC T-beams strengthened in shear using epoxy bonded glass fibre fabric. Six beams were used as control beams with and without shear reinforcements and rest three beams were strengthened in shear with one, two and three layers of GFRP in U-shape around the web of the T-beams. The experimental results had demonstrated that the contribution of externally bonded GFRP to the shear capacity was significant and was dependent on the internal transverse steel reinforcement.

Belarbi et al. (2011) had experimentally investigated the behaviour of full-scale bridge beams strengthened in shear with FRP using full-scale RC T-beams. The parameters had investigated in this study were the transverse steel reinforcement ratio and the effect of mechanical anchorage systems.

Panda et al. (2011a) had investigated experimentally the shear behaviour of nine control RC T-beams with three different stirrups spacing without GFRP wrap and another nine beams strengthened in shear with one, two and three layers of GFRP sheet on side of the web of the T-beams for each type of stirrup spacing. The authors had concluded from the experiment results that increasing the effectiveness of side-bonded GFRP sheet by 12.5–50%.

Panda et al. (2012) had experimentally investigated the effectiveness and behaviour of nine control RC T-beams with three different stirrups spacing without GFRP wrap and another nine beams strengthened in shear with one, two and three layers of GFRP sheet in the form of U-jacket around the web of T-beams for each variety of stirrup spacing. The authors had concluded from the test results that for RC T-beams strengthened in shear with U-jacketed GFRP sheets, increasing the effectiveness by 10–46%.

Panda et al. (2013a) had experimentally studied the shear strengthening performance of nine control RC T-beams and nine strengthened RC T-beams bonded by GFRP strips in U-shape and side shape with two types of orientation, i.e. at 45° and 90° to the longitudinal axis of the beam for each type of stirrup spacing. The authors had concluded from the experiment that the effectiveness was more for strengthened beam with GFRP strips at 45° orientation than 90° orientation and also observed that the effectiveness of the GFRP strips decreased as transverse steel increased.

Panda et al. (2013b) had investigated shear strengthening performance of nine control RC T-beams and nine strengthened RC T-beams bonded in shear zone with GFRP sheet in U-jacket, side-bonded and U-jacket with anchorage in each type of stirrups spacing. The test result had demonstrated that the effectiveness of GFRP sheet in U-jacket with anchorage was much better than U-jacket.

Panda et al. (2015) had investigated the strain analysis of U-wrapped GFRP sheet, transverse steel reinforcement and longitudinal steel reinforcement and observed that the strain in the U-wrapped GFRP sheet was higher in the specimens strengthened with one layer of GFRP, as compared to two and three layers in all the series. The stiffness of GFRP sheet was indirectly proportional to the strain.

2.4 Experimental Studies of Shear Effect on RC Beam–Column Joints, Strengthened with FRP

Gergely et al. (2000) had presented the experimental results of fourteen (14) 1/3-scale tests of RC beam–column joints. The variables used in the test were the composite system, the fibre orientation and the surface preparation. The tests had demonstrated the viability of CFRP composites for their use in improving the shear capacity of the beam–column joints. Based on these test results, a design aid was developed for beam–column joints with inadequate confinement and shear reinforcement.

El-Amoury and Ghobarah (2002) had studied experimentally the techniques for upgrading reinforced beam–column joints. The test specimens represented a typical joint that was built in accordance with pre-1970s codes and upgraded the shear strength of the joints and reduced the potential for bond-slip of the bottom bars of the beam. GFRP sheets were wrapped around the joint to prevent the joint shear failure. GFRP sheets were attached to bottom face of the beam to replace the inadequately anchored steel bars. Three column–beam joints were tested under quasi-static load to failure. The control specimens had showed combined brittle joint shear and bond failure modes while the rehabilitated specimens had showed a more ductile failure mode. A simple design methodology for the rehabilitation scheme was proposed.

Antonopoulos and Triantafillou (2002) had presented analytical models for the analysis of RC beam–column joints strengthened with composite materials in the form of externally bonded reinforcement comprising unidirectional strips. The tests had demonstrated that even strengthening with low quantities of FRP materials may provide significant enhancement of the shear capacity.

Antonopoulos and Triantafillou (2003) had presented the results of a comprehensive experimental program of the behaviour of shear-critical 18 exterior RC beam–column joints strengthened with FRP under simulated seismic load. The authors had concluded the load versus imposed displacement response characteristics, comprising the strength, the stiffness and the cumulative energy dissipation capacity.

2.5 Theoretical Studies on RC Beams, Strengthened in Shear with FRP

The theoretical studies were carried out by some of the researchers such as (Chaallal et al. 1998; Triantafillou 1998; Triantafillou and Antonopoulos 2000; Khalifa et al. 1998; Khalifa and Nanni 2000; Chen and Teng 2003a, b). The findings of the research were also carried out by Bousselham and Chaallal (2004) and examined and analysed the different parameters.

Khalifa et al. (1998) reviewed the research on shear strengthening with bonded FRP and slightly modified the equation proposed by Triantafillou (1998) by calibrating more test results and had presented design algorithms based on two approaches for computing the contribution of FRP to shear strength of RC members.

(a) Design approach based on effective FRP stress:

The equation presented by Triantafillou (1998) in Eurocode design format Comite Euro-International du Beton (CEB) 1992 was slightly modified by Khalifa et al. (1998) in ACI code.

$$V_f = \frac{A_f f_{fe}(\sin\beta + \cos\beta)d_f}{s_f}$$

where f_{fe} is the effective FRP stress, d_f is the effective depth of the CFRP shear reinforcement and s_f is the spacing of FRP strips. For continuous vertical shear reinforcement, the spacing of the strip, s_f and the width of the strip, w_f, are equal.

Khalifa et al. (1998) had modified the effective strain model by including additional experimental data to the model presented by Triantafillou (1998). The modified new model based on the observation that $\rho_f E_f$ does not exceed 1.1 GPa in all cases.

To eliminate the effects of various types of FRP sheet, the ratio of effective strain to ultimate strain, $R = \frac{\varepsilon_{fe}}{\varepsilon_{fu}}$, was plotted versus axial rigidity. Regression of experimental data led to the following expression, i.e. the polynomial was used as a best fit to the data in the case of $\rho_f E_f < 1.1$ GPa. This polynomial is given by

$$R = 0.5622\left(\rho_f E_f\right)^2 - 1.2188\left(\rho_f E_f\right) + 0.778 \leq 0.50$$

The upper limit of R was 0.5; this limit was suggested to maintain the shear integrity of concrete. The ratio of effective strain to ultimate strain, R, may be used as a reduction factor on the ultimate strain. The effective stress (or strain) model may only be applicable when failure is governed by FRP rupture.

(b) Design approach based on bond mechanism:

Khalifa et al. (1998) further proposed a bond mechanism design approach based on the strength model of Maeda et al. (1997). This model gives a stress (or strain) reduction factor of

$$R = \frac{f_{fe}}{f_{fu}} = \frac{\varepsilon_{fe}}{\varepsilon_{fu}} = \frac{0.0042\left(f_c'\right)^{2/3} w_{fe}}{\left(E_f t_f\right)^{0.58} \varepsilon_{fu} d_f} \leq 0.5$$

where f_c' the specified compressive strength of concrete w_{fe} is an effective width of strips. The effective width depends on the shear crack angle (assumed to be 45° and the bonded surface configuration)

$w_{fe} = d_f$ If the sheet is wrapped around the beam entirely (four sides)
$w_{fe} = d_f - L_e$ If the sheet is in the form of a U-jacket (three sides)
$w_{fe} = d_f - 2L_e$ If the sheet is bonded to only the sides of the beam (two sides)

The authors proposed design approach tends to underestimate the actual shear strength determined from experimental results but does give conservative results.

Triantafillou and Antonopoulos (2000) had published an extension work of Triantafillou (1998) and had studied a simple design model by calibrating 75 experimental data for the calculation of the FRP contribution to the shear capacity of strengthened RC beams and were presented in three design formats: Eurocode, ACI and JCI.

The FRP contribution to shear capacity V_{fd} may be written as given below:

$$V_{fd} = 0.9 \frac{\varepsilon_{fk,e}}{\gamma_f} E_f \rho_f b_w d(1 + \cot\beta) \sin\beta$$

where $\varepsilon_{fk,e}$ = characteristic value of the effective FRP strain; γ_f = partial safety factor for FRP. The characteristic value of the effective FRP strain may be calculated by multiplying the mean value of the effective FRP strain ε_{fe} by a reduction factor (α).

Triantafillou (2000) had established the tensile strength of concrete is proportional to $f_c^{'2/3}$, where f_c' is the compressive strength, ε_{fe} depends on the quantity $E_f \rho_f / f_c^{'2/3}$. The model was also separated for debonding failure and for fracture failure by the best-fit power-type expressions for the test data.

Premature shear failure due to debonding (for CFRP only):

$$\varepsilon_{fe} = 0.65 \left(\frac{f_c^{'2/3}}{E_f \rho_f} \right)^{0.56} \times 10^{-3}$$

Shear failure combined with or followed by CFRP fracture:

$$\frac{\varepsilon_{fe}}{\varepsilon_{fu}} = 0.17 \left(\frac{f_c^{'2/3}}{E_f \rho_f} \right)^{0.30}$$

Shear failure combined with or followed by aramid fibre-reinforced polymer (AFRP) fracture:

$$\frac{\varepsilon_{fe}}{\varepsilon_{fu}} = 0.048 \left(\frac{f_c^{'2/3}}{E_f \rho_f} \right)^{0.47}$$

The value $f_c^{'}$ is in MPa and E_f is in GPa.

In the model proposed by the author, no separation was made between side-bonding and U-jacketing.

Chen and Teng (2003a) had reviewed the previous data and established the FRP strengthened beams fail in shear mainly in one of the two modes: FRP rupture and FRP debonding. The authors had presented with the development of a simple, accurate and rational design proposal for the shear capacity of FRP strengthened RC beams which fails by FRP debonding.

Chen and Teng (2003b) had presented the rational design proposal for the shear capacity of FRP strengthened beams which fail in FRP rupture. The contribution of the authors on this study was the realization of the fact that the stress distribution in the FRP along the shear crack is non-uniform strain distribution in the FRP and the linear elastic brittle behaviour of FRP, and the explicit account taken of this stress non-uniformity in the new strength model. A new strength model was then developed. Finally a new design proposal was presented.

Bousselham and Chaallal (2004) carried out findings of the research and had examined and analysed the parameter on the shear behaviour of RC beams strengthened with externally bonded FRP. The authors had found that the parameters related to the properties of the FRP and to those of the shear steel reinforcement do not influence the shear behaviour of strengthened RC beams. The shear span-to-effective depth ratio (a/d), the longitudinal steel reinforcement ratio and the geometry of the beam also have influence on the shear behaviour of the RC beam. Also recommended the interaction between the FRP and the internal transverse steel reinforcement is essential for understanding the shear resistance mechanisms.

Teng et al. (2004) had presented a state-of-the-art review of existing research on shear strengthened RC beam. The methods of strengthening, experimental observations of failure process and modes had been described. The alternative FRP shear strengthening techniques, including near-surface-mounted FRP and prestressed CFRP straps, were also noted.

2.6 Numerical Studies on RC Beams, Strengthened in Shear with FRP

Some researchers had attempted to simulate the behaviour of RC beams strengthened in shear with FRP composites using the finite element method.

Arduini et al. (1997) had attempted to simulate the behaviour of RC beam strengthened with FRP composites using smeared cracking approach and FEM. The beams strengthened with FRP plates were modelled with two-dimensional plate elements in the study, however, the crack patterns of those strengthened beams were not predicted by the finite element analysis.

Tedesco et al. (1999) had studied the entire strengthened RC bridge by finite element analysis. Truss elements were used to model the FRP composites. The authors had concluded that the external bonding of FRP composites to the bridge

girders reduced the average maximum deflection at midspan by 9% and reinforcing steel stresses by 11%.

Kachlakev et al. (2001) had studied the effect of shear strengthening using ANSYS finite element model and compared the behaviour of two full-scale RC beams without stirrups and RC beam externally reinforced with GFRP on both sides of the beam. The author used a smeared cracking approach for the modelling of concrete and three-dimensional layered elements for the modelling of FRP composites for the development of three-dimensional finite element models. Finally, they concluded that finite element models show good agreement with the experimental beam test data.

Santhakumar et al. (2004) had studied the numerical analysis of retrofitted RC shear beams using finite element adopted by ANSYS. The RC beams retrofitted using CFRP composites with ±45° and 90° fibre orientations. The authors used the geometry and materials properties experimental data of Norris et al. (1997) and developed a model for the quarter portion of the full beam by taking advantage of the symmetry of the beam and loadings. Finally, the authors had concluded that the load–deflection plots obtained from the study show good agreement with the experimental plots.

2.7 Critical Observations on Existing Literature

Following points were critically observed from the existing literature.

- Generally, the strength and stiffness of beam strengthened by FRP strips or sheets as an external reinforcement increase.
- When the CFRP fibre was placed perpendicular to cracks in the beam, a large increase in strength and stiffness was observed and brittle failure occurred due to concrete rupture.
- The horizontal FRP sheet may be effective when shear span-to-effective depth ratio (*a/d*) is smaller or when failure mode is controlled by web crushing.
- Contribution of shear from CFRP reinforcement decreases with decreasing shear span-to-effective depth (*a/d*) ratio.
- Strain measurement had demonstrated that thinner the fibre used, better the utilization of the fabrics.
- The optimum combination of CFRP layers and transverse steel stirrups exist for a maximum increase in ductility.
- FRP with anchorage is more effective than U-wrap scheme. Anchorage of the FRP sheet on to the top surface of a RC beam resulted in a decrease in interface bond stresses and an increase in FRP strain at failure.

- Most of the predictive models were based on the experiments carried out on small-scale specimens. These models may produce conservative results for large-sized beams.
- The interaction between internal steel stirrups and external FRP shear reinforcement has not been considered in the FRP stress distribution.
- Most of the works have been done on the CFRP, and hence the universal model does not satisfy the test data based on GFRP and AFRP. More experimental works are required on GFRP and AFRP to modify the existing model.

2.8 Summary

The existing literature relevant to the investigation is presented in this chapter. The literature review is explained separately for experimental study, theoretical study and numerical study. The critical observation on the available literature is also presented.

References

Adhikary BB, Mutsuyoshi H, Ashrof M (2004) Shear strengthening of reinforced concrete beams using fiber reinforced polymer sheets with bonded anchorage. ACI Struct J 101(5):660–668

Al-Sulaimani GJ, Sharif A, Basunbul IA, Baluch MH, Ghaleb BN (1994) Shear repair for reinforced concrete by fiberglass plate bonding. ACI Struct J 91(3):458–464

American Concrete Institute (ACI) (1995) Building code requirements for structural concrete (ACI 318–95) and commentary (ACI 318R-95). ACI Committee 318, Detroit, Mich

American Concrete Institute (ACI) (2002) Building code requirements for reinforced concrete (ACI 318–02) and commentary-ACI 318RM-02. ACI Committee 318, Detroit, Mich

American Concrete Institute (ACI 440.2R-02) (2002) Guide for the design and construction of externally bonded FRP systems for strengthening concrete structures. ACI Committee 440, Farmington Hills, Michigan, 45 p

Antonopoulos CP, Triantafillou TC (2002) Analysis of FRP strengthened RC beam-column joints. J Compos Constr 6(1):41–51

Antonopoulos CP, Triantafillou TC (2003) Experimental investigation of FRP strengthened RC beam-column joints. J Compos Constr 7(1):39–49

Araki N, Matsuzaki Y, Nakano K, Kataoka T, Fukuyama H (1997) Shear capacity of retrofitted RC members with continuous fiber sheets. In: Non-Metallic (FRP) reinforcement for concrete structures: proceedings of the third international symposium on non-metallic (FRP) reinforcement for concrete structures, vol 1. Published by Japan Concrete Institute, Tokyo, Japan, pp 515–522

Arduini M, Di Tommaso A, Nanni A (1997) Brittle failure in FRP plate and sheet bonded beams. ACI Struct J 94(4):363–370

Baggio D, Soudki K, Noel M (2014) Strengthening of shear critical RC beams with various FRP systems. Constr Build Mater 66:634–644

Bakis CE, Bank LC, Brown VL, Cosenza E, Davalos JF, Lesko JJ, Machida A, Rizkalla SH, Triantafillou TC (2002) Fiber-reinforced polymer composites for construction state-of-the-art-review. J Compos Constr 6(2):73–87

Berset JD (1992) Strengthening of reinforced concrete beams for shear using FRP composites. MS thesis, Dept. of Civil and Environmental engineering, MIT

Bousselham A, Chaallal O (2004) Shear strengthening reinforced concrete beams with fiber-reinforced polymer: assessment of influencing parameters and required research. ACI Struct J 101(2):219–227

Bousselham A, Chaallal O (2006a) Effect of transverse steel and shear span on the performance of RC beams strengthened in shear with CFRP. Compos B 37:37–46

Bousselham A, Chaallal O (2006b) Behavior of reinforced concrete T-beams strengthened in shear with carbon fibre reinforced polymer—an experimental study. ACI Struct J 103(3):339–347

Bousselham A, Chaallal O (2008) Mechanisms of shear resistance of concrete beams strengthened in shear with externally bonded FRP. J Compos Constr 12(5):499–512

Canadian Standards Association (CSA) (1994) Design of concrete structures. A23.3-94, Rexdale, Ontario

Canadian Standards Association (CSA-S806-02) (2002) Design and construction of building components with fiber-reinforced polymer. Rexdale, Ontario, 202 p

Cao SY, Chen JF, Teng JG, Hao Z, Chen J (2005) Debonding in RC beams shear strengthened with complete FRP wraps. J Compos Constr 9(5):417–428

Carolin A, Taljsten B (2005) Experimental study of strengthening for increased shear bearing capacity. J Compos Constr 9(6):488–496

Chaallal O, Nollet MJ, Perraton D (1998) Shear strengthening of RC beams by externally bonded side CFRP strips. J Compos Constr 2(2):111–113

Chaallal O, Shahawy M, Hassan M (2002) Performance of reinforced concrete T-girders strengthened in shear with carbon fiber-reinforced polymer fabric. ACI Struct J 99(3):335–343

Chajes MJ, Januszka TF, Mertz DR, Thomson TA Jr, Finch WW Jr (1995) Shear strengthening of reinforced concrete beams using externally applied composite fabrics. ACI Struct J 92(3):295–303

Chen JF, Teng JG (2003a) Shear capacity of FRP-strengthened RC beams: FRP debonding. Constr Build Mater 17(1):27–41

Chen JF, Teng JG (2003b) Shear capacity of fiber-reinforced polymer strengthened RC beams: fiber reinforced polymer rupture. J Struct Eng 129(5):615–625

Deniaud C, Cheng JJR (2001) Shear behavior of reinforced concrete T-beams with externally bonded fiber-reinforced polymer sheets. ACI Struct J 98(3):386–394

Deniaud C, Cheng JJR (2003) Reinforced concrete T-beams strengthened in shear with fiber reinforced polymer sheets. J Compos Constr 7(4):302–310

Dolan CW, Rizkalla SH, Nanni A (eds) (1999) Fourth international symposium on fiber reinforced polymer reinforcement for reinforced concrete structures. American Concrete Institute, SP-188, Farmington Hills, Michigan

El-Amoury T, Ghobarah A (2002) Seismic rehabilitation of beam-column joints using GFRP sheets. Eng Struct. 24:1397–1407

Fardis MN, Khalili H (1981) Concrete encased in fiber glass reinforced plastic. ACI Struct J 78 (6):440–446

FIB (2001) Externally bonded FRP reinforcement for RC structures. The International Federation for Structural Concrete, Lausanne, Switzerland

Funakawa I, Shimono K, Watanabe T, Asada S, Ushijima S (1997) Experimental study on shear strengthening with continuous fiber reinforcement sheet and methyl methacrylate resin. In: Non-metallic (FRP) reinforcement for concrete structures: proceedings of the third international symposium on non-metallic (FRP) reinforcement for concrete structures, vol 1. Published by Japan Concrete Institute, Tokyo, Japan, pp 475–482

Gergely J, Pantelides CP, Reaveley LD (2000) Shear strengthening of RC T-joints using CFRP composites. J Compos Constr 4(2):56–64

Guadagnini M, Pilakoutas K, Waldron P (2006) Shear resistance of FRP RC beams: experimental study. J Compos Constr 10(6):464–473

Islam MR, Mansur MA, Maalej M (2005) Shear strengthening of RC deep beams using externally bonded FRP systems. Cement Concr Compos 27:413–420

Japan Concrete Institute (JCI) (1997) Non-metallic (FRP) reinforcement for concrete structures, 1 and 2. Tokyo, Japan

Japan Concrete Institute (JCI) (1998) Technical report on continuous fiber reinforced concrete. TC-952: Committee on Continuous Fiber Reinforced Concrete, Tokyo

Japan Society of Civil Engineers (JSCE) (2001) Recommendations for upgrading of concrete structures with use of continuous fiber sheets. Concrete Engineering Series, No. 41, Tokyo, Japan, 250 pp

Kachlakev D, Miller T, Yim S (2001) Finite element modeling of reinforced concrete structures strengthened with FRP laminates. Report for Oregon Department of Transportation, Salem, May 2001

Khalifa A, Gold WJ, Nanni A, Aziz A (1998) Contribution of externally bonded FRP to shear capacity of RC flexural members. J Compos Constr 2(4):195–201

Khalifa A, Tumialan G, Nanni A, Belarbi A (1999) Shear strengthening of continuous RC beams using externally bonded CFRP sheets. Fiber reinforced polymer reinforcement for reinforced concrete structures. In: Dolan CW, Rizkalla SH, Nanni A (eds) Proceedings of 4th international symposium, SP-188, American Concrete Institute, Farmington Hills, Mich., pp 995–1008

Khalifa A, Nanni A (2000) Improving shear capacity of existing RC T-section beams using CFRP composites. Cement Concr Compos 22:165–174

Khalifa A, Nanni A (2002) Rehabilitation of rectangular simply supported RC beams with shear deficiencies using CFRP composites. Constr Build Mater 16:135–146

Leung CKY, Chen Z, Lee S, Ng M, Xu M, Tang J (2007) Effect of size on the failure of geometrically similar concrete beams strengthened in shear with FRP strips. J Compos Constr 11(5):487–496

Li A, Assih J, Delmas Y (2001) Shear strengthening of RC beams with externally bonded CFRP sheets. J Struct Eng 127(4):374–380

Li A, Diagana C, Delmas Y (2002) Shear strengthening effect by bonded composite fabrics on RC beams. Compos B 33:225–239

Li W, Leung CKY (2017) Effect of shear span-depth ratio on mechanical performance of RC beams strengthened in shear with U-wrapping FRP strips. Compos Struct 177:141–157

Maeda T, Asano Y, Sato Y, Ueda T, Kakuta Y (1997) A study on bond mechanism of carbon fiber sheet. In: Non-metallic (FRP) reinforcement for concrete structures: proceedings of the third international symposium on non-metallic (FRP) reinforcement for concrete structures, vol. 1. Published by Japan Concrete Institute, Tokyo, Japan, pp 279–286

Malek AM, Saadatmanesh H (1998) Ultimate shear capacity of reinforced concrete beams strengthened with web-bonded fiber-reinforced plastic plates. ACI Struct J 95(4):391–399

Meier U (1987) Bridge repair with high performance composite materials. Mater Technik 4:125–128

Micelli F, Anniah RH, Nanni A (2002) Strengthening of short shear span reinforced concrete T joists with fiber reinforced plastic composites. J Compos Constr 6(4):264–271

Mosallam AS, Banerjee S (2007) Shear enhancement of reinforced concrete beams strengthened with FRP composite laminates. Compos B 38:781–793

Nanni A (1995) Concrete repair with externally bonded FRP reinforcement. Concr Int 17(6):22–26

Neale KW (2000) FRPs for structural rehabilitation: a survey of recent progress. Prog Struct Mat Eng 2(2):133–138

Norris T, Saadatmanesh H, Ehsani MR (1997) Shear and flexural strengthening of RC beams with carbon fiber sheets. J Struct Eng 123(7):903–911

Panda KC, Bhattacharyya SK, Barai SV (2010) Shear behaviour of reinforced concrete T-beams with U-bonded glass fibre reinforced plastic sheet. Indian Concr J (ICJ) 84(10):61–71

Panda KC, Bhattacharyya SK, Barai SV (2011a) Shear strengthening of RC T-beams with externally side bonded GFRP sheet. J Reinf Plast Compos 30(13):1139–154

Panda KC, Bhattacharyya SK, Barai SV (2011b) Strengthening of RC T-beams with shear deficiencies using GFRP strips. J Civil Eng Archit 05(1):56–67

Panda KC, Bhattacharyya SK, Barai SV (2011c) Influence of transverse steel on the performance of RC T-beams strengthened in shear with GFRP strips. In: Advances in FRP composite in civil engineering, vol II. Springer, India, pp 763–766

Panda KC, Bhattacharyya SK, Barai SV (2012) Shear behaviour of RC T-beams strengthened with U-wrapped GFRP sheet. Steel Compos Struct Int J 12(2):149–166
Panda KC, Bhattacharyya SK, Barai SV (2013a) Shear strengthening effect by bonded GFRP strips and transverse steel on RC T-beams. Struct Eng Mech Int J 47(1):75–98
Panda KC, Bhattacharyya SK, Barai SV (2013b) Effect of transverse steel on the performance of RC T-beams strengthened in shear zone with GFRP sheet. Constr Build Mater 41:79–90
Panda KC, Bhattacharyya SK, Barai SV (2015) Strain analysis of RC T-beams strengthened in shear with variation of U-wrapped GFRP sheet and transverse steel. Adv Struct Eng 3 (154):2001–2010
Pellegrino C, Modena C (2002) Fiber reinforced polymer shear strengthening of reinforced concrete beams with transverse steel reinforcement. J Compos Constr 6(2):104–111
Saadatmanesh H, Ehsani MRed. (1998) Second International Conference on composites in Infrastructure, ICCI, Tucson, Ariz., V. 1 & 2, p 1506
Santhakumar R, Chandrasekaran E, Dhanaraj R (2004) Analysis of retrofitted reinforced concrete shear beams using carbon fiber composites. Electr J Struct Eng 4:66–74
Sato Y, Ueda T, Kakuta Y, Tanaka T (1996) Shear reinforcing effect of carbon fiber sheet attached to side of reinforced concrete beams. In: El-Badry MM (ed) Advanced composite materials in bridges and structures (2nd international conference). Published by the Canadian Society for Civil Engineering, Montreal, Quebec, Canada, pp 621–628
Sato Y, Ueda T, Kakuta Y, Ono S (1997) Ultimate shear capacity of reinforced concrete beams with carbon fiber sheet. In: Proceedings of the third international symposium on non-metallic (FRP) reinforcement for concrete structures, vol 1. Published by Japan Concrete Institute, Tokyo, Japan, pp 499–506
Sundarraja MC, Rajamohan S (2009) Strengthening of RC beams in shear using GFRP inclined strips—an experimental study. Constr Build Mater 23(2):856–864
Sheheta E, Morphy R, Rizkalla S (1999) Fourth international symposium, fiber reinforced polymer reinforcement for concrete structures, SP-188. American Concrete Institute, Farmington Hills, Mich., p 157–167
Taerwe L, Khalil H, Matthys S (1997) Behaviour of RC beams strengthened in shear by external CFRP sheets. In: Proceedings of the third international symposium on non-metallic (FRP) reinforcement for concrete structures, vol 1. Published by Japan Concrete Institute, Tokyo, Japan, pp 483–490
Taljsten B, Elfgren L (2000) Strengthening concrete beams for shear using CFRP-materials: evaluation of different application methods. Compos B Eng 31:87–96
Taljsten B (2002) FRP strengthening of concrete structures—design guidelines in Sweden. In: Proceedings of 15th ASCE engineering mechanics conference, June 2–5. Columbia University, New York
Taljsten B (2003) Strengthening concrete beams for shear with CFRP sheets. Constr Build Mater 17(1):15–26
Tedesco JW, Stallings JM, EI-Milihmy M (1999) Finite element method analysis of a concrete bridge repaired with fiber reinforced plastic laminates. Comput Struct 72:379–407
Teng JG, Lam L, Chen JF (2004) Shear strengthening of RC T-beams with FRP composites. Prog Struct Eng Mater 6:173–184
Triantafillou TC (1998) Shear strengthening of reinforced concrete beams using epoxy bonded FRP composites. ACI Struct J 95(2):107–115
Triantafillou TC, Antonopoulos CP (2000) Design of concrete flexural members strengthened in shear with FRP. J Compos Constr 4(4):198–205
Triantafillou TC, Fardis MN (1997) Strengthening of historic masonry structures with composite materials. Mater Struct 30:486–496
Uji K (1992) Improving shear capacity of existing reinforced concrete members by applying carbon fiber sheets. Trans Jpn Concr Inst 14:253–266

Umezu K, Fujita M, Nakai H, Tamaki K (1997) Shear behavior of RC beams with aramid fiber sheet. In: Proceedings of the third international symposium on non-metallic (FRP) reinforcement for concrete structures, vol 1. Published by Japan Concrete Institute, Tokyo, Japan, pp 491–498

Uomoto T, Mutsuyoshi H, Katsuki F, Misra S (2002) Use of fiber reinforced polymer composites as reinforcing material for concrete. J Mater Civil Eng 14(3):191–209

Zhang Z, Hsu CTT, Moren J (2004) Shear strengthening of reinforced concrete deep beams using carbon fiber reinforced polymer laminates. J Compos Constr 8(5):403–414

Zhang Z, Hsu CTT (2005) Shear strengthening of reinforced concrete beams using carbon-fiber-reinforced polymer laminates. J Compos Constr 9(2):158–169

Chapter 3
Technique for Shear Strengthening—An Experimental Approach

3.1 General

This chapter presents the experimental procedure for shear strengthening of RC T-beams strengthened in shear with GFRP sheet. The job is performed primarily in two stages.

The *first stage* consists of selection and testing of relevant materials for the preparation of test specimens in the laboratory to establish the physical and mechanical properties of the materials. All materials are to be tested as per the specifications of Indian Standards. Concrete mix design is to be performed for the preparation of test samples (RC T-beams) as per the design guide lines of IS: 10262 (1982). The mix design for the present case was targeted for M30 grade of concrete. For ascertaining the properties of hardened concrete such as compressive strength, split tensile strength and stress–strain behaviour, tests on cube and cylinder samples, prepared from different batches of mix, were carried out.

The *second stage* consists of testing the beams for shear under two-point static loading system. In the present case, the experimental study was based on the testing of 45 full scale, simply supported RC T-beams of 2.5 m length. Nine beams were used as control specimens with three different stirrup spacings without GFRP wrap and the rest 36 beams were strengthened in shear with GFRP sheets and strips in different configurations, orientations and variation of layers for each variety of stirrup spacing. The tests were performed at the structural laboratory of IIT Kharagpur.

K. C. Panda et al., *Shear Strengthening of T-beam with GFRP*, Springer Transactions in Civil and Environmental Engineering, https://doi.org/10.1007/978-981-10-7760-9_3

3.2 Classification

Different forms that were selected for testing of RC T-beams are outlined in the following sections.

3.2.1 Control Specimens

Nine beams were considered as control specimens with three different spacings of transverse steel reinforcements (stirrups) without GFRP wrap as indicated below.

i. A set of three beams without any transverse steel reinforcements (stirrups), except six stirrups at four places, viz., two support points and two loading points.
ii. A set of three beams with transverse steel reinforcements (stirrups) placed at a spacing of 300 mm.
iii. A set of three beams with transverse steel reinforcements (stirrups) placed at a spacing of 200 mm.

3.2.2 RC T-beams Strengthened for Shear with Externally U-Jacketed GFRP Sheets

Nine beams were tested as RC T-beams strengthened for enhancing shear capacity using GFRP continuous sheet in the form of U-jacket with one, two and three layers for each type of stirrup spacing, described as follows:

i. Three T-beam specimens without transverse steel (stirrups) but with GFRP sheet having one, two and three layers.
ii. Three T-beam specimens with transverse steel (stirrups) spaced at 300 mm c/c and with GFRP sheet having one, two and three layers.
iii. Three T-beam specimens with transverse steel (stirrups) spaced at 200 mm c/c and with GFRP sheet having one, two and three layers.

3.2.3 RC T-beams Strengthened for Shear with Externally Side-Bonded GFRP Sheets

Nine beams were tested as RC T-beams strengthened for enhancing shear capacity using GFRP continuous sheet on two sides of the web of T-beams in one, two and three layers for each type of stirrup spacing, as indicated:

i. Three T-beam specimens without transverse steel (stirrups) but with GFRP sheet having one, two and three layers.

ii. Three T-beam specimens with transverse steel (stirrups) spaced at 300 mm c/c and with GFRP sheet having one, two and three layers.
iii. Three T-beam specimens with transverse steel (stirrups) spaced at 200 mm c/c and with GFRP sheet having one, two and three layers

3.2.4 *RC T-beams Strengthened for Shear with Externally Bonded GFRP Strips in Shear Zone*

Nine beams were tested as RC T-beams strengthened for enhancing shear capacity with externally bonded, in shear zone, with one-layer GFRP strips in U-shape, and side-bonded with orientation of the strip at 45° and 90° to the longitudinal axis of the beam for each type of stirrup spacing, as indicated:

i. Three T-beam specimens without transverse steel (stirrups) but with GFRP strips having U-shape, and side-bonded with orientation at 45° and 90° with respect to the longitudinal axis of the beam.
ii. Three T-beam specimens with transverse steel (stirrups) spaced at 300 mm c/c and with GFRP strips having U-shape, and side-bonded with orientation at 45° and 90° with respect to the longitudinal axis of the beam.
iii. Three T-beam specimens with transverse steel (stirrups) spaced at 200 mm c/c and with GFRP strips having U-shape, and side-bonded with orientation at 45° and 90° with respect to the longitudinal axis of the beam.

3.2.5 *RC T-beams Strengthened for Shear with Externally Bonded GFRP Sheet in Shear Zone*

Nine beams were tested as RC T-beams strengthened for enhancing shear capacity with externally bonded one layer GFRP sheet in shear zone in the form of U-jacket, side-bonded and U-jacket with anchorage for each type of stirrup spacing (Panda et al. 2013b), indicated as follows:

i. Three T-beam specimens without transverse steel (stirrups) but with GFRP sheet having U-jacket, side-bonded and U-jacket with anchorage.
ii. Three T-beam specimens with transverse steel (stirrups) spaced at 300 mm c/c and with GFRP sheet having U-jacket, side-bonded and U-jacket with anchorage.
iii. Three T-beam specimens with transverse steel (stirrups) spaced at 200 mm c/c and with GFRP sheet having U-jacket, side-bonded and U-jacket with anchorage.

3.3 Design of RC T-beams and Specimen Details

All the RC T-beams were designed to fail in shear as per IS 456: 2000 (Panda et al. 2011a, 2012, 2013a, b, 2015). The sizes of the RC T-beams used in the experiment were 2500 mm long, 250 mm flange width, 60 mm flange thickness, 100 mm wide web and 200 mm deep web. Based on the design, at the bottom of the RC T-beams, 2 nos. 20 mm diameter Tor steel bars were used as flexural reinforcement (area 628.31 mm^2), and at the top of the RC T-beams, 4 nos. 8 mm diameter Tor steel bars were used in one layer. The diameter of the transverse steel reinforcements (stirrups) used in the RC T-beam specimens was 6 mm. The stirrups spaced at 200 mm centres in specimens designated as S200 at 300 mm centres in specimens designated as S300, no transverse reinforcements in specimens designated as S0, are provided in the shear zone. However, to avoid local failure, six number stirrups, out of which two stirrups at each support and one at each of the loading points were provided for S0 specimens. The details of the specimens are as in Fig. 3.1. Figure 3.2 shows the reinforcement cages of the control specimens for series S0, S300 and S200.

3.4 Strengthening of Test Specimens

All T-beam specimens were provided with the same flexural reinforcement for parity. As stated earlier, the transverse steel reinforcements (stirrups) were varied and provided in three different spacings in specimens designated as S0, S300 and S200. The details of control and strengthened specimens with the strengthening schemes are summarized in a tabular form in the following subsection.

The concrete surface was smoothened before strengthening with GFRP. To achieve better bonding of the fibres on the concrete surface, a layer of epoxy-based primer, which penetrates into the concrete pores, was applied. The corners of the RC T-beams were rounded to a radius of 10 mm for avoiding the sharp edges and damage to fibre cloth. The mixing of the epoxy was done by stirring with a rod and application of epoxy onto the concrete surface was done using a brush. For first layer of GFRP, first coat of epoxy resin was applied followed by the first layer of glass fibre cloth. A roller was used on the cloth surface to ensure impregnation of the fibres in the saturant and tension was maintained to minimize intrusion of air and to squeeze out the excess epoxy. The fibre cloth was then coated with a second layer of epoxy resin to fully saturate the fibre material and the excessive resin was removed by applying hard roller. The surface coating serves as a protective layer of the fibre cloth. The beams were kept for at least 7 days for epoxy to cure and hardened before testing. The surface preparation before and after the application of GFRP layer is shown in Figs. 3.3 and 3.4.

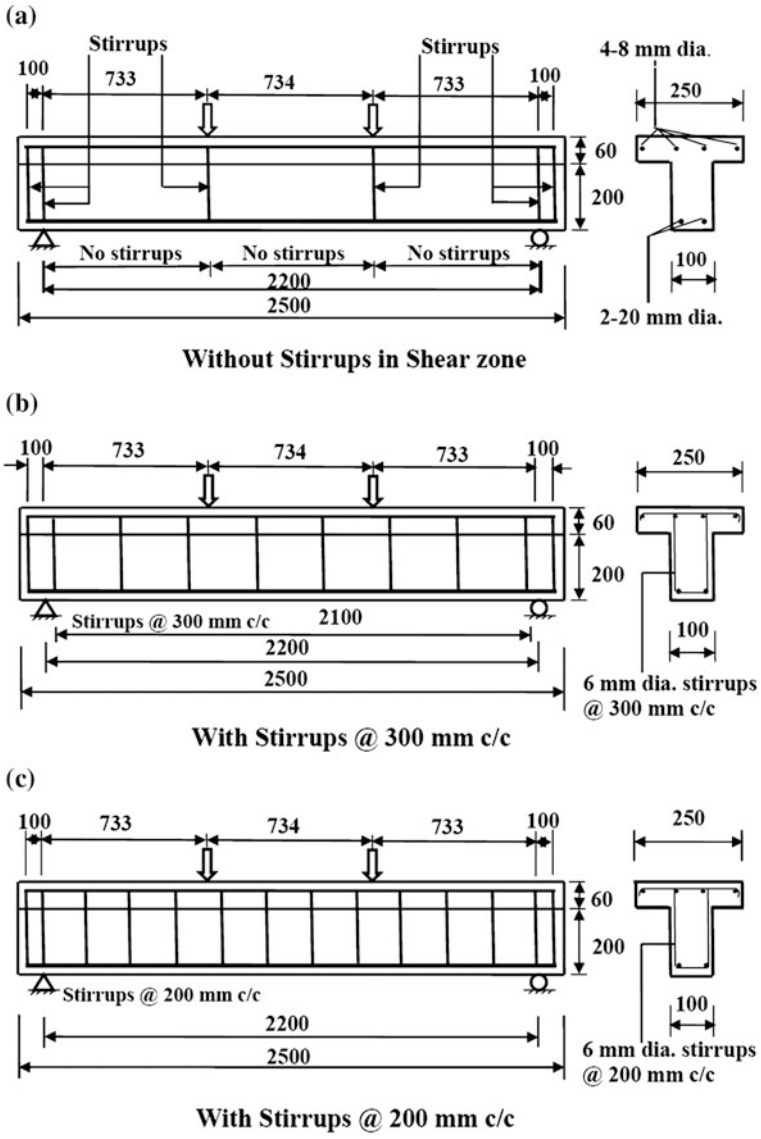

Fig. 3.1 Schematic diagrams of control specimens

3.4.1 Control RC T-beams

Nine RC T-beam specimens were prepared as control beams in three different series. As stated earlier the series S0 refers to RC T-beam specimens with no stirrups (only the stirrups were provided at the support and loading points to prevent

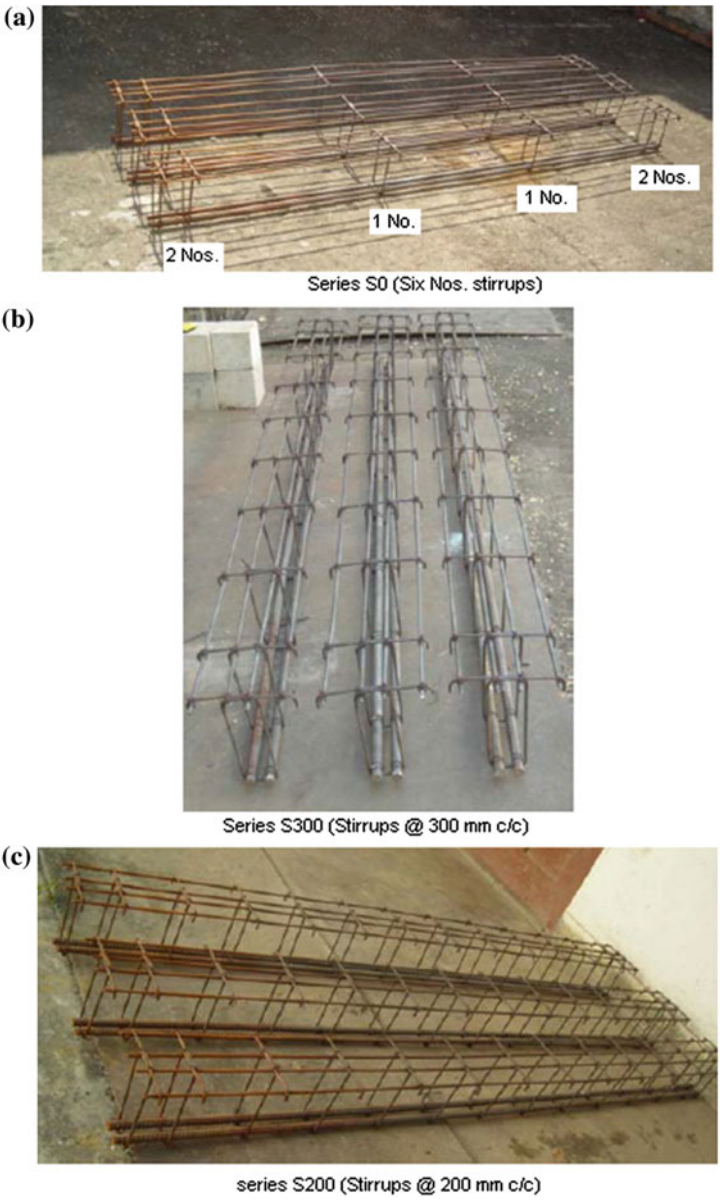

Fig. 3.2 Cages for different series of specimens

local shear failure), series S200 corresponds to RC T-beam specimens with steel stirrups spaced at 200 mm c/c and series S300 corresponds to RC T-beam specimens with steel stirrups spaced at 300 mm c/c. Thus, for example specimen S200-0L-2 is a RC T-beam with steel stirrups at a spacing of 200 mm c/c (S200),

Fig. 3.3 Specimens before applying GFRP

Fig. 3.4 Specimens after applying GFRP

Table 3.1 Details of control RC T-beams test specimens

Specimen designation	Strengthening schemes
S0-0L	Control beam without stirrups
S300-0L	Control beam with stirrups at a spacing of 300 mm c/c
S200-0L	Control beam with stirrups at a spacing of 200 mm c/c

without GFRP layer (0L) and sample number 2. The details of control RC T-beam specimens are presented in Table 3.1.

The preparation of specimens before casting for three series such as S0, S300 and S200 is shown in Fig. 3.5.

The specimens after casting and 28 days of curing are shown in Figs. 3.6 and 3.7.

Fig. 3.5 Cages of RC T-beams before casting for series S0, S300 and S200

Fig. 3.6 RC T-beams after casting

Fig. 3.7 RC T-beams after curing

3.4.2 Strengthening Schemes of RC T-beams with Externally U-Jacketed GFRP Sheets

Nine test specimens were prepared as RC T-beams strengthened in shear with externally U-jacketed GFRP sheets. The RC T-beams were strengthened with one layer, two layers and three layers of GFRP sheet in the form of continuous U-jacket around the web, the main fibre direction oriented perpendicular to the longitudinal axis of the RC T-beam (Panda et al. 2010, 2012, 2015). The RC T-beam specimens strengthened with one, two and three layers of GFRP sheet were labelled as 1L, 2L and 3L. The thickness of 1L, 2L and 3L GFRP sheet was 0.36, 0.72, 1.08 mm respectively. The strengthened specimens designated as S300-1L-CT-U-90, indicates steel stirrups @ 300 mm c/c (S300), strengthened with one layer of GFRP sheet (1L), continuous wrapping (CT), in U-jacket around the web of the T-beams (U) and orientation of the fibre angle is 90º to the longitudinal axis of the beam. The details of the specimens are listed in Table 3.2. Figure 3.8 shows the details of strengthening scheme with externally U-jacketed GFRP sheet.

Table 3.2 Details of RC T-beams strengthened in shear with U-jacketed GFRP

Specimen designation	Strengthening schemes
S0-1L-CT-U-90	Without stirrups + one layer of GFRP continuous sheet + U-jacket + orientation of the fibre 90° to the longitudinal axis of the beam
S0-2L-CT-U-90	Without stirrups + two layers of GFRP continuous sheet + U-jacket + orientation of the fibre 90° to the longitudinal axis of the beam
S0-3L-CT-U-90	Without stirrups + three layers of GFRP continuous sheet + U-jacket + orientation of the fibre 90° to the longitudinal axis of the beam
S300-1L-CT-U-90	With stirrups @ 300 mm c/c + one layer of GFRP continuous sheet + U-jacket + orientation of the fibre 90° to the longitudinal axis of the beam
S300-2L-CT-U-90	With stirrups @ 300 mm c/c + two layers of GFRP continuous sheet + U-jacket + orientation of the fibre 90° to the longitudinal axis of the beam
S300-3L-CT-U-90	With stirrups @ 300 mm c/c + three layers of GFRP continuous sheet + U-jacket + orientation of the fibre 90° to the longitudinal axis of the beam
S200-1L-CT-U-90	With stirrups @ 200 mm c/c + one layer of GFRP continuous sheet + U-jacket + orientation of the fibre 90° to the longitudinal axis of the beam
S200-2L-CT-U-90	With stirrups @ 200 mm c/c + two layers of GFRP continuous sheet + U-jacket + orientation of the fibre 90° to the longitudinal axis of the beam
S200-3L-CT-U-90	With stirrups @ 200 mm c/c + three layers of GFRP continuous + U-jacket + orientation of the fibre 90° to the longitudinal axis of the beam

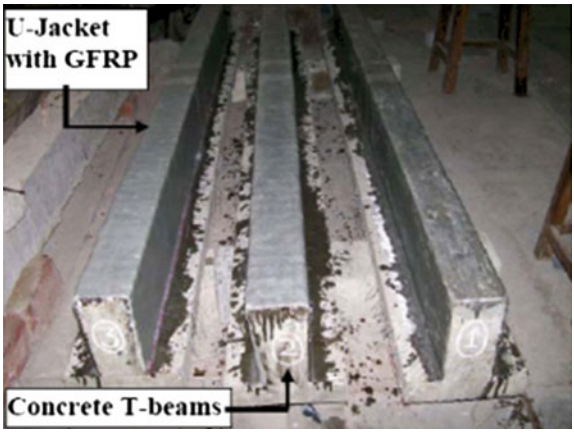

Fig. 3.8 Strengthening scheme with U-jacketed GFRP

3.4.3 Strengthening Schemes of RC T-beams with Externally Side-Bonded GFRP Sheets

Nine test specimens were prepared as RC T-beams strengthened in shear with externally side-bonded GFRP sheets. The RC T-beams were strengthened with one layer, two layers and three layers of GFRP continuous sheets on either side of the web (Panda et al. 2011a). The orientation of main fibre directions was perpendicular to the longitudinal axis of the beam. The thickness of 1L, 2L and 3L GFRP was 0.36 mm, 0.72 mm and 1.08 mm respectively. The strengthened specimens designated as S300-1L-CT-S-90, with steel stirrups @ 300 mm c/c (S300), strengthened with one layer of GFRP sheet (1L), continuously (CT) placed on sides of the web of RC T-beams (S) and fibre orientation is 90° to the longitudinal axis of the beam. The details of the RC T-beam specimens are presented in Table 3.3. Figure 3.9 shows the shear strengthening scheme details with externally side-bonded GFRP.

Table 3.3 Details of RC T-beams strengthened in shear with side-bonded GFRP

Specimen designation	Strengthening schemes
S0-1L-CT-S-90	Without stirrups + one layer of GFRP continuous sheet + side-bonded + orientation of the fibre 90° to the longitudinal axis of the beam
S0-2L-CT-S-90	Without stirrups + two layers of GFRP continuous sheet + side-bonded + orientation of the fibre 90° to the longitudinal axis of the beam
S0-3L-CT-S-90	Without stirrups + three layers of GFRP continuous sheet in the form of side-bonded + orientation of the fibre 90° to the longitudinal axis of the beam
S300-1L-CT-S-90	With stirrups @ 300 mm c/c + one layer of GFRP continuous sheet + side-bonded + orientation of the fibre 90° to the longitudinal axis of the beam
S300-2L-CT-S-90	With stirrups @ 300 mm c/c + two layers of GFRP continuous + side-bonded + orientation of the fibre 90° to the longitudinal axis of the beam
S300-3L-CT-S-90	With stirrups @ 300 mm c/c + three layers of GFRP continuous sheet + side-bonded + orientation of the fibre 90° to the longitudinal axis of the beam
S200-1L-CT-S-90	With stirrups @ 200 mm c/c + one layer of GFRP continuous sheet + side-bonded + orientation of the fibre 90° to the longitudinal axis of the beam
S200-2L-CT-S-90	With stirrups @ 200 mm c/c + two layers of GFRP continuous sheet + side-bonded + orientation of the fibre 90° to the longitudinal axis of the beam
S200-3L-CT-S-90	With stirrups @ 200 mm c/c + three layers of GFRP continuous sheet + side-bonded + orientation of the fibre 90° to the longitudinal axis of the beam

Fig. 3.9 Details of strengthening schemes with side-bonded GFRP

3.4.4 Strengthening Schemes of RC T-beams with Externally Bonded GFRP Strips in Shear Zone

Nine RC T-beam specimens were prepared and strengthened in shear with externally bonded GFRP strips in two configurations such as U-shape, and side-bonded in the shear zone (Panda et al. 2013a). The orientation of the side-bonded GFRP strips was 45° and 90° to the longitudinal axis of the beam. The width and thickness of the GFRP strips were 50 and 0.36 mm respectively. The centre to centre spacing of the GFRP strips was 100 mm for U-shape and side-bonded with orientation 90° to the longitudinal axis of the beam. The centre of first GFRP strips was placed at a distance of 50 mm from both sides of the support. Whereas for side-bonded GFRP strips with 45° orientations, bottom inner edge (nearer to the support) of the first inclined GFRP strip was placed at 50 mm distance from both sides of the support. The width of the GFRP strips at the bottom was 70 mm and centre to centre spacing of the GFRP strips was 120 mm. Totally seven GFRP strips were provided in each side of the shear zone. The strengthened RC T-beam specimen designated as S300-1L-ST-S-45 indicates steel stirrups spaced @ 300 mm c/c (S300), strengthened with one layer of GFRP (1L) strips (ST), bonded on the sides of the web of T-beams (S), and orientation of the fibre angle is 45° to the longitudinal axis of the beam. The specimen's details are presented in Table 3.4.

Figure 3.10 shows the details of strengthening scheme with externally bonded GFRP strips in shear zone.

Table 3.4 Details of RC T-beams strengthened in shear with GFRP strips

Specimen designation	Strengthening schemes
S0-1L-ST-U-90	Without stirrups + one layer of GFRP strips + U-shape + 90° orientation
S0-1L-ST-S-90	Without stirrups + one layer of GFRP strips + side-bonded + 90° orientation
S0-1L-ST-S-45	Without stirrups + one layer of GFRP strips + side-bonded + 45° orientation
S300-1L-ST-U-90	Stirrups @ 300 mm c/c + one layer of GFRP strips + U-shape + 90° orientation
S300-1L-ST-S-90	Stirrups @ 300 mm c/c + one layer of GFRP strips + side-bonded + 90° orientation
S300-1L-ST-S-45	Stirrups @ 300 mm c/c + one layer of GFRP strips + side-bonded + 45° orientation to the axis of the beam
S200-1L-ST-U-90	Stirrups @ 200 mm c/c + one layer of GFRP strips + U-shape + 90° orientation
S200-1L-ST-S-90	Stirrups @ 200 mm c/c + one layer of GFRP strips + side-bonded + 90° orientation
S200-1L-ST-S-45	Stirrups @ 200 mm c/c + one layer of GFRP strips + side-bonded + 45° orientation to the axis of the beam

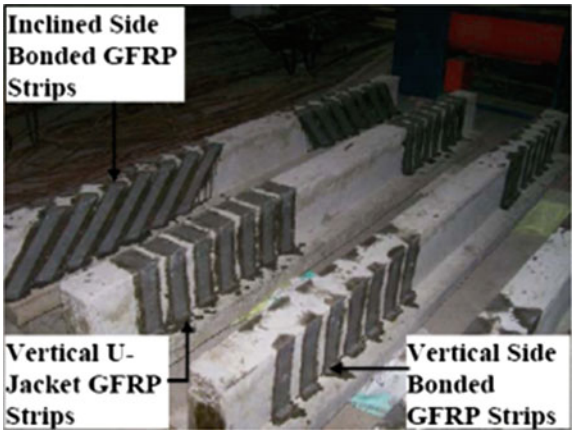

Fig. 3.10 Details of strengthening schemes with bonded GFRP strips

3.4.5 Strengthening Schemes of RC T-beams with Externally Bonded GFRP Sheet in Shear Zone

A set of 9 RC T-beam specimens were prepared. The beams were strengthened in shear with externally bonded GFRP sheet in shear zone (Panda et al. 2013b). The RC T-beams were strengthened with one layer of GFRP sheet in U-jacket (U-shape) around the web of the T-beams, side-bonded on both sides of the web of the T-beam and U-jacket (U-shape) with anchorage. The anchorage was provided by bonding a certain length of sheet to the bottom surface of the flange. The designation S200-1L-SZ-U-90 indicates, that the beam specimen is provided with steel stirrups @ 200 mm c/c (S200), strengthened with one layer of GFRP sheet (1L),

in shear zone (SZ) around the web of the T-beams (U), and orientation of the fibre angle 90° to the longitudinal axis of the beam. The details of the RC T-beam specimens are presented in Table 3.5.

The details of strengthening schemes with bonded GFRP sheet in shear zone is presented in Fig. 3.11.

Table 3.5 Details of RC T-beams strengthened in shear with externally bonded GFRP sheet in shear zone (Panda et al. 2013b)

Specimen designation	Strengthening schemes
S0-1L-SZ-S-90	Without stirrups + one layer of GFRP sheet in shear zone + side-bonded + orientation of the fibre 90° to the axis of the beam
S0-1L-SZ-U-90	Without stirrups + one layer of GFRP sheet in shear zone + U-jacket + orientation of the fibre 90° to the axis of the beam
S0-1L-SZ-UA-90	Without stirrups + one layer of GFRP sheet in shear zone + U-jacket with anchorage + orientation of the fibre 90° to the axis of the beam
S300-1L-SZ-S-90	Stirrups @ 300 mm c/c + one layer of GFRP sheet in shear zone + side-bonded + orientation of the fibre 90° to the axis of the beam
S300-1L-SZ-U-90	Stirrups @ 300 mm c/c + one layer of GFRP sheet in shear zone + U-jacket + orientation of the fibre 90° to the axis of the beam
S300-1L-SZ-UA-90	Stirrups @ 300 mm c/c + one layer of GFRP sheet in shear zone + U-jacket with anchorage + orientation of the fibre 90° to the axis of the beam
S200-1L-SZ-S-90	Stirrups @ 200 mm c/c + one layer of GFRP sheet in shear zone + side-bonded + orientation of the fibre 90° to the axis of the beam
S200-1L-SZ-U-90	Stirrups @ 200 mm c/c + one layer of GFRP sheet in shear zone + U-jacket + orientation of the fibre 90° to the axis of the beam
S200-1L-SZ-UA-90	Stirrups @ 200 mm c/c + one layer of GFRP sheet in shear zone + U-jacket with anchorage + orientation of the fibre 90° to the axis of the beam

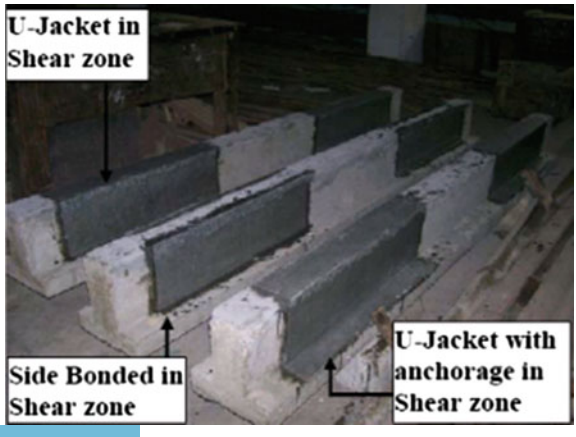

Fig. 3.11 Details of strengthening schemes with bonded GFRP sheet in shear zone

3.5 Materials Used and Their Properties

Ordinary Portland cement (OPC-43 grade) and 12.5 mm down-graded coarse aggregates were used for the preparation of concrete. The physical properties of cement and aggregates are presented in Tables 3.6 and 3.7 (Panda et al. 2011b, 2013b).

The mix design of concrete used in the experimental investigation was M30 grade. The mix proportion of the ingredients was (1:0.946:2.03). The water/cement (w/c) used 0.375 for the preparation of concrete mix. The slump test was done for each batch of concrete mixing, the slump values were varying between 30 and 50 mm. Compressive strength on cubes and cylinders were measured at 7 and 28 days of curing the sample. The split tensile strength and modulus of elasticity were calculated after 28 days. The average value of split tensile strength and modulus of elasticity was 3.00 MPa and 3.5×10^4 MPa respectively. The compressive strength test results of cubes and cylinders are listed in Table 3.8.

The transverse and longitudinal steel reinforcements used in the RC T-beam were tested in the laboratory according to the Indian Standards. The grade of longitudinal steel reinforcement Fe 415 and transverse reinforcement Fe 250 were used in the experiment. The test results of steel are presented in Table 3.9 (Panda et al. 2011a, 2012, 2013a, b).

Glass fibre fabric of thickness 0.32 mm was used for strengthening of RC T-beams. Epoxy adhesive was used to attach the glass fabric to the beam; the resin used was a 9:1 mixture of Araldite CY-230 and hardener HY-951 (Panda et al. 2010, 2011a, 2012, 2013a, b, 2015). The coupons of one layer, two layers and three layers of glass fibre composites were prepared and tested in a universal testing machine (UTM). The sketch of the coupon specimens for tension test is shown in Fig. 3.12.

Table 3.6 Physical properties of cement

Characteristics	Experimental results	Manufacturer results	Value specified by IS 8112: (1989)
Normal consistency of cement (%)	31	29	NA
Fineness of cement (m^2/Kg)	311	308	225 (min)
Setting time of cement (min)			
(a) Initial	130	125	30 (min)
(b) Final	210	220	600 (max)
Specific gravity of cement	3.10	NA	3.15
Compressive strength of cement (MPa)			
(a) 3 days strength	23.5	37	23 (min)
(b) 7 days strength	35.54	45	33 (min)
(c) 28 days strength	49.30	55	43 (min)

Cement used: Ordinary Portland Cement (43 grade)

Table 3.7 Physical properties of aggregates

Characteristics	Experimentally obtained value as per IS 383: (1970)	
	Coarse aggregate	Fine aggregate
Type of aggregate	Crushed	Natural
Maximum size of aggregate (mm)	12.5 (Angular)	4.75
Specific gravity of aggregate	2.95	2.64
Total water absorption (%)	0.53	0.30
Fineness modulus of aggregate	5.00	2.73 (Grading zone II) Medium sand
Free surface moisture (%)	Nil	2

Table 3.8 Compressive strength test results of cubes and cylinders

Specimen designation	No. of beam samples	Mean compressive strength of cube (7 days) (MPa)	Mean compressive strength of cube (28 days) (MPa)	Mean compressive strength of cylinder (7 days) (MPa)	Mean compressive strength of cylinder (28 days) (MPa)
S0-0L	3	35.71	49.61	28.42	42.16
S200-0L	3	45.40	59.78	32.52	42.67
S300-0L	3	45.00	57.62	32.92	39.53
S0-1L-CT-U-90	3	43.73	51.76	30.50	38.78
S0-2L-CT-U-90					
S0-3L-CT-U-90					
S200-1L-CT-U-90	3	40.11	51.44	31.91	41.03
S200-2L-CT-U-90					
S200-3L-CT-U-90					
S300-1L-CT-U-90	3	46.73	52.06	35.10	39.35
S300-2L-CT-U-90					
S300-3L-CT-U-90					
S0-1L-CT-S-90	3	43.86	53.21	29.14	40.09
S0-2L-CT-S-90					
S0-3L-CT-S-90					
S200-1L-CT-S-90	3	42.46	51.38	31.36	40.66
S200-2L-CT-S-90					
S200-3L-CT-S-90					
S300-1L-CT-S-90	3	44.81	53.66	29.77	40.67
S300-2L-CT-S-90					
S300-3L-CT-S-90					
S0-1L-ST-U-90	3	43.10	52.18	32.14	40.03
S0-1L-ST-S-90					
S0-1L-ST-S-45					
S200-1L-ST-U-90	3	39.90	53.62	30.02	37.83
S200-1L-ST-S-90					
S200-1L-ST-S-45					

(continued)

Table 3.8 (continued)

Specimen designation	No. of beam samples	Mean compressive strength of cube (7 days) (MPa)	Mean compressive strength of cube (28 days) (MPa)	Mean compressive strength of cylinder (7 days) (MPa)	Mean compressive strength of cylinder (28 days) (MPa)
S300-1L-ST-U-90	3	43.66	51.03	31.87	38.28
S300-1L-ST-S-90					
S300-1L-ST-S-45					
S0-1L-SZ-U-90	3	38.71	52.22	32.15	39.58
S0-1L-SZ-S-90					
S0-1L-SZ-UA-90					
S200-1L-SZ-U-90	3	43.87	62.17	33.44	40.38
S200-1L-SZ-S-90					
S200-1L-SZ-UA-90					
S300-1L-SZ-U-90	3	44.72	69.93	31.10	42.08
S300-1L-SZ-S-90					
S300-1L-SZ-UA-90					

Table 3.9 Test results of steel reinforcement

Diameter (mm)	Yield stress (MPa)	Ultimate stress (MPa)	Modulus of elasticity (GPa)	Yield strain (μstrains)
20 (Fe 415)	500	590	200	2500
8 (Fe 415)	503	646	180	2794
6 (Fe 250)	252	461	200	–

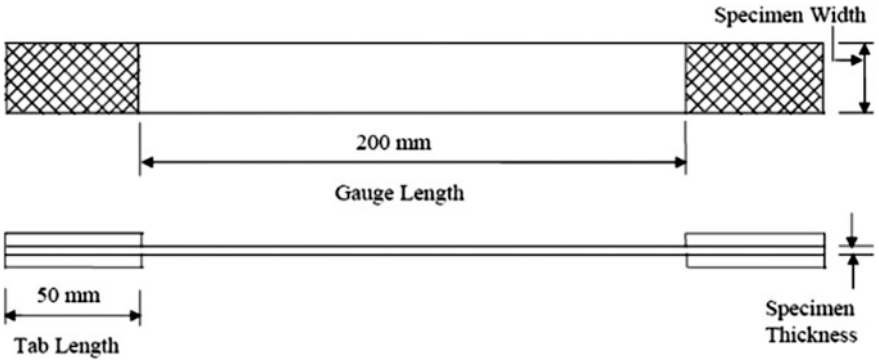

Fig. 3.12 Sketch of the coupon specimen for tension test

The thickness of one layer of GFRP was 0.36 mm. The ultimate tensile strength measured was 160 MPa and the elastic modulus was 13.18 GPa. The summary of coupon test results of GFRP is presented in Table 3.10. The UTM with coupon

Table 3.10 Summary of GFRP Coupon Test Results. (a) Test Results of One Layer GFRP Sheet. (b) Test Results of Two Layers GFRP Sheet. (c) Test Results of Three Layers GFRP Sheet

(a)				
Characteristics	Test results obtained by UTM			
	GFRP-1-S1	GFRP-1-S2	GFRP-1-S3	Average
Width (mm)	19.10	18.80	19.00	18.97
Thickness (mm)	0.36	0.36	0.36	0.36
Area (mm^2)	6.88	6.77	6.84	6.83
Ultimate load (kN)	1.10	1.10	1.15	1.12
Ultimate strength (MPa)	159.88	162.48	168.13	**163.50**
(b)				
Characteristics	Test results obtained by UTM			
	GFRP-2-S1	GFRP-2-S2	GFRP-2-S3	Average
Width (mm)	18.80	18.00	19.00	18.60
Thickness (mm)	0.72	0.72	0.72	0.72
Area (mm^2)	13.54	12.96	13.68	13.40
Ultimate load (kN)	2.50	2.10	2.20	2.27
Ultimate strength (MPa)	184.64	162.04	160.82	**169.17**

(c)							
Characteristics	Test results obtained by UTM						
	GFRP-3-S1	GFRP-3–S2	GFRP-3-S3	GFRP-3-S4	GFRP-3-S5	GFRP-3-S6	Average
Width (mm)	19.00	18.90	19.10	19.20	18.80	18.78	18.93
Thickness (mm)	1.08	1.08	1.08	1.08	1.08	1.08	1.08
Area (mm^2)	20.50	20.40	20.60	20.74	20.30	20.28	20.44
Ultimate load (kN)	4.20	3.61	3.43	4.50	3.80	3.60	3.97
Ultimate strength (MPa)	204.80	177.00	166.50	217.00	187.20	177.50	**188.34**
Modulus of elasticity (GPa)	15.48	13.47	10.91	12.30	12.55	14.36	**13.18**
Ultimate elongation (%)	1.32	1.31	1.53	1.58	1.35	1.31	1.41

Fig. 3.13 UTM showing the coupon specimen

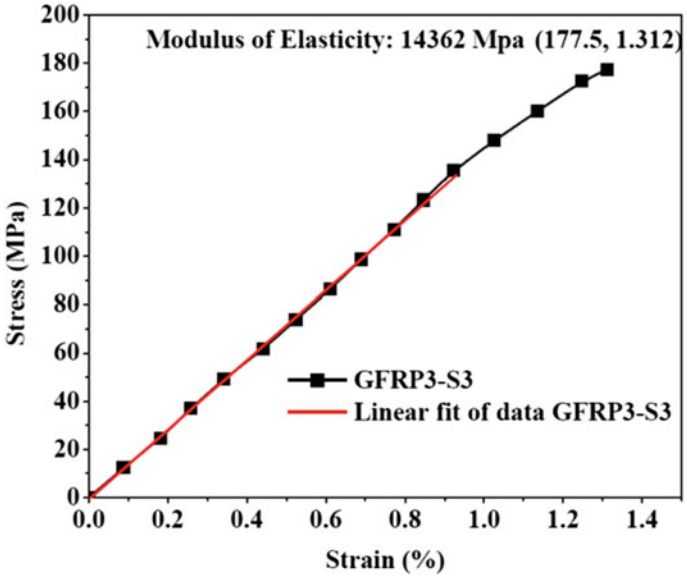

Fig. 3.14 Stress versus strain plot (GFRP3-S6)

specimen is shown in Fig. 3.13. The stress–strain plot of GFRP sheet for specimen GFRP3-S6 is shown in Fig. 3.14.

For the present work, the following experimental data were used for all calculations and interpretations.

Ultimate strength used for theoretical calculation = 160 MPa.

Average modulus of elasticity = 13.18 GPa

Ultimate elongation = (160/13180) = 0.01214 = 1.214%

3.6 Test Setup and Instrumentation

All T-beam specimens were tested using two-point loading with shear span (a) to effective depth (d) ratio equal to 3.26. The tests were conducted at the Structural Laboratory, IIT Kharagpur using 300 T capacity Universal Testing Machine. Figure 3.15 shows the details of the test setup. The load was applied monotonically to the test beam until failure. Strains, deflections and the applied load were recorded at every 6 kN load increment up to 60 kN, thereafter the load increment was 10 kN till the failure of the beam.

3.6.1 Dial Gauge Positions

Dial gauges were used to monitor vertical displacements. One dial gauge was located at the midspan of the beam. Two were located at the centre of the shear zone and the other two were located below the loading points on either side of the beam as shown in Fig. 3.16 (Panda et al. 2010, 2011a, 2012, 2013a, b, 2015).

3.6.2 Internal Strain Gauge Positions

Two types of electrical strain gauges were used in the experiment to measure the strains in GFRP sheet and strips, concrete surface, longitudinal steel and transverse steel. Gauges BKNIC-10 (Gauge length 10 mm, Gauge factor 2.00 ± 2%, Resistance 355.0 ± 0.5 Ω) placed on the surface of the longitudinal and transverse steel reinforcement and gauges BKCT-30 (Gauge length 30 mm, Gauge factor

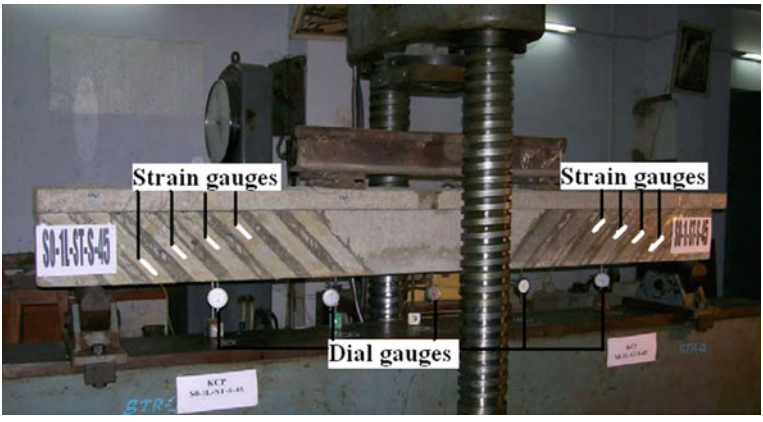

Fig. 3.15 Test setup

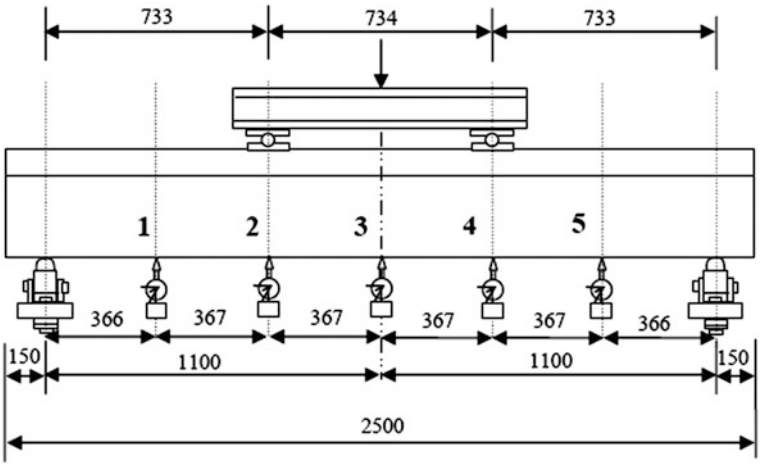

Fig. 3.16 Dial gauge positions

2.00 ± 2%, Resistance 350.5 ± 0.5 Ω) placed on the concrete surface were used in the experiment. BKNIC-10 was attached on the longitudinal and transverse steel to measure strain during the different stages of loading (Panda et al. 2010, 2011a, 2012, 2013a, b, 2015). In S0-1L-CT-S-90- and S0-2L-CT-S-90-strengthened RC T-beam specimens, one strain gauge (ISg1) was attached in the longitudinal steel surface at 150 mm distance from the left support, whereas in S0-3L-CT-S-90-strengthened specimen two strain gauges (ISg1 and ISg4) were used in the longitudinal steel surface at 150 and 650 mm distance from the left support. In S200-1L-CT-S-90- and S200-2L-CT-S-90-strengthened RC T-beam specimens, three strain gauges (ISg1, ISg2 and ISg3) were attached, one in the longitudinal steel surface at 150 mm distance from the left support and the other two strain gauges were attached in stirrups in shear zone at locations (200, 90), and (400, 145) from the support. In S200-3L-CT-S-90-strengthened specimen, four strain gauges (ISg1, ISg2, ISg3 and ISg4) were attached. Similarly, in S300-1L-CT-S-90- and S300-2L-CT-S-90-strengthened RC T-beam specimens, three strain gauges were attached, one in the longitudinal steel surface at 150 mm distance from the left support and the other two strain gauges were attached in stirrups at locations (350, 90), and (650, 145) from the support. In S300-3L-CT-S-90 strengthened specimen, four strain gauges were attached (Panda et al. 2011a). Figures 3.17 and 3.18 show the internal strain gauge location details in longitudinal steel and transverse steel for series S300.

The strain gauge position of U-jacketing was also same as used in the side-bonded strengthened T-beams.

The RC T-beams strengthened with GFRP strips, in specimen S0-1L-ST-U-90 and S0-1L-ST-S-90 one strain gauge was attached on the longitudinal steel surface at 150 mm distance from the support, whereas in S0-1L-ST-U-45 strengthened

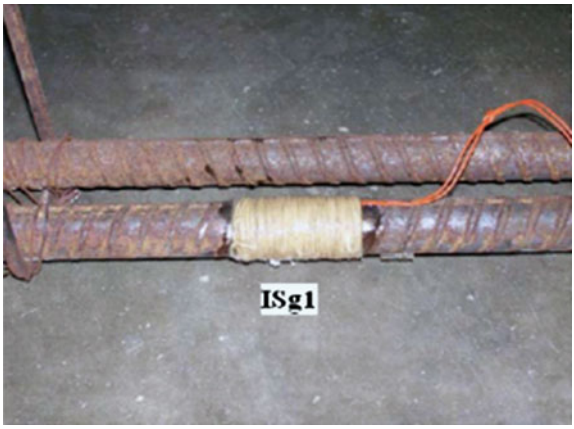

Fig. 3.17 Location of internal strain gauge in longitudinal steel

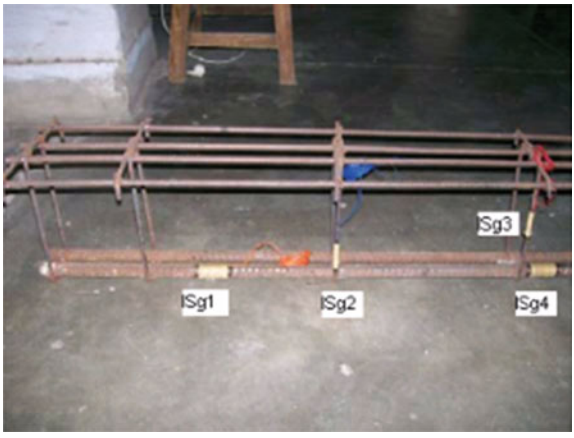

Fig. 3.18 Location of internal strain gauge in longitudinal steel and stirrups

specimen two strain gauges were attached on the longitudinal steel surface at 150 mm, 650 mm distance from the support. In S200-1L-ST-U-90, and S200-1L-ST-S-90 strengthened specimens three strain gauges were used, whereas in S200-1L-ST-S-45 strengthened specimen four strain gauges were used. The positions were the same as used in the side shape. Similar pattern was followed in S300-1L-ST-U-90, S300-1L-ST-S-90 and S300-1L-ST-S-45 strengthened specimens (Panda et al. 2011b, c, 2013a).

Similarly the RC T-beams strengthened in shear zone with GFRP sheet, in specimens S0-1L-SZ-U-90 and S0-1L-SZ-S-90 one strain gauge was attached on the longitudinal surface at 150 mm distance from the support. In S0-1L-SZ-UA-90, two strain gauges were attached on the longitudinal steel surface at 150 and 650 mm distance from the support. In S200-1L-SZ-U-90 and S200-1L-SZ-S-90, three strain gauges were attached. In S200-1L-SZ-UA-90 specimen, four strain

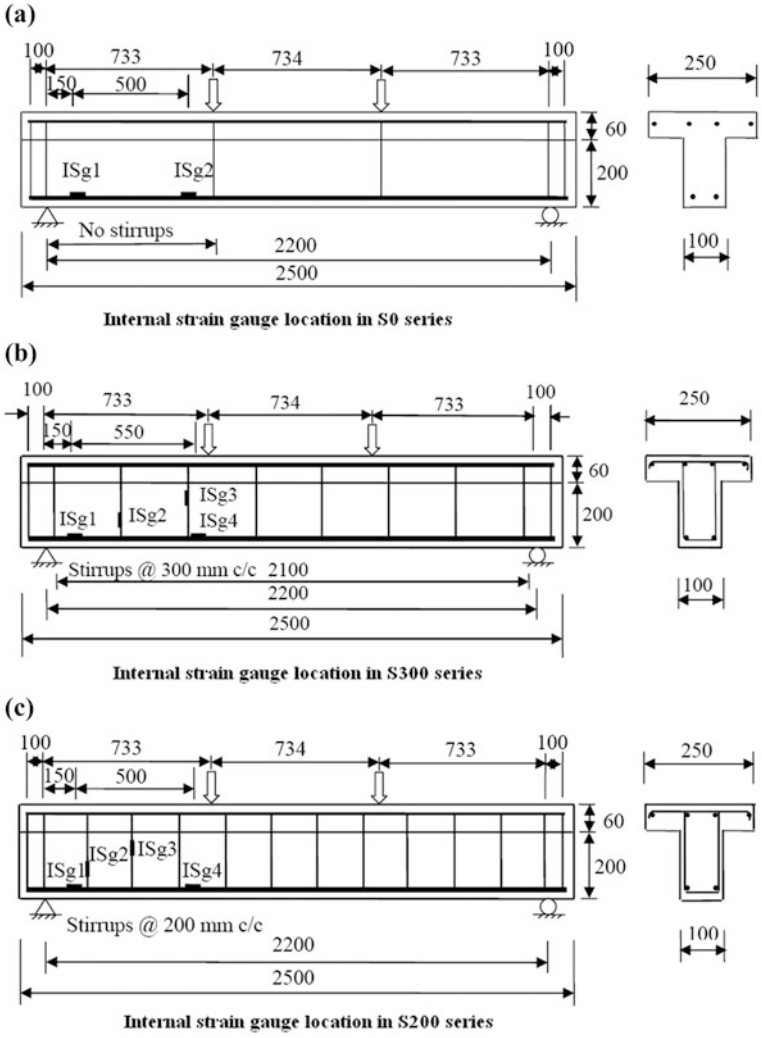

Fig. 3.19 Internal strain gauge position

gauges were attached. The positions of the strain gauges were the same as used in the side shape. The same pattern was used in S300-1L-SZ-U-90, S300-1L-SZ-S-90 and S300-1L-SZ-UA-90 specimens (Panda et al. 2013b). The schematic diagram of the internal strain gauge locations for three series is shown in Fig. 3.19.

3.6.3 External Strain Gauge Positions

BKCT-30 strain gauges were attached on the side face of the web of the RC T-beams and to the GFRP surface on the side of the web of the strengthened RC T-beams and oriented in the fibre direction.

(a) **External Strain Gauge on Control Beam**
Six strain gauges were used on the concrete surface of the control RC T-beam. Three strain gauges were attached at the middle of each side of the shear zone as a strain rosette. Figure 3.20 shows the surface strain gauges locations on control beams.

(b) **External Strain Gauge on Strengthened Beams for U-jacket with Layers**
Eight strain gauges were attached to the GFRP surface in the shear zone of the strengthened RC T-beams. Four strain gauges were attached on each side of the strengthened RC T-beam as per the probable cracking pattern position of the control RC T-beam. The coordinates of strain gauges from left support considering bottom corner as (0, 0) in strengthened RC T-beams of series S0, S300 and S200 for Sg1, Sg2, Sg3 and Sg4 were (150, 50), (250, 100), (350, 100) and (450, 150) respectively. Similarly, the coordinates for Sg5, Sg6, Sg7 and Sg8 were used from right support. The details of surface strain gauge locations of RC T-beams are shown in Fig. 3.21 (Panda et al. 2012).

(c) **External Strain Gauge on Strengthened Beams for Side-Bonding with Layers**
Eight strain gauges were mounted to the GFRP surface in the shear zone of the strengthened T-beams. The details of strain gauge positions are shown in Fig. 3.22 (Panda et al. 2011a).

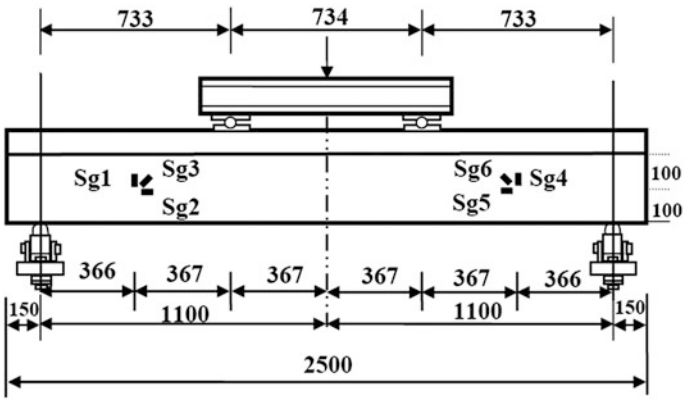

Fig. 3.20 Surface strain gauges location on control beam

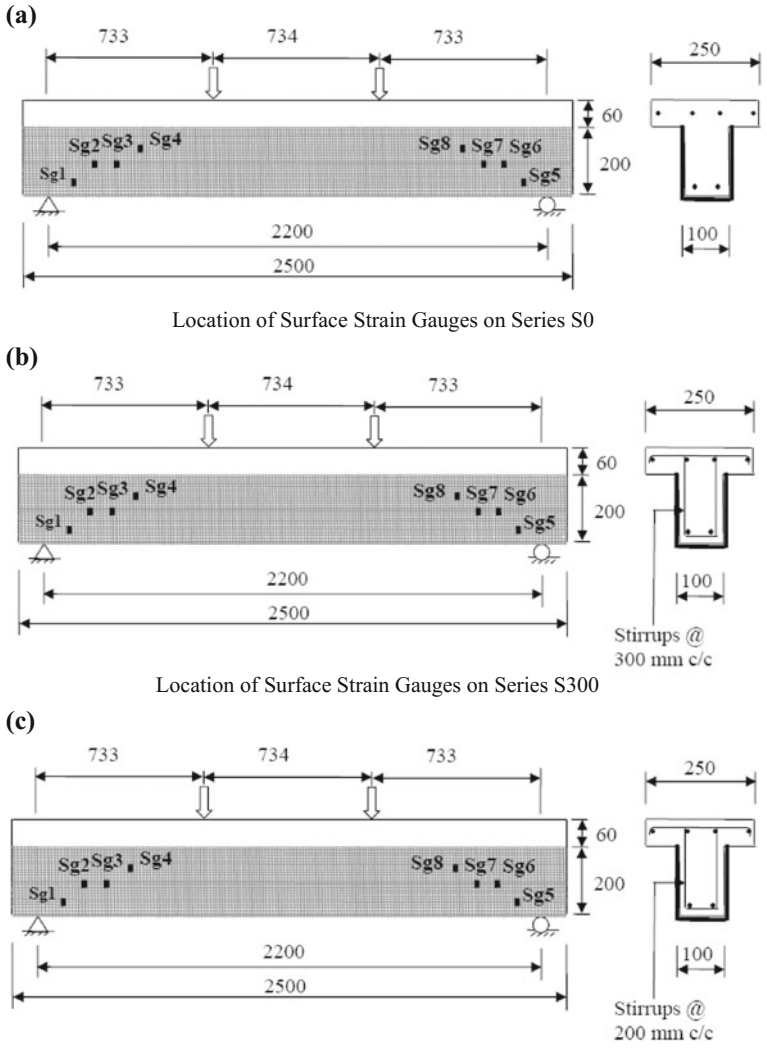

Fig. 3.21 Details of surface strain gauge positions (U-jacket)

(d) **External Strain Gauge on Strengthened Beams for GFRP Strips**
Eight strain gauges were mounted to the GFRP strips in the shear zone of the strengthened T-beams. The details of strain gauge locations are shown in Fig. 3.23 (Panda et al. 2013a).

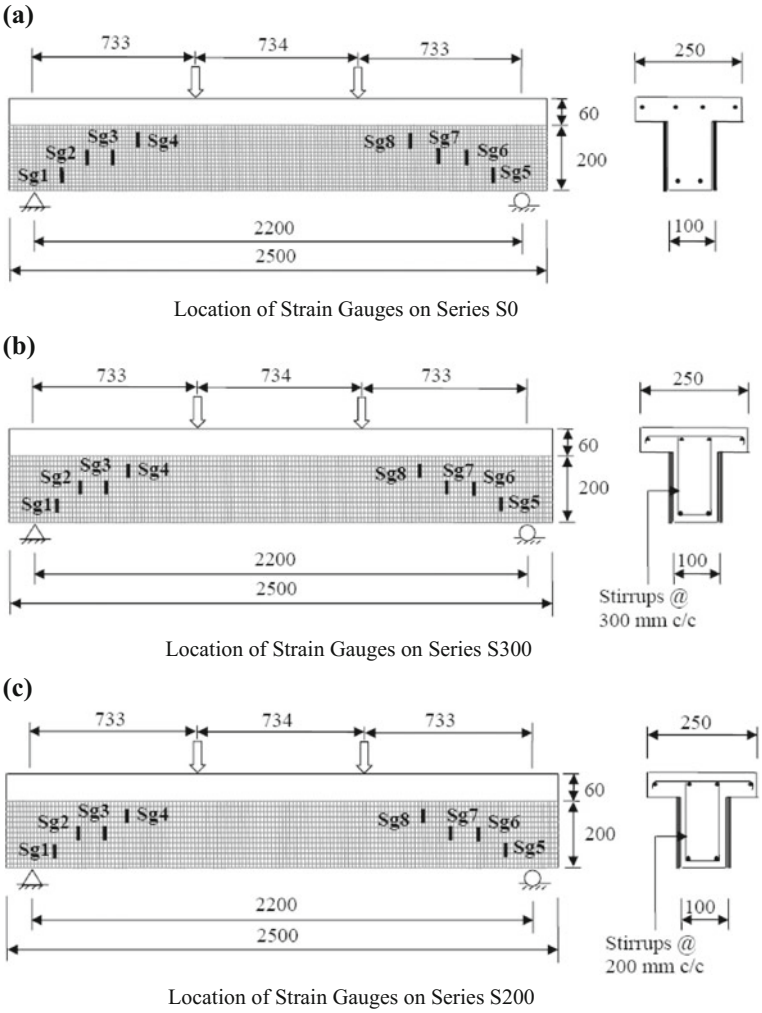

Fig. 3.22 Details of surface strain gauge positions (side-bonding)

(e) **External Strain Gauge on Strengthened Beams for GFRP Sheet in Shear Zone**

Eight strain gauges were mounted to the GFRP surface in the shear zone in S0 series. Four strain gauges were attached on each side of the strengthened beam. Whereas in S300 and S200 series 12 strain gauges were attached to the GFRP surface. Six strain gauges were attached on each side, extra two strain gauges were attached at a coordinate of (350, 100) in horizontal and diagonal direction to measure the horizontal and diagonal strain of GFRP surface. The details of strain gauge positions are shown in Fig. 3.24 (Panda et al. 2013b).

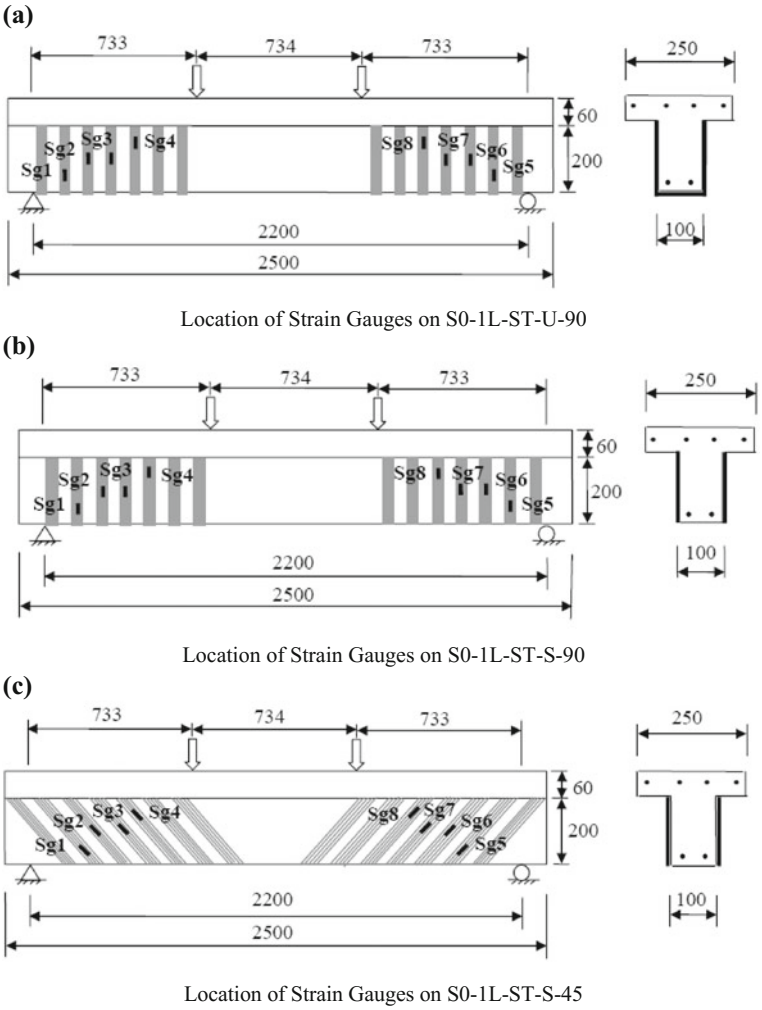

Fig. 3.23 Details of surface strain gauge positions (GFRP strips)

(d)

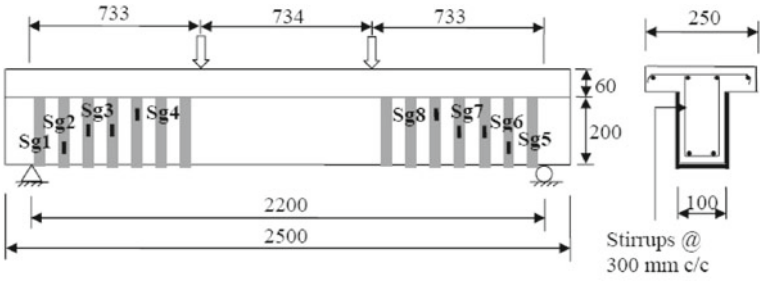

Location of Strain Gauges on S300-1L-ST-U-90

(e)

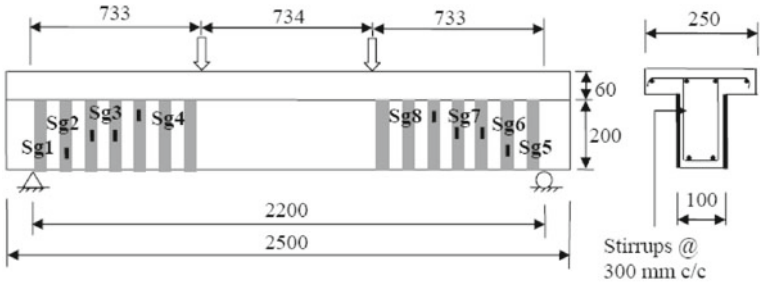

Location of Strain Gauges on S300-1L-ST-S-90

(f)

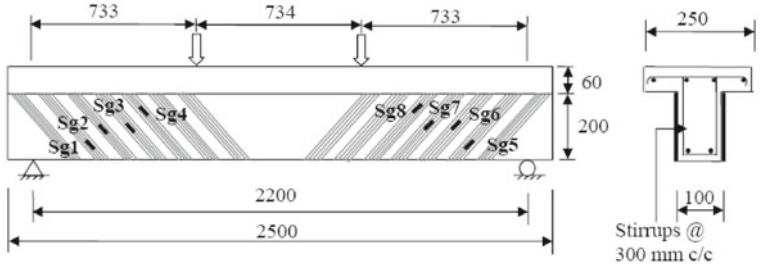

Location of Strain Gauges on S300-1L-ST-S-45

Fig. 3.23 (continued)

(g)

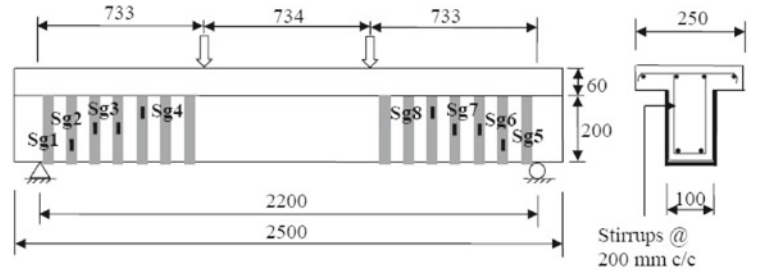

Location of Strain Gauges on S200-1L-ST-U-90

(h)

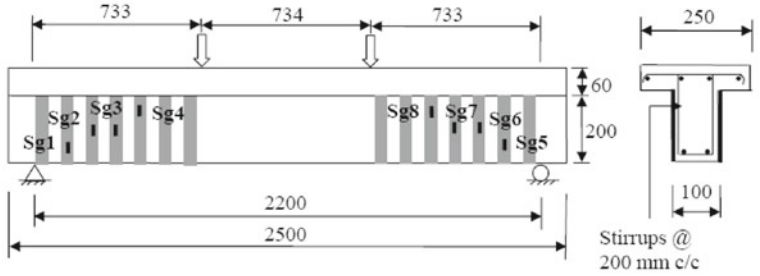

Location of Strain Gauges on S200-1L-ST-S-90

(i)

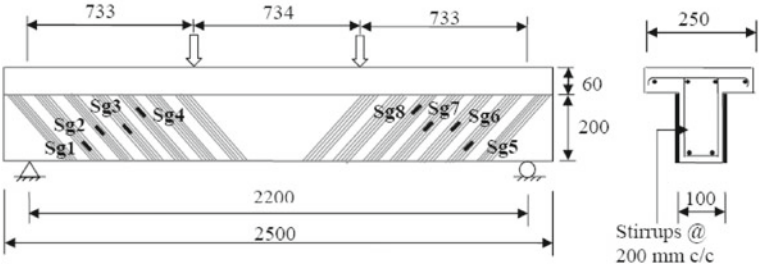

Location of Strain Gauges on S200-1L-ST-S-45

Fig. 3.23 (continued)

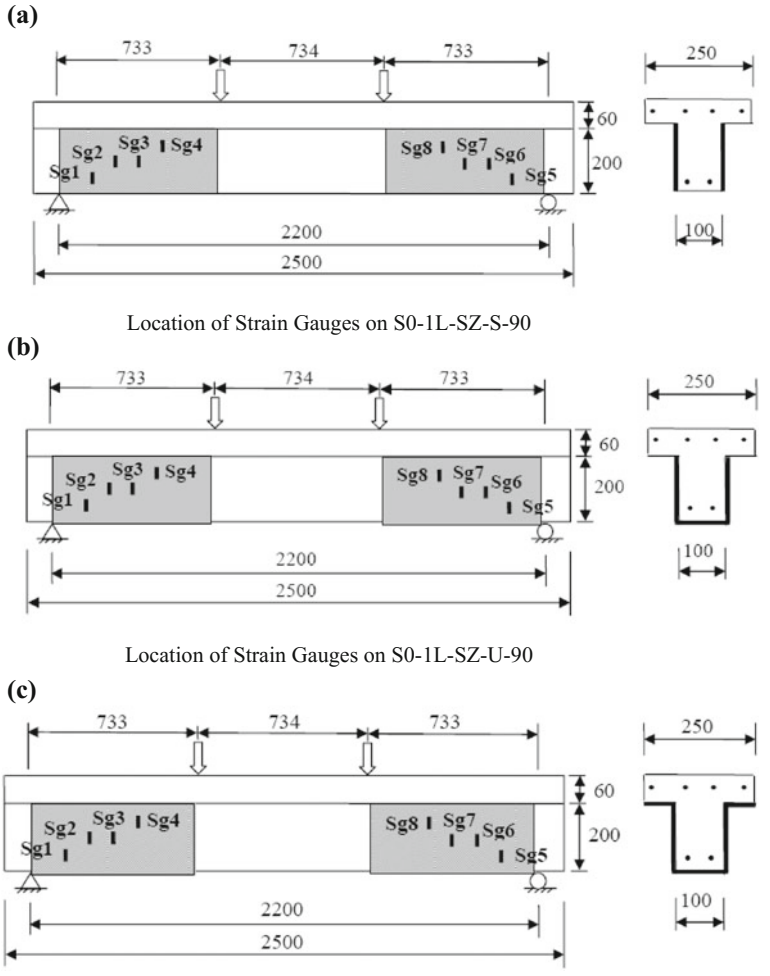

Fig. 3.24 Details of surface strain gauge positions (GFRP sheet in shear zone)

(d)

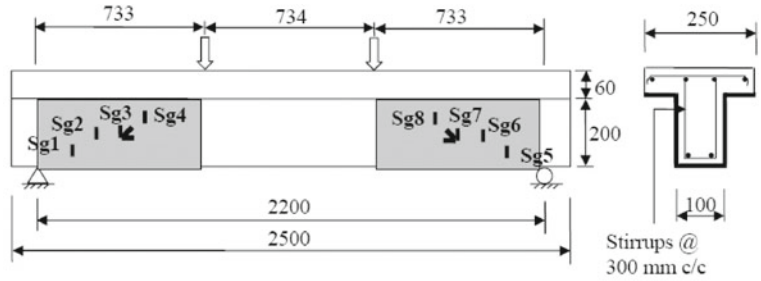

Location of Strain Gauges on S300-1L-SZ-UA-90

(e)

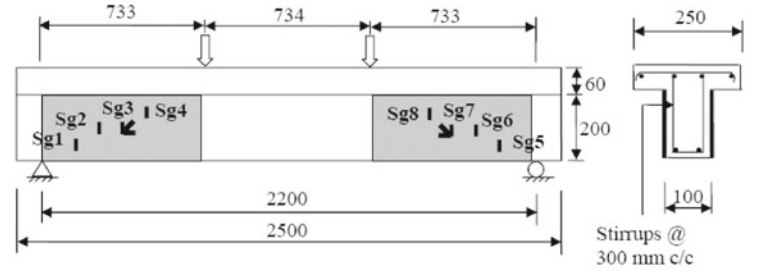

Location of Strain Gauges on S300-1L-SZ-S-90

(f)

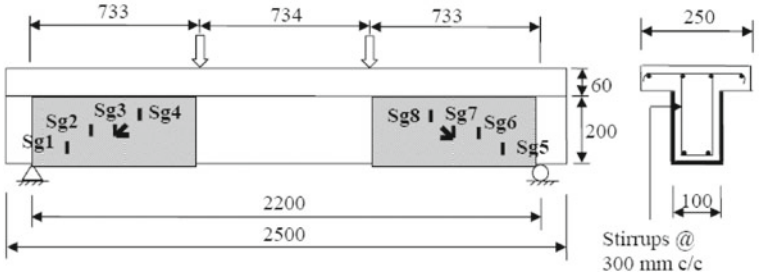

Location of Strain Gauges on S300-1L-SZ-U-90

Fig. 3.24 (continued)

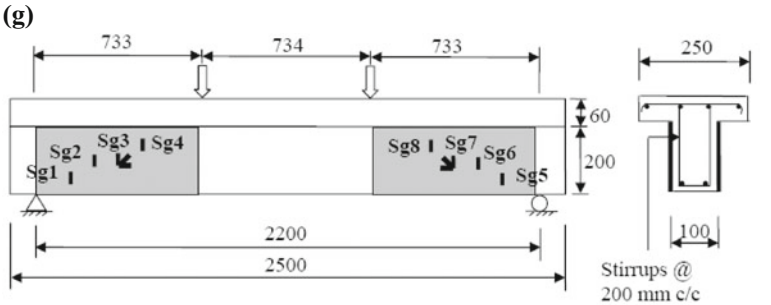

Location of Strain Gauges on S200-1L-SZ-S-90

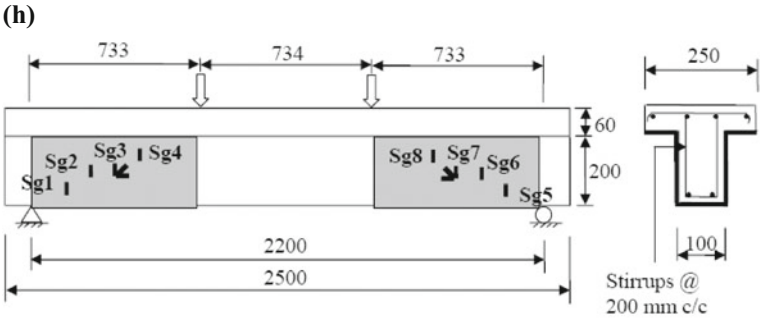

Location of Strain Gauges on S200-1L-SZ-U-90

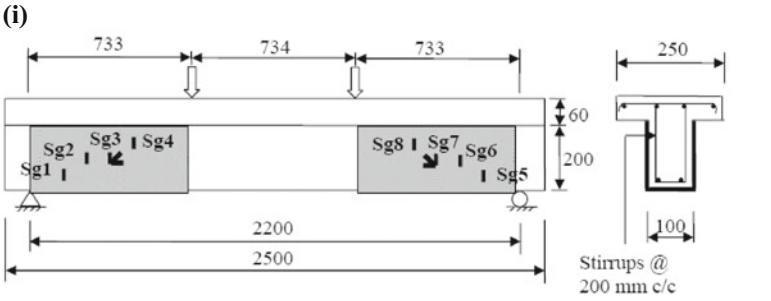

Location of Strain Gauges on S200-1L-SZ-UA-90

Fig. 3.24 (continued)

3.7 Summary

This chapter discusses the overall experimental investigation carried out during the experimental works. The detail geometry of the RC T-beams is presented for all the series. The strengthening process of RC T-beams, types of strengthening schemes with different configurations, orientations of GFRP sheets and strips are also discussed. The materials used for the experimental works with all material properties are also explained.

References

Bureau of Indian Standard, Plain and Reinforced Concrete Code of Practice IS 456: 2000, New Delhi, India, 100 pp

Bureau of Indian Standards, 43 Grade Ordinary Portland Cement Specification, (First Revision) IS: 8112-:1989. New Delhi, India

Bureau of Indian Standards, Recommended Guidelines for Concrete Mix Design IS: 10262 (1982), New Delhi, India

Bureau of Indian Standards, Indian Standard Specification for Coarse and Fine Aggregates from Natural Sources for Concrete (Second Revision) IS: 383 (1970), New Delhi, India

Panda KC, Bhattacharyya SK, Barai SV (2010) Shear behaviour of reinforced concrete T-beams with U-bonded glass fibre reinforced plastic sheet. Indian Concr J (ICJ) 84(10):61–71

Panda KC, Bhattacharyya SK, Barai SV (2011a) Shear strengthening of RC T-beams with externally side bonded GFRP sheet. J Reinf Plast Compos 30(13):1139–154

Panda KC, Bhattacharyya SK, Barai SV (2011b) Strengthening of RC T-beams with shear deficiencies using GFRP strips. J Civil Eng Archit 05(1):56–67

Panda KC, Bhattacharyya SK, Barai SV (2011c) Influence of transverse steel on the performance of RC T-beams strengthened in shear with GFRP strips. Advances in FRP composite in civil engineering, Springer, India, vol II, pp 763–766

Panda KC, Bhattacharyya SK, Barai SV (2012) Shear behaviour of RC T-beams strengthened with U-wrapped GFRP sheet. Steel Compos Struct Int J 12(2):149–166

Panda KC, Bhattacharyya SK, Barai SV (2013a) Shear strengthening effect by bonded GFRP strips and transverse steel on RC T-beams. Struct Eng Mech Int J 47(1):75–98

Panda KC, Bhattacharyya SK, Barai SV (2013b) Effect of transverse steel on the performance of RC T-beams strengthened in shear zone with GFRP sheet. Constr Build Mater 41:79–90

Panda KC, Bhattacharyya SK, Barai SV (2015) Strain analysis of RC T-beams strengthened in shear with variation of U-wrapped GFRP sheet and transverse steel. In: Advances in Structural Engineering, vol 3. Springer, India, no 154, pp 2001–2010

Chapter 4
Major Findings from Experiments on Shear Strengthening of Beams

4.1 General

This chapter presents the major findings from experiments on shear strengthening of beams. The experiments have been carried out in different phases as described in the experimental investigation, presented in Chap. 3.

In the *first phase* of experimental investigation, beams were tested as control RC T-beams in three different series S0, S300 and S200. The experimental results collected are presented herein along with the plots and discussions. In the *second phase* of the experimental investigation, beams were tested as RC T-beams strengthened in shear with one layer, two layers and three layers of externally bonded U-jacketed GFRP sheets for each variety of series. The *third phase* of experimental investigation comprises testing of RC T-beams strengthened in shear with one layer, two layers and three layers of externally bonded GFRP sheets on sides of the web of T-beams for each of series. In the *fourth phase* of experimental investigation, RC T-beams were tested as strengthened beams with externally bonded GFRP strips in different configurations and orientations for each series. In the *fifth phase* of experimental investigation, beams were tested as RC T-beams strengthened in shear with externally bonded GFRP sheet in shear zone for each series. Further, the experimental results of all the strengthened RC T-beams of each phase of the study were compared with the control specimens of same series.

4.2 Control Beams

Nine RC T-beams were used as control beams with three different stirrup spacing S0 (no stirrups), S300 (stirrups at a spacing of 300 mm) and S200 (stirrups at a spacing of 200 mm). Three specimens were tested for each of the stirrup spacing.

K. C. Panda et al., *Shear Strengthening of T-beam with GFRP*, Springer Transactions in Civil and Environmental Engineering, https://doi.org/10.1007/978-981-10-7760-9_4

The average shear strength result was used to find out the effectiveness of the RC T-beams strengthened in shear with GFRP sheets and strips. The cracking pattern and modes of failure of the specimen for each stirrups spacing were discussed. The deflection and the strain on longitudinal steel, transverse steel and on concrete surfaces were measured by using dial gauges and strain gauges as explained in Chap. 3.

4.2.1 Deflection Measurements

Dial gauges were used to measure the deflection of control beams. Figure 4.1 shows the midspan deflection of control beams for three different series. Also, the deflections at midpoint of the right and left shear zones of the control beams of three different series are shown in Fig. 4.2.

It is observed from Figs. 4.1 and 4.2 that the midspan deflection and the deflection at midpoint of the shear zone decrease as shear reinforcement increases. The deflection in S0-0L specimen is observed as 6.44 mm corresponding to the failure load of 100 kN, whereas the deflections in S300-0L and S200-0L specimens are 9.71 and 9.98 mm corresponding to the failure load of 140 and 150 kN.

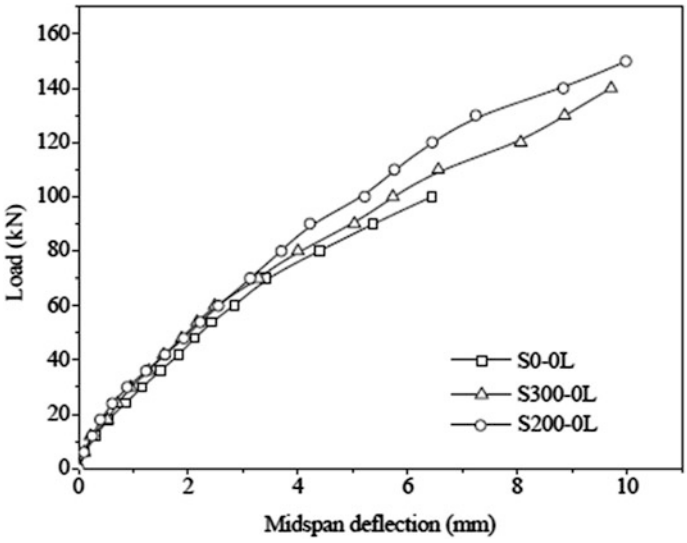

Fig. 4.1 Midspan deflection of control specimens

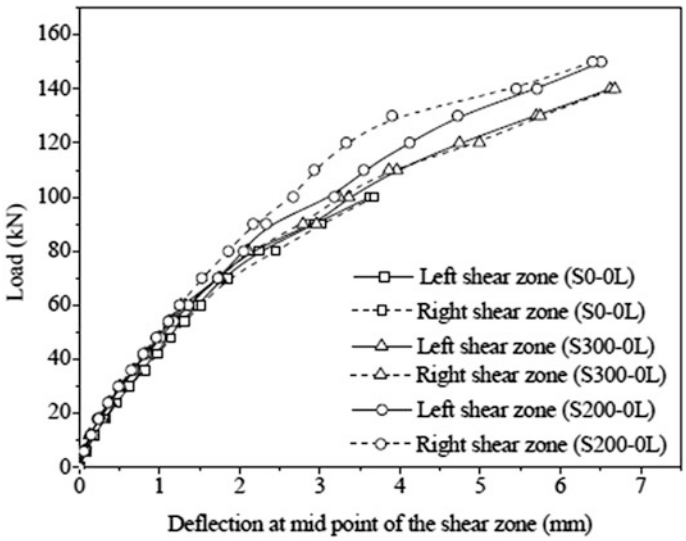

Fig. 4.2 Deflection at midpoint of the shear zones

4.2.2 Strain Measurements

The BKNIC-10 strain gauges were used to measure the strain in longitudinal and transverse steel, and BKCT-30 strain gauges were used to measure the strain on concrete surface. The strain gauge positions are indicated in Chap. 3. The strains were measured for each increment of load using digital strain indicators.

The strain gauges were attached to the concrete surface in the form of strain rosette in the shear zone on both sides of the control RC T-beams. The shear strain of concrete was calculated from the strain rosette values. The load versus shear strain graph is plotted for series S0, S300 and S200 as shown in Fig. 4.3 (Panda et al. 2013b).

It may be observed from Fig. 4.3 that the shear strain of concrete in the control RC T-beams increases slowly up to 60–70 kN loads at the initial stage of loading. Thereafter as load increases, the shear strain increases rapidly in S0-0L, S300-0L and S200-0L specimens. Further, it is observed that, at the initial stage of loading up to 70 kN load, the difference in shear strain is comparatively less for control RC T-beam specimens S0-0L, S300-0L and S200-0L. As load increases, the shear strain capacity of control RC T-beam increases with the increasing shear reinforcement. As expected, with the increase in shear reinforcement, the shear strain of the control beam also increases (Panda et al. 2013b).

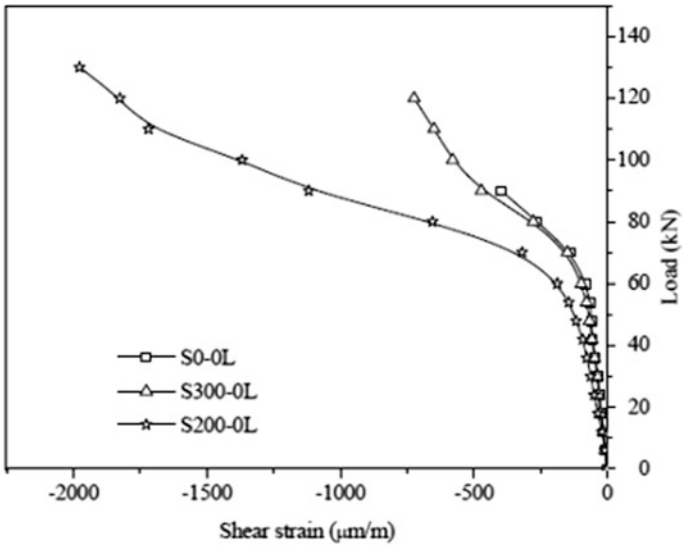

Fig. 4.3 Shear strain at centre of shear zone of the control beams

4.2.3 Cracking Pattern and Modes of Failure of Control Beams

The RC T-beam control specimens were tested with monotonically increasing load as shown in Fig. 4.4. No visible cracks were observed till a load level of 70 kN reached. Specimen S0-0L-1 exhibits diagonal shear cracks at a load of 70 kN on both the shear spans. The cracks started at the centre of the shear spans. With increasing load, the developed shear cracks were widened and propagated towards the support and loading points through the flange of the RC T-beams and leading to failure at a load of 104 kN. At the same time, a horizontal crack also appeared at the flange of the RC T-beam at a load of approximately 100 kN. It was observed that at failure, the major crack at the shear spans was inclined at an angle of approximately 42° with horizontal and the width of the crack was approximately 8 mm.

Figure 4.5a shows the cracking pattern of full beam specimen. Figure 4.5b shows the enlarged view-A of the cracks generated in the test specimen S0-0L-1.

The cracking pattern of RC T-beam specimen S300-0L-2 is shown in Fig. 4.6. The inclined cracks of specimen appeared in the shear span after 70 kN load.

The diagonal shear cracks propagated at a load of 90 kN on both the shear spans. As load increased in the control RC T-beam specimen S300-0L-2, the inclined crack widened and propagated towards the support and loading points through the flange, and ultimately failed at a load of 146 kN. It was observed that the angle of the inclined crack and maximum crack width in right shear span was approximately 45° with horizontal and 3 mm, respectively, whereas in left shear span, it was approximately 40° with horizontal and 4 mm, respectively. Also, a crack appeared

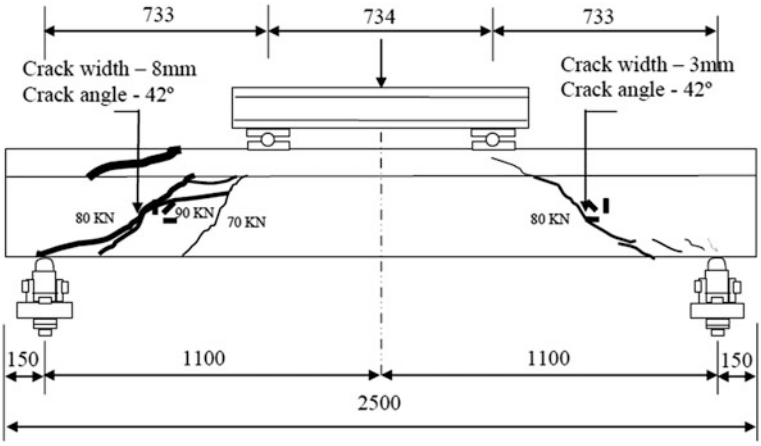

Fig. 4.4 Schematic diagram showing cracking pattern of specimen S0-0L-1

(a) Cracking Pattern of Full Beam Specimen

(b) Enlarged View-A

Fig. 4.5 Cracking pattern and modes of failure of beam specimen S0-0L-1

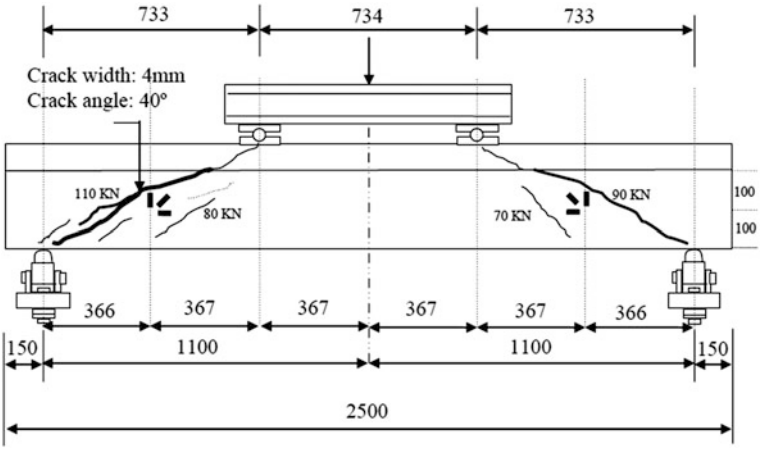

Fig. 4.6 Schematic diagram showing cracking pattern of specimen S300-0L-2

at the top of the flange of the RC T-beam and propagated in longitudinal direction from the loading position for some distance and takes a turn in 90° angle.

Figure 4.7a shows the cracking pattern of the full beam specimen. Figure 4.7b shows the enlarged view-A of the cracks generated in the part of the beam specimen.

Specimen S200-0L-3 exhibits diagonal shear cracks at a load of 90 kN on left shear span and at a load of 100 kN in right shear span as shown in Fig. 4.8.

The initiation of cracks takes place at the centre of both the shear spans. As the load increased, the cracks widen and propagated towards the support and loading points through the flange and lead to failure at a load of 156 kN. The maximum crack width observed in the web was 10 mm. The crack angle in the web was approximately 44° with the horizontal and became horizontal as it reaches near the support and the flange in both the shear spans.

The cracking pattern of the full beam specimen is shown in Fig. 4.9a, and a part of the beam specimen (enlarged view-B) is shown in Fig. 4.9b.

4.2.4 Shear Resistance of Control Beam

The shear resistance of the control beam specimens as obtained from the experimental results along with the mode of failure is listed in Table 4.1. The average value of three specimens of each series is used for the calculations.

The experimental total shear resistance ($V_{n,\text{test}}$) of control beam specimen (S0-0L) is equal with the resistance provided by the concrete ($V_{c,\text{test}}$), as there is no shear reinforcement present in the specimen. Whereas in S300-0L and S200-0L specimens, the total shear resistance is the sum of the resistance provided by the concrete ($V_{c,\text{test}}$)

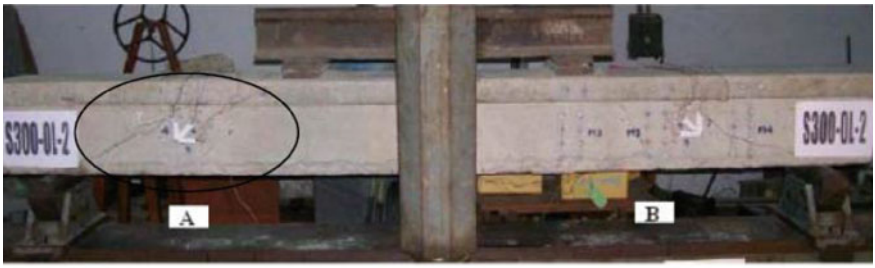

(a) Cracking Pattern of Full Beam Specimen

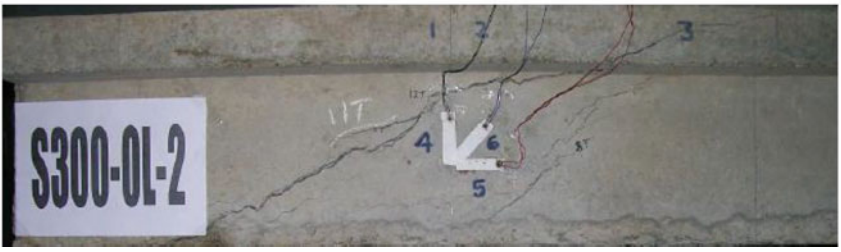

(b) Enlarged View-A

Fig. 4.7 Cracking pattern and modes of failure of beam specimen S300-0L-2

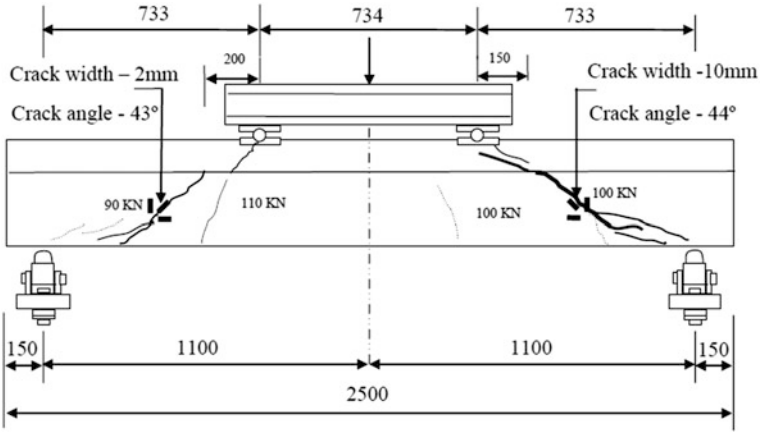

Fig. 4.8 Schematic diagram showing cracking pattern of specimen S200-0L-3

(a) Cracking Pattern of Full Beam Specimen

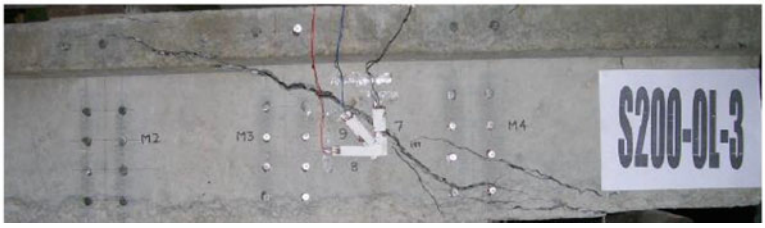

(b) Enlarged View-B

Fig. 4.9 Cracking pattern and modes of failure of beam specimen S200-0L-3

Table 4.1 Experimental results of control beam specimen

Specimen designation	Total load at failure (kN)	Total shear resistance $V_{n,\text{test}}$ (kN)	Average total shear resistance $V_{n,\text{test}}$ (kN)	Resistance due to concrete $V_{c,\text{test}}$ (kN)	Resistance due to steel $V_{s,\text{test}}$ (kN)	Modes of failure
S0-0L-1	104	52	50	50	–	Shear
S0-0L-2	100	50				Shear
S0-0L-3	96	48				Shear
S300-0L-1	136	68	70.5	50	20.5	Shear
S300-0L-2	146	73				Shear
S300-0L-3	141	70.5				Shear
S200-0L-1	174	87	80	50	30	Shear
S200-0L-2	150	75				Shear
S200-0L-3	156	78				Shear

and the transverse steel reinforcement ($V_{s,\text{test}}$). The experimental shear contribution of transverse steel reinforcement is obtained by subtracting ($V_{n,\text{test}}$) of the control beam without transverse steel reinforcement from ($V_{n,\text{test}}$) of the control beam with transverse steel reinforcement.

4.3 RC T-beams Strengthened in Shear with Externally U-Jacketed GFRP Sheets

Nine RC T-beams were strengthened in shear with one, two and three layers of externally U-jacketed GFRP continuous sheet in each series (Panda et al. 2010, 2012, 2015). Figure 4.10 shows the detail strengthening configuration for three series S0, S300 and S200. The shear contribution of GFRP sheet for different numbers of layers as compared with the control specimens is calculated.

4.3.1 Shear Strength Contribution by U-Wrapped GFRP

The experimental results of RC T-beams strengthened in shear with GFRP continuous sheets in U-jacket for different layers are calculated and given in Table 4.2.

The shear capacity of the GFRP sheet of the strengthened RC T-beams ($V_{f,\text{test}}$) is obtained by subtracting $V_{n,\text{test}}$ of the strengthened RC T-beams with GFRP sheets from $V_{n,\text{test}}$ of the corresponding control RC T-beam. The $V_{n,\text{test}}$ of the control RC T-beam is the average total shear resistance.

(a) **S0 Series**

From Table 4.2, it is observed that for strengthened RC T-beam specimen S0-1L-CT-U-90, the load at ultimate failure is 136 kN, compared to 100 kN for Control RC T-beam specimen S0-0L. The gain of 36% in load carrying capacity observed in strengthened specimen S0-1L-CT-U-90. As GFRP thickness on the gain in strength is concerned, the addition of second and third layers of GFRP sheet, that is, for strengthened RC T-beam specimens S0-2L-CT-U-90 and S0-3L-CT-U-90, the loads at ultimate failure are 142 and 146 kN, respectively. The percentage gain in strength is 42 and 46%, respectively, as compared with control RC T-beam specimen S0-0L. It may be noted that the gain in shear capacity of the RC T-beam with two and three layers of GFRP sheet is comparatively less than one layer of GFRP sheet (Panda et al. 2012).

(b) **S300 Series**

From Table 4.2, it is observed that for strengthened RC T-beam specimen S300-1L-CT-U-90, the load at ultimate failure is 156 kN, compared to 141 kN for control RC T-beam specimen S300-0L. A gain in strength of 10.64% is observed. The addition of second and third layers of GFRP sheet in specimen S300-2L-CT-U-90 and S300-3L-CT-U-90, the loads at ultimate failure are 160 and 184 kN, respectively. The gain in strength for these two groups is 13.47 and 30.5%, respectively, compared to the control RC T-beam specimen S300-0L. It is observed that the gain in strength is not much between single and double layer specimens, but as compared with control RC T-beam specimen S300-0L, very less. Whereas in

(a)

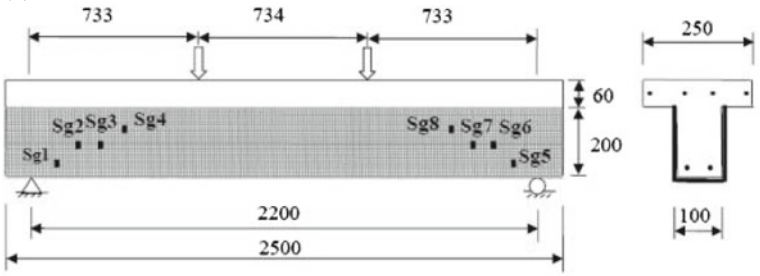

RC T-Beams with one, two and three layers of GFRP sheet of Series S0

(b)

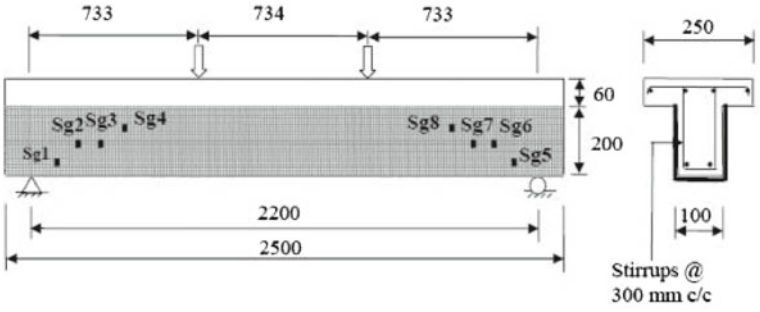

RC T-Beams with one, two and three layers of GFRP sheet of Series S300

(c)

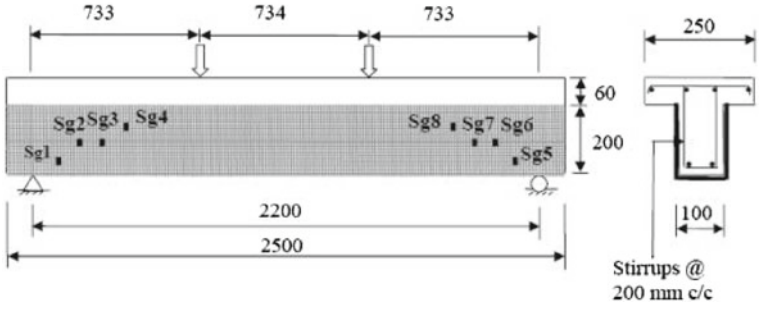

RC T-Beams with one, two and three layers of GFRP sheet of Series S200

Fig. 4.10 RC T-beams strengthened in shear with U-jacketed GFRP sheet

Table 4.2 Shear contribution of GFRP sheets (U-jacket)

Specimen	Load at failure (kN)	Total shear resistance $V_{n,\text{test}}$ (kN)	Resistance due to concrete $V_{c,\text{test}}$ (kN)	Resistance due to steel $V_{s,\text{test}}$ (kN)	Shear resistance due to GFRP $V_{f,\text{test}}$ (kN)	Gain in shear resistance due to GFRP (%)	Mode of failure
S0-0L	100	50	50	00	00	00	Shear
S300-0L	141	70.5	50	20.5	00	00	Shear
S200-0L	160	80	50	30	00	00	Shear
S0-1L-CT-U-90	136	68	50	00	18	36	Rupture failure
S0-2L-CT-U-90	142	71	50	00	21	42	GFRP debonding and rupture failure
S0-3L-CT-U-90	146	73	50	00	23	46	GFRP debonding
S300-1L-CT-U-90	156	78	50	20.5	7.5	10.64	Rupture failure
S300-2L-CT-U-90	160	80	50	20.5	9.5	13.47	GFRP debonding
S300-3L-CT-U-90	184	92	50	20.5	21.5	30.5	GFRP debonding
S200-1L-CT-U-90	182	91	50	30	11	13.75	GFRP debonding and rupture failure
S200-2L-CT-U-90	208	104	50	30	24	30	GFRP debonding
S200-3L-CT-U-90	192	96	50	30	16	20	GFRP debonding

three layers S300-3L-CT-U-90 specimen, the gain in strength is considerable, as compared with the control specimen S300-0L (Panda et al. 2012).

(c) **S200 Series**

From Table 4.2, it is clearly observed for S200 series, the loads at ultimate failure of strengthened RC T-beam specimens S200-1L-CT-U-90, S200-2L-CT-U-90 and S200-3L-CT-U-90 are 182, 208 and 192 kN, respectively, compared to 160 kN for control RC T-beam specimen S200-0L. This indicates an increase of 13.75, 30 and 20%, respectively, on loads over control RC T-beam specimen (Panda et al. 2012).

It is observed from the series S0, S300 and S200 that the gain in shear strength due to GFRP sheet of RC T-beams strengthened in shear with GFRP sheets without transverse steel reinforcement is more as compared with RC T-beams strengthened in shear with GFRP sheets with adequate transverse steel reinforcement. It is expected that, the presence of transverse steel reinforcements, the effectiveness of GFRP sheet towards the total shear strength get decreases.

4.3.2 Deflection of T-beams with U-Wrapped GFRP

The midspan deflection with load for the RC T-beams of series S0, S300 and S200 with varying layers of GFRP sheets in U-jacket around the web of the T-beams as obtained from the experiment is shown in Figs. 4.11, 4.12 and 4.13 (Panda et al. 2012).

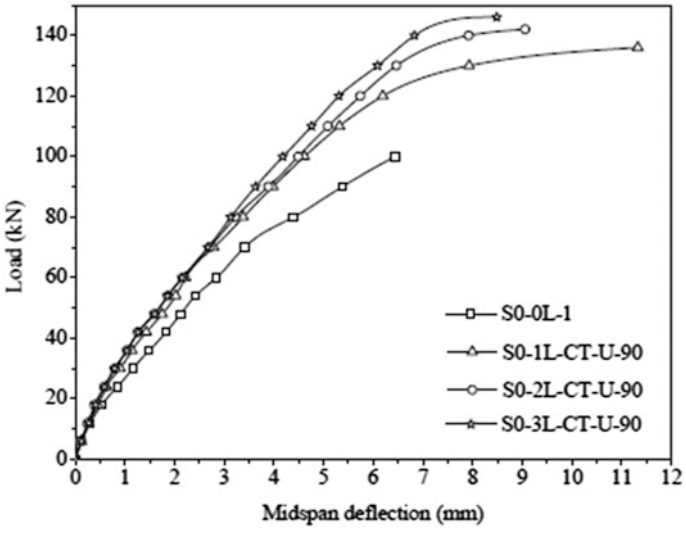

Fig. 4.11 Load versus midspan deflection of U-wrapped beam for series S0

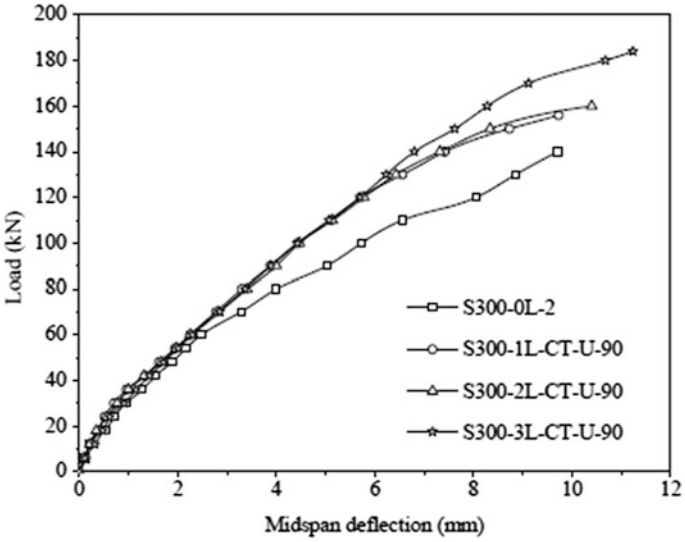

Fig. 4.12 Load versus midspan deflection of U-wrapped beam for series S300

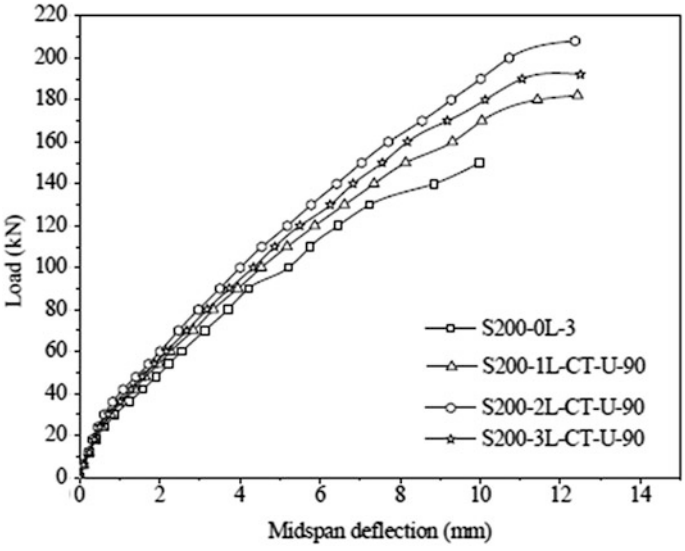

Fig. 4.13 Load versus midspan deflection of U-wrapped beam for series S200

It is observed from Fig. 4.11 that the deflection in RC T-beams, strengthened in shear with GFRP sheet is less as compared to the control RC T-beam specimen for the same load. As expected, RC T-beams strengthened with three layers of GFRP sheet carry more load than the other specimens. However, RC T-beam strengthened

with single layer of GFRP sheet, though carries lesser load than strengthening with three layers of GFRP sheet, undergoes relatively more deflection.

As observed from Fig. 4.12, the deflection of control and strengthened RC T-beam specimens is almost same up to 60 kN loads. It is observed that the deflection in RC T-beams bonded with GFRP sheet is less in comparison to control RC T-beams with the increase in loads. However, the deflection of the strengthened RC T-beams with different layers of GFRP sheet is almost equal up to 120 kN load. As expected, RC T-beams strengthened with three layers of GFRP sheet carry more load than the other two strengthened beams with one and two layers of GFRP sheet and also demonstrate more ductility.

As observed from Fig. 4.13, the midspan deflection of control and strengthened RC T-beams of series S200 is nearly equal up to 20 kN loads. Further, as the load increases, the deflection in control RC T-beam specimen becomes more as compared with strengthened RC T-beams for the same amount of load. Beam strengthened with two layers of GFRP sheet carry more load than the others. It is also observed that all the strengthened RC T-beams of this series show almost same deflection.

It is observed that the ductility of the RC T-beams strengthened in shear with U-wrapped GFRP sheet increases as shear reinforcement and GFRP layer increase.

4.3.3 Modes of Failure of T-beams with U-Wrapped GFRP

The modes of failure of the control and strengthened RC T-beams of series S0, S300 and S200 with one, two and three layers of GFRP sheets are as shown in Fig. 4.14.

(a) **S0 Series**

The rupture failure of GFRP layer is observed in shear zone in the specimens S0-1L-CT-U-90 and S0-2L-CT-U-90, whereas the debonding failure of the GFRP layer from the concrete surface is observed in the specimen S0-3L-CT-U-90 as shown in Fig. 4.14a. It is observed during experimentation that at an ultimate load of 136 and 142 kN, the GFRP layer gets ruptured in the specimen S0-1L-CT-U-90 and S0-2L-CT-U-90 in the similar area as observed in the control beam specimen earlier. Whereas in S0-3L-CT-U-90 specimen the GFRP layer gets debonded from the concrete surface at a load of 146 kN (Panda et al. 2012). Also in S0-2L-CT-U-90 specimen, the GFRP layer debonded from the concrete surface immediately before the rupture failure. These two specimens GFRP debonding gets initiated from the top surface of the web of the T-beams only. At the time of ultimate failure, a horizontal crack is appeared at the side face of the flange for a distance of 210 mm, and then the crack inclined for a distance of 200 mm approximately in S0-1L-CT-U-90 specimen. In S0-2L-CT-U-90 specimen, the inclined crack appeares on the side face of the flange and covers for a distance of

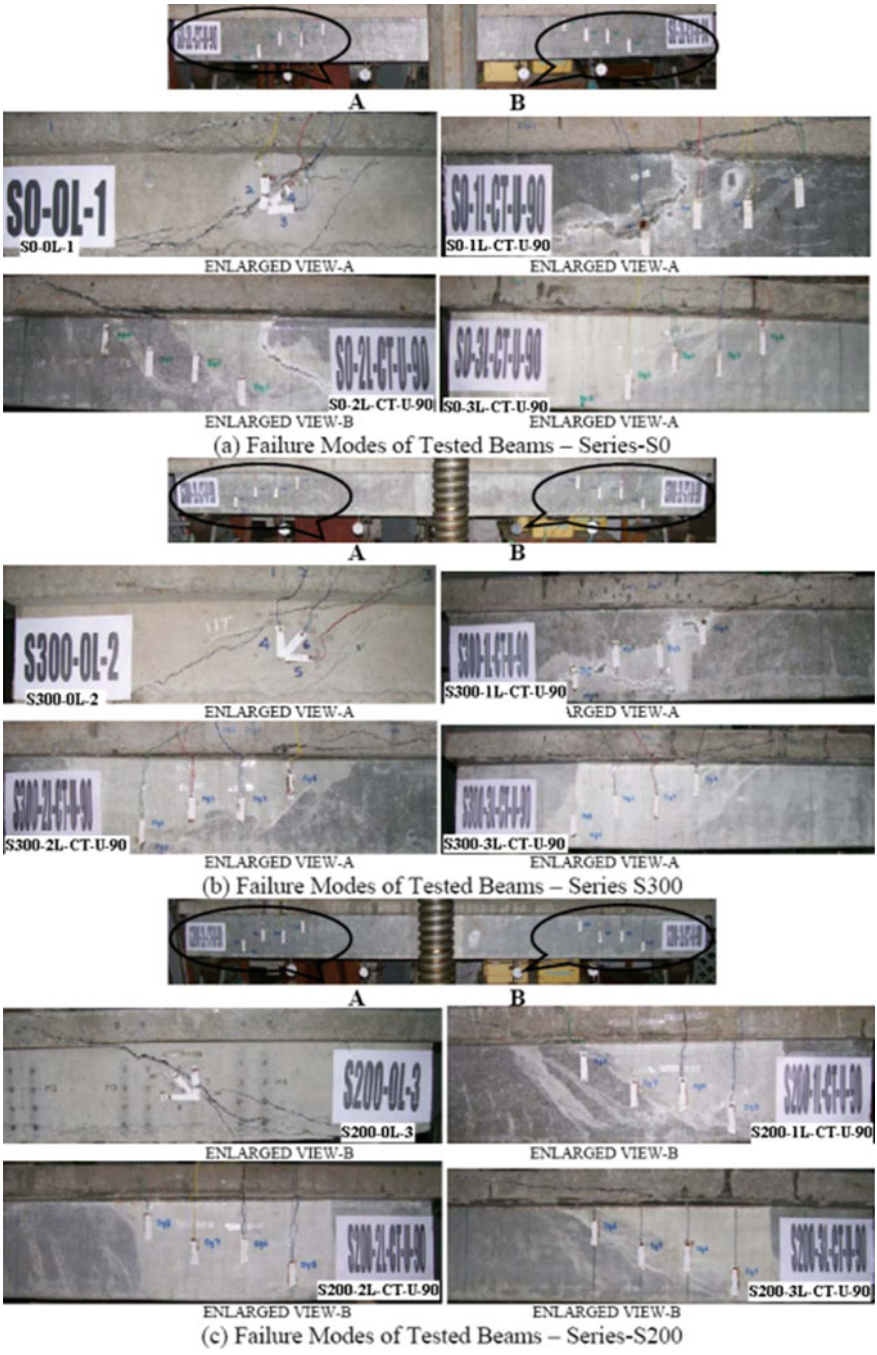

Fig. 4.14 Failure modes of tested beams (U-jacket)

150 mm approximately, and then followed by a horizontal crack for a distance of 100 mm at the flange-web junction. Whereas in S0-3L-CT-U-90 specimen, the horizontal crack appeared on the side face of the flange; it covers a distance of approximately 450 mm from the loading point towards support. Also, two hair cracks appeared at the top of the flange from the loading point: the first one propagated along longitudinal direction, whereas the second one in transverse direction covering the full width of the flange.

(b) **S300 Series**

The rupture failure of GFRP layer is observed in shear zone in the specimen S300-1L-CT-U-90, whereas the debonding of GFRP layer from the concrete surface is observed in the S300-2L-CT-U-90 and S300-3L-CT-U-90 specimens as shown in Fig. 4.14b. It is observed during experimental programme that at an ultimate load of 156 kN, the GFRP layer gets ruptured in the specimen S300-1L-CT-U-90 in the similar area as observed in the control T-beam specimen earlier. Whereas in S300-2L-CT-U-90 and S300-3L-CT-U-90 specimens, the GFRP layer gets debonded from the concrete surface at a load of 160 and 184 kN, respectively (Panda et al. 2012). An inclined crack also appeared at the side of the flange of the T-beams and propagated approximately 300 mm distance from the loading position. Also, a crack appeared at the top of the flange of the T-beams.

(c) **S200 Series**

The debonding of GFRP layer from the concrete surface is observed in the specimens S200-1L-CT-U-90, S200-2L-CT-U-90 and S200-3L-CT-U-90 as shown in Fig. 4.14c. It is observed during experimentation that at an ultimate load of 182 kN, the GFRP layer gets debonded in the specimen S200-1L-CT-U-90. The debonding gets initiated from the top surface of the web of the T-beams. The rupture failure of GFRP layer is also observed along the diagonal shear failure line. Whereas in specimens S200-2L-CT-U-90 and S200-3L-CT-U-90, the GFRP layer gets debonded from the concrete surface at 208 and 192 kN, respectively (Panda et al. 2012). These two specimens the debonding gets initiated from the top surface of the web only, no rupture failure is observed. An inclined crack is also appeared at the side of the flange of the T-beams from loading points, and it propagates a distance of about 185, 200 and 380 mm in S200-1L-CT-U-90, S200-2L-CT-U-90 and S200-3L-CT-U-90 specimens, respectively.

The failure modes of RC T-beams strengthened in shear with U-jacketed GFRP wrap clearly indicates that in single layer wrapping most of the failure is due to GFRP sheet rupture, whereas for two and three layers the failure is due to GFRP debonding.

4.3.4 Strain in U-Wrapped GFRP Sheet

(a) **S0 Series**

The variation of vertical strains in GFRP sheet due to shear force for different layers of GFRP in S0 series is shown in Fig. 4.15 (Panda et al. 2015).

The strain in the GFRP sheet in all the strain gauges did not contribute to the load carrying capacity in the initial stages of loading (Bousselham and Chaallal 2006). It is observed that, in single layer specimen (S0-1L-CT-U-90), the strain in the strain gauge Sg1 increases slowly up to 55 kN shear force. Thereafter, as shear force increases, the curve suddenly increased and attained the maximum value of 7747 μstrains at 65 kN shear force. Whereas in two (S0-2L-CT-U-90) and three (S0-3L-CT-U-90) layer specimens, the strain in the GFRP started increasing in all the strain gauges after 35 kN shear force. The maximum strain observed in Sg1 strain gauge is 3978 and 3581 μstrains at 70 kN shear force.

In series S0, the strain in the GFRP sheet is higher in the specimens strengthened with one layer of GFRP as compared to two and three layers. It is also observed that in all the specimens, the GFRP strain is higher at 150 mm distance from the support.

(b) **S300 Series**

The variation of vertical strains in GFRP sheet due to shear force for various layers of GFRP in S300 series are shown in Fig. 4.16.

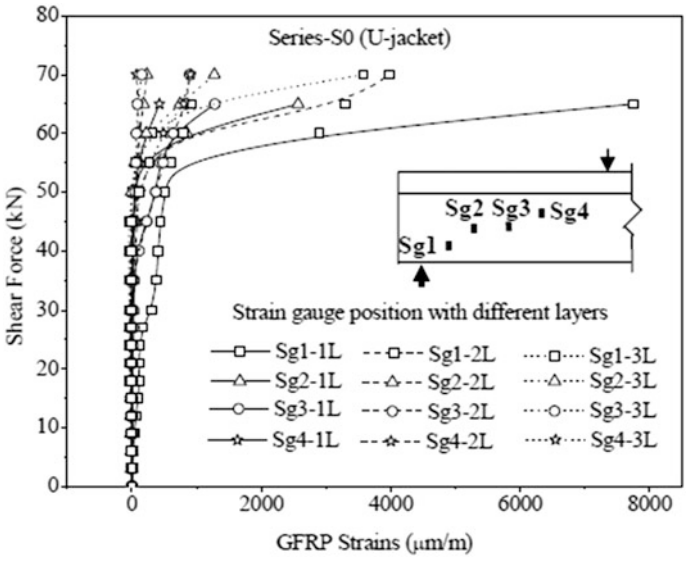

Fig. 4.15 Variation of vertical strains in GFRP sheet for series S0

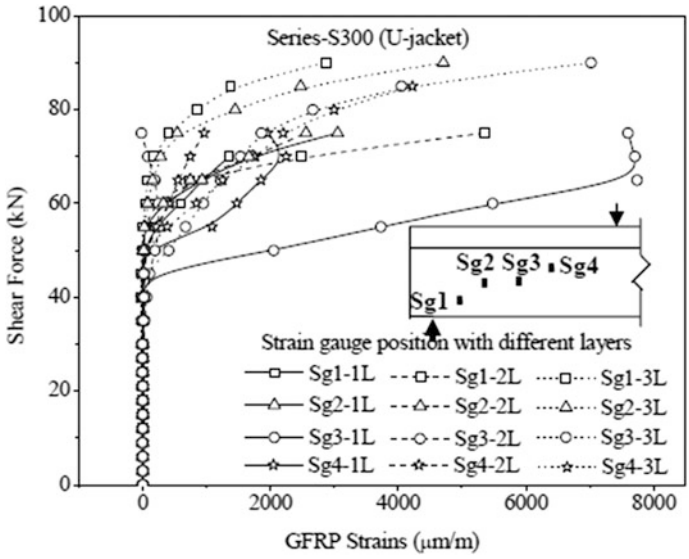

Fig. 4.16 Variation of vertical strains in GFRP sheet for series S300

The strain in the GFRP sheet in all the strain gauges did not contribute to the load carrying capacity up to 45 kN shear force approximately. After 45 kN shear force, the strain started increasing steadily in the single layer (S300-1L-CT-U-90) GFRP sheet and reached the maximum value of 7739 μstrains at 65 kN shear force in strain gauge Sg3. Whereas in two (S300-2L-CT-U-90) and three (S300-3L-CT-U-90) layers specimens, the strain corresponding to this shear force is very less. Maximum strain observed in two and three layers specimen is 5348 and 7018 μstrains in Sg1 and Sg3 strain gauges at 75 and 90 kN shear force, respectively.

In series S300, the strain in the GFRP sheet is higher in the specimens strengthened with one layer of GFRP, as compared to two and three layers. It is also observed that in one and three layers specimen, the GFRP strains are higher at 350 mm distance from the support, whereas in two layers specimen, it is 150 mm distance from the support.

(c) **S200 Series**

The variation of vertical strains in GFRP sheet due to shear force for different layers of GFRP in S200 series specimens are shown in Fig. 4.17.

The strain in the GFRP sheet in all the strain gauges did not contribute to the load carrying capacity in the initial stages of loading up to between 50 and 55 kN shear force approximately (Bousselham and Chaallal 2006), except the strain gauge Sg8 in S200-2L-CT-U-90 specimen, where it starts at a shear force of 40 kN. Thereafter, as shear force increased, the strain in the GFRP sheet started increasing steadily in all the strain gauges up to a maximum threshold, and the maximum

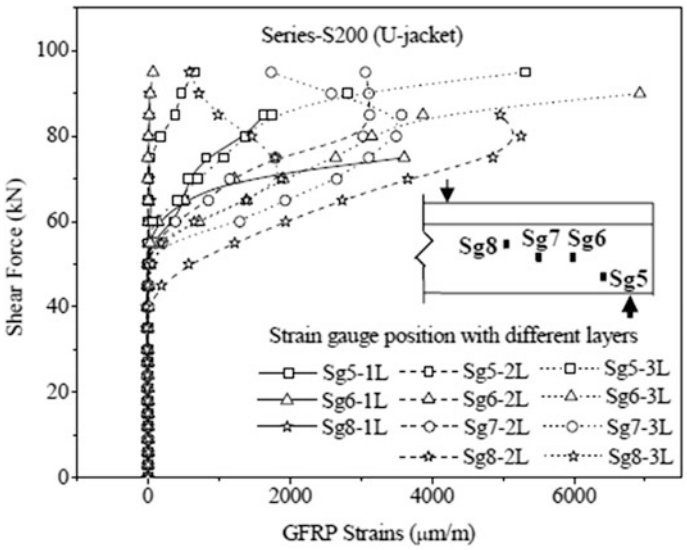

Fig. 4.17 Variation of vertical strains in GFRP sheet for series S200

strain reached in one (S200-1L-CT-U-90) layer specimen is 3609 μstrains in Sg6 strain gauge. Whereas in two (S200-2L-CT-U-90) and three (S200-3L-CT-U-90) layers specimen, the maximum strain observed is 5255 μstrains in Sg8 strain gauge and 6927 μstrains in Sg6 strain gauge, respectively. It is also observed in S200-2L-CT-U-90 specimen, the maximum strain in Sg7 and Sg8 strain gauges is 3121 μstrains at 85 kN shear force and 5255 μstrains at 80 kN shear force, respectively, whereas in S200-3L-CT-U-90 specimen, the maximum strain observed is 3571 μstrains at 85 kN shear force and 1878 μstrains at 70 kN shear force, respectively. Beyond the maximum threshold, the GFRP strain started decreasing, as the shear force increased. However, no debonding is observed. The GFRP contribution to the shear capacity is even greater since the shear force is increased (Bousselham and Chaallal 2006). As expected, the decrease in GFRP strain is due to a local debonding of the GFRP sheet. Though, it is generally seen as layer increases and also towards the top of the web. It may also be observed from S200 series that as transverse steel and GFRP layer both increase, the utilization of strain in the GFRP sheet is more and more, and attains the maximum strain.

In series S200, the GFRP strain is higher in the specimens strengthened with three layers of GFRP, as compared to one and two layers of GFRP. It is also observed that in one- and three-layered specimens, the GFRP strain is higher at 250 mm distance from the support, whereas in two layer specimen, it is 450 mm distance from the support.

4.3.5 *Transverse Steel Strain in T-beams with U-Wrapped GFRP*

The curves representing the variation of strains in the transverse steel reinforcement due to shear force for series S200 and S300 are shown in Figs. 4.18 and 4.19 (Panda et al. 2015).

It is observed from Figs. 4.18 and 4.19 that, like GFRP, the transverse steel reinforcement did not contribute to the load carrying capacity in the initial stage of loading (Bousselham and Chaallal 2006). This contribution is more effective after the diagonal cracking (Panda et al. 2015). In the control specimen S200-0L, it occurred at a shear force of approximately 35 kN. Whereas for the strengthened specimens S200-1L-CT-U-90, S200-2L-CT-U-90 and S200-3L-CT-U-90, it occurred at a shear force of approximately 40, 45 and 50 kN, respectively. In series S300, in the control specimen S300-0L, it occurred at a shear force of approximately 24 kN, whereas for the strengthened specimen S300-1L-CT-U-90, S300-2L-CT-U-90 and S300-3L-CT-U-90, it occurred at shear force of approximately 27, 30 and 35 kN, respectively. Thereafter, as shear force increases, the strain in the transverse steel get increases. It may be observed that the strain in the transverse steel is less in strengthened T-beams as compared to the control T-beam for the same amount of shear force (Panda et al. 2013b, 2015). It is also observed that the strain in the specimens strengthened with three layers of GFRP sheet is less as compared to the specimens strengthened with one layer of GFRP.

It may also be observed that the addition of the GFRP delayed the contribution of transverse steel to the load carrying capacity of the specimens; also as layers are

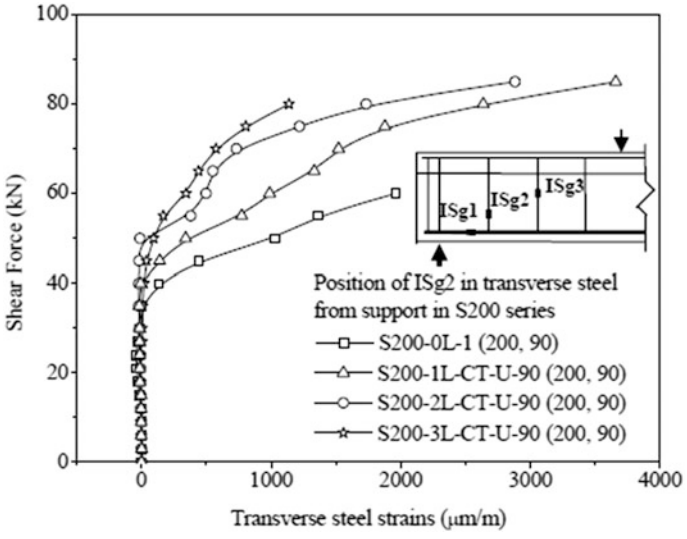

Fig. 4.18 Variation of strain in transverse steel of U-wrapped GFRP for S200 series

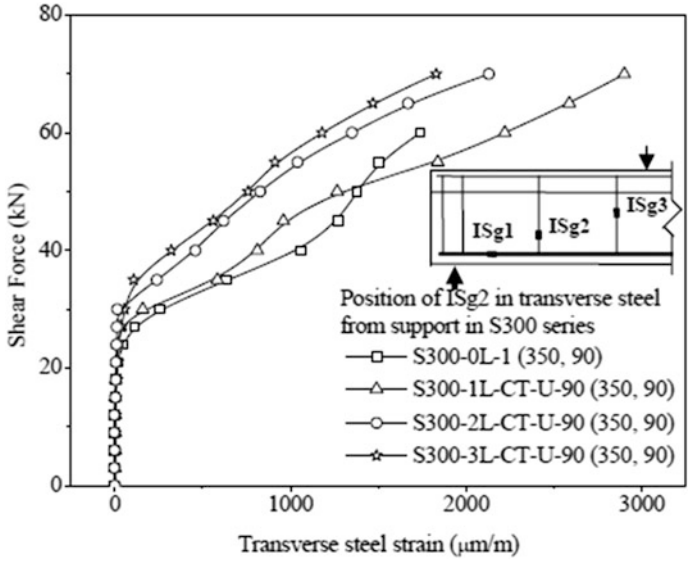

Fig. 4.19 Variation of strain in transverse steel of U-wrapped GFRP for S300 series

concerned, the addition of second and third layers of GFRP resulted in an additional decrease of the strains in the transverse steel, previously observed by Bousselham and Chaallal (2006) using CFRP as strengthening material.

4.3.6 Longitudinal Steel Strain in T-beams with U-Wrapped GFRP

The curve representing the variation of strains in the tensile longitudinal steel reinforcement due to shear force for varying layers of series S0, S300 and S200 is shown in Fig. 4.20.

The strain gauge ISg1 is located in tensile longitudinal steel reinforcement at a distance of 150 mm from the support for the RC T-beams of series S0, S200 and S300, respectively. As observed from Fig. 4.20, the strain near the support point is very small in the initial stages of loading in series S0, S200 and S300. As shear force increases, the strain in the longitudinal steel increases linearly up to about 35 kN shear force till the diagonal shear cracks appear in the concrete. After the appearance of diagonal shear cracks in the concrete, the longitudinal steel reinforcement resists the further increments of shear force. It may be observed that the strain in the longitudinal steel, in T-beams strengthened with GFRP sheet, is less as compared with control T-beam for the same amount of shear force for all the series (Panda et al. 2015).

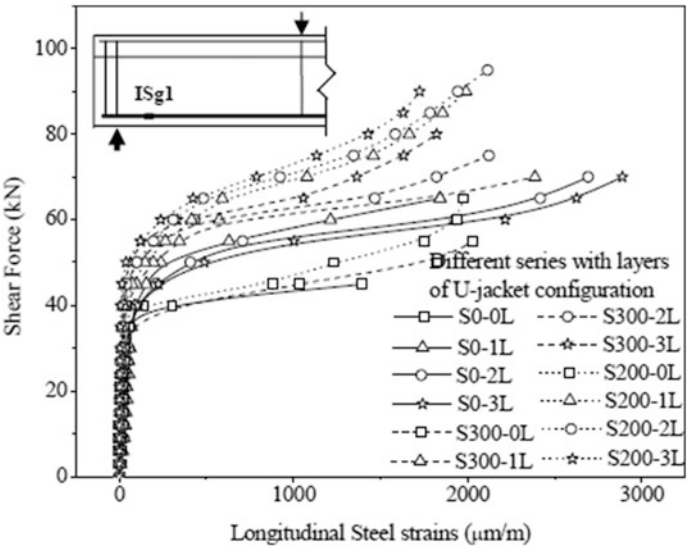

Fig. 4.20 Variation of strain in longitudinal steel for varying layers (U-jacket)

It is concluded that the presence of GFRP eased the strains in the longitudinal steel reinforcement at a given shear force; the longitudinal steel seems to be less strained in strengthened specimens as compared with control specimen, previously observed by Bousselham and Chaallal (2006) using CFRP as strengthening material. It is also observed that as transverse steel reinforcement increases, the longitudinal steel seems to be less strained for the same amount of shear force. So far, as the number of GFRP layers is concerned, the longitudinal steel is less strained in three-layered specimen as compared to single layer specimen.

4.3.7 Interaction Between Transverse Steel Reinforcement and GFRP Layers

(a) **Optimum GFRP Ratio**

The contribution of the transverse steel reinforcement and of the GFRP wrap on the ultimate shear capacity may be explained by the gain in shear capacity. The gain in shear capacity is expressed as a percentage of ultimate shear capacity of control specimen (S0-0L). If the ultimate shear capacity of control specimen is V_0 and that of the strengthened specimen is V_1, then the gain in shear capacity may be expressed as $g = [(V_1 - V_0)/V_0] \times 100\%$. The transverse steel reinforcement ratio is expressed as $\rho_s = [A_{sw}/(sb_w)] \times 100\%$. The variation of gain in shear capacity with transverse steel reinforcement ratio is shown in Fig. 4.21.

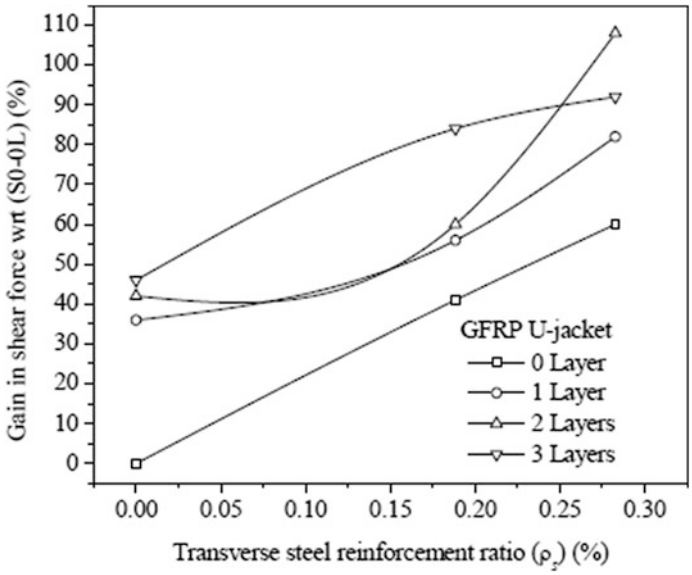

Fig. 4.21 Gain in shear force versus transverse steel reinforcement ratio

The control specimen (S0-0L), without stirrups, resists the shear by the concrete only since no stirrup is intercepted the diagonal shear crack. It may be observed that from Fig. 4.21, the gain in shear capacity in the entire strengthened RC T-beams with respect to (S0-0L) increases, as the transverse steel reinforcement ratio increases. As expected, beams strengthened with three layers of GFRP, the gain in shear capacity tends to decrease after 0.19% of transverse steel reinforcement ratio, whereas in two layers shows the increased value. The maximum increase in shear capacity for specimen strengthened with three layers of GFRP is observed against 0 and 0.19% transverse steel reinforcement ratio, whereas the specimen strengthened with two layers of GFRP, the maximum increase in shear capacity is observed against 0.28% of transverse steel reinforcement ratio.

Figures 4.22 and 4.23 show the gain in shear force as a percentage of control specimens (S0-0L) versus total shear reinforcement ratio $\rho_{\text{total}} = (m\rho_f + \rho_s)$, where ρ_f is the FRP shear reinforcement ratio, ρ_s is the transverse steel reinforcement ratio and m is the non-dimensional number. It may be observed that the gain in shear force in strengthened beams is mainly due to both GFRP reinforcement ratio and transverse steel reinforcement ratio. The results presented in Fig. 4.22 are for all the U-jacketed beams with variation of GFRP sheets. A good correlation may be proposed with a second-degree polynomial as observed in Fig. 4.23.

(b) **Ductility of Strengthened T-beams**

The midspan deflection gain versus total shear reinforcement ratio (ρ_{total}) of T-beams strengthened in shear with U-jacketed GFRP sheet is shown in Fig. 4.24.

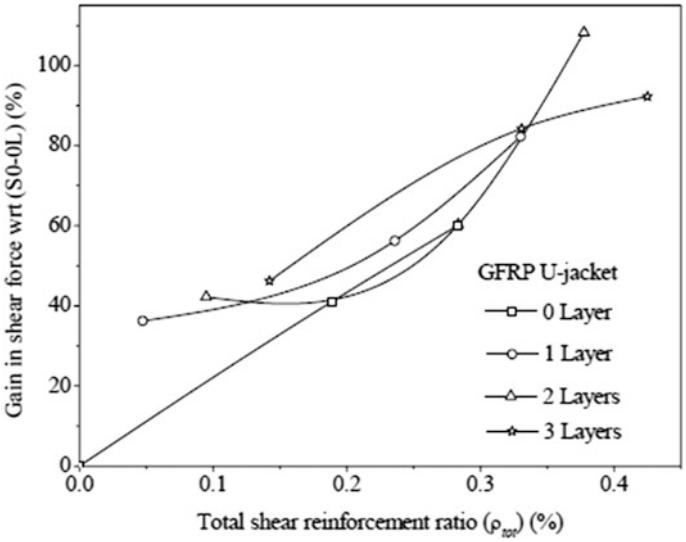

Fig. 4.22 Gain in shear force versus total shear reinforcement ratio

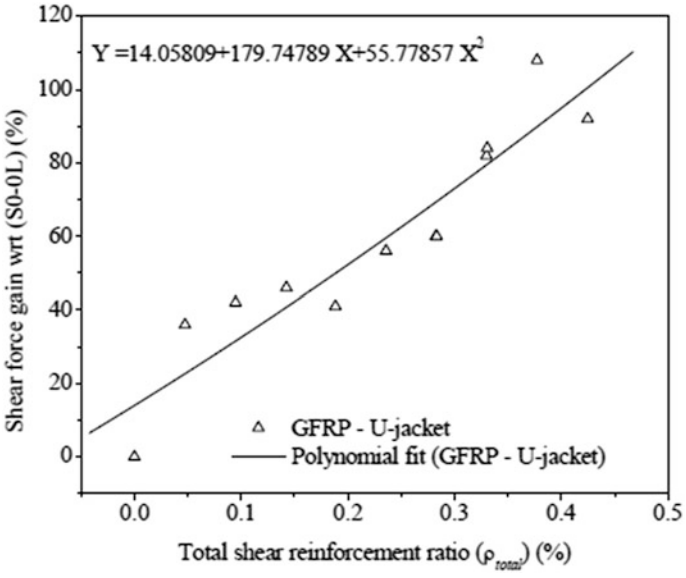

Fig. 4.23 Gain in shear force versus total shear reinforcement ratio (correlation)

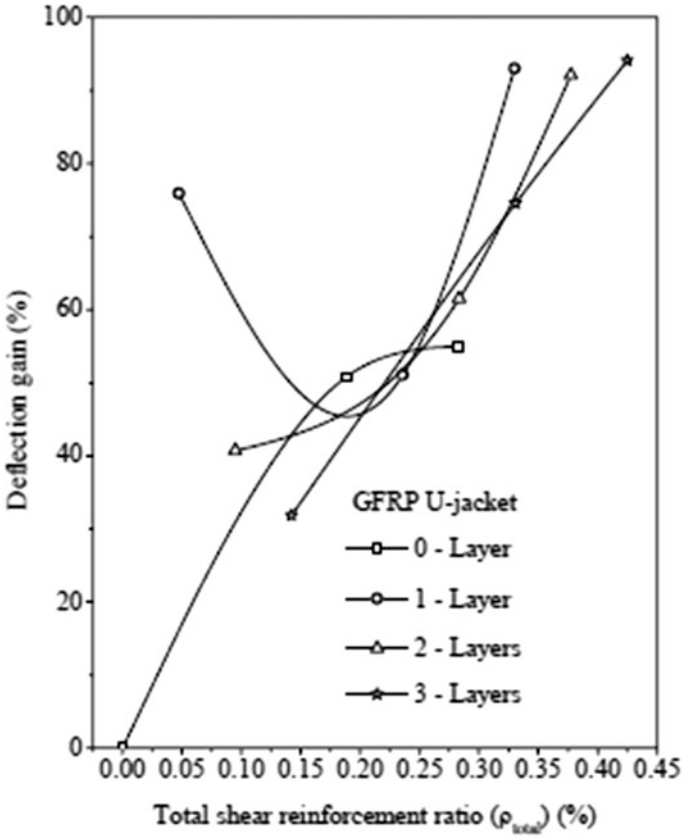

Fig. 4.24 Midspan deflection gain versus total shear reinforcement ratio

It may be observed that the midspan deflection of specimen (S0-0L) is more as strengthened with one layer of GFRP (S0-1L-CT-U-90); however, the value goes on decreasing order as GFRP layer increases from one to three layers. As the combination of transverse steel and GFRP layers is concerned, the maximum gain in deflection shows 76% in one layer GFRP strengthened T-beams corresponding to 0.047% of total shear reinforcement ratio; thereafter, it goes on decreasing order as total shear reinforcement ratio increases and shows 45% corresponding to 0.2% of total shear reinforcement ratio. Once again, the deflection increases to 93% at 0.33% of total shear reinforcement ratio. Whereas in two layers, the maximum gain in deflection is observed 40.7, 61.5 and 92% corresponding to the total shear reinforcement ratio of 0.095, 0.283 and 0.378%, and in three layers, the maximum gain in deflection is observed 31.83, 74.5 and 94.1% corresponding to the total shear reinforcement ratio of 0.142, 0.33 and 0.425%, respectively. It may be observed that the addition of the second layer, the maximum gain in deflection slowly increases as the total shear reinforcement ratio increases from 0.095 to

0.283%, thereafter suddenly increases up to the total shear reinforcement ratio 0.378%. However, the addition of the third layer, the maximum gain in deflection increases linearly from 0.142 to 0.425%. It may be concluded that the ductility of concrete beams loaded in shear depends directly on both the internal transverse steel and external GFRP wrap. Overall, in global point of view, the ductility increases as total shear reinforcement ratio increases.

4.4 RC T-beams Strengthened in Shear with Externally Side-Bonded GFRP Sheets

Nine RC T-beams were strengthened in shear with one, two and three layers of GFRP continuous sheet in side of the web of the T-beams for each series (Panda et al. 2011a). Figure 4.25 shows the detail strengthening configuration for three series S0, S300 and S200. The shear contribution of GFRP sheet for different numbers of layers as compared with the control specimens is calculated.

4.4.1 Shear Strength Contribution by Side-Bonded GFRP

The experimental results of RC T-beams strengthened in shear with side-bonded GFRP continuous sheet for different layers are calculated and presented in Table 4.3 (Panda et al. 2011a).

(a) **S0 Series**

From Table 4.3, it is observed that for strengthened specimen S0-1L-CT-S-90, the load at ultimate failure is 132 kN, compared to 100 kN for S0-0L control specimen. This shows that there is a gain of 32% in load carrying capacity. As for the influence of the GFRP thickness on the gain in strength of the RC T-beams is concerned, the addition of second and third layers of GFRP sheet, that is, for S0-2L-CT-S-90 and S0-3L-CT-S-90, the loads at ultimate failure are 138 and 150 kN, respectively. The percentage gain in strength is 38 and 50%, respectively, as compared with the control specimen S0-0L (Panda et al. 2011a). It may be noted that the gain in shear capacity of the RC T-beams strengthened with two layers of side-bonded GFRP sheet is comparatively less than one layer of GFRP sheet. Whereas in three layers, to some extent, it is better.

(b) **S300 Series**

From Table 4.3, it is observed that for strengthened specimen S300-1L-CT-S-90, the load at ultimate failure is 176 kN, compared to 141 kN for control T-beam specimen S300-0L. This indicates a gain in strength of 24.82% that is observed. The addition of second and third layers of side-bonded GFRP sheet in series

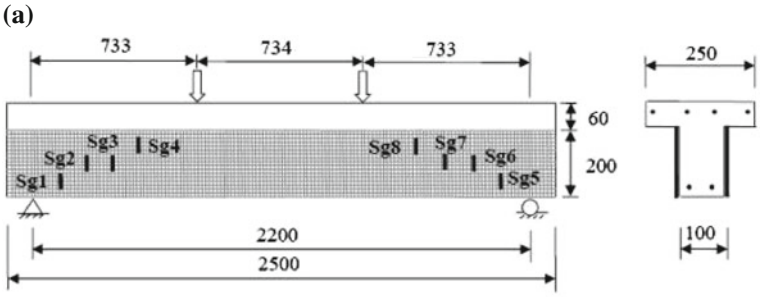

RC T-Beams with one, two and three layers of GFRP sheet of Series S0

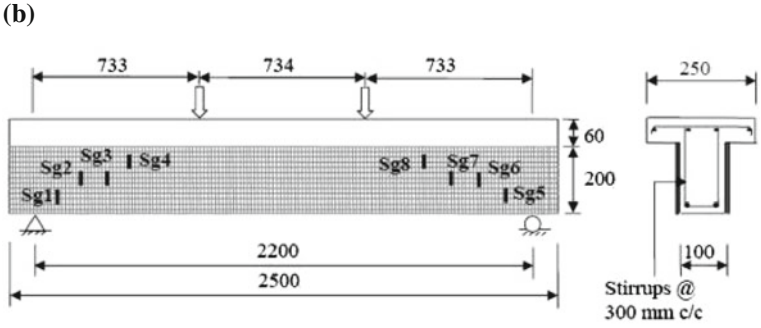

RC T-Beams with one, two and three layers of GFRP sheet of Series S300

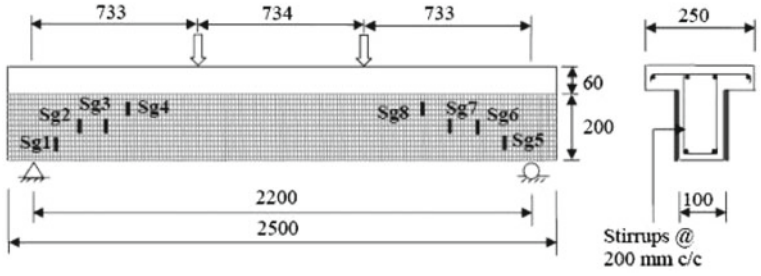

RC T-Beams with one, two and three layers of GFRP sheet of Series S200

Fig. 4.25 RC T-beams strengthened in shear with side-bonded GFRP sheet

S300-2L-CT-S-90 and S300-3L-CT-S-90, the loads at ultimate failure are 180 and 182 kN, respectively. The gain in strength for these two strengthened RC T-beam specimens is 27.66 and 29.08%, respectively, compared to the control RC T-beam specimen S300-0L (Panda et al. 2011a). It is observed that the gain in strength is not much difference in RC T-beam with side-bonded GFRP sheet in single, double

Table 4.3 Shear contribution of GFRP sheets (side-bonded)

Specimen designation	Load at failure (kN)	Total shear resistance $V_{n,test}$ (kN)	Resistance due to concrete $V_{c,test}$ (kN)	Resistance due to steel $V_{s,test}$ (kN)	Shear resistance due to GFRP $V_{f,test}$ (kN)	Gain in shear resistance due to GFRP (%)	Mode of failure
S0-0L	100	50	50	00	00	00	Shear
S300-0L	141	70.5	50	20.5	00	00	Shear
S200-0L	160	80	50	30	00	00	Shear
S0-1L-CT-S-90	132	66	50	00	16	32	Rupture failure
S0-2L-CT-S-90	138	69	50	00	19	38	GFRP debonding
S0-3L-CT-S-90	150	75	50	00	25	50	GFRP debonding
S300-1L-CT-S-90	176	88	50	20.5	17.5	24.82	GFRP debonding and rupture failure
S300-2L-CT-S-90	180	90	50	20.5	19.5	27.66	GFRP debonding
S300-3L-CT-S-90	182	91	50	20.5	20.5	29.08	GFRP debonding
S200-1L-CT-S-90	180	90	50	30	10	12.50	GFRP debonding
S200-2L-CT-S-90	186	93	50	30	13	16.25	GFRP debonding
S200-3L-CT-S-90	196	98	50	30	18	22.50	GFRP debonding

and triple layers, but as compared with control RC T-beam specimen S300-0L shows a better result.

(c) **S200 Series**

From Table 4.3, it is observed that for S200 series, the loads at ultimate failure of S200-1L-CT-S-90, S200-2L-CT-S-90 and S200-3L-CT-S-90 specimens are 180, 186 and 196 kN, respectively, compared to 160 kN for control RC T-beam specimen S200-0L. This shows a gain in strength of strengthened RC T-beams, i.e. 12.50, 16.25 and 22.50%, respectively, over control RC T-beam specimens (Panda et al. 2011a). It may be noted that the gain in shear capacity of the RC T-beams strengthened in shear with side-bonded one, two and three layers of GFRP sheet is proportionately increased as compared with control RC T-beam specimen (S200-0L). The gain in shear capacity of S200 series is also less as compared with S0 and S300 series.

It is observed from the series S0, S300 and S200 that the gain in shear strength due to GFRP of RC T-beams strengthened in shear with GFRP sheets on side of the web of the T-beams without transverse steel reinforcement is more as compared with RC T-beams strengthened in shear with GFRP sheets with adequate transverse steel reinforcement (Panda et al. 2011a).

4.4.2 Deflection of T-beams with Side-Bonded GFRP

The variation of midspan deflection with load for the RC T-beams of series S0, S300 and S200 with varying layers of GFRP sheets bonded on side of the web of the T-beams as obtained from the experiment is shown in Figs. 4.26, 4.27 and 4.28 (Panda et al. 2011a).

As observed from Fig. 4.26, for series S0, the maximum deflection of S0-1L-CT-S-90, S0-2L-CT-S-90 and S0-3L-CT-S-90 is 7.18, 8.08 and 9.13 mm corresponding to the failure load of 132, 138 and 150 kN. Whereas in control RC T-beam specimen S0-0L, the maximum deflection is 6.44 mm corresponding to 100 kN load (Panda et al. 2011a). It is observed that the deflection in RC T-beams strengthened with GFRP sheet is less in comparison to the control RC T-beam with the increase in loads. As expected, beams strengthened with three layers of GFRP sheet on side of the web of the T-beams carry more load than the other two and also demonstrate more ductility.

As observed from Fig. 4.27, for series S300, the deflection of control and strengthened RC T-beams is almost same up to 60 kN loads. It is observed that the deflection in RC T-beams strengthened with side-bonded GFRP sheet is less as compared with control RC T-beams with the increase in loads. The maximum deflection of the strengthened RC T-beams is observed in S300-1L-CT-S-90, S300-2L-CT-S-90 and S300-3L-CT-S-90, which is 10.88, 11.14 and 11.42 mm corresponding to the failure load of 176, 180 and 182 kN, whereas in control RC

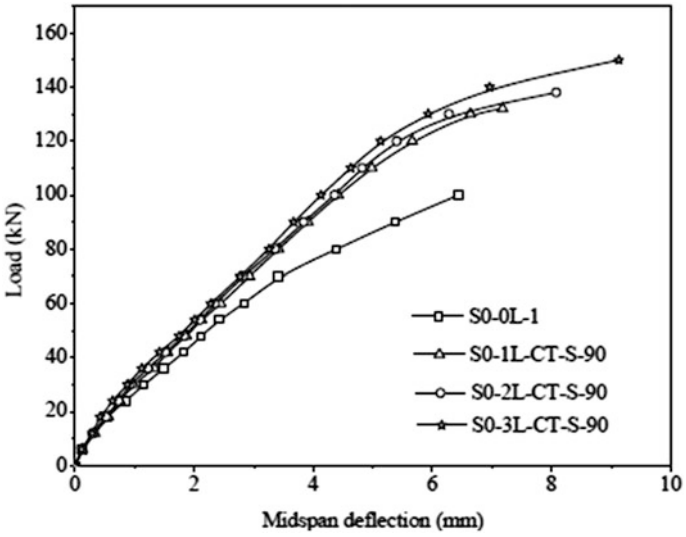

Fig. 4.26 Load versus midspan deflection of side-bonded T-beams for series S0

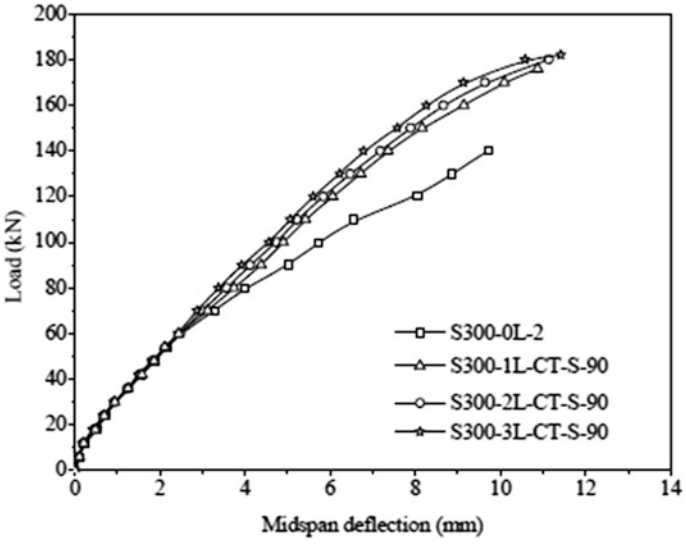

Fig. 4.27 Load versus midspan deflection of side-bonded T-beams for series S300

T-beam, the value is 9.71 mm corresponding to 140 kN load (Panda et al. 2011a). As expected, RC T-beams strengthened with three (3) layers of GFRP sheet carry more load than the other two and also demonstrate more ductility.

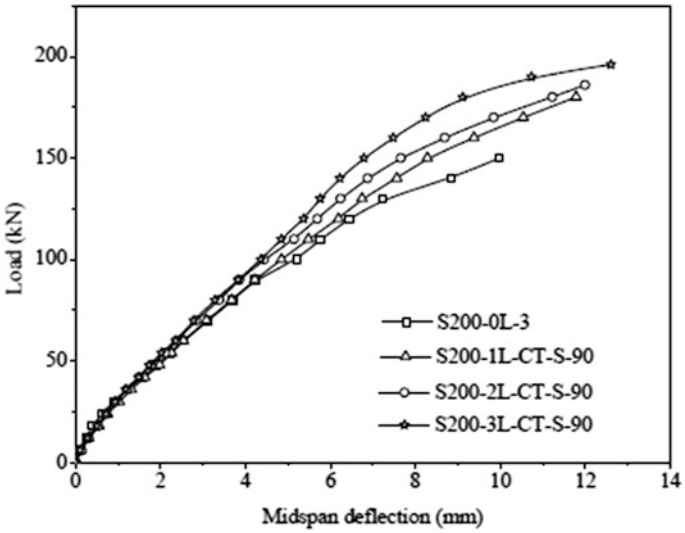

Fig. 4.28 Load versus midspan deflection of side-bonded T-beams for series S200

As observed from Fig. 4.28, the deflection of control and strengthened RC T-beams with side-bonded GFRP sheet of series S200 is nearly equal up to 50 kN loads. Further, as the load increases, the deflection in control RC T-beam specimen becomes more as compared with strengthened RC T-beams for the same amount of load. The maximum deflection of the strengthened RC T-beams observed in S200-1L-CT-S-90, S200-2L-CT-S-90 and S200-3L-CT-S-90 is 11.78, 11.99 and 12.60 mm corresponding to the failure load of 180, 186 and 196 kN, whereas in control RC T-beam (S200-0L) the value is 9.98 mm corresponding to the load of 150 kN (Panda et al. 2011a). As expected, beams strengthened in shear with side-bonded three (3) layers of GFRP sheet carry more load than the other two and also demonstrate more ductility.

It is observed that, as GFRP layer and shear reinforcement increases, the ductility of the beams strengthened in shear with side-bonded GFRP sheet increases.

4.4.3 Modes of Failure of T-beams with Side-Bonded GFRP

The failure modes of the control and side-bonded strengthened RC T-beams of series S0, S300 and S200 with one, two and three layers of GFRP continuous sheets are as shown in Fig. 4.29.

(a) **S0 Series**

The rupture failure of GFRP layer in shear zone is observed in the RC T-beam strengthened with side-bonded GFRP sheet in specimen S0-1L-CT-S-90. Whereas

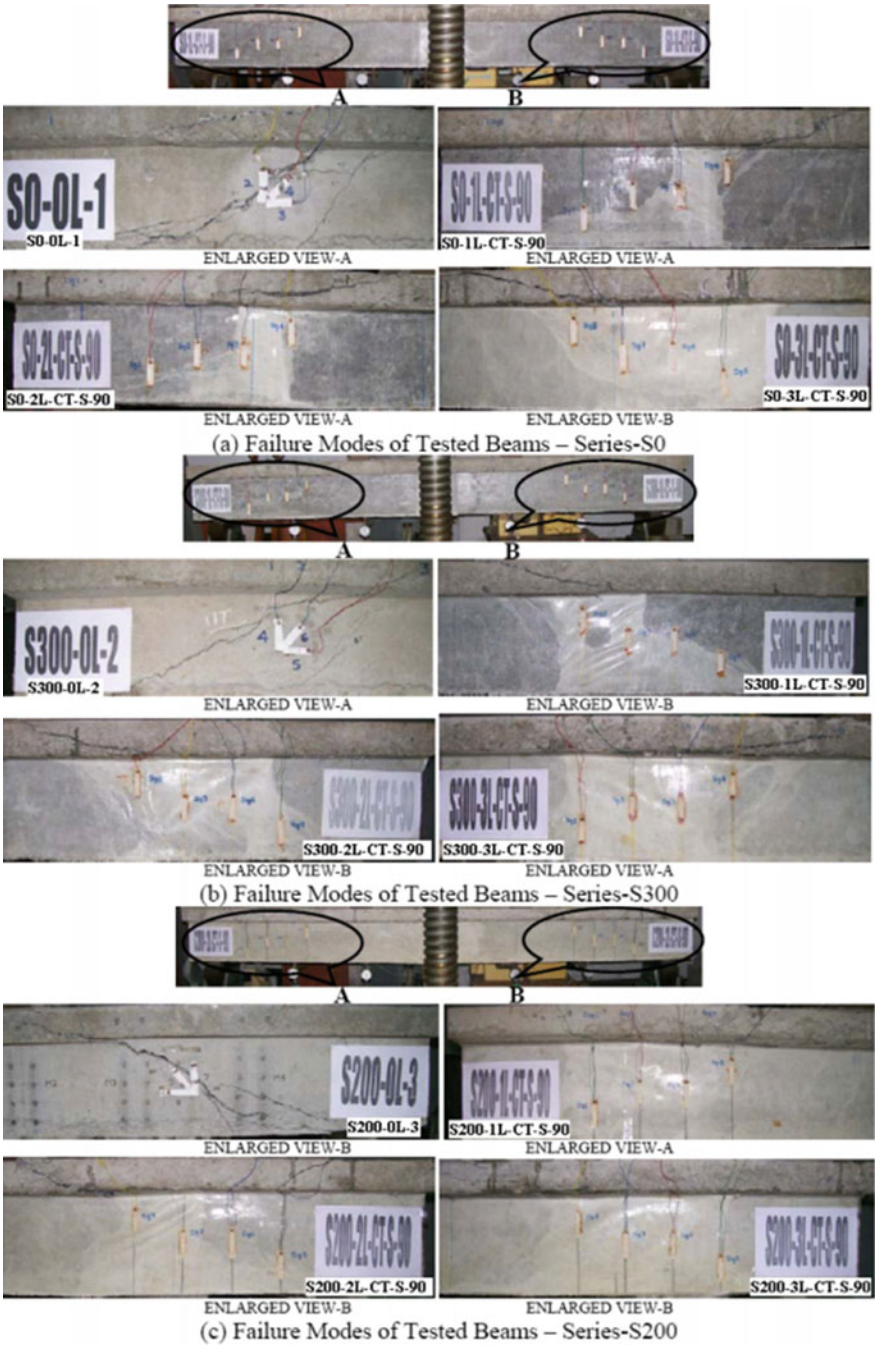

Fig. 4.29 Failure modes of tested beams (side-bonded)

the debonding of the GFRP layer from the concrete surface is observed in the specimens S0-2L-CT-S-90 and S0-3L-CT-S-90 as shown in Fig. 4.29a. It is observed that at an ultimate load of 132 kN, the GFRP layer gets ruptured in the strengthened specimen S0-1L-CT-S-90 in the similar area as observed in the control RC T-beam. Whereas in strengthened beams S0-2L-CT-S-90 and S0-3L-CT-S-90, the GFRP layer gets debonded from the concrete surface at a load of 138 and 150 kN, respectively (Panda et al. 2011a). The GFRP debonding gets initiated from the bottom of the web of the RC T-beams. An inclined crack also appeared at the side of the flange in all the strengthened RC T-beams, and then propagated in longitudinal direction from the loading position for a distance of 250, 450 and 300 mm, respectively.

(b) **S300 Series**

The debonding of GFRP layer from the concrete surface is observed in all the strengthened RC T-beam specimens of series S300 as shown in Fig. 4.29b. It is observed during experimentation that at an ultimate load of 176 kN, the GFRP layer gets debonded in the strengthened specimen S300-1L-CT-S-90. The debonding gets initiated from the bottom of the web of the RC T-beams. The GFRP layer also ruptured along the diagonal shear failure line. Whereas in strengthened RC T-beams S300-2L-CT-S-90 and S300-3L-CT-S-90, the GFRP gets debonded from the concrete surface in the same area as observed in control beam S300-0L at a load of 180 and 182 kN, respectively. In all the strengthened beams, an inclined crack appeared at the sides of the flange of the RC T-beams and propagates in longitudinal direction for a distance of approximately 320, 310 and 275 mm towards the support.

(c) **S200 Series**

The debonding of GFRP layer from the concrete surface is observed in all the strengthened RC T-beam of series S200 as shown in Fig. 4.29c. It is observed during experimentation that the GFRP layer gets debonded in the strengthened specimens S200-1L-CT-S-90, S200-2L-CT-S-90 and S200-3L-CT-S-90 at an ultimate load of 180, 186 and 196 kN, respectively (Panda et al. 2011a). The debonding gets initiated from the bottom of the web of the RC T-beams and it propagates towards the top. In all the specimens, an inclined crack also appears at the side of the flange of the strengthened RC T-beam from loading position and it propagates towards support for a distance of about 380, 325, 300 mm approximately.

The cracking pattern and failure modes of RC T-beams strengthened in shear with side-bonded GFRP sheets clearly indicates that almost all the failure takes place due to GFRP debonding, except the specimen S0-1L-CT-S-90 (Panda et al. 2011a).

4.4.4 Strain in Side-Bonded GFRP Sheet

(a) **S0 Series**

The variation of vertical strains in GFRP sheet due to shear force for different layers of GFRP in S0 series specimens are shown in Fig. 4.30.

The strain in the RC T-beams with side-bonded GFRP sheet in all the strain gauges did not contribute to the load carrying capacity in the initial stages. It is observed that, in single layer strengthened specimen S0-1L-CT-S-90, the strain in the strain gauge Sg3 gets increased after 35 kN shear force. Thereafter, as shear force increases, the curve suddenly increases and reaches the maximum value of 8404 μstrains at 60 kN shear force. Whereas in S0-2L-CT-S-90 strengthened specimen, the strain in the GFRP sheet started increasing in all the strain gauges after 40 kN shear force. The maximum strain observed in Sg4 strain gauge is 7502 μstrains at 65 kN shear force. In S0-3L-CT-S-90 specimen, the strain decreases after 30 kN shear force till obtained the maximum compression at 45 kN shear force. Once again as shear force increases, the strain increases slowly up to 65 kN shear force. Thereafter, the strain suddenly increases in Sg2 and Sg4 strain gauges. The maximum value is observed 7423 μstrains in Sg2 strain gauge at 75 kN shear force.

In series S0, the strain in the side-bonded GFRP sheet is higher in the specimens strengthened with one layer of GFRP, as compared to two and three layers.

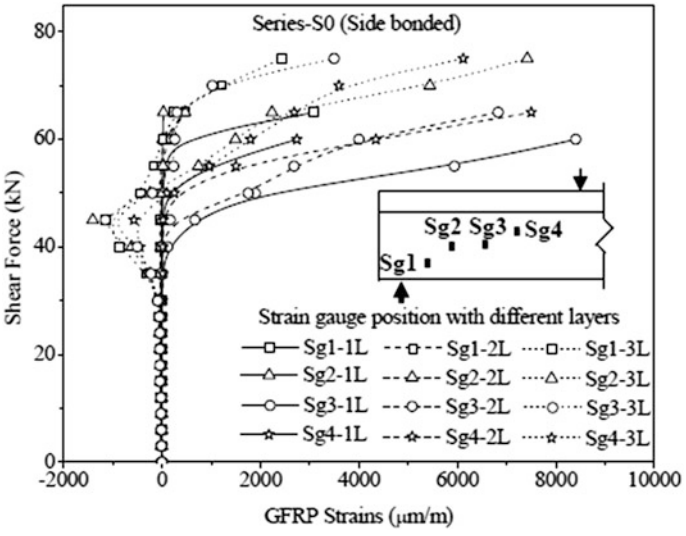

Fig. 4.30 Variation of vertical strains in side-bonded GFRP for series S0

(b) **S300 Series**

The variation of vertical strains in GFRP sheet due to shear force for different layers of GFRP in series S300 specimens are shown in Fig. 4.31.

The strain in the side-bonded GFRP sheets in all the strain gauges did not contribute to the load carrying capacity up to approximately 35 kN shear force in all the specimens. As shear force increases, the strain in the GFRP sheet increases slowly in S300-1L-CT-S-90 and S300-2L-CT-S-90 up to 60 kN shear force except the strain gauge Sg7 in S300-1L-CT-S-90 specimen. Thereafter, the strain suddenly increases and reaches the maximum value of 7538 μstrains at 88 kN shear force and 5338 μstrains at 85 kN shear force in Sg6 strain gauge in S300-1L-CT-S-90 and S300-2L-CT-S-90 specimens, respectively. Whereas in three-layered specimen S300-3L-CT-S-90, the strain increases suddenly after 45 kN shear force in Sg6 strain gauge and reaches the maximum value of 6642 μstrains at 90 kN shear force.

In series S300, the strain in the GFRP sheet is higher in the specimens strengthened with one layer of GFRP, as compared to two and three layers. It is also observed that in all the strengthened beams, the GFRP strain is higher at 250 mm distance from the support.

(c) **S200 Series**

The variation of vertical strains in GFRP sheet due to shear force for different layers of GFRP in S200 series specimens are shown in Fig. 4.32.

The strain in the side-bonded GFRP sheet in all the strain gauges did not contribute to the load carrying capacity in the initial stages of loading up to 35 kN shear force in S200-1L-CT-S-90 specimen, up to 45 kN shear force in

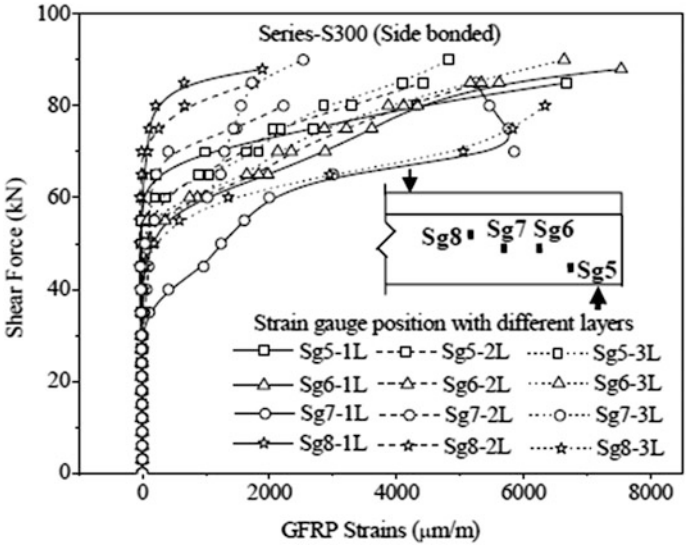

Fig. 4.31 Variation of vertical strains in side-bonded GFRP for series S300

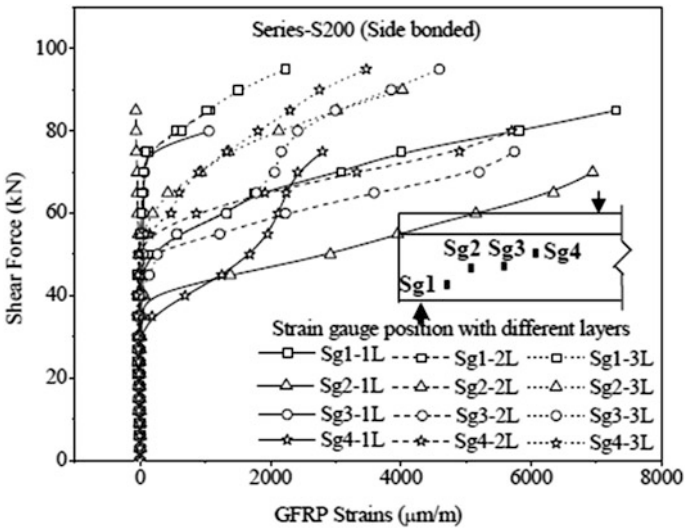

Fig. 4.32 Variation of vertical strains in side-bonded GFRP for series S200

S200-2L-CT-S-90 specimen and up to 50 kN shear force in S200-3L-CT-S-90 specimen, respectively. Thereafter, as shear force increases, the strain increases in all the strain gauges. The maximum strain observed in one layer (S200-1L-CT-S-90) strengthened RC T-beam specimen in Sg1 strain gauge is 7302 μstrains at 85 kN shear force. Whereas in two (S200-2L-CT-S-90) and three (S200-3L-CT-S-90) layers strengthened RC T-beam specimen, the maximum strain observed is 5747 μstrains at 75 kN shear force in Sg3 strain gauge and 4594 μstrains at 95 kN shear force in Sg3 strain gauge, respectively.

In series S200, the strain in the side-bonded GFRP sheet is higher in the specimens strengthened with one layer of GFRP, as compared to two and three layers. In one layer strengthened RC T-beam specimen, the maximum is strain observed at a distance of 150 mm distance from the support, whereas in two and three layers strengthened specimen, the distance is 350 mm.

4.4.5 Transverse Steel Strain in T-beams with Side-Bonded GFRP

The curves representing variation of strains in the transverse steel reinforcement with shear force for series S200 and S300 are shown in Figs. 4.33 and 4.34.

It is observed that, like GFRP, the transverse steel reinforcement did not contribute to the load carrying capacity in the initial stage of loading. This contribution is more effective after the diagonal cracking (Bousselham and Chaallal 2006). In the

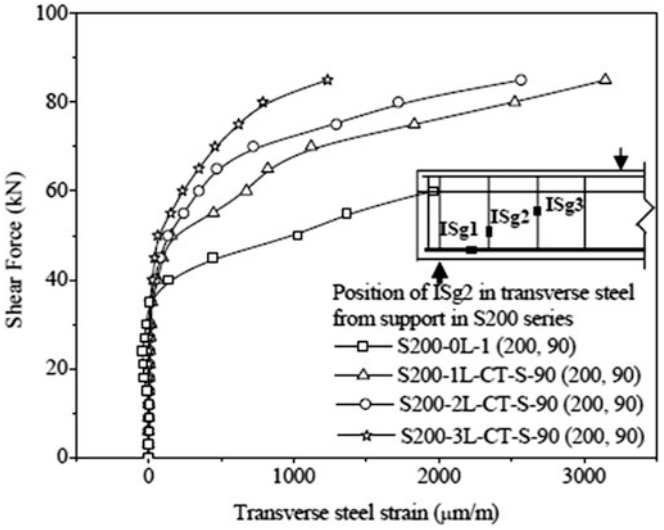

Fig. 4.33 Variation of strain in transverse steel of side-bonded GFRP for S200 series

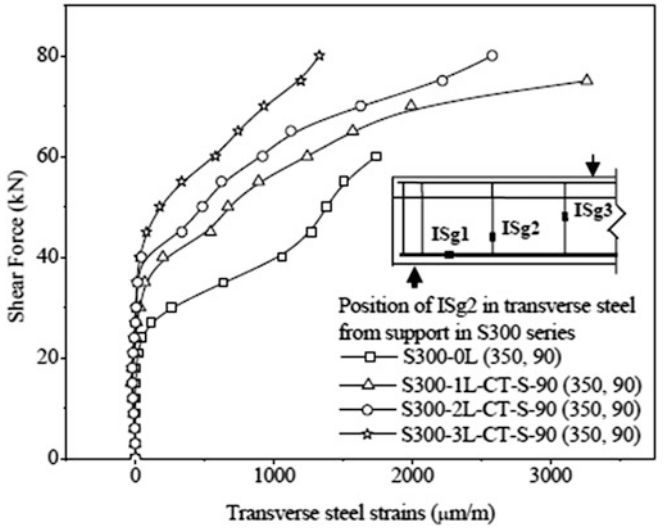

Fig. 4.34 Variation of strain in transverse steel of side-bonded GFRP for S300 series

control specimen S200-0L, it occurred at a shear force of approximately 35 kN. Whereas for the strengthened specimens S200-1L-CT-S-90, S200-2L-CT-S-90 and S200-3L-CT-S-90, it occurred between 40 and 45 kN shear force approximately. Thereafter, as shear force increases, the strain in the transverse steel in all the strain

gauge increases. In control RC T-beam specimen the maximum strain observed is 1962 μstrains at 60 kN shear force. Whereas the strain in strengthened RC T-beam specimens corresponding to this shear force is 676, 348 and 234 μstrains in one, two and three layers. The maximum strain is also observed in S200-1L-CT-S-90, S200-2L-CT-S-90 and S200-3L-CT-S-90 strengthened specimens, which is 3148, 2568 and 1234 μstrains, respectively, at a shear force of 85 kN.

In the S300 series, in the control RC T-beam specimen S300-0L, it occurred at a shear force of approximately 25 kN, whereas for the strengthened RC T-beam specimens S300-1L-CT-S-90, S300-2L-CT-S-90 and S300-3L-CT-S-90, it occurred at a shear force of approximately 30, 35 and 40 kN, respectively. Thereafter, as shear force increases, the strain in the transverse steel increases. In control RC T-beam specimen, the maximum strain is observed 1740 μstrains at 60 kN shear force, whereas the strain in strengthened RC T-beam specimens corresponding to this shear force is 1242, 918 and 578 μstrains in one, two and three layers. The maximum strain observed in S300-1L-CT-S-90, S300-2L-CT-S-90 and S300-3L-CT-S-90 strengthened specimens is 3262, 2578 and 1328 μstrains, respectively.

It is observed that the strain in the transverse steel is less in strengthened RC T-beams as compared to the control RC T-beam for the same amount of shear force. It is also observed that the strain in the RC T-beam specimens strengthened with three layers of side-bonded GFRP sheet is less as compared to the specimens strengthened with one layer of side-bonded GFRP sheet. It may be concluded that the addition of the GFRP sheet delayed the contribution of transverse steel to the shear carrying capacity of the specimens. The addition of second and third layers of GFRP sheet resulted in an additional decrease of the strains in the transverse steel (Bousselham and Chaallal 2006).

4.4.6 *Longitudinal Steel Strain in T-beams with Side-Bonded GFRP*

The curve representing the variation of strains in the tensile longitudinal steel reinforcement due to shear force for varying layers of series S0, S300 and S200 is shown in Fig. 4.35.

The strain gauge ISg1 is located in tensile longitudinal steel reinforcement at a distance of 150 mm from the support for the RC T-beams of series S0, S300 and S200, respectively. As observed from Fig. 4.35, the strain in the longitudinal steel near the support point is very small at the initial stages of loading in all the series. As shear force increases, the strain increases linearly up to about 35 kN shear force as the diagonal shear cracks appear in the concrete. After the appearance of diagonal shear cracks in the concrete, the longitudinal steel reinforcement resists the further increment of shear force (Panda et al. 2013b).

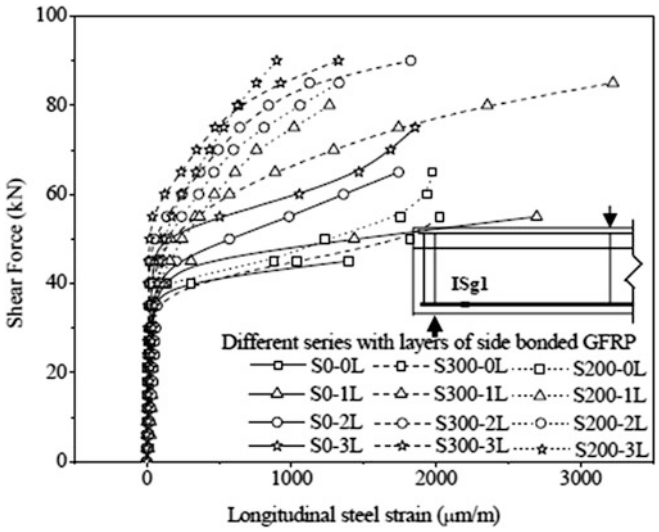

Fig. 4.35 Variation of strain in longitudinal steel for varying layers of all the series (side-bonded)

In S0 series, in control RC T-beam specimen S0-0L, the strain suddenly increased after 35 kN shear force and attained the maximum value of 1392 μstrains at 45 kN shear force, whereas in strengthened RC T-beam specimens S0-1L-CT-S-90, S0-2L-CT-S-90 and S0-3L-CT-S-90, the strain corresponding to this shear force is 305, 203 and 48 μstrains. Thereafter, as shear force increases, the strain suddenly increases in strengthened RC T-beam specimens and attains the maximum value of 2697 μstrains at 55 kN shear force in one layer strengthened specimen, 1742 μstrains at 65 kN shear force in two layer strengthened specimen and 1856 μstrains at 75 kN shear force in three layer strengthened specimen, respectively.

In S300 series, in control RC T-beam specimen S300-0L, the strain suddenly increases after 35 kN shear force and attains the maximum value of 2028 μstrains at 55 kN shear force, whereas in strengthened RC T-beam specimens S300-1L-CT-S-90, S300-2L-CT-S-90 and S300-3L-CT-S-90, the strain corresponding to this shear force is 334, 136 and 38 μstrains. Thereafter, as shear force increases, the strain increases gradually and attains the maximum value of 3226 μstrains at 85 kN, 1826 and 1326 μstrains at 90 kN shear force in one, two and three layer strengthened specimens, respectively.

In S200 series, in control RC T-beam specimen S200-0L, the strain suddenly increases after 40 kN shear force and attains the maximum value of 1976 μstrains at 65 kN shear force, whereas in strengthened RC T-beam specimens S200-1L-CT-S-90, S200-2L-CT-S-90 and S200-3L-CT-S-90, the strain corresponding to this shear force is 611, 464 338 μstrains. Thereafter, as shear force increases, the strain increases gradually in strengthened specimens and attains the maximum value of 1264 μstrains at 80 kN, 1330 μstrains at 85 kN and

898 μstrains at 90 kN shear force in S200-1L-CT-S-90, S200-2L-CT-S-90 and S200-3L-CT-S-90, respectively.

It is observed that the strain in the longitudinal steel, in RC T-beams strengthened with GFRP sheet on side of the web of the T-beams, is less as compared with control RC T-beam specimen for the same amount of shear force for all the series. It may be concluded that the presence of GFRP sheet eased the strains in the longitudinal steel reinforcement at a given applied shear force; the longitudinal steel seems to be less strained in strengthened RC T-beams as compared with control RC T-beam. It is also observed that, as shear reinforcement increases, the strain in the longitudinal steel is less for the same amount of shear force.

4.4.7 *Interaction Between Transverse Steel Reinforcement and GFRP Layers*

(a) **Optimum GFRP Ratio**

The gain in shear capacity is expressed as a percentage of ultimate shear capacity of control RC T-beam specimen (S0-0L). The variation of gain in shear capacity with transverse steel reinforcement ratio is shown in Fig. 4.36.

It is observed from Fig. 4.36, the gain in shear capacity in the entire strengthened T-beams with respect to the (S0-0L) specimen increases as the transverse steel reinforcement ratio increases. As expected, RC T-beams strengthened with one and two layers of GFRP increase steadily up to 0.19% transverse steel reinforcement

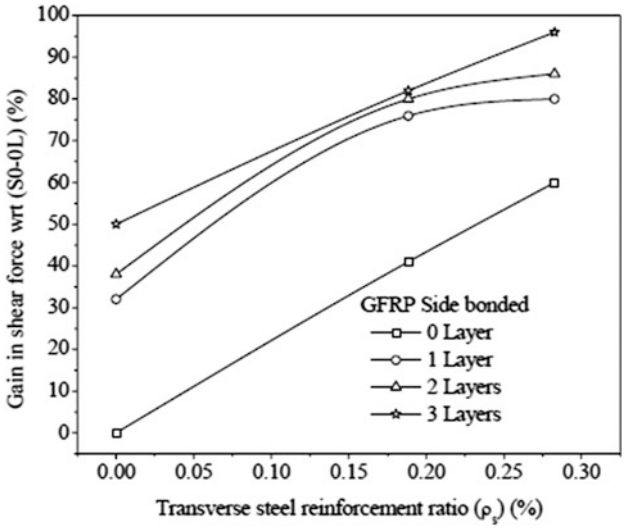

Fig. 4.36 Gain in shear force versus transverse steel reinforcement ratio

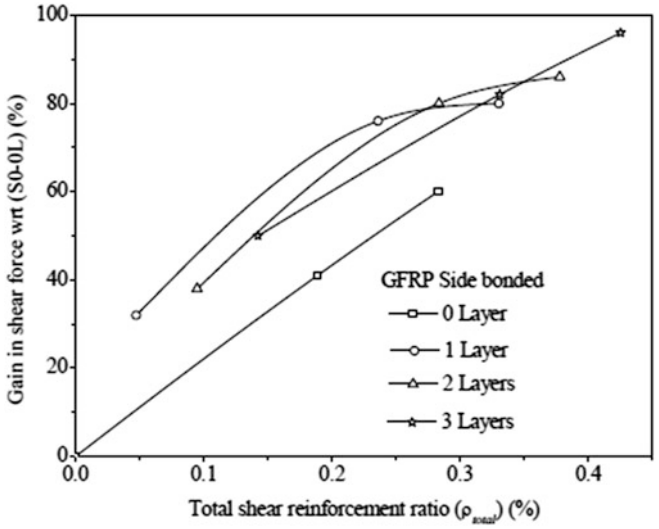

Fig. 4.37 Gain in shear force versus total shear reinforcement ratio

ratio. Thereafter, the gain in shear capacity is shown, no appreciable difference, as transverse steel reinforcement ratio increases. The maximum value of gain in shear capacity is attained in one and two layers of GFRP are 80 and 86% corresponding to the 0.28% of transverse steel reinforcement ratio. Whereas in three layers, the gain in shear capacity increases steadily from 0 to 0.28% and attains the maximum value of 96% corresponding to the transverse steel reinforcement ratio 0.28%.

The variation of gain in shear capacity with total shear reinforcement ratio (ρ_{total}) is shown in Fig. 4.37.

It is observed from Fig. 4.37, the gain in shear force correspond to one, two three layers specimen is more as compared with zero layer (control) specimen. As the total shear reinforcement ratio increases, the gain in shear force in one and two layers specimen increases steadily up to 0.236 and 0.238%, respectively. Thereafter, the gain in shear force is not changed appreciable amount, and it reaches the 80 and 86% corresponding to the total reinforcement ratio of 0.33 and 0.37%. Whereas in three layers specimen, it increases steadily and attains the maximum value of 96% corresponding to the total shear reinforcement ratio 0.425%. Figure 4.38 proposed a correlation for variation of gain in shear capacity with total shear reinforcement ratio.

It may be concluded that the gain in shear force in strengthened T-beams is mainly due to both GFRP reinforcement and transverse steel reinforcement. The interaction between transverse steel reinforcement and GFRP layers plays a significant role in gain the shear capacity of the strengthened T-beams.

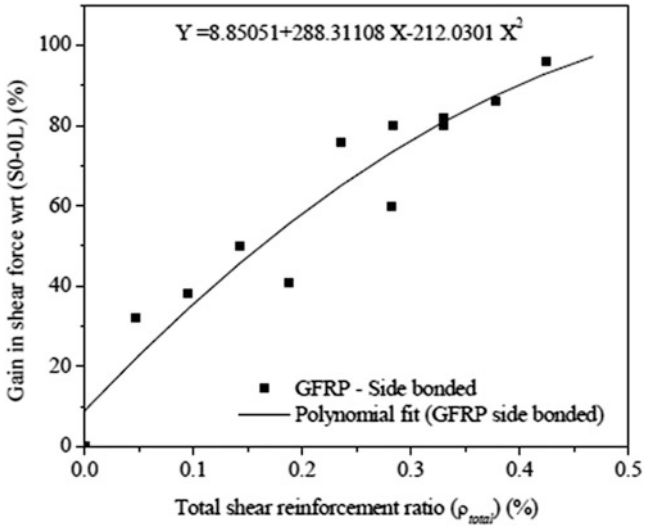

Fig. 4.38 Gain in shear force versus total shear reinforcement ratio (correlation)

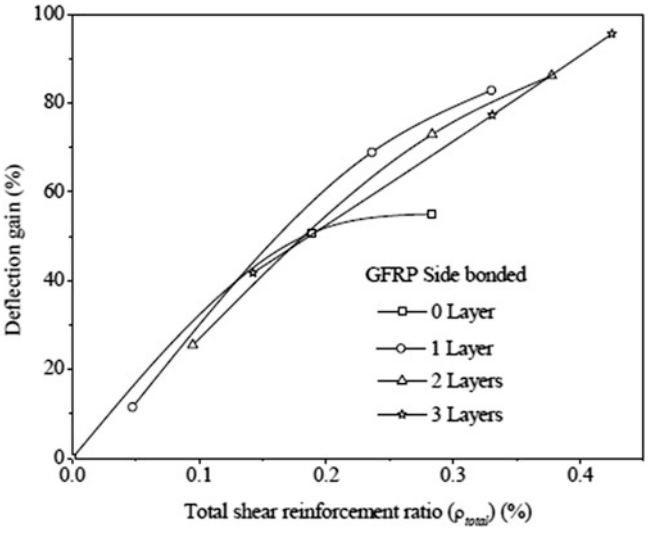

Fig. 4.39 Midspan deflection gain versus total shear reinforcement ratio

(b) **Ductility of Strengthened T-beams**

The gain in deflection versus the total shear reinforcement ratio (ρ_{total}) of the T-beams strengthened in shear with GFRP sheets on side of the web of the T-beams is shown in Fig. 4.39.

The deflection gain is expressed in terms of the midspan deflection of S0-0L specimen. It may be observed that the gain in deflection increases as the total shear reinforcement ratio increases in all the specimens. The maximum gain in deflection observed in three-layered specimen is 95% corresponding to the total shear reinforcement ratio (ρ_{total}) of 0.425%, whereas in one and two layers specimen, the maximum gain is 82.9 and 86% corresponding to the total shear reinforcement ratio (ρ_{total}) of 0.33 and 0.377%.

It may be concluded that the increase of layers and transverse steel reinforcement, increases the ductility of the GFRP strengthened RC T-beams.

4.5 RC T-beams Strengthened in Shear Zone with Externally Bonded GFRP Strips

Nine RC T-beams were strengthened in shear zone with GFRP strips in U-shape and side-bonded with orientation of the strips at 45° and 90° to the longitudinal axis of the beam in each series (Panda et al. 2011b, c 2013a).

Figure 4.40 shows the detail strengthening configuration for three series S0, S300 and S200. The shear contribution of GFRP strips for different configurations and orientations as compared with control specimens is calculated.

4.5.1 Shear Strength Contribution by GFRP Strips

The experimental results of RC T-beams strengthened in shear with GFRP strips for different configurations and orientations are calculated and presented in Table 4.4 (Panda et al. 2013a).

(a) **S0 Series**

From Table 4.4, it is observed that for strengthened RC T-beam specimen S0-1L-ST-S-90, the load at ultimate failure is 116 kN, compared to 100 kN for control RC T-beam specimen S0-0L. This indicates that there is a gain of 16% strength over the control specimen. As for the influence of the configuration and orientation of GFRP strips on the gain in strength, that is, for S0-1L-ST-U-90 and S0-1L-ST-S-45, the loads at ultimate failure are 124 and 146 kN, respectively. The percentage gain in strength is 24 and 46%, respectively, on loads over control specimen S0-0L (Panda et al. 2011b, 2013a). It is expected that without transverse steel reinforcement, the strengthened RC T-beams with GFRP side strips perpendicular to the diagonal shear cracks outperformed those strengthened with vertical GFRP strips at 90° to the longitudinal axis of the beam.

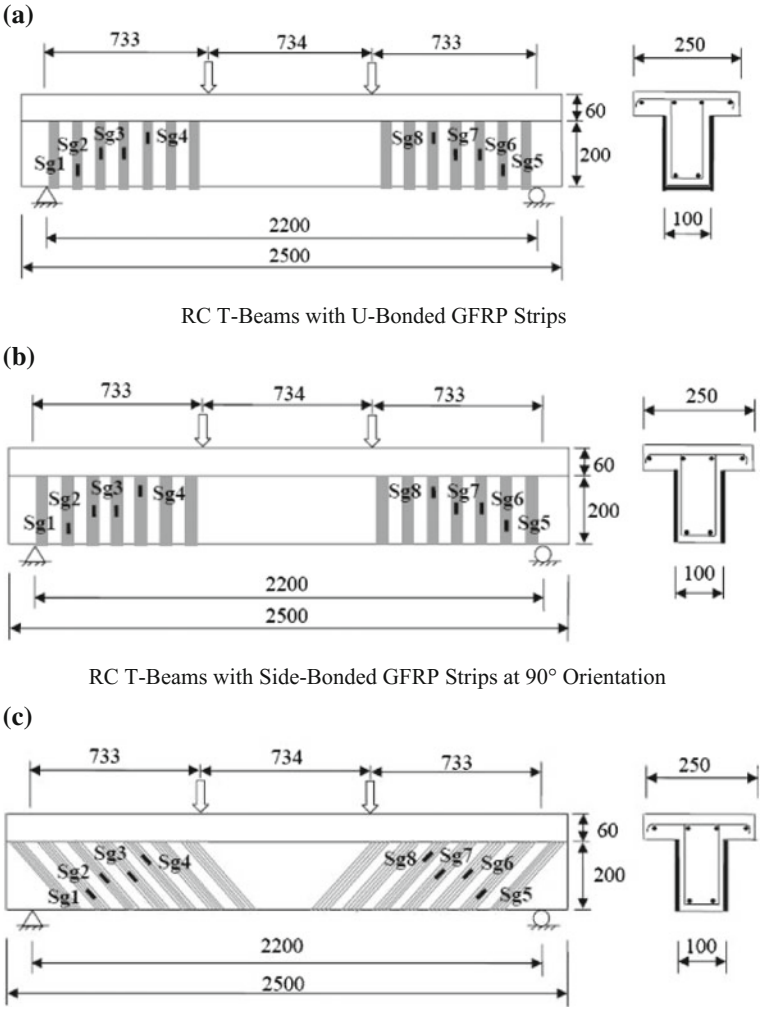

Fig. 4.40 RC T-beams strengthened in shear with GFRP strips for all the series

(b) **S300 Series**

From Table 4.4, it is observed that for strengthened RC T-beam specimen S300-1L-ST-S-90, the ultimate failure load is 154 kN, compared to 141 kN for control RC T-beam specimen S300-0L. A percentage gain in strength of 9.22% is observed over the control specimen. As GFRP configuration and orientation on the gain in strength observed, that is, for S300-1L-ST-U-90 and S300-1L-ST-S-45, the loads at ultimate failure are 164 and 166 kN, respectively. The percentage gain in strength for these two strengthened specimens is 16.31 and 17.73%, respectively, as

Table 4.4 Shear contribution of GFRP strips

Specimen designation	Load at failure (kN)	Total shear resistance $V_{n,test}$ (kN)	Resistance due to concrete $V_{c,test}$ (kN)	Resistance due to steel $V_{s,test}$ (kN)	Shear resistance due to GFRP $V_{f,test}$ (kN)	Gain in shear resistance due to GFRP (%)	Mode of failure
S0-0L	100	50	50	00	00	00	Shear
S300-0L	141	70.5	50	20.5	00	00	Shear
S200-0L	160	80	50	30	00	00	Shear
S0-1L-ST-S-90	116	58	50	00	08	16	GFRP debonding
S0-1L-ST-S-45	146	73	50	00	23	46	GFRP debonding and rupture failure
S0-1L-ST-U-90	124	62	50	00	12	24	GFRP debonding and rupture failure
S300-1L-ST-S-90	154	77	50	20.5	6.5	9.22	GFRP debonding
S300-1L-ST-S-45	166	83	50	20.5	12.5	17.73	GFRP debonding and rupture failure
S300-1L-ST-U-90	164	82	50	20.5	11.5	16.31	GFRP debonding and rupture failure
S200-1L-ST-S-90	172	86	50	30	06	7.5	GFRP debonding
S200-1L-ST-S-45	182	91	50	30	11	13.75	GFRP debonding and rupture failure
S200-1L-ST-U-90	186	93	50	30	13	16.25	GFRP debonding and rupture failure

compared with the control specimen S300-0L (Panda et al. 2013a). As expected, with transverse steel reinforcement at 300 mm stirrup spacing, the RC T-beams strengthened with GFRP strips on side of the web of the T-beams at 45° orientation to the longitudinal axis of the beam carry more loads than the other.

(c) **S200 Series**

From Table 4.4, it is observed that for strengthened RC T-beam specimen of S200 series, the ultimate failure load of S200-1L-ST-S-90, S200-1L-ST-U-90 and S200-1L-ST-S-45 specimens is 172, 186 and 182 kN, respectively, compared to 160 kN for control RC T-beam specimen S200-0L. This indicates a gain in strength 7.5, 16.25 and 13.75%, respectively, on loads over control specimen (Panda et al. 2013a). As expected, with transverse steel reinforcement at 200 mm stirrup spacing, the RC T-beams strengthened with U-shape GFRP strips carry more loads than the other.

It is concluded from the three series that the shear strength contribution of GFRP strips for different configurations and orientations, without transverse steel reinforcements, is relatively more effective than with transverse steel reinforcements.

4.5.2 Deflection of T-beams Bonded with GFRP Strips

The load versus midspan deflection for the RC T-beams of series S0, S300 and S200 with varying configuration U-shape and side-bonded with orientation of the GFRP strips at 90° and 45° to the longitudinal axis of the beam as obtained from the experiment is shown in Figs. 4.41, 4.42 and 4.43.

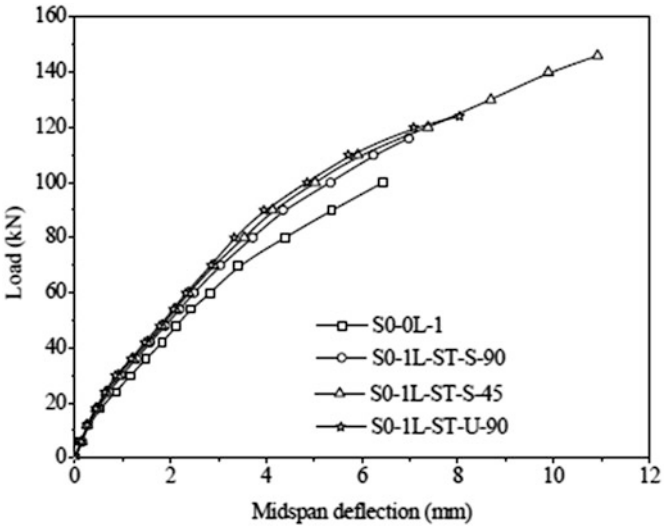

Fig. 4.41 Load versus midspan deflection of T-beam with GFRP strips for series S0

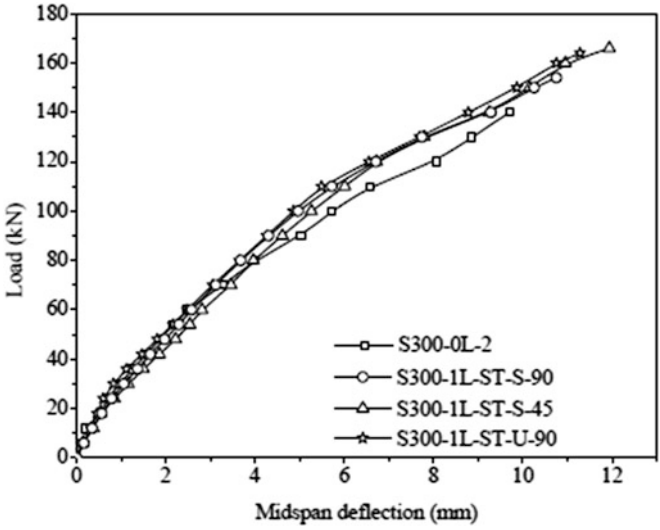

Fig. 4.42 Load versus midspan deflection of T-beams with GFRP strips for series S300

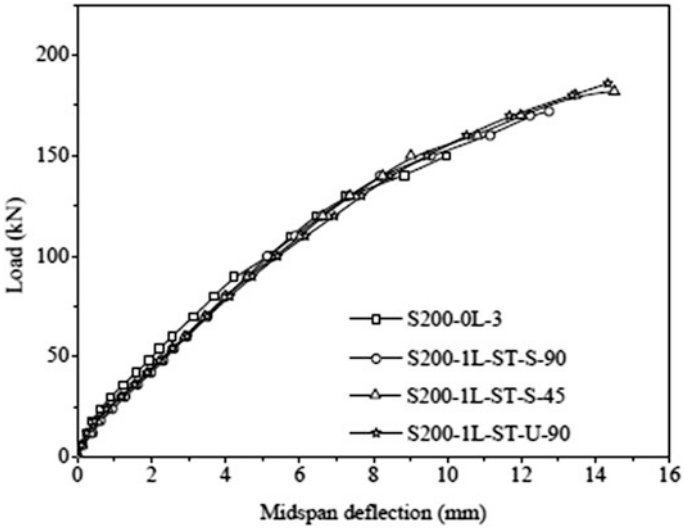

Fig. 4.43 Load versus midspan deflection of T-beams with GFRP strips for series S200

It is observed from Fig. 4.41, the maximum deflection of strengthened RC T-beam specimens S0-1L-ST-S-90, S0-1L-ST-S-45 and S0-1L-ST-U-90 is 6.98, 10.92 and 8.04 mm corresponding to the ultimate failure load of 116, 146 and 124 kN. Whereas in control RC T-beam specimen S0-0L, the maximum deflection

is 6.44 mm corresponding to 100 kN failure load (Panda et al. 2011b, 2013a). It is also observed that the midspan deflection of RC T-beams, strengthened in shear with GFRP strips is less as compared to the control RC T-beam for the same load. As expected, RC T-beams strengthened with GFRP strips with orientation of the strip at 45° to the longitudinal axis of the beam carry more load and also demonstrate more ductility.

As observed from Fig. 4.42, for S300 series, the deflection of control and strengthened RC T-beams is almost same up to 80 kN loads. It is also observed that the deflection in RC T-beams strengthened with GFRP strips is less in comparison to the control RC T-beams with the same amount of load. The maximum deflection of strengthened RC T-beam specimens S300-1L-ST-S-90, S300-1L-ST-S-45 and S300-1L-ST-U-90 is 10.75, 11.94 and 11.28 mm corresponding to the failure load of 154, 166 and 164 kN, respectively, whereas in control RC T-beam, the value is 9.71 mm corresponding to the failure load of 140 kN (Panda et al. 2013a). As expected, RC T-beam strengthened with GFRP strips on side of the web of the T-beams, with orientation of the strip at 45° to the longitudinal axis of the beam, carries more load and also demonstrates more ductility.

As observed from Fig. 4.43, the midspan deflection of control and strengthened RC T-beams of series S200 is almost equal. The maximum deflection of RC T-beam strengthened with GFRP strips for specimens S200-1L-ST-S-90, S200-1L-ST-S-45 and S200-1L-ST-U-90 is 12.75, 14.51 and 14.34 mm corresponding to the failure load of 172, 182 and 186 kN. In control RC T-beam (S200-0L), the value is 9.98 mm corresponding to the failure load of 150 kN. The RC T-beams strengthened with U-shape GFRP strips carry more load, whereas the RC T-beams strengthened with side shape GFRP strips at 45° orientation to the longitudinal axis of the beam show slightly more deflection.

It is concluded from the three series, the midspan deflection of RC T-beams strengthened with GFRP strips in different configurations and orientations, and with adequate amount of transverse steel reinforcements gave more deflection than RC T-beam without any transverse steel reinforcements.

4.5.3 Modes of Failure of T-beams Bonded with GFRP Strips

The failure modes of strengthened RC T-beams of series S0, S300 and S200 with U-shape, and side-bonded GFRP strips at 45° and 90° to the longitudinal axis of the beam are shown in Fig. 4.44.

(a) **S0 Series**

It is observed in strengthened RC T-beam with side-bonded GFRP strips in 90° orientation, in specimen S0-1L-ST-S-90, the diagonal shear crack initiated at a load of 80 kN. The crack propagated as the load increases in a similar manner as

Fig. 4.44 Failure modes of tested beams (GFRP strips)

observed in the control RC T-beam specimen S0-0L. The failure occurred due to debonding of GFRP strips over the main diagonal shear crack at an ultimate load of 116 kN. At the same time, the diagonal shear crack propagated to the loading position through the flange (Panda et al. 2011b, 2013a). In left side of the RC T-beam (view-A), the second, third, fourth and fifth strips get debonded from the concrete surface. Similarly, in right side of the RC T-beam, strips second, third and fourth get debonded from the concrete surface.

It is observed, in strengthened T-beam S0-1L-ST-S-45, the diagonal shear crack initiated at a load of 80 kN in the concrete surface (Panda et al. 2011b, 2013a). Thereafter, with increasing the load, the width of the diagonal shear crack increases slowly. At the same time, the strain in the GFRP strips increases slowly until the load reached the ultimate strength of the control RC T-beam. Once the diagonal shear cracks occurred in the shear span, the strain in the GFRP strip increases rapidly and continues until the beam gets failed. The ultimate failure of the strengthened RC T-beam is attained at a load of 146 kN. The failure of the GFRP strips is occurred due to debonding of the GFRP strip and GFRP rupture from the concrete surface.

It is observed in strengthened RC T-beam with U-bonded GFRP strips, in S0-1L-ST-U-90 specimen, the diagonal shear crack initiated at a load of 70 kN. As load increases, the width of the crack gets increased. The debonding of the most of the GFRP strips is caused from the concrete surface at an ultimate load of 124 kN (Panda et al. 2011b, 2013a). In left side (view-A) of the RC T-beam, GFRP rupture and debonding have been caused in the second GFRP strip. Figure 4.44a shows the cracking pattern and failure modes of the tested beams of series S0.

(b) **S300 Series**

It is observed in strengthened RC T-beam of S300 series with side-bonded GFRP strips in 90° orientation, in specimen S300-1L-ST-S-90, the diagonal shear crack started at a load of 90 kN. With increasing load, the width of the crack also increased. At the same time, the GFRP strip, which crosses the shear crack, increased. The ultimate failure of the strengthened RC T-beam is caused due to debonding of the GFRP strips at a load of 154 kN (Panda et al. 2013a). It is observed during experimentation that there is GFRP debonding in left shear span of the RC T-beam (view-A) for the second, third, fourth and fifth GFRP strips. The second GFRP strip is debonded for a length of 50 mm and gets initiated from the bottom of the strip, whereas the third, fourth and fifth GFRP strips get initiated from the top of the strip and are developed approximately for a length of 150, 160 and 140 mm, respectively.

It is observed in strengthened RC T-beam of S300 series with side-bonded GFRP strips in 45° orientation, in specimen S300-1L-ST-S-45, the diagonal shear crack initiated at a load of 90 kN. Once the diagonal shear cracks occurred in the shear span, the strain in the GFRP strip increased suddenly and continued till the failure of the strengthened RC T-beam. The ultimate failure of the RC T-beam is attained at a load of 166 kN (Panda et al. 2013a). The failure of the GFRP strips is caused due to debonding and rupture of the GFRP strips. It is also observed during

experimentation, in left shear span of the beam (view-A), the debonding of the second and third GFRP strips gets initiated from the bottom and is developed for a length of 170 and 140 mm, respectively. Whereas the fourth GFRP strip debonded the whole surface, and the fifth GFRP strip is debonded from the top and developed for a length of 80 mm. However, the other side of the RC T-beam, the GFRP strip gets ruptured at the ultimate failure of the beam.

It is observed in RC T-beam strengthened in shear with U-shape GFRP strips of series S300, in S300-1L-ST-U-90 specimen, the diagonal shear crack initiated at a load of 90 kN. The ultimate failure of the strengthened RC T-beam is caused at a load of 164 kN. The failure of the GFRP strips is caused due to debonding and rupture of the GFRP strips (Panda et al. 2013a). It is observed during experimentation, in left shear span of the RC T-beam (view-A), the failure of the second GFRP strip is caused by GFRP rupture. The rupture takes place at a height 70 mm from the bottom of the strip. Whereas the third, fourth and fifth GFRP strips get debonded from the concrete surface. The third GFRP strip is debonded the whole surface. Debonding of the fourth and fifth GFRP strip started from the top of the strip and is developed approximately 130 mm length and 80 mm length approximately. Figure 4.44b shows the cracking pattern and modes of failure of the tested beams of series S300.

(c) **S200 Series**

It is observed in strengthened RC T-beam of S200 series with side-bonded GFRP strips in 90° orientation, in S200-1L-ST-S-90 specimen, the diagonal shear crack initiated at a load of 110 kN. As load increases, the width of the crack also gets increased. The failure of the GFRP strips is caused mainly due to debonding of the GFRP strips from the concrete surface at a load of 172 kN. It is also observed during experimentation, in left shear span, the debonding of a second GFRP strip gets initiated from the bottom and is developed for a length of 60 mm, the third GFRP strip is ruptured at a height of 75 mm from the bottom. Whereas the debonding of fourth and fifth GFRP strips gets initiated from the top and is developed for a length of 150 and 40 mm, respectively. In right shear span (view-B), the strips second and third get debonded from the bottom and are developed approximately 100 and 80 mm length, respectively. Whereas the fourth and fifth strips debonded from the top and were developed approximately 150 and 110 mm length, respectively.

It is observed in strengthened RC T-beam of S200 series with side-bonded GFRP strips in 45° orientation, in specimen S200-1L-ST-S-45, the diagonal shear crack originated at a load of 110 kN in both sides of the shear span. As load increases, the width of the shear crack is also increased; consequently, the strain in the GFRP strips started increasing until the load reached the ultimate strength of the control RC T-beam. The ultimate failure of the strengthened RC T-beam is attained at a load of 182 kN. The failure of the strengthened RC T-beam is caused due to rupture of the GFRP strips. In left shear span (view-A), first GFRP strip is debonded

30 mm length from the bottom, second GFRP strip debonded from the bottom for a length of 160 mm, third GFRP strip debonded from the top for a length of 220 mm, and fourth GFRP strip ruptured at a distance of 120 mm from the top of the strip. In right shear span, the GFRP strips second, third, fourth and fifth ruptured at a length of 80, 110, 110 and 170 mm from the bottom of the strip.

It is observed in RC T-beam strengthened in shear with U-shape GFRP strips of series S200, in specimen S200-1L-ST-U-90, the diagonal shear crack originated at a load of 110 kN. The ultimate failure of the strengthened RC T-beam is attained at a load of 186 kN due to debonding and rupture of the GFRP strips. In left shear span (view-A), the debonding of the first GFRP strip is started from the bottom and is developed approximately for a length of 70 mm. The second and third GFRP strips are debonded the whole surface, and the fourth strip debonded from the top and developed approximately for a length of 40 mm. In right shear span, first, second and third GFRP strips debonded from the bottom and were developed for a length of 60, 70 and 150 mm, respectively. At the time of ultimate failure, the diagonal shear crack is propagated towards loading position through the flange. Figure 4.44c shows the cracking pattern and modes of failure of the tested beams of series S200.

The modes of failure of RC T-beams strengthened in shear with GFRP strips indicate in all the series that the side-bonded GFRP strip and at 90° orientation to the longitudinal axis of the beam fails due to GFRP debonding, whereas for side-bonded GFRP strip with 45° orientation to the longitudinal axis of the beam and U-shaped GFRP strip the fails due to GFRP debonding and rupture.

4.5.4 Strain in GFRP Strips

(a) **S0 Series**

The variation of vertical strains in GFRP strip with shear force for different configurations and orientations of GFRP strips in S0 series is presented in Fig. 4.45.

The strain in the GFRP strips in all the strain gauges of the strengthened RC T-beams did not contribute to the shear carrying capacity at the initial stages of loading. In specimen S0-1L-ST-S-90, the strain in the GFRP strip in most of the strain gauges started increasing between 40 and 45 kN shear force approximately. Thereafter, as shear force increases, the strain in the GFRP strips suddenly increases and attains the maximum value of 8884 μstrains at 58 kN shear force. Whereas in strengthened RC T-beam specimen S0-1L-ST-S-45, the strain in the GFRP strip started increasing in all the strain gauges between 40 and 50 kN shear force. The maximum strain observed is 9932 μstrains at 70 kN shear force in Sg8 strain gauge. In S0-1L-ST-U-90 strengthened specimen, the strain in the GFRP strip started increasing after 35 kN shear force and attained the maximum value of 9076 μstrains at 62 kN shear force (Panda et al. 2011b).

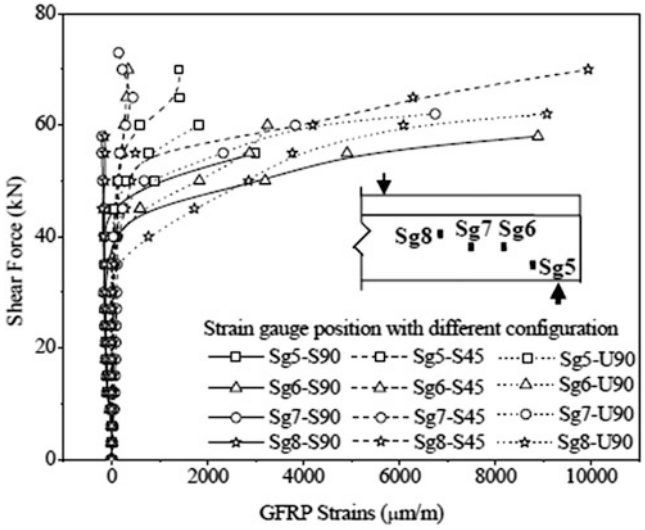

Fig. 4.45 Variation of vertical strain in GFRP strip for series S0

RC T-beams strengthened in shear with side-bonded GFRP strips, in series S0, the strain is higher for specimens with GFRP strip at 45° orientation to the longitudinal axis of the beam, whereas in 90° orientation, GFRP strain is less.

(b) **S300 Series**

The variation of vertical strains in GFRP strip with shear force for different configurations and orientations of GFRP strips in S300 series specimens is presented in Fig. 4.46.

The strain in the GFRP strip in all the strain gauges of RC T-beams did not contribute to the shear carrying capacity approximately between 35 and 40 kN shear force. As shear force increases, the GFRP strain increases suddenly in strengthened RC T-beam specimens S300-1L-ST-S-90 and S300-1L-ST-S-45, and attains the maximum value 7497 μstrains at 60 kN shear force and 7917 μstrains at 65 kN shear force, respectively (Panda et al. 2013a). Whereas in S300-1L-ST-U-90 strengthened specimen, the strain in the GFRP strips increases slowly up to 50 kN shear force, thereafter as shear force increases, the GFRP strain increases suddenly and attains the maximum value of 9450 μstrains at 65 kN shear force.

In series S300, the maximum strain is observed in RC T-beams strengthened with GFRP strips in U-shape. Whereas in side-bonded, the GFRP strain is higher in the specimen strengthened with the GFRP strips on side of the web of the T-beams at 45° orientation to the longitudinal axis of the beam.

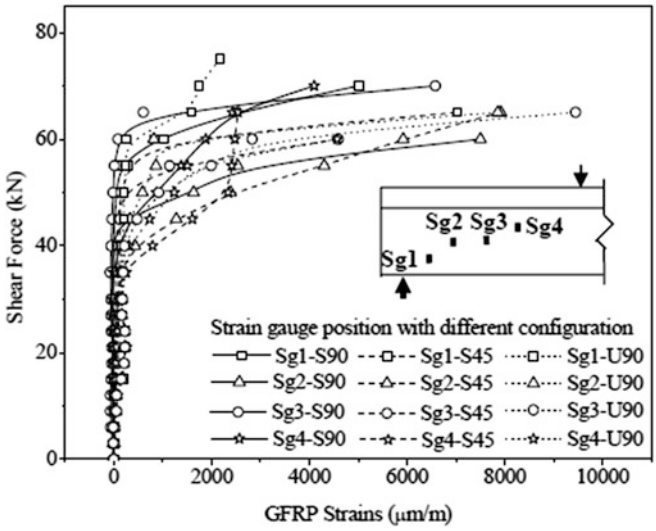

Fig. 4.46 Variation of vertical strain in GFRP strip for series S300

(c) **S200 Series**

The variation of vertical strains in GFRP strip due to shear force for different configurations and orientations of GFRP strips in S200 series specimens is presented in Fig. 4.47.

The strain in the GFRP strips in all the strain gauges of RC T-beams did not contribute to the shear carrying capacity at the initial stages of loading or very negligible amount up to approximately between 40 and 50 kN shear force in all the specimens (Panda et al. 2013a). Thereafter, as shear force increases, the maximum GFRP strain in strengthened RC T-beam specimen (S200-1L-ST-S-90) is measured 7548 μstrains at 85 kN shear force in Sg5 strain gauge. Whereas in S200-1L-ST-S-45 and S200-1L-ST-U-90 strengthened specimens, the value is 7716 μstrains at 85 kN shear force in Sg5 strain gauge and 8978 μstrains at 80 kN shear force in Sg6 strain gauges, respectively.

In series S200, the maximum strain is observed in U-shape strengthened RC T-beam. Whereas in side-bonded strengthened T-beams, the maximum strain is observed for 45° orientations of GFRP strips.

It may be noted that, without any transverse steel reinforcement, the strain is higher in RC T-beams strengthened with the GFRP strips in 45° orientation, whereas with adequate amount of transverse steel reinforcements, the strain is higher in beams strengthened with the GFRP strips in U-shape.

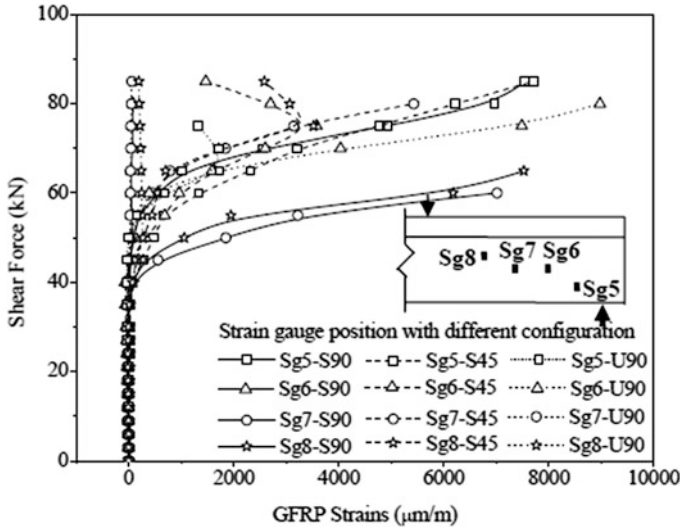

Fig. 4.47 Variation of vertical strains in GFRP strip for series S200

4.5.5 Transverse Steel Strain in T-beams Bonded with GFRP Strips

The curves representing the shear force versus the strains in the transverse steel reinforcement of RC T-beams strengthened in shear with GFRP strips of series S200 and S300 and for strain gauge ISg3 and ISg2 are shown in Figs. 4.48 and 4.49.

It is observed that in RC T-beams strengthened in shear with GFRP strips, the transverse steel reinforcement did not contribute to the shear carrying capacity at the initial stage of loading (Panda et al. 2013b). This contribution is more effective after the diagonal cracking. In the control RC T-beam specimen S200-0L, and strengthened RC T-beam specimens S200-1L-ST-S-90 and S200-1L-ST-U-90, it occurred between 35 and 40 kN shear force. Whereas in strengthened specimen S200-1L-ST-S-45, the contribution is effective from the beginning and shows lesser value up to 40 kN shear force. Thereafter, the strain in the transverse steel in the entire strengthened RC T-beam gets increased with the increase in shear forces. The maximum strain observed in control specimen is 1983 μstrains at 60 kN shear force, whereas the strain in strengthened RC T-beams corresponding to this shear force is 1905, 1152, 624 μstrains in S200-1L-ST-S-90, S200-1L-ST-S-45 and S200-1L-ST-U-90. The maximum strain also observed in S200-1L-ST-S-90, S200-1L-ST-S-45 and S200-1L-ST-U-90 strengthened specimens is 2606 μstrains at 65 kN shear force and 1864 and 1422 μstrains at 75 kN shear force, respectively.

In the series S300, in the control RC T-beam specimen (S300-0L), the contribution of transverse steel reinforcement to the shear carrying capacity is occurred

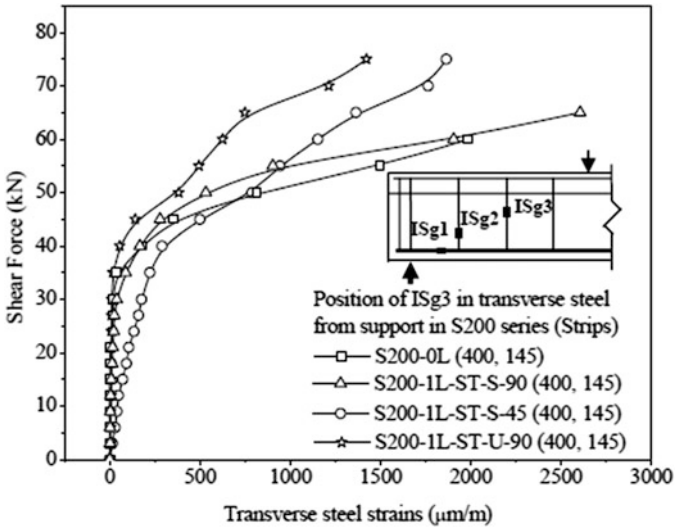

Fig. 4.48 Variation of strain in transverse steel of RC T-beam bonded with GFRP strips for S200 series

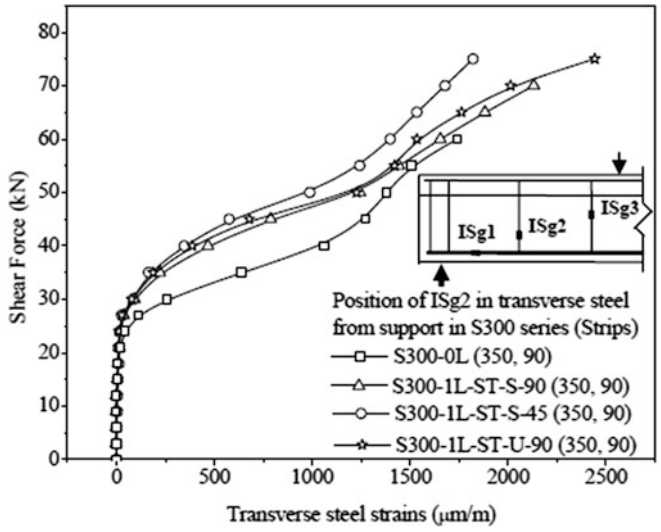

Fig. 4.49 Variation of strain in transverse steel of RC T-beams bonded with GFRP strips for S300 series

approximately after 25 kN shear force, whereas for the strengthened RC T-beam specimens S300-1L-ST-S-90, S300-1L-ST-S-45 and S300-1L-ST-U-90, it occurred between the shear force of 25–30 kN. Thereafter, as shear force increases, the strain in the transverse steel increases Panda et al. (2011C). In control RC T-beam specimen, the maximum strain is observed 1740 μstrains at 60 kN shear force, whereas the strain in strengthened RC T-beams corresponding to this shear force is 1654, 1534 and 1398 μstrains in S200-1L-ST-S-90, S200-1L-ST-U-90 and S200-1L-ST-S-45. The maximum strain is also observed in strengthened RC T-beams 2132 μstrains at 70 kN shear force, and 1822 and 2443 μstrains at 75 kN shear force, respectively (Panda et al. 2011a, c).

It is observed that the strain in the transverse steel is less in strengthened RC T-beams as compared to the control RC T-beam for the same amount of shear force. So far as the configuration of GFRP strips is concerned, the strain in the transverse steel with U-bonded GFRP strips is less as compared to the side-bonded GFRP strips for S200 series, whereas in S300 series, it is more as compared with the diagonal side strips.

4.5.6 *Longitudinal Steel Strain in T-beams Bonded with GFRP Strips*

The variation of strain in longitudinal steel with shear force for different configurations and orientations of GFRP strips for series S0, S300 and S200 is shown in Fig. 4.50 (Panda et al. 2013a).

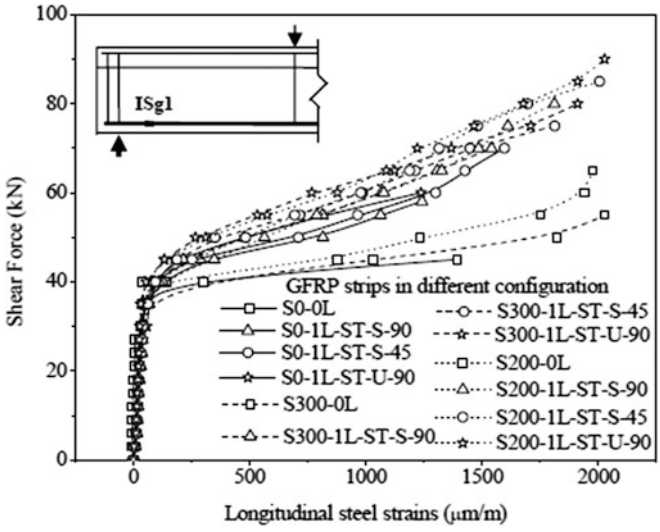

Fig. 4.50 Variation of strain in longitudinal steel for different configurations

It is observed from Fig. 4.50, at the initial stages of loading, the strain in the longitudinal steel is very small near the support point. As shear force increases, the strain in the longitudinal steel increases linearly up to about 35 kN shear force as the diagonal shear cracks appear in the concrete. After the diagonal shear cracks appear in the concrete, the longitudinal steel reinforcement resists the further increments of shear force. In series S0, in control RC T-beam specimen S0-0L, the strain suddenly increases after 35 kN shear force and attains the maximum value of 1392 μstrains at 45 kN shear force. Whereas in strengthened RC T-beam specimens S0-1L-ST-S-90, S0-1L-ST-S-45 and S0-1L-ST-U-90, the strain corresponding to this shear force is 288, 215 and 176 μstrains. Further, with increasing shear force, the longitudinal steel strain increases suddenly in strengthened RC T-beams and attains the maximum value of 1242 μstrains at 58 kN shear force in S0-1L-ST-S-90, 1596 μstrains at 70 kN shear force in S0-1L-ST-S-45 and 1238 μstrains at 60 kN shear force in S0-1L-ST-U-90 specimen (Panda et al. 2011b). Similarly, in series S300, in control RC T-beam S300-0L, the strain in the longitudinal steel suddenly increases after 35 kN shear force and attains the maximum value of 2028 μstrains at 55 kN shear force. Whereas in strengthened RC T-beam specimens S300-1L-ST-S-90, S300-1L-ST-S-45 and S300-1L-ST-U-90, the strain corresponding to this shear force is 815, 717 and 534 μstrains. Thereafter, as shear force increases, the longitudinal steel strain increases gradually in strengthened RC T-beams and attains the maximum value of 1541 μstrains at 70 kN shear force in S300-1L-ST-S-90 specimen, 1813 μstrains at 75 kN shear force in S300-1L-ST-S-45 specimen and 1912 μstrains at 80 kN shear force in S300-1L-ST-U-90 specimen. Similarly, in series S200, in control RC T-beam S200-0L, the strain suddenly increases after 35 kN shear force and attains the maximum value of 1976 μstrains at 65 kN shear force. Whereas in strengthened RC T-beam specimens S200-1L-ST-S-90, S200-1L-ST-S-45 and S200-1L-ST-U-90, the strain corresponding to this shear force is 1327, 1188 and 1088 μstrains. Thereafter, as shear force increases, the longitudinal steel strain increases gradually in strengthened RC T-beams and attains the maximum value of 1812 μstrains at 80 kN shear force in S200-1L-ST-S-90 specimen, 2006 μstrains at 85 kN shear force in S200-1L-ST-S-45 specimen and 2028 μstrains at 90 kN shear force in S200-1L-ST-U-90 specimen.

It is noted that the strain in the longitudinal steel, in RC T-beams strengthened with GFRP strips, is less in comparison to the control RC T-beam for the same amount of shear force in all the series. It is also observed that the strain in the longitudinal steel in RC T-beam strengthened with U-shape GFRP strips is less in comparison to the side-bonded GFRP strips for the same amount of shear force (Panda et al. 2011b, 2013a). It is also expected that, as transverse steel reinforcement increases, the longitudinal steel is less strained for the same amount of shear force.

4.6 RC T-beams Strengthened in Shear Zone with Externally Bonded GFRP Sheet

Nine RC T-beams were strengthened in shear zone with externally bonded GFRP sheet in U-shape, side-bonded and U-shaped with anchorage for each of the series (Panda et al. 2013b). The detail strengthening configuration for three series is shown in Fig. 4.51. The shear strength contribution of GFRP sheet for different configurations is calculated and presented in Table 4.5.

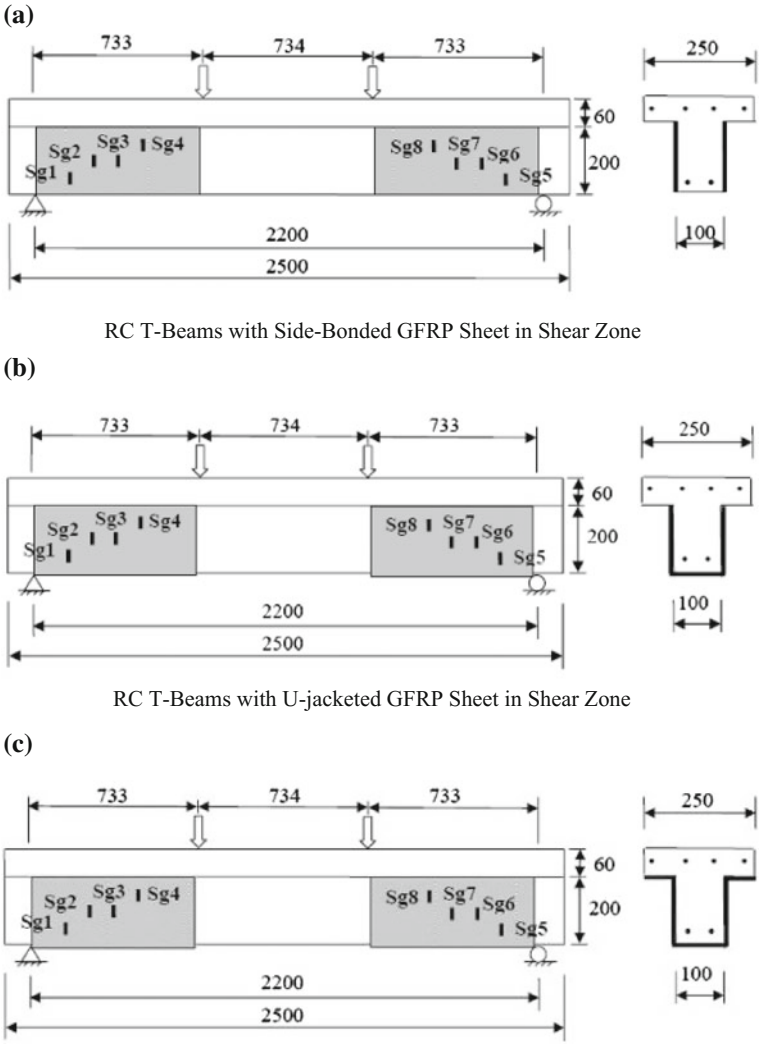

Fig. 4.51 RC T-beams strengthened in shear zone with GFRP for all the series

Table 4.5 Shear strength contribution of GFRP sheet in shear zone

Specimen	Load at failure (kN)	Total shear resistance $V_{n,\text{test}}$ (kN)	Resistance due to concrete $V_{c,\text{test}}$ (kN)	Resistance due to steel $V_{s,\text{test}}$ (kN)	Shear resistance due to GFRP $V_{f,\text{test}}$ (kN)	Gain in shear resistance due to GFRP (%)	Modes of failure
S0-0L	100	50	50	00	00	00	Shear
S300-0L	141	70.5	50	20.5	00	00	Shear
S200-0L	160	80	50	30	00	00	Shear
S0-1L-SZ-S-90	130	65	50	00	15	30	GFRP debonding
S0-1L-SZ-U-90	132	66	50	00	16	32	GFRP debonding and rupture failure
S0-1L-SZ-UA-90	140	70	50	00	20	40	GFRP debonding and rupture failure
S300-1L-SZ-S-90	178	89	50	20.5	18.5	26.24	Rupture failure
S300-1L-SZ-U-90	180	90	50	20.5	19.5	27.66	Rupture failure
S300-1L-SZ-UA-90	192	96	50	20.5	25.5	36.17	Rupture failure
S200-1L-SZ-S-90	184	92	50	30	12	15	Rupture failure
S200-1L-SZ-U-90	188	94	50	30	14	17.5	Rupture failure
S200-1L-SZ-UA-90	196	98	50	30	18	22.5	Rupture failure

4.6.1 Shear Strength Contribution by GFRP Sheet

The experimental results of RC T-beams strengthened in shear zone with GFRP sheet in different configurations were calculated and presented in Table 4.5 (Panda et al. 2013b).

(a) **S0 Series**

From Table 4.5, it is observed that for strengthened RC T-beam specimen S0-1L-SZ-S-90, the load at ultimate failure is 130 kN, compared to 100 kN for S0-0L control beam. There is a gain in strength of 30% observed. As the configuration of GFRP sheet is concerned on gain in strength, that is, for S0-1L-SZ-U-90 and S0-1L-SZ-UA-90, the loads at ultimate failure are 132 and 140 kN, respectively. This shows a percentage gain in strength, which is 32 and 40%, respectively, on loads over control specimen S0-0L. It is expected from the result that, without transverse steel reinforcement, the RC T-beams strengthened in shear zone with GFRP sheet in U-shape with anchorage outperformed those strengthened with U-shape and side-bonded (Panda et al. 2013b).

(b) **S300 Series**

From Table 4.5, it is observed that for strengthened RC T-beam S300-1L-SZ-S-90, the ultimate failure load is 178 kN, compared to 141 kN for control RC T-beam S300-0L. A gain in strength of 26.24% is observed. As GFRP sheet configuration is concerned on the gain in strength, that is, for strengthened specimens S300-1L-SZ-U-90 and S300-1L-SZ-UA-90, the ultimate failure load is 180 and 192 kN, respectively. The gain in strength for these two strengthened specimens is 27.66 and 36.17%, respectively, on loads over control specimen S300-0L (Panda et al. 2013b). It may be noted that the gain in shear capacity of the RC T-beams, with transverse steel reinforcement at 300 mm stirrup spacing, strengthened with GFRP sheet in shear zone in U-jacket with anchorage carry more loads than the other two side-bonded and U-jacket strengthened beam.

(c) **S200 Series**

From Table 4.5, for S200 series, it is observed that the loads at ultimate failure of strengthened RC T-beam specimens S200-1L-SZ-S-90, S200-1L-SZ-U-90 and S200-1L-SZ-UA-90 are 184, 188 and 196 kN, respectively, compared to 160 kN for control RC T-beam specimen S200-0L. The gain in strength is 15, 17.50 and 22.50%, respectively, on over control RC T-beam specimens (Panda et al. 2013b). It may be expected that the gain in shear capacity of the RC T-beams, with transverse steel reinforcement at 200 mm stirrup spacing, the T-beams strengthened with GFRP sheet in U-jacket with anchorage carry more loads than the other two strengthened specimens, i.e. U-jacket and side-bonded.

It is observed from the three series, the shear strength contribution of GFRP sheet without any transverse steel reinforcement bonded in shear zone is relatively more effective as compared with adequate transverse steel reinforcements. As per as

the configuration of strengthened RC T-beam is concerned, U-shape with anchorage is much more effective than side-bonded and U-shape.

4.6.2 *Deflection of T-beams Bonded with GFRP in Shear Zone*

The midspan deflection with load for the RC T-beams of three series with three types of configurations of GFRP sheet such as side-bonded, U-shape and U-shape with anchorage is as shown in Figs. 4.52, 4.53 and 4.54 (Panda et al. 2013b).

It is observed from Fig. 4.52, for series S0, the maximum deflection of strengthened RC T-beam specimens S0-1L-SZ-S-90, S0-1L-SZ-U-90 and S0-1L-SZ-UA-90 is 8.52, 9.13 and 9.82 mm corresponding to the failure load of 130, 132 and 140 kN, whereas in control RC T-beam S0-0L, the maximum deflection is 6.44 mm corresponding to the failure load of 100 kN. It is observed that the midspan deflection of RC T-beams, strengthened in shear zone with GFRP sheet in different configurations, is less as compared to the control RC T-beam for the same amount of load. Beams strengthened with GFRP sheet in shear zone with U-shape with anchorage configuration carry more loads and also demonstrate more ductility than the other two strengthened beams (Panda et al. 2013b).

As observed from Fig. 4.53 (Panda et al. 2013b), the deflection of control and strengthened RC T-beams of series S300 is almost equal up to 60 kN loads. Further, as load increases, the deflection in RC T-beams strengthened with GFRP

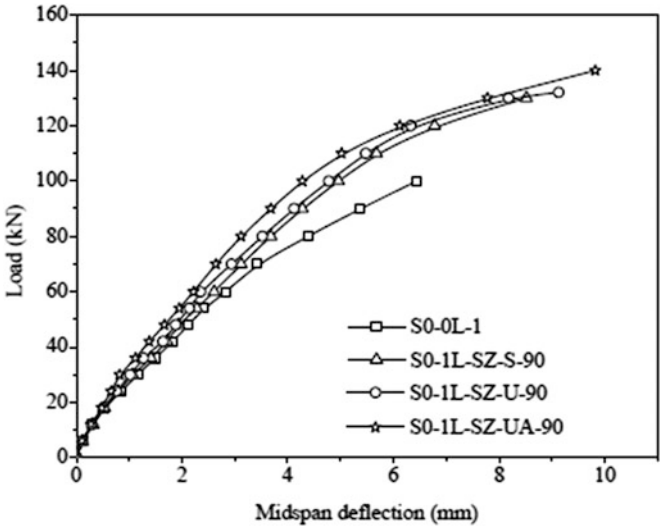

Fig. 4.52 Load versus midspan deflection of series S0 (GFRP in shear zone)

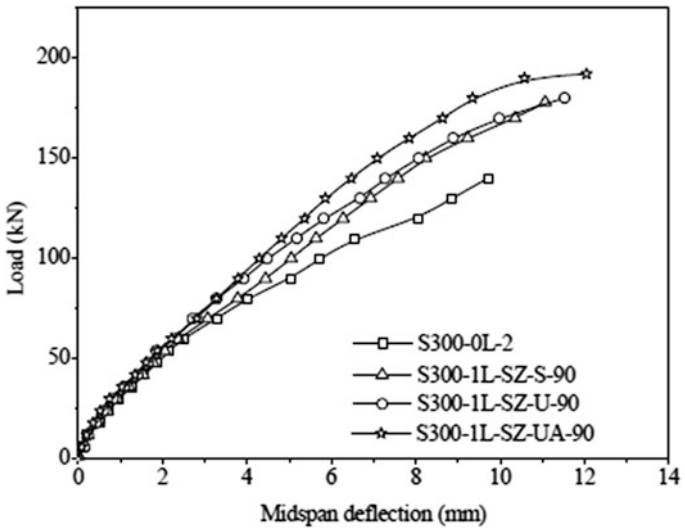

Fig. 4.53 Load versus midspan deflection of series S300 (GFRP in shear zone)

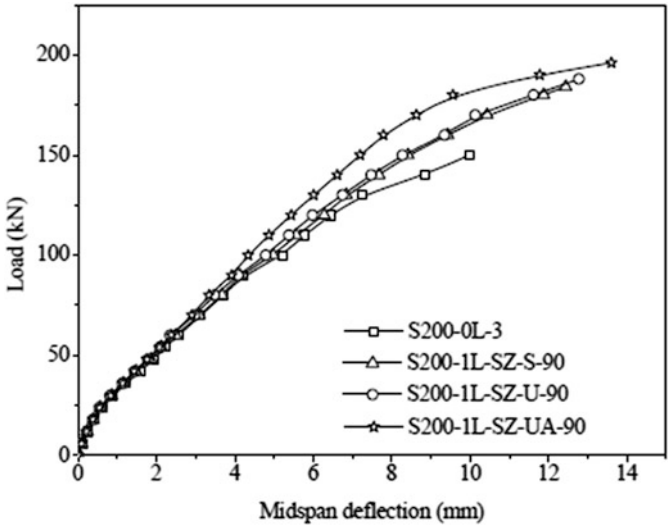

Fig. 4.54 Load versus midspan deflection of series S200 (GFRP in shear zone)

sheet in shear zone is less as compared to the control RC T-beam specimen for the same amount of load. The maximum deflection of strengthened RC T-beam specimens, i.e. S300-1L-SZ-S-90, S300-1L-SZ-U-90 and S300-1L-SZ-UA-90, is 11.07, 11.53 and 12.05 mm corresponding to the failure load of 178, 180 and 192 kN, respectively, whereas in control RC T-beam, the value is 9.71 mm

corresponding to the failure load of 140 kN. It is noted that RC T-beam strengthened in shear with GFRP sheet in U-shape with anchorage carries more load than the other two and also demonstrates more ductility.

As observed from Fig. 4.54, the deflection of control and strengthened RC T-beams for S200 series is almost same up to 70 kN loads. The maximum deflection of RC T-beams strengthened with GFRP sheet in different configurations such as S200-1L-SZ-S-90, S200-1L-SZ-U-90 and S200-1L-SZ-UA-90 is 12.44, 12.78 and 13.61 mm corresponding to the failure load of 184, 188 and 196 kN, whereas in control RC T-beam S200-0L, the value is 9.98 mm corresponding to the failure load of 150 kN.

It is observed from series S0, S300 and S200, the RC T-beam strengthened with GFRP sheet in U-shape with anchorage carries more loads and demonstrates more ductility. The ductility of the RC T-beam also increases with increasing transverse steel reinforcements (Panda et al. 2013b).

4.6.3 Modes of Failure of T-beams Bonded with GFRP in Shear Zone

The cracking pattern and failure modes of the control and strengthened RC T-beams with three types of configuration such as side-bonded, U-shape and U-shape with anchorage of series S0, S300 and S200 (Panda et al. 2013b) are shown in Fig. 4.55.

(a) **S0 Series**

The debonding and rupture failure of GFRP sheet from the concrete surface in the strengthened RC T-beams is shown in Fig. 4.55a. It is observed during experimentation that the GFRP sheet gets debonded in the strengthened RC T-beam specimen S0-1L-SZ-S-90 at an ultimate load of 130 kN. The debonding of the GFRP sheet is initiated from the bottom and propagated towards the top. At the same time, an inclined crack also appears at the side of the flange of the RC T-beams and propagates in longitudinal direction from the loading position for a distance of 250 mm, whereas, in strengthened RC T-beam specimens S0-1L-SZ-U-90 and S0-1L-SZ-UA-90, initially the GFRP sheet gets debonded from the concrete surface. Thereafter, the GFRP sheet gets ruptured at the bottom surface and is propagated towards the support at a load of 132 and 140 kN, respectively. These two strengthened specimens GFRP gets debonded from the top of the GFRP sheet and is propagated towards the bottom. An inclined crack also appears at the side of the flange of the RC T-beam from the loading position and propagates approximately 300, and 200 mm distance towards the support. At the top of the flange of the T-beams, some cracks also appear and propagate from the loading position towards the support for a length of 300 and 350 mm in S0-1L-SZ-U-90 and S0-1L-SZ-UA-90 strengthened specimens, respectively (Panda et al. 2013b).

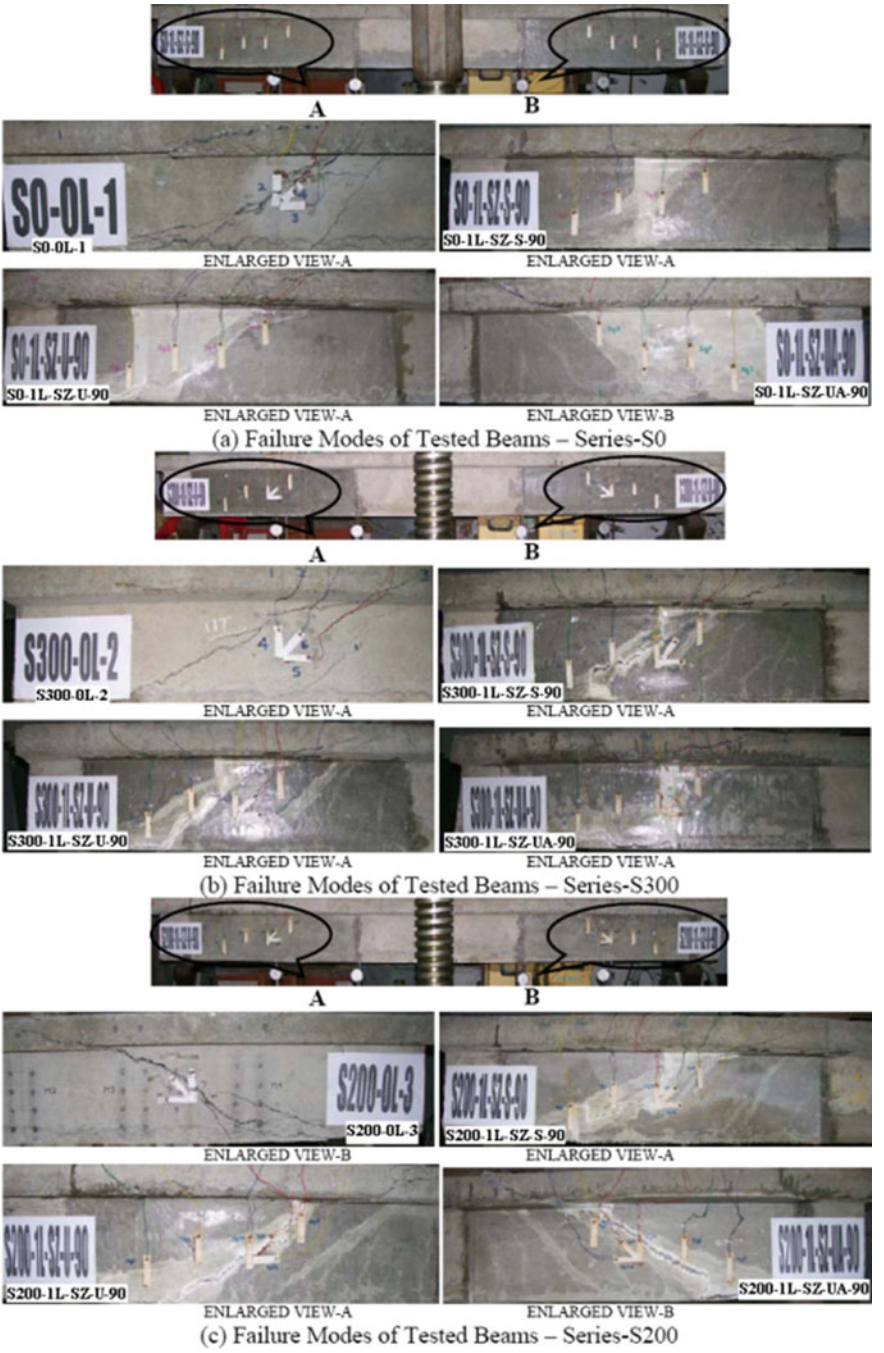

Fig. 4.55 Failure modes of tested beams (GFRP sheet in shear zone)

(b) **S300 Series**

The rupture failure of GFRP sheet from the concrete surface is observed in the strengthened RC T-beams as shown in Fig. 4.55b. It is observed during experiment that the GFRP sheet gets ruptured in the strengthened RC T-beam specimens S300-1L-SZ-S-90, S300-1L-SZ-U-90 and S300-1L-SZ-UA-90 at an ultimate load of 178, 180 and 192 kN, respectively, over the same shear crack location as observed in the control specimen S300-0L. An inclined crack also appears at the side of the flange of the RC T-beams at the same time and propagates in longitudinal direction from the loading position towards support for a distance of 200, 275 and 450 mm distance, respectively. The GFRP sheet also gets ruptured at the bottom of the RC T-beam at the support point. The developed GFRP rupture propagates from the support along the horizontal direction for a distance of about 200 and 350 mm for strengthened specimen S300-1L-SZ-U-90 and S300-1L-SZ-UA-90, respectively (Panda et al. 2013b).

(c) **S200 Series**

In the strengthened RC T-beams with GFRP sheet in shear zone, in series S200, the rupture failure of GFRP sheet observed from the concrete surface is shown in Fig. 4.55c. It is observed during experimentation that the GFRP sheet gets ruptured in the strengthened RC T-beam specimens S200-1L-SZ-S-90, S200-1L-SZ-U-90 and S200-1L-SZ-UA-90 at an ultimate load of 184, 188 and 196 kN, respectively, over the same shear crack location as observed in control specimen S200-0L. An inclined crack also appears at the same time in the side face of the flange of the RC T-beams from loading point propagates in longitudinal direction for a distance of about 200 mm approximately in all the specimens (Panda et al. 2013b).

The failure modes of RC T-beams strengthened in shear zone with GFRP sheet with adequate shear reinforcements and three types of GFRP configuration such as side-bonded, U-shape and U-shape with anchorage indicates that, most of the failure is due to GFRP sheet rupture, whereas without shear reinforcements the failure is due to the combination of both GFRP sheet rupture and GFRP debonding (Panda et al. 2013b).

4.6.4 Strain in GFRP Sheet of T-beams Bonded in Shear Zone

(a) **S0 Series**

The variation of vertical strains in GFRP sheet due to shear force for different configurations of GFRP sheet in S0 series specimens is shown in Fig. 4.56 (Panda et al. 2013b).

It is observed in the RC T-beams strengthened in shear zone with GFRP sheet, the strain in the GFRP sheet did not contribute to the shear carrying capacity at the

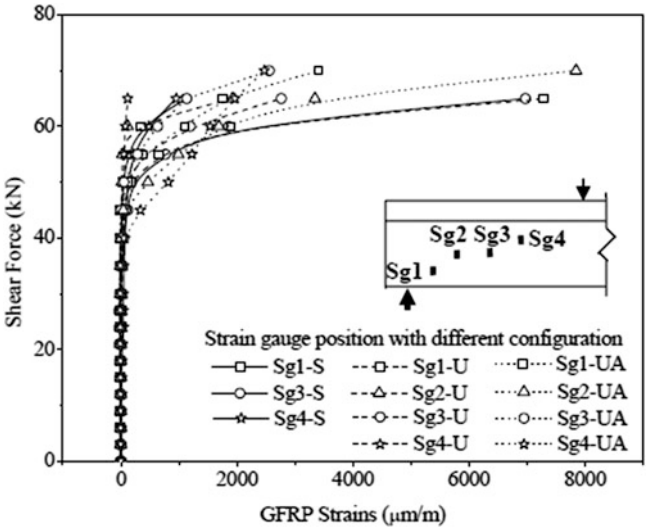

Fig. 4.56 Variation of vertical strains in GFRP sheet for series S0

initial stage of loading in all the strain gauges. It is more effective after 35 kN shear force (Panda et al. 2013b). As shear force increases in the strengthened RC T-beams, the strain in the GFRP slowly increases up to 50 kN shear force. Thereafter, in strengthened RC T-beam specimens S0-1L-SZ-S-90, S0-1L-SZ-U-90 and S0-1L-SZ-UA-90, the curve suddenly increases and attains the maximum value of 6974 μstrains at 65 kN shear force in Sg3 strain gauge, 7295 μstrains at 65 kN shear force in Sg1 strain gauge and 7848 μstrains at 70 kN shear force in Sg2 strain gauge, respectively.

In series S0, as the configuration of GFRP sheet is concerned, the strain in the GFRP sheet is higher in the RC T-beam bonded with U-shape with anchorage as compared with side-bonded and U-shape (Panda et al. 2013b).

(b) **S300 Series**

The variation of vertical strains in GFRP sheet due to shear force for different configurations of GFRP sheet in S300 series specimens is shown in Fig. 4.57 (Panda et al. 2013b).

It is observed in S300 series, the strain in GFRP sheets in all the strain gauges did not contribute to the shear carrying capacity between 40 and 45 kN shear force approximately in all the specimens (Panda et al. 2013b). As shear force increases, the strain in the GFRP sheet increases suddenly in the strengthened RC T-beam specimen S300-1L-SZ-S-90 after 50 kN shear force and attains the maximum value of 6609 μstrains at 85 kN shear force in Sg3 strain gauge. Whereas the maximum GFRP strain attained in the strengthened RC T-beam specimens S300-1L-SZ-U-90 and S300-1L-SZ-UA-90 is 7250 μstrains at 85 kN shear force and 9677 μstrains at 95 kN shear force in Sg2 and Sg3 strain gauges, respectively.

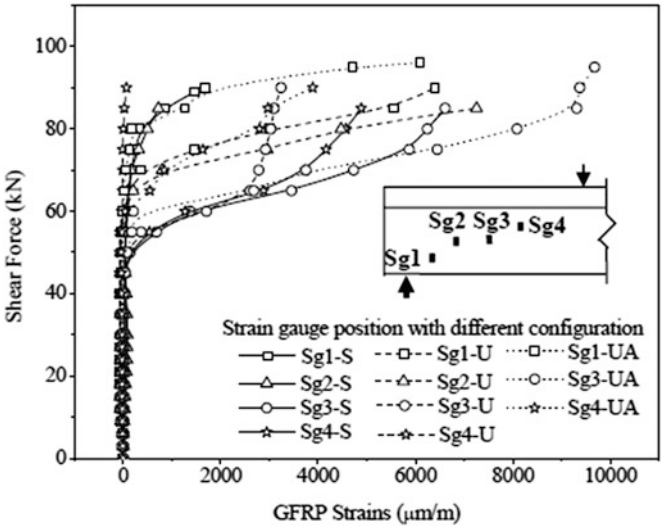

Fig. 4.57 Variation of vertical strains in GFRP sheet for series S300

In series S300, the strain in the GFRP sheet is higher in the specimens strengthened with U-shape with anchorage configuration as compared to side-bonded and U-shape configuration. It may also be observed that the strain in the GFRP sheet is higher between 250 and 350 mm distance from the support (Panda et al. 2013b).

(c) **S200 Series**

The variation of vertical strains in GFRP sheet due to shear force for different configurations of GFRP sheet in S200 series specimens is shown in Fig. 4.58 (Panda et al. 2013b).

It is observed in S200 series, the strain in the GFRP sheet in all the strain gauges did not contribute to the shear carrying capacity at the initial stages of loading up to between 45 and 55 kN shear force except the strain gauge Sg4 in S200-1L-SZ-S-90 and S200-1L-SZ-UA-90 specimens. Thereafter, as shear force increases, the GFRP strain increases in all the strain gauges. The maximum vertical GFRP strain of strengthened RC T-beams in three different configurations, i.e. S200-1L-SZ-S-90, S200-1L-SZ-U-90 and S200-1L-SZ-UA-90, measured 6642 μstrains at 90 kN shear force, 6841 μstrains at 85 kN shear force and 8746 μstrains at 80 kN shear force in Sg3 strain gauge, respectively (Panda et al. 2013b).

In series S200, the strain in the GFRP sheet is higher in the RC T-beam specimen bonded with GFRP sheet in U-shape with anchorage configuration, as compared to the side-bonded and U-shape. It is also observed that in all the strengthened RC T-beam specimens the maximum strain observed at a distance of 350 mm distance from the support.

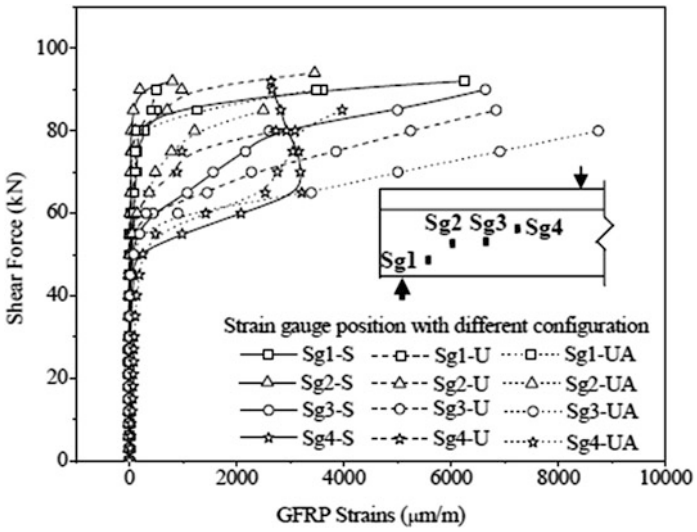

Fig. 4.58 Variation of vertical strains in GFRP sheet for series S200

4.6.5 Transverse Steel Strain in T-beams Bonded with GFRP Sheet in Shear Zone

The variation of strains in the transverse steel reinforcement with shear force of series S200 and S300 for strain gauge ISg2 is shown in Figs. 4.59 and 4.60 (Panda et al. 2013b).

It is observed from Fig. 4.59, in series S200, at the initial stage of loading, the transverse steel reinforcement did not contribute to the shear carrying capacity. This contribution is more effective after the failure of diagonal cracking. In the control RC T-beam specimen (S200-0L), and strengthened RC T-beam specimens S200-1L-SZ-S-90, S200-1L-SZ-U-90 and S200-1L-SZ-UA-90, it occurred between 35 and 50 kN shear force (Panda et al. 2013b). As shear force increases, the strain in the transverse steel increases slowly up to 65 kN shear force. Thereafter, the strain suddenly increases till failure of the RC T-beam. In ISg2 strain gauge, the maximum strain observed in control RC T-beam specimen is 1962 μstrains at 60 kN shear force, whereas in strengthened RC T-beams corresponding to this shear force is 557, 540 and 383 μstrains in S200-1L-SZ-S-90, S200-1L-SZ-U-90 and S200-1L-SZ-UA-90. The maximum strain is also observed in S200-1L-SZ-S-90, S200-1L-SZ-U-90 and S200-1L-SZ-UA-90; strengthened RC T-beam specimens are 3212 and 3020 μstrains at 90 kN shear force and 2788 μstrains at 95 kN shear force, respectively.

As observed from Fig. 4.60, in series S300, the contribution of transverse steel to the shear carrying capacity of control beam specimen S300-0L is occurred at a shear force of 25 kN approximately. Whereas for the strengthened RC T-beam

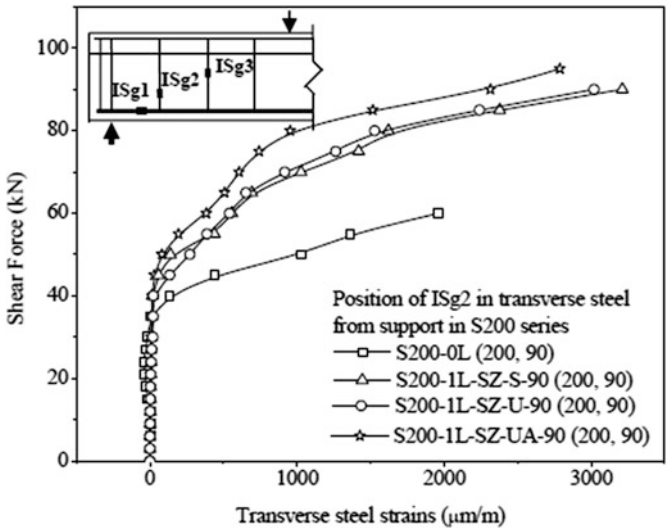

Fig. 4.59 Variation of strain in transverse steel of T-beams bonded with GFRP in shear zone for series S200

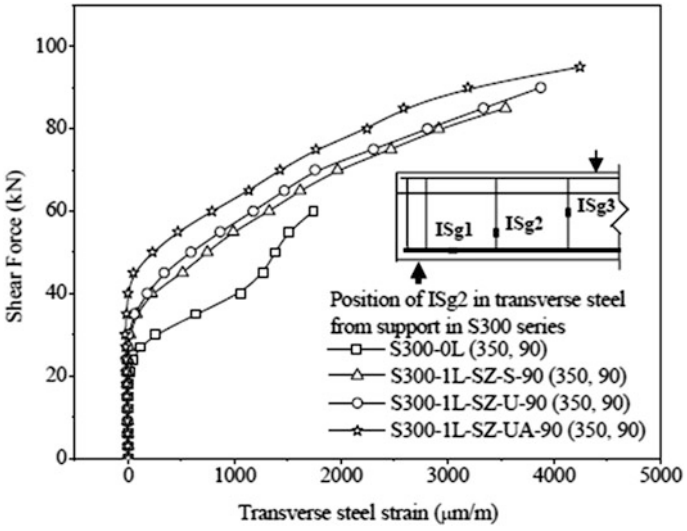

Fig. 4.60 Variation of strain in transverse steel of T-beams bonded with GFRP in shear zone for series S300

specimens S300-1L-SZ-S-90, S300-1L-SZ-U-90, and S300-1L-SZ-UA-90, it occurred between 35 and 45 kN shear force. Thereafter, as shear force increases, the strain in the transverse steel increases. In control RC T-beam specimen, the

maximum strain observed is 1740 μstrains at 60 kN shear force, whereas the strain in strengthened RC T-beams corresponding to this shear force is 1324, 1176 and 786 μstrains in S300-1L-SZ-S-90, S300-1L-SZ-U-90 and S300-1L-SZ-UA-90. The maximum strain is also observed in S300-1L-SZ-S-90, S300-1L-SZ-U-90 and S300-1L-SZ-UA-90 beams, which is 3545 μstrains at 85 kN shear force, 3876 μstrains at 90 kN shear force and 4245 μstrains at 95 kN shear force, respectively (Panda et al. 2013b).

It is observed that the strain in the transverse steel is less in strengthened of RC T-beam as compared to the control RC T-beam for the same amount of shear force. It is also observed that the strain in the transverse steel is less in the RC T-beam strengthened with GFRP sheet in U-shape with anchorage as compared to the side-bonded and U-shape in both the series (Panda et al. 2013b).

4.6.6 *Longitudinal Steel Strain in T-beams Bonded with GFRP Sheet in Shear Zone*

The variation of strain in longitudinal steel reinforcement with shear force for RC T-beams strengthened in shear zone with GFRP sheet in different configurations is shown in Fig. 4.61 (Panda et al. 2013b).

It is observed from Fig. 4.61, at the initial stage of loading, the strain in the longitudinal steel near the support point is very small in all the configurations of GFRP sheet such as U-shape, side-bonded and U-shape with anchorage. As shear

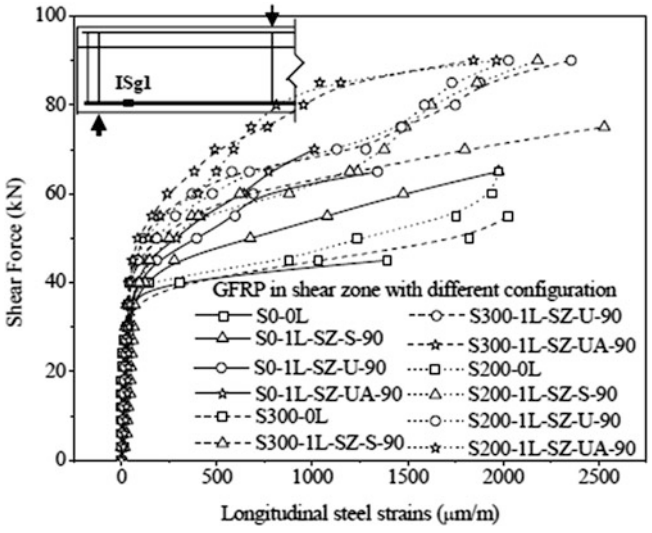

Fig. 4.61 Variation of strain in longitudinal steel of T-beams strengthened in shear zone with GFRP for different configurations

force increases, the strain in the longitudinal steel increases linearly up to approximately between 35 and 40 kN shear force till the diagonal shear crack failure appears in the concrete. After the appearance of diagonal shear cracks, the longitudinal steel reinforcement resists the further increments of shear force (Panda et al. 2013b).

In series S0, in control RC T-beam S0-0L, the strain suddenly increases in the longitudinal steel after 35 kN shear force and attains the maximum value of 1392 μstrains at 45 kN shear force, whereas in strengthened RC T-beam specimens S0-1L-SZ-S-90, S0-1L-SZ-U-90 and S0-1L-SZ-UA-90, the strain corresponding to this shear force is 276, 184 and 131 μstrains. Thereafter, as shear force increases, the strain in the longitudinal steel increases suddenly in strengthened RC T-beams and attains the maximum value of 1976 and 1341 μstrains at 65 kN shear force in S0-1L-SZ-S-90 and S0-1L-SZ-U-90 specimen, respectively. Whereas in S0-1L-SZ-UA-90 specimen, the value is 1010 μstrains at 70 kN shear force (Panda et al. 2013b).

In series S300, in control RC T-beam S300-0L, the strain in the longitudinal steel suddenly increases after 35 kN shear force and attains the maximum value of 2028 μstrains at 55 kN shear force, whereas in strengthened RC T-beam specimens S300-1L-SZ-S-90, S300-1L-SZ-U-90 and S300-1L-SZ-UA-90, the strain corresponding to this shear force is 368, 187 and 159 μstrains. Thereafter, as shear force increases, the strain in the longitudinal steel increases gradually in strengthened RC T-beams and attains the maximum value of 2529 μstrains at 75 kN shear force, 2356 μstrains at 90 kN shear force and 1844 μstrains at 90 kN shear force in S300-1L-SZ-S-90, S300-1L-SZ-U-90 and S300-1L-SZ-UA-90, respectively (Panda et al. 2013b).

In series S200, in control RC T-beam S200-0L, the strain in the longitudinal steel suddenly increases after 35 kN shear force and attains the maximum value of 1976 μstrains at 65 kN shear force. Whereas in strengthened RC T-beam specimens S200-1L-SZ-S-90, S200-1L-SZ-U-90 and S200-1L-SZ-UA-90, the strain corresponding to this shear force is 1196, 670 and 497 μstrains. Thereafter, as shear force increases, the strain in the longitudinal steel increases gradually in strengthened RC T-beams and attains the maximum value of 2180, 2027 and 1964 μstrains at 45 kN shear force in S200-1L-SZ-S-90, S200-1L-SZ-U-90 and S200-1L-SZ-UA-90, respectively (Panda et al. 2013b).

It is observed that the strain in the longitudinal steel, in RC T-beams strengthened with GFRP sheet in shear zone, is less as compared with control RC T-beam for the same amount of shear force for series S0, S300 and S200. As the configuration of GFRP sheet is concerned, the strain in the longitudinal steel in the RC T-beams strengthened with GFRP sheet in U-shape with anchorage is less as compared to the side-bonded and U-shape GFRP sheet (Panda et al 2013b). It may be expected that as transverse steel shear reinforcement increases, the strain in the longitudinal steel is less for the same amount of shear force.

4.7 Summary

This chapter presented the experimental results those were obtained from the experimental investigation carried out in the laboratory for RC T-beams strengthened in shear with GFRP sheets and strips. Various strengthening schemes with a number of layers, configuration and orientations are discussed. The effectiveness of the strengthened T-beams is presented. The main focus of the chapter has been the presentation of different modes of failures for different strengthening schemes and strain analysis for GFRP sheets and strips, transverse steel and longitudinal steel. Interaction between GFRP layers and transverse steel reinforcement is also discussed for U-jacket and side-bonded configuration.

The following conclusions may be drawn on the basis of effectiveness of the control and strengthened RC T-beams, different modes of failure observed during the experimental works, strain analysis of GFRP, transverse and longitudinal steel and ductility of the beams.

- The test results indicate that for control specimens, the value for nominal shear predicted by ACI is underestimated in the range of 75–105%.
- The RC T-beams strengthened in shear with U-jacketed and side-bonded GFRP continuous sheet throughout the span with different numbers of layers, GFRP strips in shear zone with different configurations and orientations and GFRP sheet in shear zone with different configurations increase the effectiveness by 7.5–50%.
- The gain in shear capacity is significant in all the GFRP strengthened RC T-beams. However, it is observed that one layer of GFRP is comparatively more effective than two and three layers of GFRP. This may be due to the fact that with increasing number of GFRP layers, the possibility of delamination increases (Panda et al. 2011a).
- The modes of failure of strengthened RC T-beams in shear with U-jacket and side-bonded GFRP wrap indicates that in single layer wrapping most of the failure is due to rupture of GFRP sheet, whereas for two and three layers, the failure is due to GFRP debonding.
- The load–strain curves indicate that the strain in the GFRP sheet is higher in the RC T-beam specimens strengthened with one layer of GFRP, as compared to two and three layers in all the series. Whereas for S200 and S300 series, the combination of transverse steel and GFRP layer both resulted in larger strain capacity.
- The addition of internal transverse steel in the RC T-beams resulted in a significant decrease of the gain in shear capacity due to GFRP sheet. But the combination of transverse steel and GFRP layers plays an important role to gain the shear capacity.
- The load–deflection plot clearly indicates that the RC T-beams strengthened in shear with GFRP sheets or strips have a significant effect on beam ductility.

- The ductility of RC T-beams loaded in shear depends directly on both the internal transverse steel reinforcement and external GFRP wrap. The ductility of RC T-beams increases as total shear reinforcement ratio increases.
- The gain in shear capacity is significant in all the strengthened RC T-beams bonded with GFRP strips in shear zone. But so far as the configuration and orientation of GFRP strip are concerned, side-bonded configuration with orientation of the GFRP strip at 45° to the longitudinal axis of the beam is more effective than U-shape and side-bonded with orientation 90°.
- The failure mode of RC T-beams strengthened in shear with side-bonded GFRP strips indicates that the GFRP strip at 90° to the longitudinal axis of the beam fails due to GFRP debonding, whereas for 45° orientations and U-shaped GFRP strip the fails is due to both GFRP rupture and debonding.
- The gain in shear capacity is significant in all the RC T-beams strengthened in shear zone with GFRP sheet. But so far as the configuration of GFRP sheet is concerned, U-shape with anchorage is more effective than side-bonded and U-shape. The contribution of shear capacity from the GFRP sheet is decreased as transverse steel reinforcement increases in all the series (Panda et al. 2013b).
- The modes of failure of RC T-beams strengthened in shear zone with GFRP sheet with adequate shear reinforcements indicate that in single layer wrapping with all types of configurations, most of the failure is due to GFRP sheet rupture, whereas without shear reinforcements the failure is due to the combination of both debonding of GFRP sheet and GFRP rupture (Panda et al. 2013b).
- The transverse steel is more strained in control specimens, as compared with strengthened specimens. This indicates that the addition of GFRP reduced the strain in transverse steel. But, so far as the number of layers is concerned, the addition of second and third layers of GFRP sheets resulted in the decrease of strains in the transverse steel.
- As far as configuration of GFRP strips is concerned, the U-shape of GFRP strip resulted in an additional decrease of strains in the transverse steel reinforcement as compared with side-bonded GFRP strip. As far as side-bonded orientation is concerned, the strain in the transverse steel at 45° orientation of GFRP strip with the longitudinal axis of the beam is less as compared with 90° orientation of GFRP strip.
- As far as the configuration of GFRP sheet in shear zone is concerned, U-shape with anchorage results in additional decrease of strain in the transverse steel reinforcement as compared with side-bonded and U-shape beams (Panda et al. 2013b).
- The longitudinal steel is more strained in control specimens, as compared with strengthened specimens. This indicates that the addition of GFRP helps in reducing the strain in longitudinal steel.
- As far as configuration of GFRP strips is concerned, U-shape GFRP strips resulted in a decrease of strains in the longitudinal steel reinforcement as compared with side-bonded GFRP strips. Also, as far as orientation is concerned, the strain in the longitudinal steel at 45° orientation of GFRP strip is less as compared with 90°orientation of GFRP strip.

- As far as configuration of GFRP sheet in shear zone is concerned, U-shape with anchorage resulted in an additional decrease of strains in the longitudinal steel reinforcement as compared with side-bonded and U-shape beams (Panda et al. 2013b).

It is observed that the maximum gain in shear capacity is achieved in RC T-beams strengthened in shear zone with one layer GFRP sheet in U-jacket with anchorage and RC T-beams strengthened in shear zone with GFRP strips at 45° to the longitudinal axis.

References

Bousselham A, Chaallal O (2006) Effect of transverse steel and shear span on the performance of RC beams strengthened in shear with CFRP. Compos B 37:37–46

Panda KC, Bhattacharyya SK, Barai SV (2010) Shear behaviour of reinforced concrete T-beams with U-bonded glass fibre reinforced plastic sheet. Ind Concr J (ICJ) 84(10):61–71

Panda KC, Bhattacharyya SK, Barai SV (2011a) Shear strengthening of RC T-beams with externally side bonded GFRP sheet. J Reinf Plast Compos 30(13):1139–1154

Panda KC, Bhattacharyya SK, Barai SV (2011b) Strengthening of RC T-beams with shear deficiencies using GFRP strips. J Civ Eng Archit 05(1):56–67

Panda KC, Bhattacharyya SK, Barai SV (2011c) Influence of transverse steel on the performance of RC T-beams strengthened in shear with GFRP strips. Advances in FRP Composite in Civil Engineering, Springer, India, vol II, pp 763–766

Panda KC, Bhattacharyya SK, Barai SV (2012) Shear behaviour of RC T-beams strengthened with U-wrapped GFRP sheet. Steel Compos Struct Int J 12(2):149–166

Panda KC, Bhattacharyya SK, Barai SV (2013a) Shear strengthening effect by bonded GFRP strips and transverse steel on RC T-beams. Struct Eng Mech Int J 47(1):75–98

Panda KC, Bhattacharyya SK, Barai SV (2013b) Effect of transverse steel on the performance of RC T-beams strengthened in shear zone with GFRP sheet. Constr Build Mater 41:79–90

Panda KC, Bhattacharyya SK, Barai SV (2015) Strain analysis of RC T-beams strengthened in shear with variation of U-wrapped GFRP sheet and transverse steel. Adv Struct Eng (Springer, India) 3(154):2001–2010

Chapter 5
Theoretical Approach to Shear Strengthening of Beams

5.1 General

The shear strength of RC T-beams with and without GFRP obtained from experimental investigation is compared to the shear strength computed by the guidelines given in different standards such as American Concrete Institute (ACI 318-02), Canadian Standard Association (CSA A23.3-94) and Indian Standard (IS 456: 2000) building codes (without the provision of FRP) and also ACI 440.2R-02 guidelines (with the provision of FRP). Best-fit curves are plotted with the results obtained from the experiments performed on RC T-beams strengthened in shear with GFRP sheets. The effectiveness of RC T-beams strengthened in shear with GFRP sheet may be calculated using the proposed best-fit curves and the design approach proposed by Khalifa et al. (1998).

5.2 Shear Strength Using Standards

Section 5.2.1 presents guidelines of the shear strength of beams without provision of FRP as per the building codes, ACI and CSA. Section 5.2.2 presents the guidelines on the shear strength of beams with the provision of FRP as per the ACI design approach (ACI 440.2R-02).

K. C. Panda et al., *Shear Strengthening of T-beam with GFRP*, Springer Transactions in Civil and Environmental Engineering, https://doi.org/10.1007/978-981-10-7760-9_5

5.2.1 Shear Strength Using Building Codes (Without Provision of FRP)

(a) **Shear Strength by ACI Building Code**

The shear strength of the RC beam may be calculated using the ACI building code, ACI 318-02. The ACI guidelines proposed an equation for calculating the shear strength in RC beams without shear reinforcement as indicated in Eq. (5.1).

$$V_c = \left(0.16\sqrt{f_c'} + 17.2\rho_w \frac{V_u d}{M_u}\right) b_w d \tag{5.1}$$

where b_w is the width of the beam; d is the effective depth of beam; f_c' the compressive strength of concrete cylinder; ρ_w is the longitudinal steel tensile reinforcement ratio; V_u and M_u are the shear and moment at the critical section, respectively.

ACI building code states that for RC beams with transverse steel reinforcement, the nominal shear strength, V_n, is composed of the shear contribution of concrete, V_c, and the contribution of transverse steel reinforcement, V_s, as given in Eq. (5.2).

$$V_n = V_c + V_s \tag{5.2}$$

where V_c is calculated as given in Eq. (5.1) and V_s is expressed as given in Eq. (5.3)

$$V_s = A_{sw} f_y d/s \tag{5.3}$$

In Eq. (5.3), A_{sw} is the area of vertical shear reinforcement, f_y is the yield stress of stirrups, d is the effective depth of beam, s is the spacing of stirrups and ρ_s is the transverse steel reinforcement ratio. The ACI building code also states that the shear contribution of concrete and the contribution of shear reinforcement must not be taken greater than 0.3 $\sqrt{f_c'}$ and 0.66 $\sqrt{f_c'}$, respectively.

(b) **As per ACI 318M-95 Shear Design Approach for Beams**

$$V_n = V_c + V_s \tag{5.4}$$

$$V_c = \left(\sqrt{f_c'}/6\right) b_w d \quad \text{(For non-prestressed beams)} \tag{5.5}$$

$$V_s = A_{sw} f_y d/s \leq (2/3)\sqrt{f_c'} b_w d \tag{5.6}$$

where V_c is the nominal shear strength contribution of concrete; V_s is the nominal shear strength contribution of shear reinforcement; A_{sw} is the area of shear reinforcement

in mm^2; s is the stirrups' spacing; f_c' is the compressive strength of concrete in MPa; f_y is the yield stress of stirrups in MPa.

(c) **CSA (Canadian Standards Association) Building Code**

The shear strength of RC T-beams can be calculated using the Canadian building code, a simplified method (A23.3 C1.11.3) presented in the Canadian building code for the shear design (CSA 1994, 2002).

In Canadian building code, the shear strength of an RC beam is composed of the shear contribution of concrete and the contribution of transverse steel reinforcement as expressed in Eq. (5.2). Two equations for the shear contribution of concrete, V_c, are given depending on the amount of transverse steel reinforcement and the effective depth d of the beam as indicated in Eqs. (5.7) and (5.8).

$$V_c = \left(0.2\sqrt{f_c'}\right) b_w d \tag{5.7}$$

When $A_{sw} \geq \frac{6\sqrt{f_c'} b_w s}{f_y}$ and $d \leq 300$ mm

$$V_c = \left[\left(\frac{260}{1000 + d}\right)\sqrt{f_c'}\right] b_w d \geq \left(0.1\sqrt{f_c'}\right) b_w d \tag{5.8}$$

When $A_{sw} < \frac{6\sqrt{f_c'} b_w s}{f_y}$ and $d > 300$ mm.

The shear strength contribution of the transverse steel reinforcement, V_s, is same as expressed in the ACI building code as given by Eq. (5.3).

5.2.2 *Shear Strength of Strengthened RC Beams Using ACI 440.2R-02*

(a) **Design of Material Properties**

The properties of the material reported by the manufacturers, such as ultimate tensile strength, do not consider long-term exposure to environmental conditions and should be considered as initial properties. The material properties used in the design should be reduced based on the environmental exposure condition.

The design ultimate tensile strength is determined using the environmental reduction factor given in Table 8.1 of the ACI 440.2R-02 guidelines for the appropriate fibre type and exposure condition.

$$\text{Design ultimate tensile strength } = f_{\text{fu}} = C_E f_{\text{fu}}^* \tag{5.9}$$

where

f_{fu} Design ultimate tensile strength of FRP in MPa
C_E Environmental reduction factor
f_{fu}^* Ultimate tensile strength of FRP as reported by the manufacturer in MPa

Similarly, the design rupture strain should also be reduced for environmental exposure conditions.

$$\text{Design rupture strain} = \varepsilon_{fu} = C_E \varepsilon_{fu}^* \tag{5.10}$$

ε_{fu} Design rupture strain of FRP reinforcement, (mm/mm)
ε_{fu}^* Ultimate rupture strain of the FRP reinforcement, (mm/mm)

The material used in the experimental work was glass fibre and epoxy resin, and the exposure condition was internal exposure. The environmental reduction factor (C_E) is used as 0.75 for present calculation (Table 8.1 of the ACI 440.2R-02 document).

(b) **Nominal Shear Strength of Strengthened RC Beam**

The design guidelines proposed by ACI 440.2R-02 is applicable to RC beams externally strengthened with FRP. According to the ACI design guidelines, the nominal shear strength of a strengthened RC member wrapped with FRP may be determined by adding thel contribution of the FRP reinforcement to the contribution of steel and the concrete as shown in Eq. (5.11)

$$V_n = V_c + V_S + V_f \tag{5.11}$$

(c) **Design Shear Strength of Strengthened RC Beam**

The design shear strength of strengthened RC beam may be calculated as given in Eq. (5.12)

$$\phi V_n = \phi(V_c + V_s + \psi_f V_f) \tag{5.12}$$

where ψ_f is the additional reduction factor is applied to the contribution of FRP system as given in Table 10.1 of the ACI 440.2R-02 guidelines. The experimental work presented in Chap. 4 was based on U-wraps and side-bonded FRP on RC T-beams. For bond-critical shear reinforcement, an additional reduction factor of 0.85 is recommended. The design shear strength may be calculated using the strength reduction factor ϕ, required by ACI 318-99. The strength reduction factor of 0.85 is recommended.

(d) **Shear Strength Contribution of FRP Reinforcement**

The shear strength provided by the FRP shear reinforcement of strengthened RC beam may be determined by calculating the force resulting from tensile stress in the FRP across the assumed crack.

The shear strength contribution of FRP in strengthened RC beam is given by Eq. (5.13)

$$V_f = \frac{A_{fe} f_{fe} (\sin\beta + \cos\beta) d_f}{s_f} \tag{5.13}$$

where

$$A_{fe} = 2nt_f w_f \tag{5.14}$$

The tensile stress in the FRP shear reinforcement at the ultimate stage is directly proportional to the strain that is developed in the FRP shear reinforcement at the ultimate stage.

$$f_{fe} = \varepsilon_{fe} E_f \tag{5.15}$$

where

A_{fe} Area of GFRP shear reinforcement
t_f Thickness of the GFRP sheet on one side of the RC beam (for both sides of the RC beam $2t_f$)
w_f Width of the GFRP strip
d_f Effective depth of the GFRP shear reinforcement
b_w Width of the beam cross section
s_f Spacing of GFRP strips

A_{fe} is calculated by the total thickness of the sheet and the width of the GFRP strip w_f in the longitudinal direction. For multilayered RC beam, n times the area of GFRP shear reinforcement A_{fe}. Where, n is the number of layers.

For continuous vertical GFRP shear reinforcement, the spacing of the GFRP strip, s_f, and the width of the GFRP strip, w_f, are equal. The dimensions used for vertical and inclined GFRP strips are shown in Figs. 5.1 and 5.2.

(e) **Effective Strain in FRP Laminates**

The effective strain in FRP laminate is the maximum strain that is calculated in the FRP system at an ultimate stage of loading and is governed by the failure mode of the FRP system and the strengthened reinforced concrete beam. The effective strain, ε_{fe} in FRP is assumed to be smaller than ultimate strain, ε_{fu}. This may be calculated as

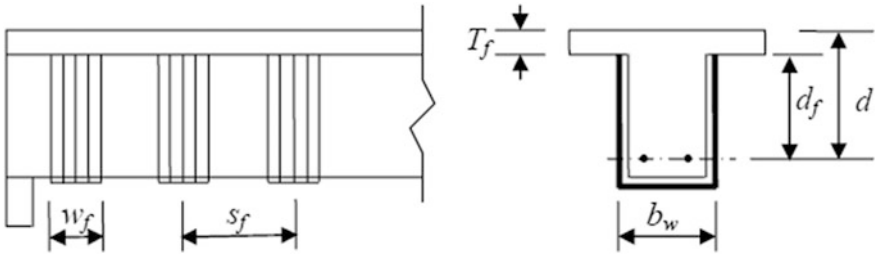

Fig. 5.1 Dimensions used for GFRP strips (vertical)

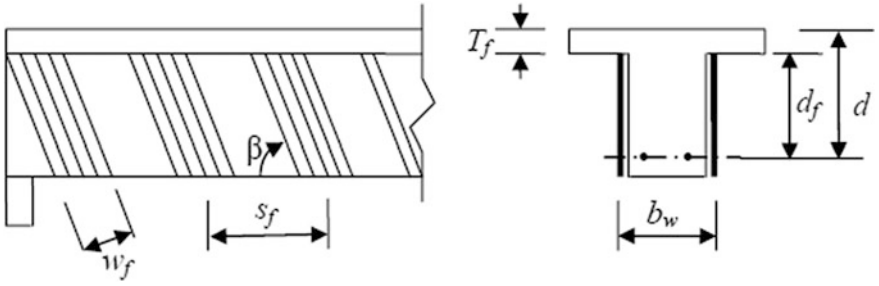

Fig. 5.2 Dimensions used for GFRP strips (inclined)

$$\varepsilon_{fe} = 0.004 \leq 0.75\varepsilon_{fu} \text{ (For full wrapped beams)} \tag{5.16}$$

$$\varepsilon_{fe} = k_v\varepsilon_{fu} \leq 0.004 \text{ (For U-wraps or bonding to two sides)} \tag{5.17}$$

where k_v = bond reduction coefficient for shear.

(f) **Reduction Coefficient Based on Rupture Failure Mode**

The reduction coefficient for rupture failure mode is calculated using the model proposed by Khalifa et al. (1998). There is no particular guideline indicated for strengthening of the RC beam with GFRP. The reduction coefficient presented in Eq. (5.18) is a function of $\rho_f E_f$ for $\rho_f E_f \leq 0.7$ GPa.

$$R = 0.5622\left(\rho_f E_f\right)^2 - 1.218\left(\rho_f E_f\right) + 0.778 \tag{5.18}$$

where

ρ_f GFRP shear reinforcement ratio = $(2t_f/b_w)(w_f/s_f)$
E_f Tensile modulus of elasticity of GFRP

(g) **Reduction Coefficient Based on Debonding Failure Mode**

ACI 440.2R-02 design approach presented the reduction coefficient based on debonding failure mode. Where, k_v is used as bond reduction coefficient.

The bond reduction coefficient (k_v) is a function of the concrete strength, the type of wrapping scheme used and the stiffness of the FRP laminate. Equations (5.19)–(5.22) are used to determine the bond reduction coefficient.

$$k_v = \frac{k_1 k_2 L_e}{11{,}900\ \varepsilon_{fu}} \leq 0.75 \tag{5.19}$$

where L_e = Active bond length over which the majority of the bond stress is maintained. Equation (5.20) is used to find out active bond length.

$$L_e = \frac{416}{\left(nt_f E_f\right)^{0.58}} \tag{5.20}$$

k_1 and k_2 are two modification factors that account for the concrete strength and the type of FRP wrapping scheme used, respectively. The modification factors are expressed in Eqs. (5.21) and (5.22).

$$k_1 = \left(\frac{f_c'}{27}\right)^{2/3} \tag{5.21}$$

$$k_2 = \frac{d_f - L_e}{d_f} \text{ for U-wrap strengthening scheme,}$$
$$\text{and } k_2 = \frac{d_f - 2L_e}{d_f} \quad \text{for two sides-bonded strengthening scheme} \tag{5.22}$$

where f_c' and E_f are in MPa.

(h) **Total Shear Reinforcement Limits**

Both the contribution of the FRP shear reinforcement and the steel shear reinforcement of the RC beams strengthened in shear with FRP is used to determine the total shear reinforcement. The total shear reinforcement should be limited based on the criteria given for steel alone in ACI 318-99 guidelines as stated in Eq. (5.23).

$$V_s + V_f \leq 0.66\sqrt{f_c'} b_w d \tag{5.23}$$

5.3 Best-Fit Curves on the Basis of Test Results

An extensive review of the literature (Tables 2.1 and 2.2) was conducted for the purpose of compiling a database of experimental results of RC beams strengthened in shear with FRP. All the specimens in the database were simply supported RC rectangular beam and T-beams. The database was presented by Triantafillou and Antonpoulos (2000) and Bousselham and Chaallal (2004) and was upgraded in this study. A plot between $R = \varepsilon_{fe}/\varepsilon_{fu}$, and $E_f\rho_f/f_c'^{2/3}$ is presented in Fig. 5.3, by using the experimental data available on CFRP, GFRP and AFRP in the literature (Panda et al. 2011).

Further, using these existing data points, the best-fit curve was plotted as shown in Fig. 5.4. The best-fit curve indicates the nonlinear variation for plot between $R = \varepsilon_{fe}/\varepsilon_{fu}$, and $E_f\rho_f/f_c'^{2/3}$ as proposed by Khalifa et al. (1998), and Triantafillou and Antonopoulos (2000).

From the present investigation, six best-fit curves are plotted based on the experimental results obtained from 36 RC T-beams strengthened in shear with GFRP sheets. Three curves are plotted for each category of configurations such as side-bonded and U-jacket strengthening scheme. Each category is based on the variation of transverse steel reinforcement ratio ($\rho_s = [A_{sw}/(sb_w)] \times 100\%$) used. The transverse steel in the first category of GFRP strengthened RC T-beams, without transverse steel reinforcements, i.e. no stirrups in the shear zone ($\rho_s = 0\%$). The transverse steel in the second category of GFRP strengthened RC T-beams, with 0.19% of transverse steel reinforcement ratio, i.e. the spacing of the stirrups @ 300 mm c/c throughout the span of the strengthened beams ($\rho_s = 0.19\%$). The transverse steel in the third category of GFRP strengthened RC T-beams, with 0.28% of transverse steel reinforcement ratio, i.e. the spacing of the stirrups @ 200 mm c/c throughout the span of the strengthened beams ($\rho_s = 0.28\%$). Average maximum GFRP strain value obtained from the experiments from left and right side of the of the RC T-beams strengthened in shear with GFRP is used in the study. The experimental

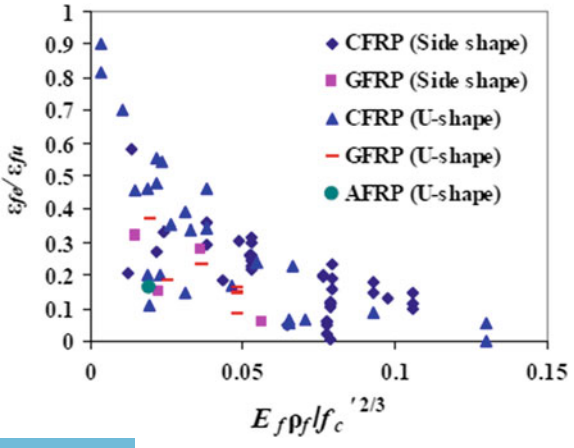

Fig. 5.3 Ratio of $\varepsilon_{fe}/\varepsilon_{fu}$ in terms of $E_f\rho_f/f_c'^{2/3}$ for CFRP, GFRP and AFRP

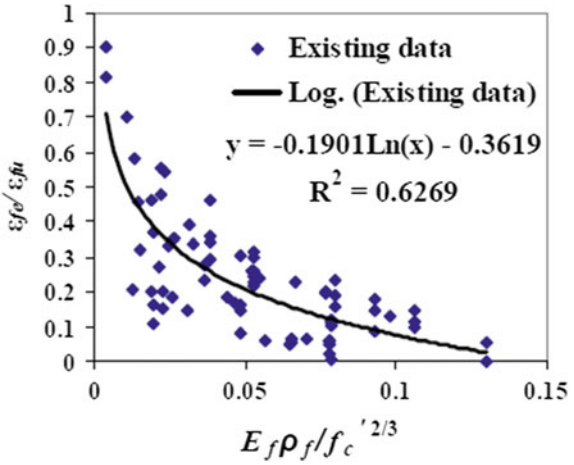

Fig. 5.4 Ratio of $\varepsilon_{fe}/\varepsilon_{fu}$ in terms of $E_f\rho_f/f_c'^{2/3}$ for existing data (best-fit curve)

data used in the study includes only one type of fibre material, i.e. GFRP sheet and strips, two types of configuration, i.e. U-jackets, and side-bonded, two types of distributions, i.e. continuous GFRP sheet and GFRP strips, two types of fibre orientations, i.e. 45° and 90° to the longitudinal axis of the beam, number of GFRP layers, i.e. single, double, as well as triple and three variations of transverse steel reinforcements, i.e. without stirrups and with stirrups @ 300 and @ 200 mm c/c.

It is well established that the tensile strength of concrete is proportional to $f_c'^{2/3}$ (Triantafillou and Antonopoulos 2000), where f_c' is the compressive strength of concrete. The effective strain depends on the quantity $E_f\rho_f/f_c'^{2/3}$. The ratio of effective strain to ultimate strain, $R = \varepsilon_{fe}/\varepsilon_{fu}$, is plotted versus axial rigidity $E_f\rho_f/f_c'^{2/3}$. The test results obtained from the experimental investigations (Panda et al. 2010, 2011, 2012, 2013a, b, 2015) are presented in Tables 5.1, 5.2, 5.3, 5.4, 5.5 and 5.6. The test data is used to produce the plot between the $R = \varepsilon_{fe}/\varepsilon_{fu}$, and $E_f\rho_f/f_c'^{2/3}$ and fitted six curves.

5.3.1 *U-Jacket Without Transverse Steel Reinforcements*

Best fit curve—1 is plotted on test data of beams strengthened in shear with GFRP sheets in the form of U-jacket without transverse steel reinforcements ($\rho_s = 0\%$). The details of test data on U-jacket without transverse steel reinforcements ($\rho_s = 0\%$) are given in Table 5.1.

The experimental data provided in Table 5.1 is used to produce the plot as shown in Fig. 5.5, which gives $R = \varepsilon_{fe}/\varepsilon_{fu}$ in terms of the quantity $E_f\rho_f/f_c'^{2/3}$.

It can be clearly seen that R decreases as $E_f\rho_f/f_c'^{2/3}$ increases. This indicates that as the stiffness of the GFRP sheet increases, effective strain decreases.

Table 5.1 Details of test data on U-jacket without transverse steel reinforcements ($\rho_s = 0\%$)

Specimen designation	f_c' (MPa)	b_w (mm)	d (mm)	d_f (mm)	t_f (mm)	ρ_f (%)	ρ_s (%)	ρ_w (%)	E_f (GPa)	$\varepsilon_{fu} \times 10^{-3}$	$\varepsilon_{fe} \times 10^{-3}$
S0-1L-CT-U-90	38.78	100	225	165	0.36	0.72	0	2.79	13.18	12.14	7.747
S0-2L-CT-U-90	38.78	100	225	165	0.72	1.44	0	2.79	13.18	12.14	5.278
S0-3L-CT-U-90	38.78	100	225	165	1.08	2.16	0	2.79	13.18	12.14	4.378
S0-1L-SZ-U-90	39.58	100	225	165	0.36	0.72	0	2.79	13.18	12.14	7.190
S0-1L-ST-U-90	40.03	100	225	165	0.36	0.36	0	2.79	13.18	12.14	9.229
S0-1L-SZ-UA-90	39.58	100	225	165	0.36	0.72	0	2.79	13.18	12.14	7.345

Table 5.2 Details of test data on U-jacket with transverse steel reinforcements (ρ_s = 0.19%)

Specimen designation	f_c' (MPa)	b_w (mm)	d (mm)	d_f (mm)	t_f (mm)	ρ_f (%)	ρ_s (%)	ρ_w (%)	E_f (GPa)	$\varepsilon_{fu} \times 10^{-3}$	$\varepsilon_{fe} \times 10^{-3}$
S300-1L-CT-U-90	39.35	100	225	165	0.36	0.72	0.19	2.79	13.18	12.14	7.127
S300-2L-CT-U-90	39.35	100	225	165	0.72	1.44	0.19	2.79	13.18	12.14	5.148
S300-3L-CT-U-90	39.35	100	225	165	1.08	2.16	0.19	2.79	13.18	12.14	4.318
S300-1L-SZ-U-90	42.08	100	225	165	0.36	0.72	0.19	2.79	13.18	12.14	6.950
S300-1L-ST-U-90	38.28	100	225	165	0.36	0.36	0.19	2.79	13.18	12.14	8.980
S300-1L-SZ-UA-90	42.08	100	225	165	0.36	0.72	0.19	2.79	13.18	12.14	7.877

Table 5.3 Details of test data on U-jacket with transverse steel reinforcement (ρ_s = 0.28%)

Specimen designation	f_c' (MPa)	b_w (mm)	d (mm)	d_f (mm)	t_f (mm)	ρ_f (%)	ρ_s (%)	ρ_w (%)	E_f (GPa)	$\varepsilon_{fu} \times 10^{-3}$	$\varepsilon_{fe} \times 10^{-3}$
S200-1L-CT-U-90	41.03	100	225	165	0.36	0.72	0.28	2.79	13.18	12.14	5.265
S200-2L-CT-U-90	41.03	100	225	165	0.72	1.44	0.28	2.79	13.18	12.14	4.862
S200-3L-CT-U-90	41.03	100	225	165	1.08	2.16	0.28	2.79	13.18	12.14	4.490
S200-1L-SZ-U-90	40.38	100	225	165	0.36	0.72	0.28	2.79	13.18	12.14	6.347
S200-1L-ST-U-90	37.83	100	225	165	0.36	0.36	0.28	2.79	13.18	12.14	8.882
S200-1L-SZ-UA-90	40.38	100	225	165	0.36	0.72	0.28	2.79	13.18	12.14	7.046

Table 5.4 Details of test data on side-bonded without transverse steel reinforcements ($\rho_s = 0\%$)

Specimen designation	f_c' (MPa)	b_w (mm)	d (mm)	d_f (mm)	t_f (mm)	ρ_f (%)	ρ_s (%)	ρ_w (%)	E_f (GPa)	$\varepsilon_{fu} \times 10^{-3}$	$\varepsilon_{fe} \times 10^{-3}$
S0-1L-CT-S-90	40.09	100	225	165	0.36	0.72	0	2.79	13.18	12.14	7.293
S0-2L-CT-S-90	40.09	100	225	165	0.72	1.44	0	2.79	13.18	12.14	5.443
S0-3L-CT-S-90	40.09	100	225	165	1.08	2.16	0	2.79	13.18	12.14	5.321
S0-1L-SZ-S-90	39.58	100	225	165	0.36	0.72	0	2.79	13.18	12.14	6.861
S0-1L-ST-S-90	40.03	100	225	165	0.36	0.36	0	2.79	13.18	12.14	8.504
S0-1L-ST-S-45	40.03	100	225	165	0.36	0.42	0	2.79	13.18	12.14	9.604

Table 5.5 Details of test data on side-bonded with transverse steel reinforcements (ρ_s = 0.19%)

Specimen designation	f_c' (MPa)	b_w (mm)	d (mm)	d_f (mm)	t_f (mm)	ρ_f (%)	ρ_s (%)	ρ_w (%)	E_f (GPa)	$\varepsilon_{fu} \times 10^{-3}$	$\varepsilon_{fe} \times 10^{-3}$
S300-1L-CT-S-90	40.67	100	225	165	0.36	0.72	0.19	2.79	13.18	12.14	6.891
S300-2L-CT-S-90	40.67	100	225	165	0.72	1.44	0.19	2.79	13.18	12.14	4.893
S300-3L-CT-S-90	40.67	100	225	165	1.08	2.16	0.19	2.79	13.18	12.14	4.644
S300-1L-SZ-S-90	42.08	100	225	165	0.36	0.72	0.19	2.79	13.18	12.14	6.248
S300-1L-ST-S-90	38.28	100	225	165	0.36	0.36	0.19	2.79	13.18	12.14	6.775
S300-1L-ST-S-45	38.28	100	225	165	0.36	0.42	0.19	2.79	13.18	12.14	7.215

Table 5.6 Details of test data on side-bonded with transverse steel reinforcements (ρ_s = 0.28%)

Specimen designation	f_c' (MPa)	b_w (mm)	d (mm)	d_f (mm)	t_f (mm)	ρ_f (%)	ρ_s (%)	ρ_w (%)	E_f (GPa)	$\varepsilon_{fu} \times 10^{-3}$	$\varepsilon_{fe} \times 10^{-3}$
S200-1L-CT-S-90	40.66	100	225	165	0.36	0.72	0.28	2.79	13.18	12.14	6.688
S200-2L-CT-S-90	40.66	100	225	165	0.72	1.44	0.28	2.79	13.18	12.14	4.695
S200-3L-CT-S-90	40.66	100	225	165	1.08	2.16	0.28	2.79	13.18	12.14	3.749
S200-1L-SZ-S-90	40.38	100	225	165	0.36	0.72	0.28	2.79	13.18	12.14	6.080
S200-1L-ST-S-90	37.83	100	225	165	0.36	0.36	0.28	2.79	13.18	12.14	6.960
S200-1L-ST-S-45	37.83	100	225	165	0.36	0.42	0.28	2.79	13.18	12.14	8.065

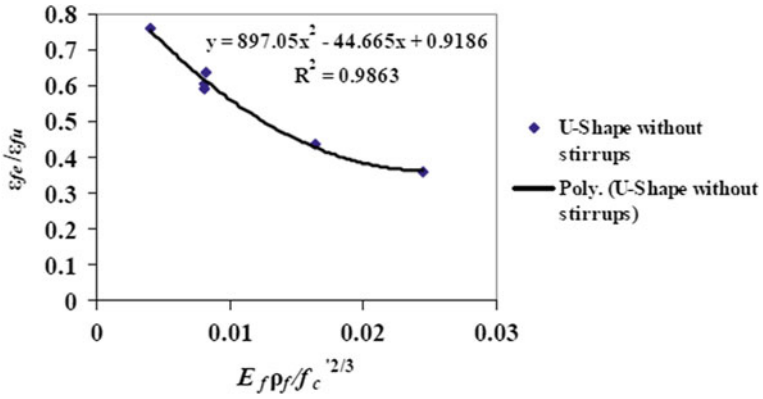

Fig. 5.5 Ratio of $\varepsilon_{fe}/\varepsilon_{fu}$ in terms of $E_f\rho_f/f_c'^{2/3}$

The relation between $R = \varepsilon_{fe}/\varepsilon_{fu}$ and $E_f\rho_f/f_c'^{2/3}$ is obtained here from the best-fit polynomial expressions as given in Eq. (5.24).

$$R = \frac{\varepsilon_{fe}}{\varepsilon_{fu}} = 897.05x^2 - 44.645x + 0.9186 \tag{5.24}$$

where $x = E_f\rho_f/f_c'^{2/3}$.

The value varies between $0.004 \leq x \leq 0.024$.
$R^2 = 0.9863$.

5.3.2 U-Jacket with 0.19% of Transverse Steel Reinforcement Ratio

Best-fit curve—2 is plotted on test data of beams strengthened in shear with GFRP sheets in the form of U-jacket with transverse steel reinforcements ($\rho_s = 0.19\%$). The details of test data on U-jacket with transverse steel reinforcements ($\rho_s = 0.19\%$) are given in Table 5.2.

The experimental data provided in Table 5.2 is used to produce the plot as shown in Fig. 5.6, which gives R in terms of the quantity $E_f\rho_f/f_c'^{2/3}$. It can be clearly seen that R decreases as $E_f\rho_f/f_c'^{2/3}$ increases.

The relation between $R = \varepsilon_{fe}/\varepsilon_{fu}$ and $E_f\rho_f/f_c'^{2/3}$ is obtained here from the best-fit polynomial expressions as given in Eq. (5.25).

$$R = \frac{\varepsilon_{fe}}{\varepsilon_{fu}} = 940.14x^2 - 45.365x + 0.9051 \tag{5.25}$$

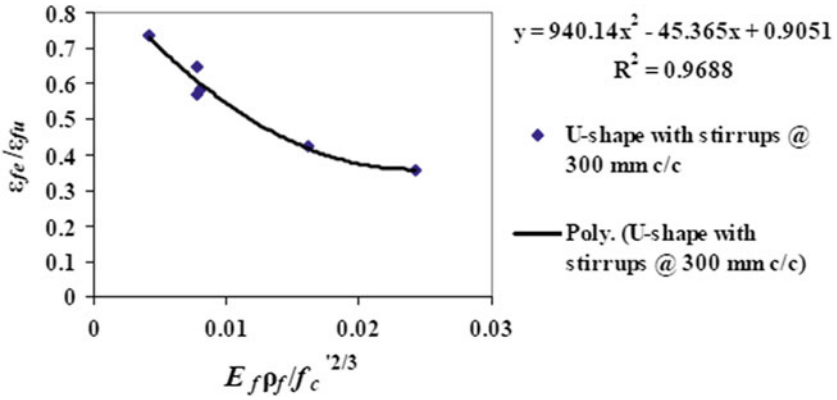

Fig. 5.6 Ratio of $\varepsilon_{fe}/\varepsilon_{fu}$ in terms of $E_f\rho_f/f_c'^{2/3}$

where $x = E_f\rho_f/f_c'^{2/3}$.

The value varies between $0.004 \leq x \leq 0.024$.

$R^2 = 0.9688$.

5.3.3 U-Jacket with 0.28% of Transverse Steel Reinforcement Ratio

Best fit curve—3 is plotted on test data of beams strengthened in shear with GFRP sheets in the form of U-jacket with transverse steel reinforcements ($\rho_s = 0.28\%$). The details of test data on U-jacket with transverse steel reinforcements ($\rho_s = 0.28\%$) are given in Table 5.3.

The experimental data provided in Table 5.3 is used to produce the plot as shown in Fig. 5.7, which gives R in terms of the quantity $E_f\rho_f/f_c'^{2/3}$. It can be clearly seen that R decreases as $E_f\rho_f/f_c'^{2/3}$ increases.

The relation between $R = \varepsilon_{fe}/\varepsilon_{fu}$ and $E_f\rho_f/f_c'^{2/3}$ is obtained here from the best-fit polynomial expressions as given in Eq. (5.26).

$$R = \frac{\varepsilon_{fe}}{\varepsilon_{fu}} = 1658.9x^2 - 62.073x + 0.9232 \tag{5.26}$$

where $x = E_f\rho_f/f_c'^{2/3}$.

The value varies between $0.004 \leq x \leq 0.024$.

$R^2 = 0.8203$.

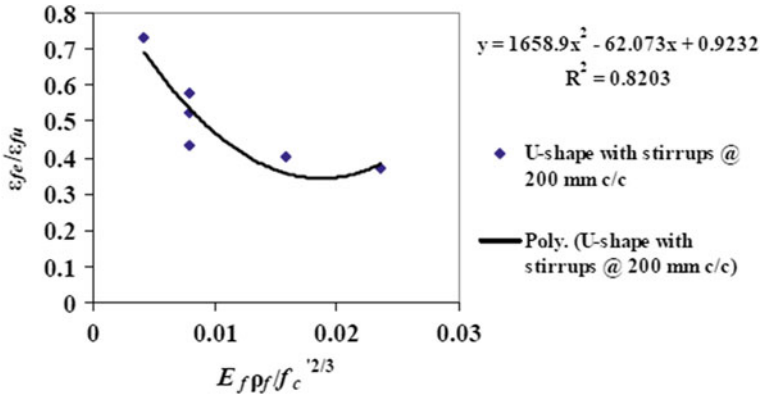

Fig. 5.7 Ratio of $\varepsilon_{fe}/\varepsilon_{fu}$ in terms of $E_f\rho_f/f_c'^{2/3}$

5.3.4 Side-Bonded Without Transverse Steel Reinforcements

Best fit curve—4 is plotted on test data of beams strengthened in shear with GFRP sheets on side of the web of the T-beams without transverse steel reinforcements ($\rho_s = 0\%$). The details of test data on side-bonded without transverse steel reinforcements ($\rho_s = 0\%$) are given in Table 5.4.

The experimental data provided in Table 5.4 is used to produce the plot as shown in Fig. 5.8, which gives R in terms of the quantity $E_f\rho_f/f_c'^{2/3}$. It can be clearly seen that R decreases as $E_f\rho_f/f_c'^{2/3}$ increases.

The relation between $R = \varepsilon_{fe}/\varepsilon_{fu}$ and $E_f\rho_f/f_c'^{2/3}$ is obtained here from the best-fit power expressions as given in Eq. (5.27).

$$R = \frac{\varepsilon_{fe}}{\varepsilon_{fu}} = 0.1237x^{-0.3255} \tag{5.27}$$

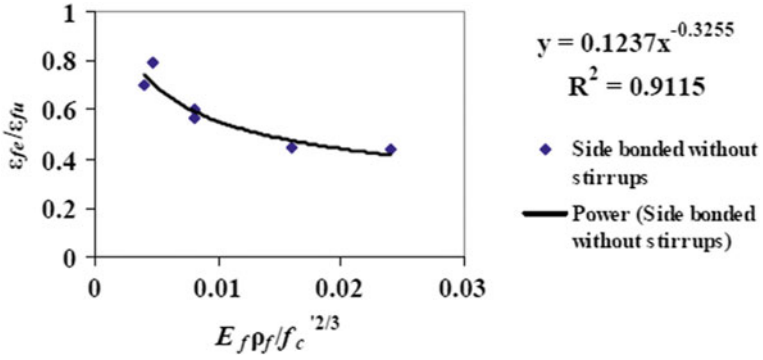

Fig. 5.8 Ratio of $\varepsilon_{fe}/\varepsilon_{fu}$ in terms of $E_f\rho_f/f_c'^{2/3}$

where $x = E_f\rho_f/f_c'^{2/3}$

The value varies between $0.004 \leq x \leq 0.024$.

$R^2 = 0.9115$.

5.3.5 Side-Bonded with 0.19% of Transverse Steel Reinforcement Ratio

Best-fit curve—5 is plotted on test data of beams strengthened in shear with GFRP sheets on side of the web of the T-beams with transverse steel reinforcements ($\rho_s = 0.19\%$). The details of test data on side-bonded with transverse steel reinforcements ($\rho_s = 0.19\%$) are given in Table 5.5.

The experimental data provided in Table 5.5 is used to produce the plot as shown in Fig. 5.9, which gives R in terms of the quantity $E_f\rho_f/f_c'^{2/3}$. It can be clearly seen that R decreases as $E_f\rho_f/f_c'^{2/3}$ increases.

The relation between $R = \varepsilon_{fe}/\varepsilon_{fu}$ and $E_f\rho_f/f_c'^{2/3}$ is obtained here from the best-fit polynomial expressions as given in Eq. (5.28).

$$R = \frac{\varepsilon_{fe}}{\varepsilon_{fu}} = 396.37x^2 - 21.96x + 0.6738 \tag{5.28}$$

where $x = E_f\rho_f/f_c'^{2/3}$.

The value varies between $0.004 \leq x \leq 0.024$.

$R^2 = 0.9037$.

5.3.6 Side-Bonded with 0.28% of Transverse Steel Reinforcement Ratio

Best fit curve—6 is plotted on test data of beams strengthened in shear with GFRP sheets on side of the web of the T-beams with transverse steel reinforcements

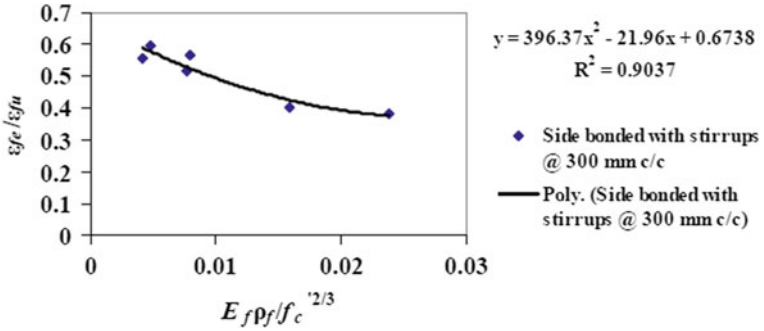

Fig. 5.9 Ratio of $\varepsilon_{fe}/\varepsilon_{fu}$ in terms of $E_f\rho_f/f_c'^{2/3}$

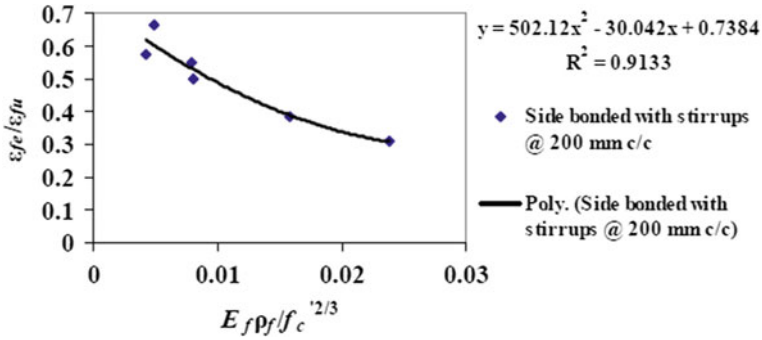

Fig. 5.10 Ratio of $\varepsilon_{fe}/\varepsilon_{fu}$ in terms of $E_f\rho_f/f_c'^{2/3}$

($\rho_s = 0.28\%$). The details of test data on side-bonded with transverse steel reinforcements ($\rho_s = 0.28\%$) are given in Table 5.6.

The experimental results provided in Table 5.6 are used to produce the plot as shown in Fig. 5.10, which gives R in terms of the quantity $E_f\rho_f/f_c'^{2/3}$. It can be clearly seen that R decreases as $E_f\rho_f/f_c'^{2/3}$ increases.

The relation between $R = \varepsilon_{fe}/\varepsilon_{fu}$ and $E_f\rho_f/f_c'^{2/3}$ is obtained here from the best-fit polynomial expressions as given in Eq. (5.29).

$$R = \frac{\varepsilon_{fe}}{\varepsilon_{fu}} = 502.12x^2 - 30.042x + 0.7384 \tag{5.29}$$

where $x = E_f\rho_f/f_c'^{2/3}$.

The value varies between $0.004 \leq x \leq 0.024$.

$R^2 = 0.9133$.

5.4 Comparison of Experimental and Theoretical Results

Following section presents the comparison of test results of control beams obtained from the experimental studies and the theoretical value calculated from the different standards. Section 5.4.2 presents the comparison of the test results of strengthened beams obtained from the experimental investigations and theoretical value obtained from the ACI 440.2R-02 design approach.

5.4.1 Comparison of Test Results of Control Beams with Different Standards

The total shear resistance of the control beams from the experimental studies and the calculated value from the different standards ACI 318-02, CSA (A23.3-C1.11.3), and IS 456: 2000 is listed in Table 5.7.

Table 5.7 Comparison of test results of control specimen with different standards

Specimen designation	Test results $V_{n,\text{test}}$ (kN)	ACI 318-95 $V_{n,\text{theor}}$ (kN)	Increase in test results (%)	$\frac{V_{n,\text{test}}}{V_{n,\text{theor}}}$ ratio as per ACI	CSA (A23.3-C1.11.3) $V_{n,\text{theor}}$ (kN)	Increase in test results (%)	$\frac{V_{n,\text{test}}}{V_{n,\text{theor}}}$ ratio as per CSA	IS 456: 2000 $V_{n,\text{theor}}$ (kN)	Increase in test results (%)	$\frac{V_{n,\text{test}}}{V_{n,\text{theor}}}$ ratio as per IS
S0-0L-1	52.0	26.68	94.90	1.95	29.22	77.96	1.78	22.16	134.70	2.35
S0-0L-2	50.0	26.68	87.41	1.87	29.22	71.12	1.71	22.16	125.63	2.26
S0-0L-3	48.0	26.68	79.91	1.80	29.22	64.27	1.64	22.16	116.60	2.17
S300-0L-1	68.0	36.55	86.05	1.86	38.89	74.85	1.75	31.38	116.70	2.17
S300-0L-2	73.0	36.55	99.72	2.00	38.89	87.70	1.88	31.38	132.60	2.33
S300-0L-3	70.5	36.55	92.89	1.93	38.89	81.28	1.81	31.38	124.66	2.25
S200-0L-1	87.0	42.72	103.65	2.03	45.30	92.05	1.92	36.00	141.70	2.42
S200-0L-2	75.0	42.72	75.56	1.75	45.30	65.56	1.65	36.00	108.30	2.08
S200-0L-3	78.0	42.72	82.58	1.83	45.30	72.18	1.72	36.00	116.70	2.17

It may be observed that the theoretical results obtained from the different standard give conservative value as compared with the test results.

5.4.2 *Comparison of Test Results of Strengthened Beams with ACI Design Approach*

The test results obtained from the experimental studies of the RC T-beams strengthened in shear with GFRP sheets is compared with the theoretical value obtained from ACI 440.2R-02 design approach.

The total shear strength of the RC T-beams strengthened in shear with GFRP sheets obtained from the different phases of experimental investigations and the theoretical shear strength calculated using the ACI 440.2R-02 design approach is listed in tables in the following paragraph.

(a) **RC T-beams Strengthened in Shear with U-Jacketed GFRP Sheets**

The comparison of test results (Panda et al. 2012) and theoretical shear resistance results predicted by ACI 440.2R-02 guidelines of RC T-beams strengthened in shear with externally U-jacketed GFRP sheets is listed in Table 5.8.

It is observed that without transverse steel reinforcements the shear strength contribution of GFRP is more as compared with transverse steel reinforcements. It is expected that with no transverse steel, the guidelines underestimate the shear resistance due to GFRP. It may also be observed that, as layer increases, the experimental and ACI predicted results come almost closure to each other.

(b) **RC T-beams Strengthened in Shear with Side-Bonded GFRP Sheets**

The comparison of test results (Panda et al. 2011) and theoretical shear resistance results predicted by ACI 440.2R-02 guidelines of RC T-beams strengthened in shear with externally side-bonded GFRP sheets is listed in Table 5.9.

It is observed that the shear strength contribution of GFRP sheet in strengthened RC T-beams without transverse steel reinforcements and with 0.19% of transverse steel reinforcement is more as compared with 0.28% of transverse steel reinforcements. It is expected that with no transverse steel and for 0.19% transverse steel reinforcement, the ACI guidelines underestimate the shear resistance due to GFRP, whereas for 0.28% transverse steel reinforcements the experimental result and theoretical results predicted by ACI guidelines come closer to each other.

(c) **RC T-beams Strengthened in Shear Zone with GFRP Strips**

The comparison of test results (Panda et al. 2013a) and theoretical shear resistance results predicted by ACI 440.2R-02 guidelines of RC T-beams strengthened in shear with externally bonded GFRP strips is listed in Table 5.10.

It is observed that the shear strength contribution of GFRP from the experimental study is giving more value as compared with the ACI design approach. It may also

Table 5.8 Comparison of experimental and ACI-predicted shear resistance results

Specimen	Experimental results						Theoretical results predicted by ACI 440.2R-02 design approach			
	Load at failure (kN)	$V_{n,\text{test}}$ (kN)	$V_{c,\text{test}}$ (kN)	$V_{s,\text{test}}$ (kN)	$V_{f,\text{test}}$ (kN)	$\frac{V_{f,\text{test}}}{V_{n,\text{test,rif}}} \times 100$ (%)	$V_{f,\text{theor}}$ (kN)	$V_{c,\text{theor}}$ (kN)	$V_{s,\text{theor}}$ (kN)	$\phi V_{n,\text{theor}}$ (kN)
S0-0L	100	50.0	50	–	–	–	–	26.68	–	22.68
S300-0L	141	70.5	50	20.5	–	–	–	25.95	10.60	31.07
S200-0L	160	80.0	50	30.0	–	–	–	26.82	15.90	36.31
S0-1L-CT-U-90	136	68.0	50	–	18.0	36.00	6.26	25.73	–	26.25
S0-2L-CT-U-90	142	71.0	50	–	21.0	42.00	11.84	25.73	–	30.16
S0-3L-CT-U-90	146	73.0	50	–	23.0	46.00	18.79	25.73	–	35.02
S300-1L-CT-U-90	156	78.0	50	20.5	7.5	10.64	6.26	25.90	10.60	35.54
S300-2L-CT-U-90	160	80.0	50	20.5	9.5	13.47	12.05	25.90	10.60	39.73
S300-3L-CT-U-90	184	92.0	50	20.5	21.5	30.50	18.79	25.90	10.60	44.60
S200-1L-CT-U-90	182	91.0	50	30.0	11.0	13.75	6.26	26.37	15.90	40.45
S200-2L-CT-U-90	208	104.0	50	30.0	24.0	30.00	12.36	26.37	15.90	44.86
S200-3L-CT-U-90	192	96.0	50	30.0	16.0	20.00	18.79	26.37	15.90	49.51

Table 5.9 Comparison of experimental and ACI-predicted shear resistance results

Specimen	Experimental results						Theoretical results predicted by ACI 440.2R-02 design approach			
	Load at failure (kN)	$V_{n,\text{test}}$ (kN)	$V_{c,\text{test}}$ (kN)	$V_{s,\text{test}}$ (kN)	$V_{f,\text{test}}$ (kN)	$\frac{V_{f,\text{test}}}{V_{n,\text{test,rif}}} \times 100$ (%)	$V_{f,\text{theor}}$ (kN)	$V_{c,\text{theor}}$ (kN)	$V_{s,\text{theor}}$ (kN)	$\phi V_{n,\text{theor}}$ (kN)
S0-0L	100	50.0	50	–	–	–	–	26.68	–	22.68
S300-0L	141	70.5	50	20.5	–	–	–	25.95	10.60	31.07
S200-0L	160	80.0	50	30.0	–	–	–	26.82	15.90	36.31
S0-1L-CT-S-90	132	66.0	50	–	16.0	32.00	6.26	26.11	–	26.72
S0-2L-CT-S-90	138	69.0	50	–	19.0	38.00	12.53	26.11	–	31.25
S0-3L-CT-S-90	150	75.0	50	–	25.0	50.00	18.79	26.11	–	35.77
S300-1L-CT-S-90	176	88.0	50	20.5	17.5	24.82	6.26	26.27	10.60	35.86
S300-2L-CT-S-90	180	90.0	50	20.5	19.5	27.66	12.53	26.27	10.60	40.40
S300-3L-CT-S-90	182	91.0	50	20.5	20.5	29.08	18.79	26.27	10.60	44.92
S200-1L-CT-S-90	180	90.0	50	30.0	10.0	12.50	6.26	26.27	15.90	40.37
S200-2L-CT-S-90	186	93.0	50	30.0	13.0	16.25	12.53	26.27	15.90	44.90
S200-3L-CT-S-90	196	98.0	50	30.0	18.0	22.50	18.79	26.27	15.90	49.42

Table 5.10 Comparison of experimental and ACI-predicted shear resistance results

Specimen	Experimental results						Theoretical results predicted by ACI 440.2R-02 design approach			
	Load at failure (kN)	$V_{n,\text{test}}$ (kN)	$V_{c,\text{test}}$ (kN)	$V_{s,\text{test}}$ (kN)	$V_{f,\text{test}}$ (kN)	$\frac{V_{f,\text{test}}}{V_{n,\text{test,rif}}} \times 100$ (%)	$V_{f,\text{theor}}$ (kN)	$V_{c,\text{theor}}$ (kN)	$V_{s,\text{theor}}$ (kN)	$\phi V_{n,\text{theor}}$ (kN)
S0-0L	100	50.0	50	–	–	–	–	26.68	–	22.68
S300-0L	141	70.5	50	20.5	–	–	–	25.95	10.60	31.07
S200-0L	160	80.0	50	30.0	–	–	–	26.82	15.90	36.31
S0-1L-ST-U-90	124	62.0	50	–	12.0	24.00	3.13	26.09	–	24.44
S0-1L-ST-S-90	116	58.0	50	–	8.0	16.00	3.13	26.09	–	24.44
S0-1L-ST-S-45	146	73.0	50	–	23.0	46.00	5.20	26.09	–	25.93
S300-1L-ST-U-90	164	82.0	50	20.5	11.5	16.31	3.13	25.59	10.60	33.02
S300-1L-ST-S-90	154	77.0	50	20.5	6.5	9.22	3.13	25.59	10.60	33.02
S300-1L-ST-S-45	166	83.0	50	20.5	12.5	17.73	5.20	25.59	10.60	34.52
S200-1L-ST-U-90	186	93.0	50	30.0	13.0	16.25	3.13	25.45	15.90	37.41
S200-1L-ST-S-90	172	86.0	50	30.0	6.0	7.50	3.13	25.45	15.90	37.41
S200-1L-ST-S-45	182	91.0	50	30.0	11.0	13.75	5.20	25.45	15.90	38.90

be observed that the shear strength contribution of GFRP strips from the experimental study significantly decreases as transverse steel reinforcement increases, whereas in ACI design approach, the value remains same for all variation of transverse steel reinforcements.

(d) **RC T-beams Strengthened in Shear Zone with GFRP Sheet**

The comparison of test results (Panda et al. 2013b) and theoretical shear resistance results predicted by ACI 440.2R-02 guidelines of RC T-beams strengthened in shear with externally bonded GFRP sheet in the shear zone is listed in Table 5.11.

It is observed that the shear strength contribution of GFRP sheet in the shear zone from the experimental study is more than theoretical values. Whereas in ACI design approach, the value remains the same for all variations of transverse steel reinforcements.

5.5 General Discussion

The equations presented in ACI design approach based on the various data used include three types of fibre material such as CFRP, AFRP and GFRP, three types of strengthening configurations such as completely wrapped, U-jacket, and bonded on two sides, continuous FRP sheet as well as strips, 45° and 90° fibre orientations and number of plies. Although all the data followed nearly the same trend as shown in Fig. 5.3, only a single curve fit was proposed. Based on the present experimentation, a plot of reduction factor (effective strain/ultimate strain) versus stiffness was compiled for various cases. Using these curves, a realistic assessment of the shear strength of GFRP wrapped beam can be made. This will enhance the design capability than the existing ones. Further, it is observed that the variation of reduction factor with stiffness as per ACI design guideline has the similar trend as that of the present experimental results. It is conjectured that the nonlinear variation of the plot is due to the change in stiffness for the addition of different layers of GFRP.

5.6 Summary

The chapter presented theoretical and comparative studies. Based on these studies, it may be concluded that the experimental value of shear strength contribution of control RC T-beams is more as compared to the theoretical values obtained from ACI, CSA and IS standards. The ACI, CSA and IS standards give conservative results for control RC T-beams.

The experimental values of shear strength contribution of GFRP sheet and strips are more as compared to the theoretical values obtained from the ACI 440.2R-02 design approach. The ACI design approach gives conservative results for RC T-beams strengthened in shear with GFRP sheets or strips.

Table 5.11 Comparison of experimental and ACI-predicted shear resistance results

Specimen	Experimental results						Theoretical results predicted by ACI 440.2R-02 design approach			
	Load at failure (kN)	$V_{n,\text{test}}$ (kN)	$V_{c,\text{test}}$ (kN)	$V_{s,\text{test}}$ (kN)	$V_{f,\text{test}}$ (kN)	$\frac{V_{f,\text{test}}}{V_{n,\text{test,rif}}} \times 100$ (%)	$V_{f,\text{theor}}$ (kN)	$V_{c,\text{theor}}$ (kN)	$V_{s,\text{theor}}$ (kN)	$\phi V_{n,\text{theor}}$ (kN)
S0-0L	100	50.0	50	–	–	–	–	26.68	–	22.68
S300-0L	141	70.5	50	20.5	–	–	–	25.95	10.60	31.07
S200-0L	160	80.0	50	30.0	–	–	–	26.82	15.90	36.31
S0-1L-SZ-S-90	130	65.0	50	–	15.0	30.00	6.26	25.96	–	26.59
S0-1L-SZ-U-90	132	66.0	50	–	16.0	32.00	6.26	25.96	–	26.59
S0-1L-SZ-UA-90	140	70.0	50	–	20.0	40.00	6.26	25.96	–	26.59
S300-1L-SZ-S-90	178	89.0	50	20.5	18.5	26.24	6.26	26.66	10.60	36.19
S300-1L-SZ-U-90	180	90.0	50	20.5	19.5	27.66	6.26	26.66	10.60	36.19
S300-1L-SZ-UA-90	192	96.0	50	20.5	25.5	36.17	6.26	26.66	10.60	36.19
S200-1L-SZ-S-90	184	92.0	50	30.0	12.0	15.00	6.26	26.18	15.90	40.29
S200-1L-SZ-U-90	188	94.0	50	30.0	14.0	17.50	6.26	26.18	15.90	40.29
S200-1L-SZ-UA-90	196	98.0	50	30.0	18.0	22.50	6.26	26.18	15.90	40.29

The theoretical observation indicates that as stiffness of the GFRP sheet increases, the shear contribution of GFRP obtained from the ACI 440.2R-02 guidelines, approaches closer to the test results.

References

American Concrete Institute (ACI) (1995) Building code requirements for structural concrete (ACI 318-95) and commentary (ACI 318R-95). ACI Committee 318, Detroit, Mich

American Concrete Institute (ACI) (2002) Building code requirements for reinforced concrete (ACI 318-02) and commentary-ACI 318RM-02. ACI Committee 318, Detroit, Mich

American Concrete Institute (ACI 440.2R-02) (2002) Guide for the design and construction of externally bonded FRP systems for strengthening concrete structures. ACI Committee 440, Farmington Hills, Michigan, 45 p

Antonopoulos CP, Triantafillou TC (2002) Analysis of FRP strengthened RC beam column joints. J Compos Constr 6(1):41–51

Antonopoulos CP, Triantafillou TC (2003) Experimental investigation of FRP strengthened RC beam-column joints. J Compos Constr 7(1):39–49

Bousselham A, Chaallal O (2004) Shear strengthening reinforced concrete beams with fiber-reinforced polymer: assessment of influencing parameters and required research. ACI Struct J 101(2):219–227

Canadian Standards Association (CSA) (1994) Design of concrete structures. A23.3-94, Rexdale, Ontario

Canadian Standards Association (CSA-S806-02) (2002) Design and construction of building components with fiber-reinforced polymer. Rexdale, Ontario, 202pp

Indian Standard, Plain and Reinforced Concrete Code of Practice IS 456: 2000, 100pp

Khalifa A, Gold WJ, Nanni A, Aziz A (1998) Contribution of externally bonded FRP to shear capacity of RC flexural members. J Compos Constr 2(4):195–201

Panda KC, Bhattacharyya SK, Barai SV (2010) Shear behaviour of reinforced concrete T-beams with U-bonded glass fibre reinforced plastic sheet. Indian Concr J (ICJ) 84(10):61–71

Panda KC, Bhattacharyya SK, Barai SV (2011) Shear strengthening of RC T-beams with externally side bonded GFRP sheet. J Reinf Plastic Compos 30(13):1139–1154

Panda KC, Bhattacharyya SK, Barai SV (2012) Shear behaviour of RC T-beams strengthened with U-wrapped GFRP sheet. Steel Compos Struct Int J 12(2):149–166

Panda KC, Bhattacharyya SK, Barai SV (2013a) Shear strengthening effect by bonded GFRP strips and transverse steel on RC T-beams. Struct Eng Mech Int J 47(1):75–98

Panda KC, Bhattacharyya SK, Barai SV (2013b) Effect of transverse steel on the performance of RC T-beams strengthened in shear zone with GFRP sheet. Constr Build Mater 41:79–90

Panda KC, Bhattacharyya SK, Barai SV (2015) Strain analysis of RC T-beams strengthened in shear with variation of U-wrapped GFRP sheet and transverse steel. Adv Struct Eng 3 (154):2001–2010

Triantafillou TC, Antonopoulos CP (2000) Design of concrete flexural members strengthened in shear with FRP. J Compos Constr 4(4):198–205

Chapter 6
Numerical Approach to Shear Strengthening of Beams

6.1 General

Finite element method (FEM) is used to study the behaviour of RC T-beams strengthened in shear with GFRP sheet under two-point loading condition. The finite element analysis is carried out in this study using ANSYS finite element software. Specimens without GFRP as control beams, designated as S0-0L, S300-0L and S200-0L and beams strengthened with GFRP sheets in U-jacket for specimens S0-1L-CT-U-90, S300-1L-CT-U-90 and S200-1L-CT-U-90 (Panda et al. 2012) are analysed. The main focus of the chapter is on the development of the model for full-size beams, elements used for the development of the model, geometry of the models, loading and boundary conditions and comparison of results with experiment. The formulation of the FEM models is discussed in the following sections.

6.2 Element Formulation

Commercially available ANSYS software has been used for the numerical study. The elements selected for the study are described below.

6.2.1 Reinforced Concrete

Solid65 is an eight-noded solid element with three degrees of freedom at each node and translations in the x, y and z directions. This element is used to model the concrete beams with or without steel reinforcement bars. The solid element is capable of representing plastic deformation, cracking in three orthogonal directions and also crushing of concrete. Isotropic material properties are considered for the elements (Kachlakev et al. 2001). The geometry of Solid65 element is shown in Fig. 6.1.

K. C. Panda et al., *Shear Strengthening of T-beam with GFRP*, Springer Transactions in Civil and Environmental Engineering, https://doi.org/10.1007/978-981-10-7760-9_6

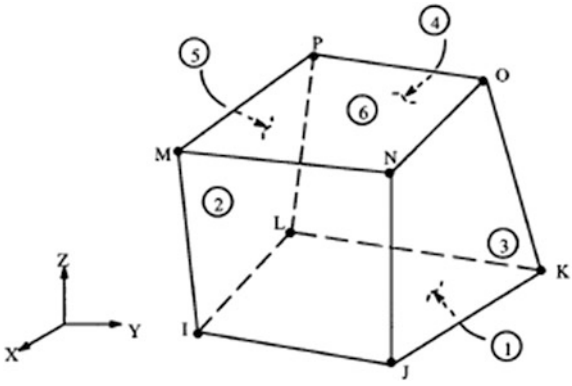

Fig. 6.1 Solid65 element (ANSYS 1998)

Link8 element is a two-noded element with three degrees of freedom at each node and translations in the *x*, *y* and *z* directions. This element is used to model the steel reinforcement bar. The element is also capable of representing plastic deformation. The geometry of this element type shown in Fig. 6.2.

6.2.2 FRP Composites

Solid46 is a layered solid element with three degrees of freedom at each node and translations in the *x*, *y* and *z* directions. This element is used to model the FRP composites. The geometry of Solid46 elements is shown in Fig. 6.3.

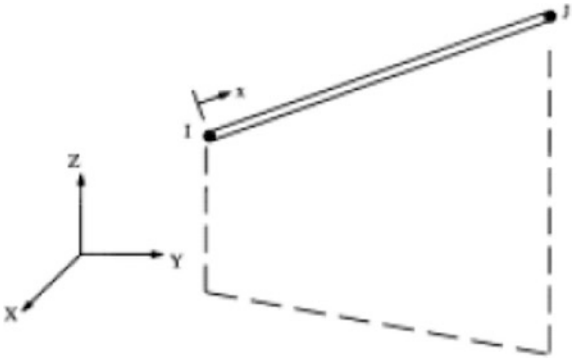

Fig. 6.2 Link8 element (ANSYS 1998)

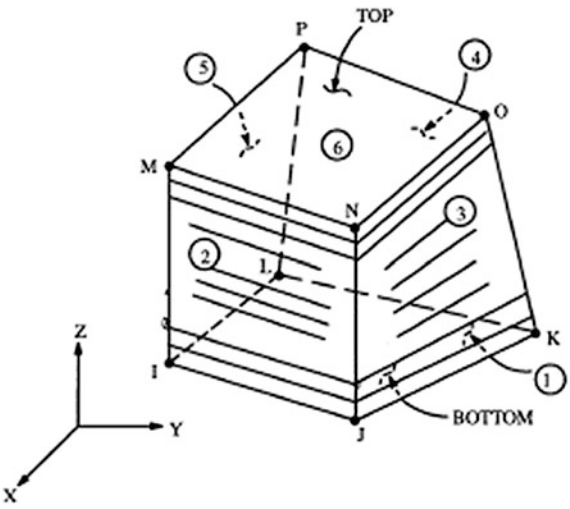

Fig. 6.3 Solid46 element (ANSYS 1998)

6.3 Model Description

With the help of commercially available software (ANSYS), the finite element analysis was carried out using previously discussed elements. The details are given below.

6.3.1 Geometry of the Model

The detailed geometry of the full-size RC T-beams, used for the experimental investigation, is explained in Chap. 3. The development of the model of RC T-beams using finite element software (ANSYS) is presented in Fig. 6.4.

The dimensions of the models are the same as used in the experimental investigation. The line sketch of the models of series S0, S300 and S200 is presented in Figs. 6.5, 6.6 and 6.7.

The models for strengthened RC T-beams of S0-1L-CT-U-90, S300-1L-CT-U-90 and S200-1L-CT-U-90 (Panda et al. 2012) are presented in Figs. 6.11, 6.12 and 6.13.

In the strengthened RC T-beam models, the Link8 element is used to represent the steel reinforcement bar. The model simplified by ignoring the anchorage portion of steel reinforcement bar. In this study, the perfect bond between the materials is assumed for developing the model. The Link8 element for steel reinforcement bar is connected between the nodes of each adjacent concrete Solid65 element, so that the two different materials share the same node. The same approach is also followed for

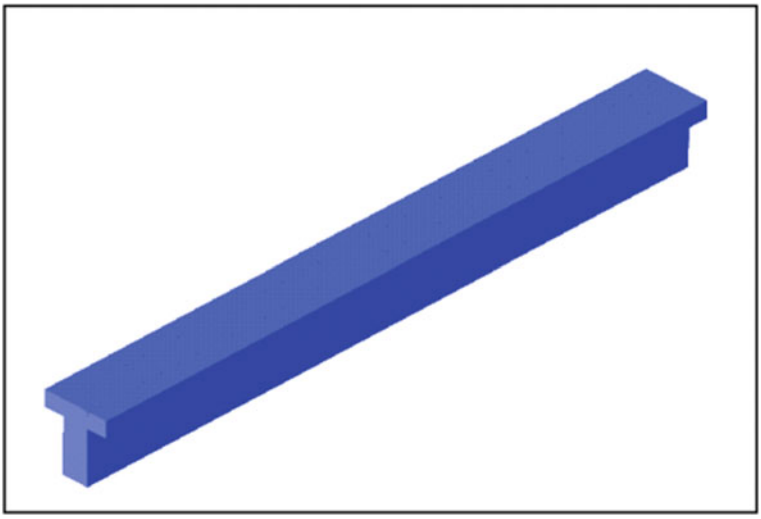

Fig. 6.4 Geometry of the model of all the series

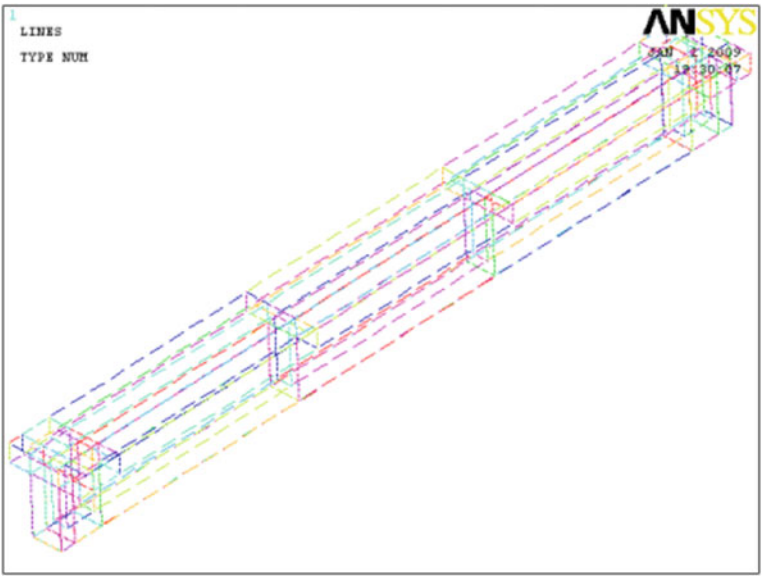

Fig. 6.5 Line sketch of the model of series S0

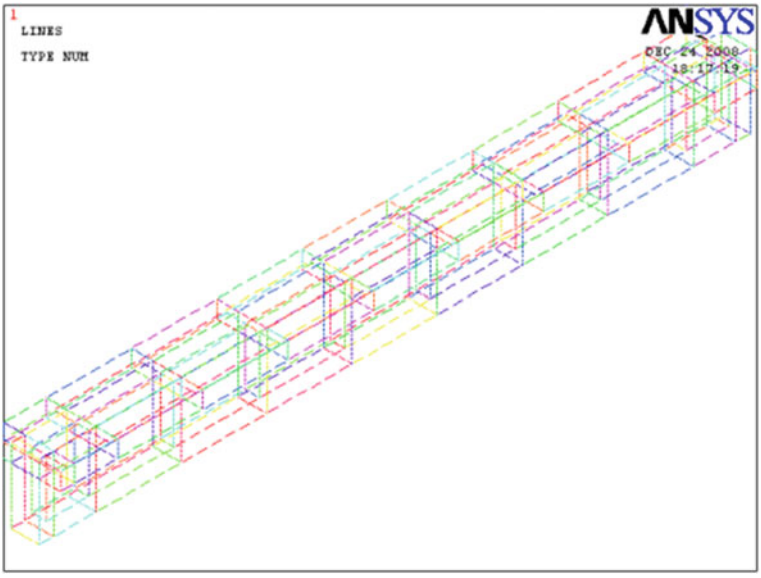

Fig. 6.6 Line sketch of the model of series S300

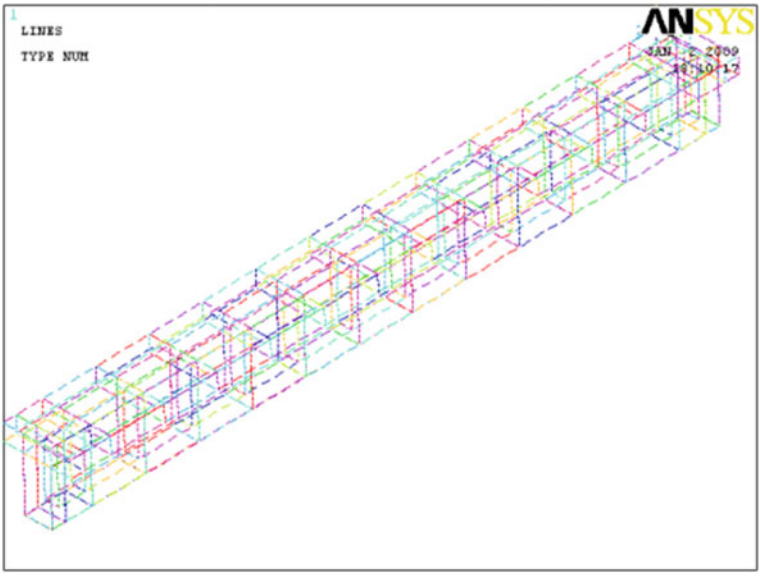

Fig. 6.7 Line sketch of the model of series S200

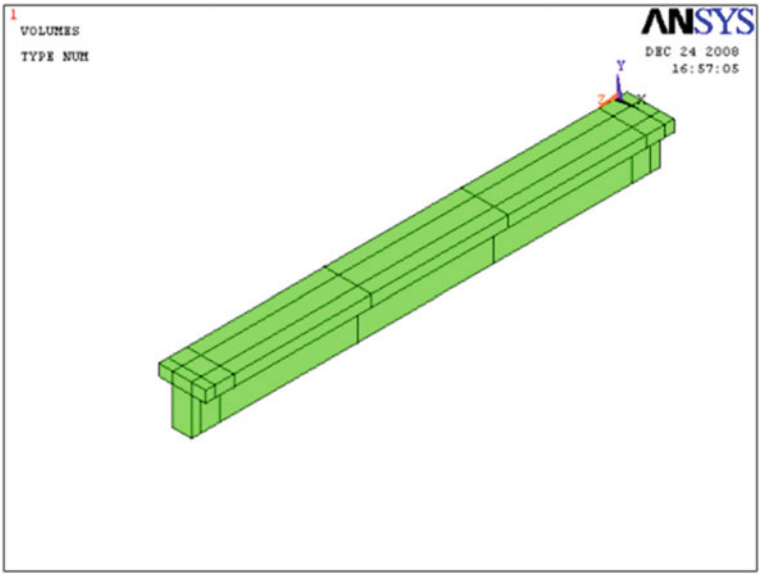

Fig. 6.8 Model of series S0

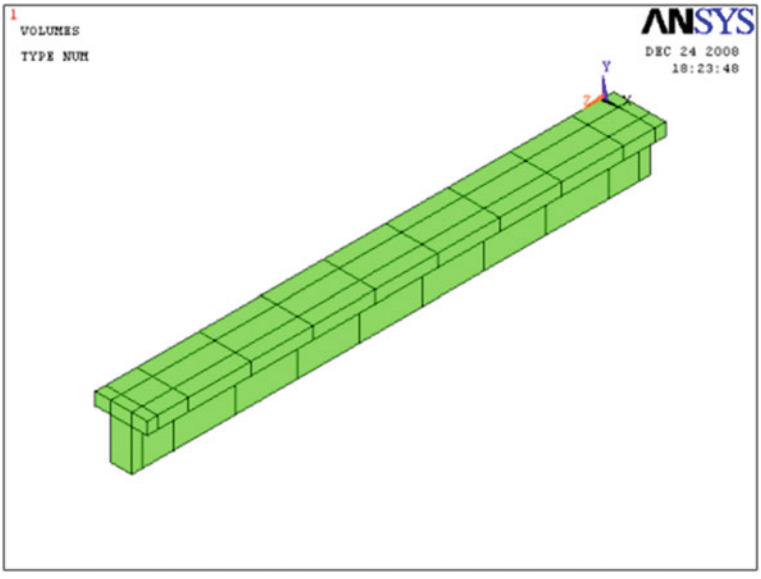

Fig. 6.9 Model of series S300

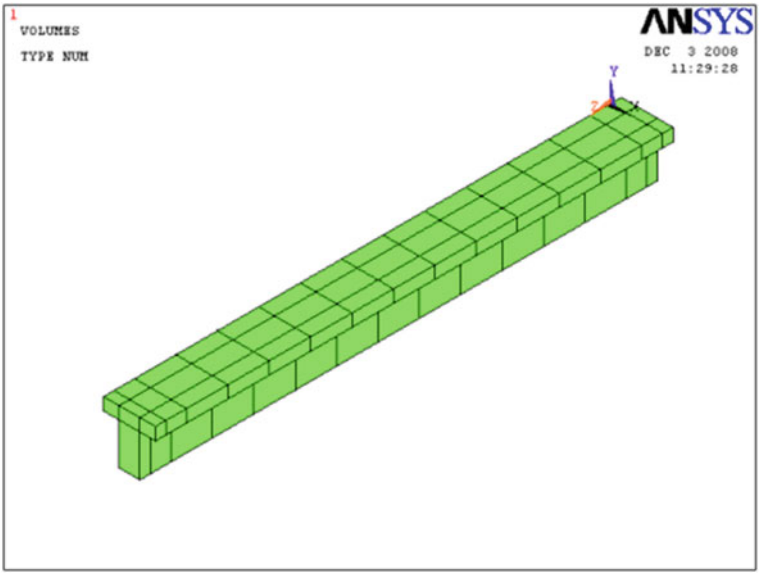

Fig. 6.10 Model of series S200

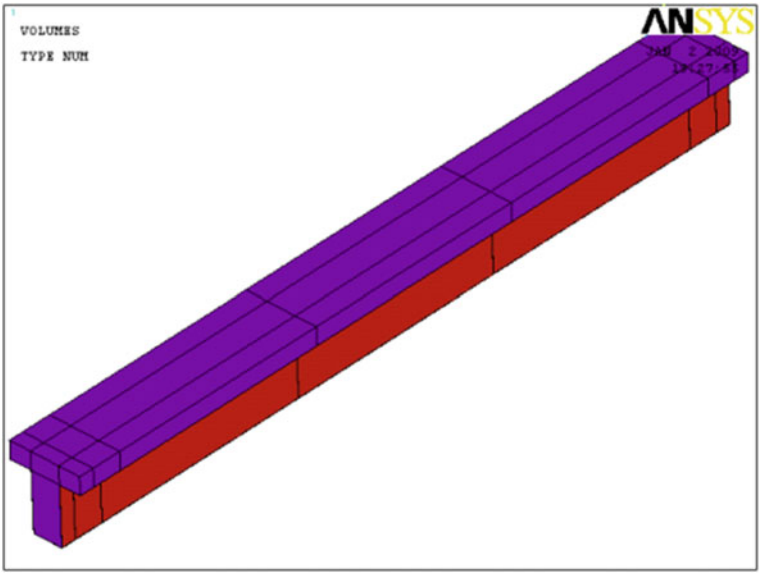

Fig. 6.11 Model of S0-1L-CT-U-90

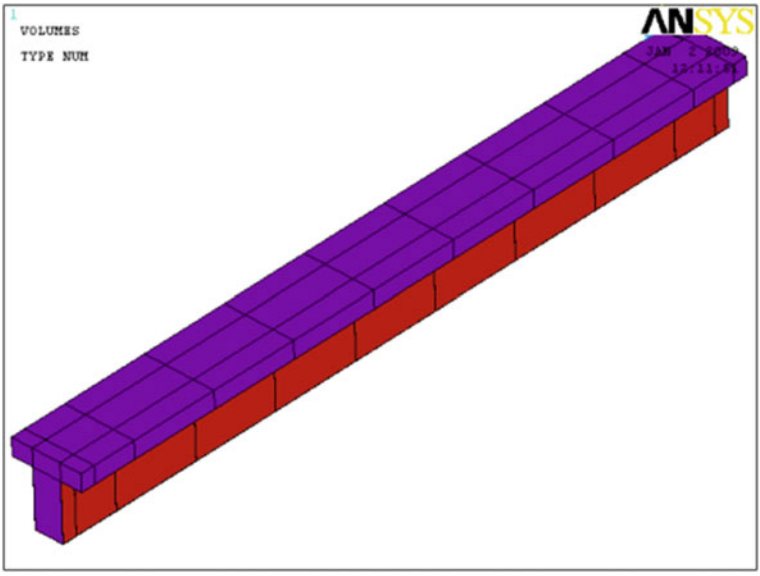

Fig. 6.12 Model of S300-1L-CT-U-90

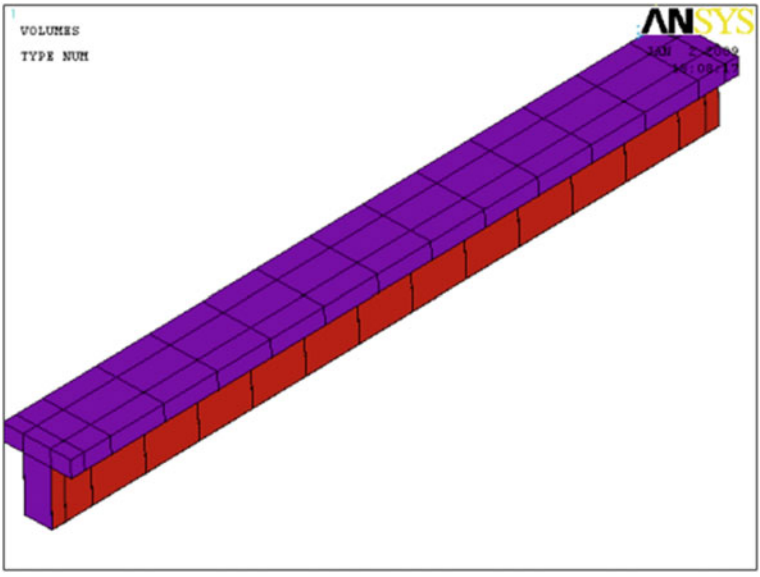

Fig. 6.13 Model of S200-1L-CT-U-90

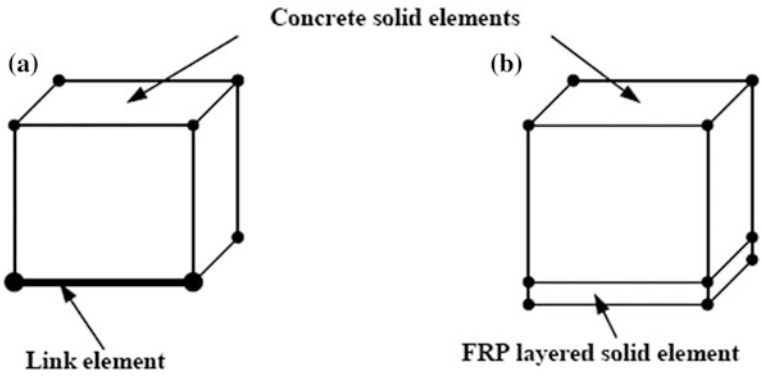

Fig. 6.14 Element connectivity: **a** concrete Solid65 and Link8 elements; **b** Solid65 and Solid46 FRP-layered elements

GFRP sheets. Solid46, layered solid elements, are used to model the GFRP sheets. To satisfy the perfect bond between the concrete surface and FRP sheet, nodes of the Solid46 FRP-layered solid elements are connected to those of adjacent Solid65 concrete solid elements. Figure 6.14a presents the connectivity between the concrete solid element and link element and Fig. 6.14b presents the connectivity between the concrete solid element and FRP-layered solid element.

6.3.2 Finite Element Discretization

After modeling the control and strengthened RC T-beams, the model is divided into a number of small elements. An important step in finite element modeling is the selection of the mesh density. In the present model, the element length used along the cross section is 5 mm and along the longitudinal direction is 50 mm, which gives the most desirable conserving results. Numbers of elements used in this study are given in Table 6.1.

Table 6.1 Numbers of elements used

Model	Number of elements			
	Concrete	Steel reinforcement	GFRP composites	Total
S0-0L	71,400	1074	–	72,474
S300-0L	70,000	1588	–	71,588
S200-0L	70,000	2108	–	72,108
S0-1L-CT-U-90	72,624	1074	5202	78,900
S300-1L-CT-U-90	71,200	1588	5100	77,888
S200-1L-CT-U-90	71,200	2108	5100	78,408

The finite element discretization of the steel reinforcement for specimens of series S0, S300 and S200 is shown in Figs. 6.15, 6.16 and 6.17.

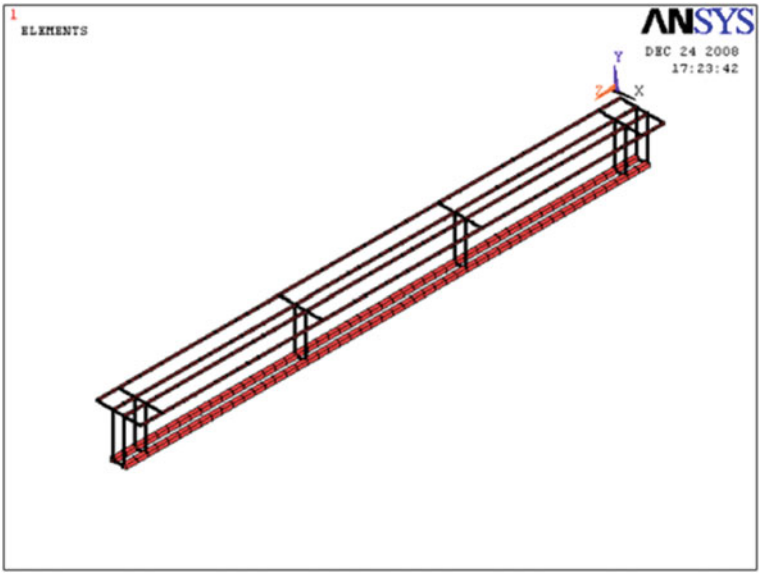

Fig. 6.15 Element discretization of the steel reinforcements of series S0

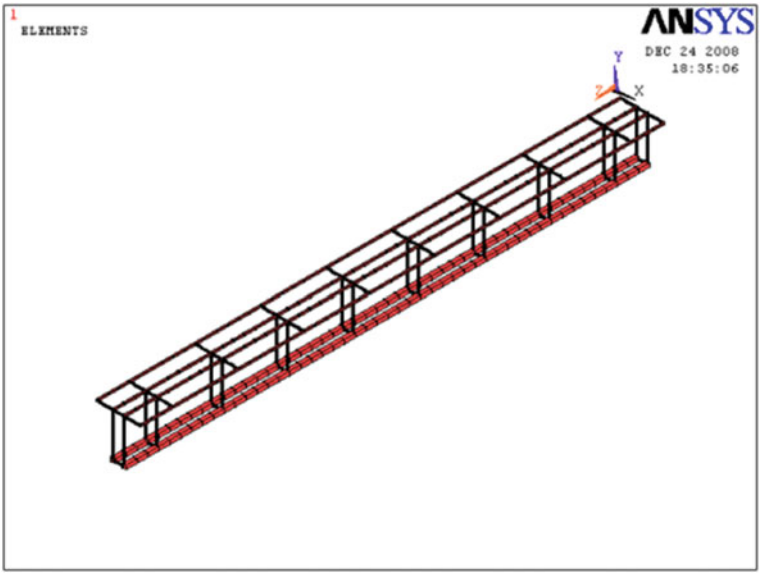

Fig. 6.16 Element discretization of the steel reinforcements of series S300

The detail discretization of the RC T-beams and the U-jacket GFRP sheet is shown in Figs. 6.18 and 6.19.

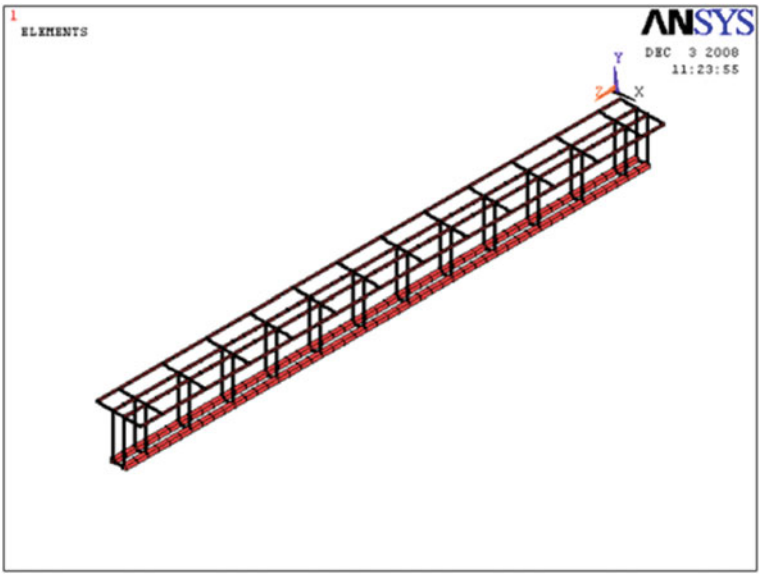

Fig. 6.17 Element discretization of the steel reinforcements of series S200

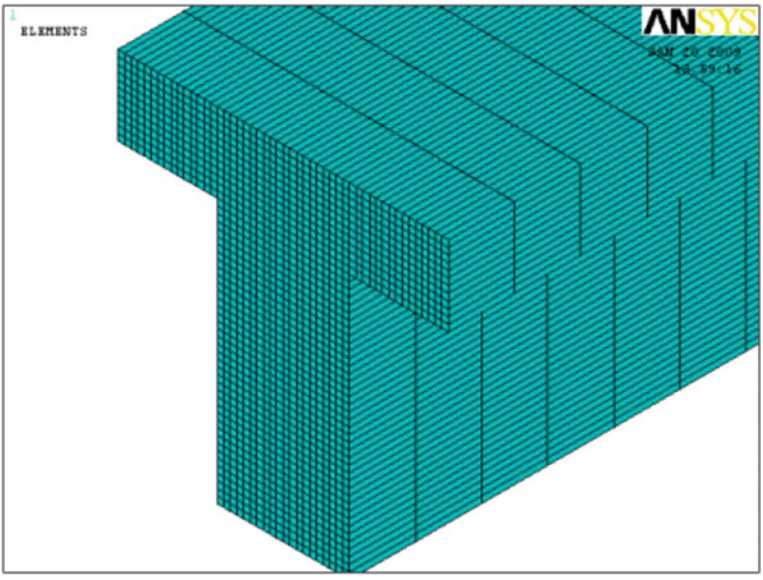

Fig. 6.18 Element discretization of RC T-Beams

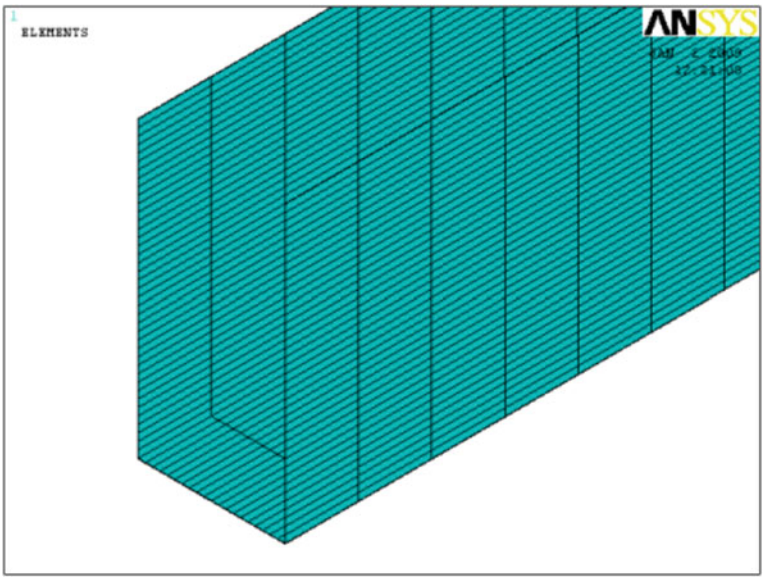

Fig. 6.19 Element discretization of GFRP U-jacket

6.3.3 Loading and Boundary Conditions

Minor change is made in the loading in the FEM models as compared to the experimental investigation. In S0-0L, and S0-1L-CT-U-90 specimens, the load is applied at a distance of 735 mm from both ends of the supports, whereas in the experimental investigation it is 733 mm. In S300-0L, S200-0L, S300-1L-CT-U-90 and S200-1L-CT-U-90 (Panda et al. 2012), the loading point is located at a distance of 750 mm from both ends of the supports. The displacement in the vertical direction at the support point is considered as zero. The loading and boundary conditions of a typical finite element model is shown in Figs. 6.20 and 6.21.

6.3.4 Material Properties

The material properties used in the FEM models of control and strengthened RC T-beams are presented in Tables 6.2, 6.3 and 6.4 for concrete, steel and GFRP respectively.

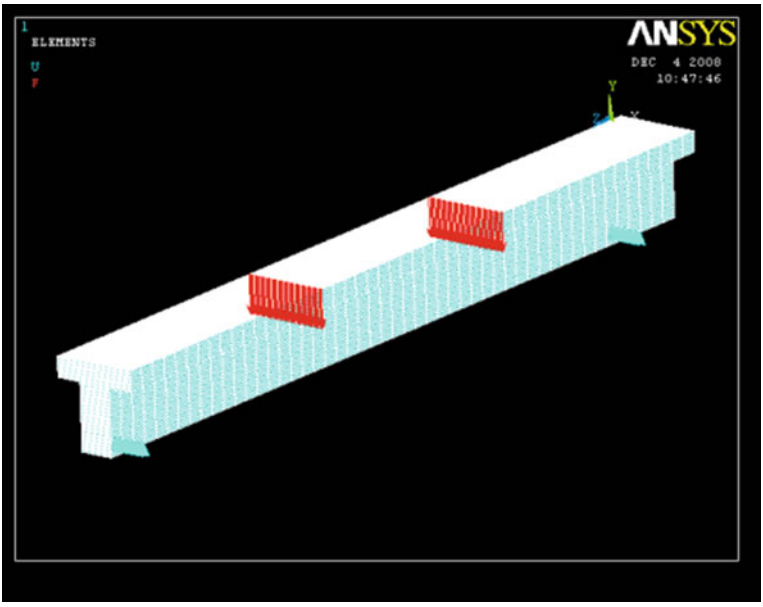

Fig. 6.20 Loading and boundary conditions

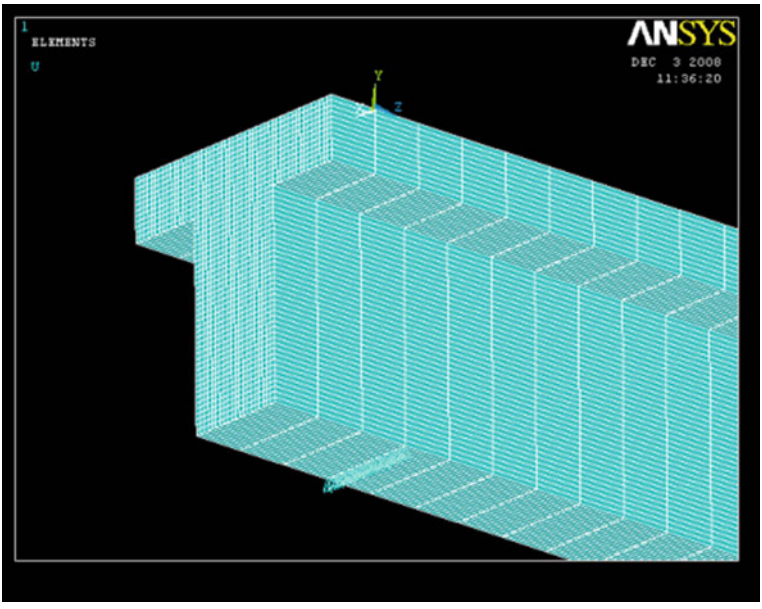

Fig. 6.21 Support at nodal points (one side view)

Table 6.2 Summary of material properties for concrete

Modulus of elasticity of concrete	E_c	GPa	35
Poisson's ratio for concrete	v_c	–	0.20
Density of plain concrete	$\rho_{concrete}$	kg/m^3	2400
Cement volume fraction	C	%	0.25
Sand volume fraction	FA	%	0.24
Aggregate volume fraction	CA	%	0.51

Table 6.3 Summary of Material Properties for Steel

Modulus of elasticity of steel	E_s	GPa	200
Poisson's ratio for steel	v_s	–	0.30
Density of steel	ρ_{steel}	kg/m^3	7800

Table 6.4 Summary of material properties for GFRP

Modulus of elasticity—*X* direction	E_x	GPa	13.18
Modulus of elasticity—*Y* direction	E_y	GPa	5.0
Modulus of elasticity—*Z* direction	E_z	GPa	3.0
Poisson's ratio—*XY* plane	v_{xy}	–	0.22
Poisson's ratio—*XZ* plane	v_{xz}	–	0.23
Poisson's ratio—*YZ* plane	v_{yz}	–	0.24
Shear modulus—*XY* plane	G_{xy}	GPa	1.0
Shear modulus—*XZ* plane	G_{xz}	GPa	1.1
Shear modulus—*YZ* plane	G_{yz}	GPa	1.2
Density of GFRP	ρ_{GFRP}	kg/m^3	1300

6.4 Comparison of Experimental and ANSYS Results

The variation of midspan deflections with load obtained using ANSYS models are compared with the experimental results. It is observed that the results obtained using FEM analyses are closer to the experimental results.

(a) **Control Beams**

The deflections of control RC T-beams of three different series are computed at the midspan of the beams. The variation of midspan deflection with load obtained from experimental and ANSYS results for all the control RC T-beams of S0-0L, S300-0L and S200-0L are shown in Figs. 6.22, 6.23 and 6.24. The results computed for the RC T-beams from the finite element analysis agree quite well with the experimental plot up to approximately 60 kN load. Thereafter as load increased, the finite element load–deflection plot shows lesser value than the experimental plot.

(b) **Strengthened Beams**

The variation of midspan deflection with load obtained from experimental and ANSYS results for all the strengthened RC T-beams of S0-1L-CT-U-90, S300-1L-CT-U-90 and S200-1L-CT-U-90 (Panda et al. 2012) are shown in

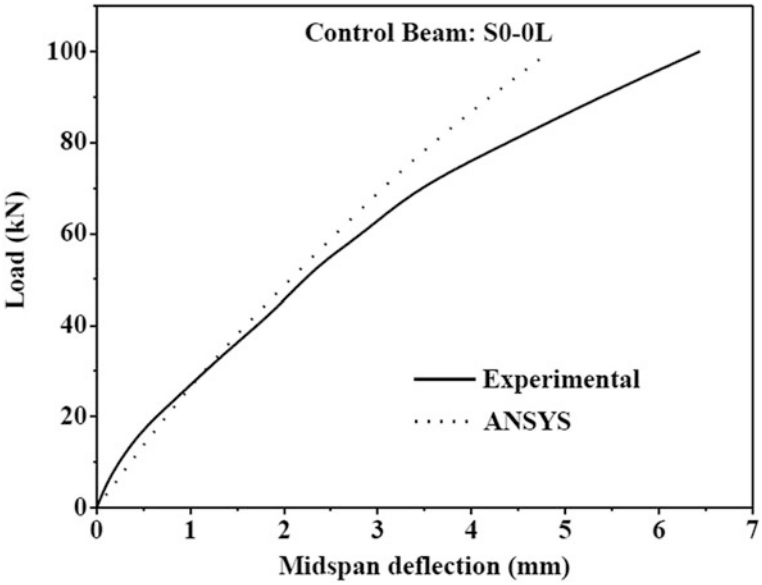

Fig. 6.22 Load versus midspan deflection of control beam S0-0L

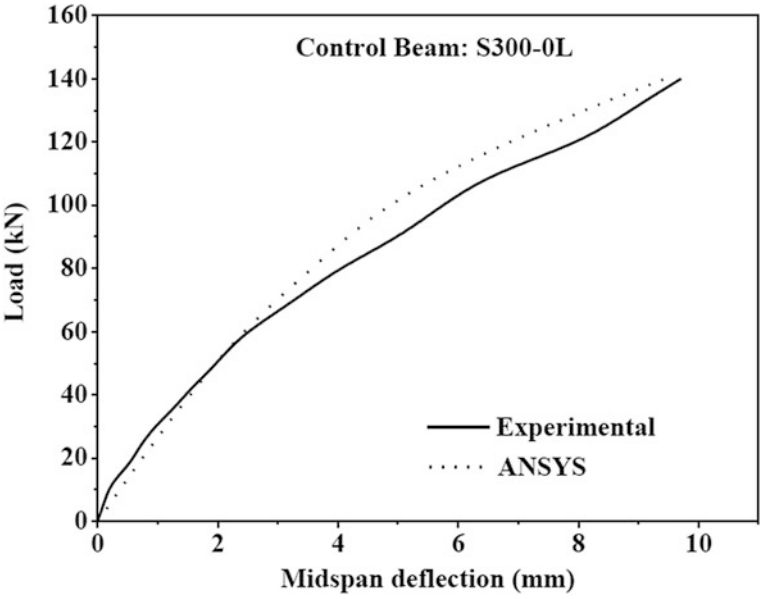

Fig. 6.23 Load versus midspan deflection of control beam S300-0L

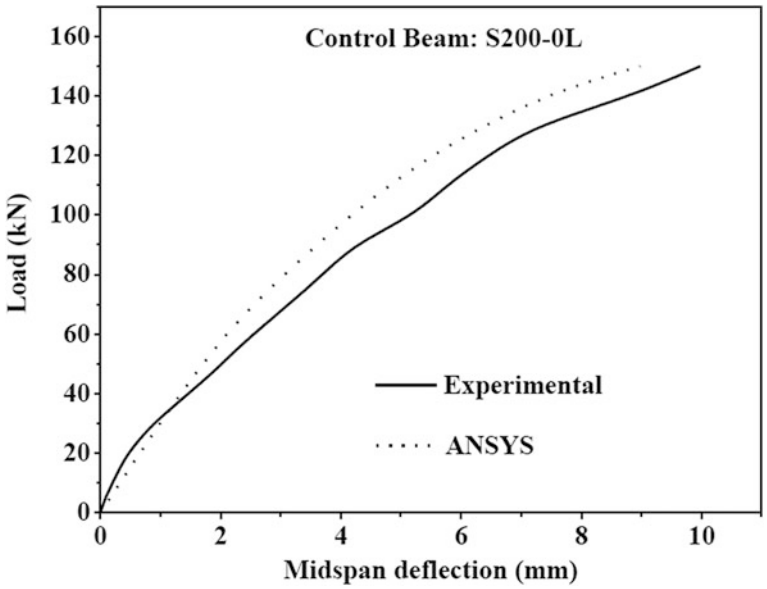

Fig. 6.24 Load versus midspan deflection of control beam S200-0L

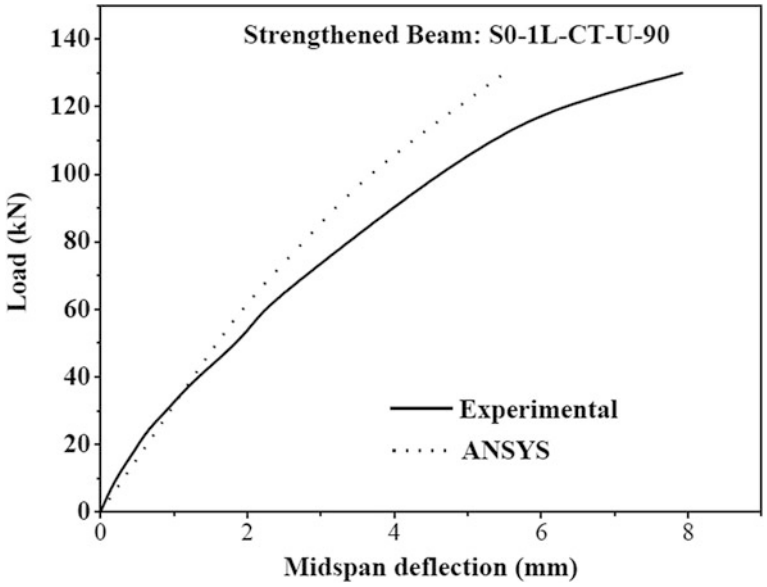

Fig. 6.25 Load versus midspan deflection of beam S0-1L-CT-U-90

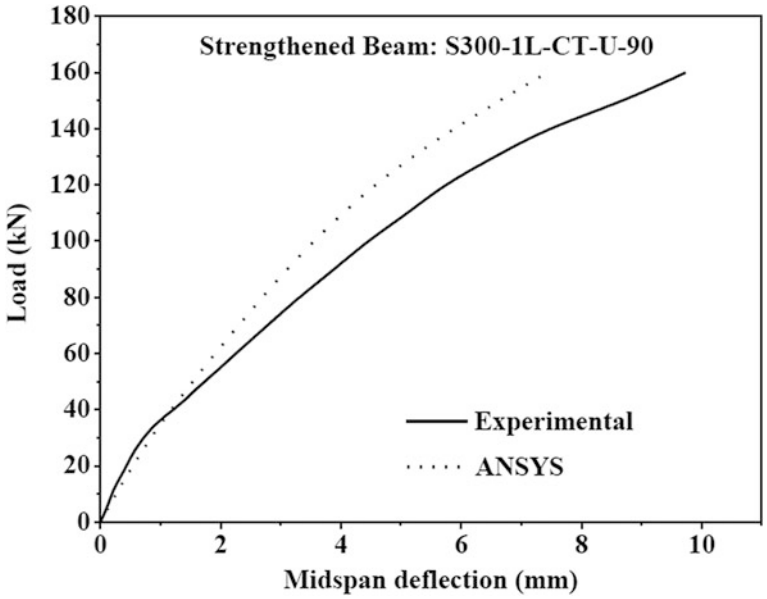

Fig. 6.26 Load versus midspan deflection of beam S300-1L-CT-U-90

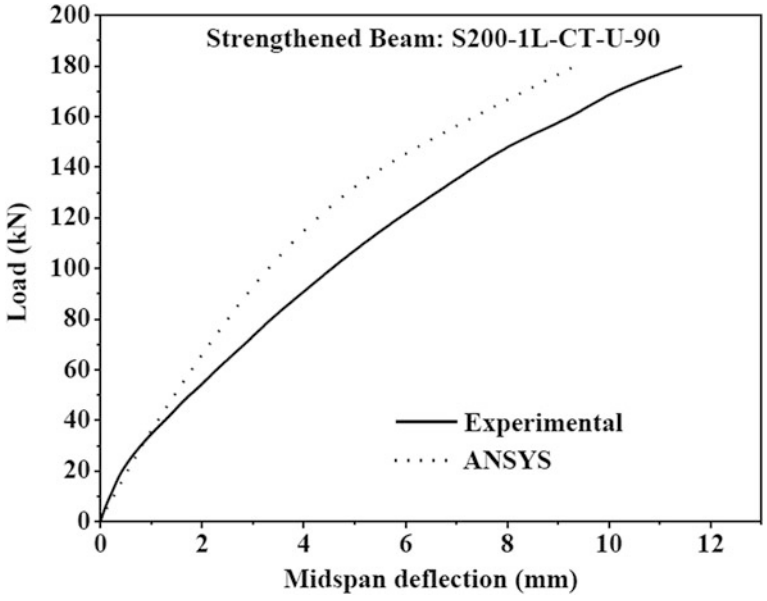

Fig. 6.27 Load versus midspan deflection of beam S200-1L-CT-U-90

Figs. 6.25, 6.26 and 6.27. It is observed that, the load–deflection plots for the RC T-beams from the finite element analysis agree quite well with the experimental results up to approximately 40 kN load. Thereafter as load increased the numerical values demonstrated less than the experimental results.

6.5 Summary

Six RC T-beams were analysed. Out of six beams, three beams are for the control RC T-beam and the rest three beams for the RC T-beams are strengthened in shear with U-jacketed GFRP sheet. The general behaviour of the finite element models represented by the load–deflection plots at midspan of the beam shows reasonable agreement with the test results at the initial stage of loading. However, after initiation of crack the finite element model shows relatively more stiffness than the experimental plot. In the present work, only the deflection at the midspan of the beams is computed. For control specimens, the result matches up to cracking (60–70 kN) load. The objective of carrying out the numerical result was to get an insight of the experiments done. However, the limitation of the present FEM analysis is the consideration of linear analysis instead of nonlinear one. The results indicated that the wrapped beams demonstrate a nonlinear behaviour at around a load of 40 kN. This requires to be further investigated to support the observation.

References

ANSYS (1998) ANSYS User's Manual revision 8. ANSYS Inc., Canonsburg

Kachlakev D, Miller T, Yim S (2001) Finite element modeling of reinforced concrete structures strengthened with FRP laminates. Report for Oregon Department of Transportation, Salem

Panda KC, Bhattacharyya SK, Barai SV (2012) Shear behaviour of RC T-beams strengthened with U-wrapped GFRP sheet. Steel Compos Struct Int J 12(2):149–166

Index

K. C. Panda et al., *Shear Strengthening of T-beam with GFRP*, Springer Transactions in Civil and Environmental Engineering, https://doi.org/10.1007/978-981-10-7760-9